

**Functional Interactions Between Ribosome and Nascent Peptide  
Mediated By Small Molecules**

BY  
SHANMUGAPRIYA SOTHISELVAM  
B.Tech. Anna University, 2010

DISSERTATION  
Submitted as partial fulfillment of the requirements for the degree of  
Doctor of Philosophy in Pharmacognosy in the Graduate College of the  
University of Illinois at Chicago, 2016

Chicago, Illinois

Committee Members:

Alexander S. Mankin, Advisor and Chair

Nora Vázquez-Laslop, Co-advisor

Michael J. Federle, Medicinal Chemistry and Pharmacognosy

Miljan Simonović, Biochemistry and Molecular Genetics

Brian K. Kay, Biological Sciences

Yury Polikanov, Biological Sciences

*I dedicate this dissertation to my parents,  
Logasundari and Sothiselvam,  
as I owe them everything I am and hope to be.*

## ACKNOWLEDGEMENTS

I was extremely fortunate to have Drs. Nora Vazquez-Laslop and Alexander (Shura) Mankin as mentors for my Ph.D. I have learned and benefitted a lot from their critical inputs on various aspects during the course of my graduate work. I cannot thank Nora enough, for being available always, for her constant advice, criticisms and for being extremely supportive professionally and personally all of which has helped me a lot in doing well throughout grad school. I am very thankful to both of them for encouraging my career interests and letting me to pursue internships at industries during grad school. They have been a great source of inspiration and I am indebted to them for their guidance.

I am extremely grateful to the current and past members of the Mankin lab (Jacqueline LaMarre, Bindiya Kaushal, Anna Ochabowicz, Krishna Kannan, Pulkit Gupta, Dorota Klepacki, Teresa Szal, Cedric Orelle, Mashal AlMutairi, James Marks, Sezen Meydan, Tanja Florin, Tonu Margus, Michael Graf, Anusha Paul Raj, Amira Kefi, Jiyoung Lee and Maxim Svetlov) and members of the Lee lab (Tamiko Oguri and Jerry Woo) for their friendship and making the lab feel like a home away from home. Dorota, is the most patient person I have known and I owe her for teaching me all the experimental skills I learned in the Mankin Lab. Special thanks to Krishna Kannan for his helpful discussions, guidance from time to time and constantly pushing me to achieve above and beyond and Pulkit Gupta for his guidance during my rotation in the Mankin lab, which paved the way for me joining the lab subsequently.

## **ACKNOWLEDGEMENTS (continued)**

I would like to thank my prelim and doctoral defense committee members (Dr. Michael Federle, Dr. Brian Kay, Dr. Yury Polikanov, Dr. Zain Paroo and Dr. Miljan Simonovic) for their time and feedback.

I would like to thank summer and rotation students Rasha Shalaby, Alvin Godnina, Trupti Patel, Lauren Callahan and Vladimir Yurukov for the opportunity to mentor them and hone my teaching skills and their contributions to my projects.

Thanks to Center for Pharmaceutical Biotechnology administrative staff (Elizabeth Woods, Emily Lam, Yi Dong, Linda Ly, Mary Ann and Rachel Morrow) for their help with all the administrative issues.

Finally, I would like to thank my friends and family for being there for me whenever I needed them. Special thanks to my husband, Raajan Aravindhan for supporting my career aspirations and being very understanding especially during the final weeks of wrapping up this dissertation work.

## TABLE OF CONTENTS

<u>Chapter</u>	<u>Page</u>
<b>1. Introduction</b>	1
1.1 Ribosome: the protein synthesis factory	1
1.2 Ribosome stalling and regulation of gene expression	3
1.3 Nascent peptide and small molecule mediated regulation of translation	6
1.4 Antibiotic and nascent peptide dependent ribosome stalling and inducible expression of resistance genes	8
1.4.1 Macrolide antibiotics allosterically predispose the ribosome for translation arrest	17
1.4.2 Ribosome can discriminate its catalytic substrates based on their charge and size	19
1.4.3 Context specific translation arrest mediated by macrolide antibiotics	20
1.5 Cited Literature	22
<b>2. Macrolide antibiotics allosterically predispose the ribosome for translation arrest</b>	27
2.1 Introduction and rationale	27
2.2 Materials and Methods	31
2.3 Results	38
2.3.1 The Position of the Conserved RLR Motif Varies in the Leader Peptides of Macrolide Resistance Genes	38
2.3.2 Tunnel-Bound Antibiotic Inhibits Formation of Peptide Bond Between MRL Peptide and the Incoming Aminoacyl-tRNA	42
2.3.3 Known Nascent Peptide Ribosomal Sensors Are Not Involved in Drug Induced Stalling with the MRL Peptide	45
2.3.4 Structurally Diverse Antibiotics Promote Ribosome Stalling with RLR Peptides	46
2.3.5 Binding of Antibiotics in the NPET Allosterically Alters the Conformation of the PTC	49
2.3.6 MD Simulations Substantiate the Existence of a Structural Link Between the NPET and the PTC	50
2.4 Discussion	57
2.5 Cited Literature	62
<b>3. Antibiotic bound ribosome discriminates its catalytic substrates based on charge</b>	66
3.1 Introduction and rationale	66
3.2 Materials and Methods	71
3.3 Results	77

## **TABLE OF CONTENTS (continued)**

3.3.1	Antibiotic-mediated translation arrest at the MRLR ORF is independent of the mRNA sequence and tRNA structure	77
3.3.2	Only the templates encoding Arg or Lys in the second and fourth codons are conducive to ERY induced translation arrest	77
3.3.3	The presence of Arg or Lys in the donor and acceptor substrates is critical for arrest of translation by diverse macrolide antibiotics	80
3.3.4	Arg- and Lys- acceptor substrate analogs react poorly with the MRL-tRNA donor in the presence and in the absence of antibiotic	85
3.3.5	The positive charge of the A site substrates is the predominant factor that makes them poor acceptors of the MRL peptide	89
3.4	Discussion	97
3.5	Cited Literature	103
<b>4.</b>	<b>Context specific action of macrolide antibiotics in facilitating translation arrest</b>	<b>106</b>
4.1	Introduction and rationale	106
4.2	Materials and Methods	109
4.3	Results	112
4.3.1	Nascent peptide sequence preceding the RLR stalling motif affects macrolide-dependent translation arrest	112
4.3.2	ERY remains bound to the ribosome, which translates through the RLR sequence	118
4.3.3	The counter-stalling sequence of the <i>ermDL</i> M3 mutant can operate inside the gene	119
4.3.4	The N-terminal sequence of the ErmDL peptide acts as an independent stalling module that promotes translation arrest even at non-optimal stalling motifs	123
4.4	Discussion	128
4.5	Cited Literature	135
	<b>Appendices</b>	<b>139</b>
	Appendix A	139
	Appendix B	180
	Appendix C	181
	Appendix D	190
	<b>VITA</b>	<b>191</b>

## LIST OF FIGURES

<u>Figure</u>		<u>Page</u>
1.1	The ribosome and its exit tunnel	2
1.2	Examples of regulatory nascent peptides and their arrest sequences	7
1.3	Structure of macrolide antibiotics and their binding site in the ribosomal exit tunnel	10
1.4	The regulatory uORFs and the encoded leader peptides of representative macrolide resistance genes	12
1.5	Inducible expression of antibiotic resistance by programmed translation arrest	13
1.6	Models of leader peptides in the drug bound exit tunnel	16
2.1	Antibiotic and nascent peptide in the ribosomal exit tunnel	30
2.2	Antibiotic-dependent ribosome stalling occurs at the R/K-L-R/K motif of leader peptides with heterogeneous N-termini	39
2.3	The N-terminal segment preceding the RLLR motif is dispensable for antibiotic-mediated translation arrest	40
2.4	Drug-dependent ribosome stalling is abolished by the N-terminal truncations of ErmCL	41
2.5	Antibiotic inhibits the ability of the ribosome carrying the MRL nascent peptide to catalyze peptidyl transfer	43
2.6	Characterization of peptidyl-tRNA in the stalled complex	44
2.7	None of the tested nucleotides in the ribosomal exit tunnel is critical for antibiotic-induced translation arrest with the MRL peptide	47
2.8	Diverse macrolides induce ribosome stalling with the MRL nascent peptide	48
2.9	Binding of antibiotics in the NPET affect the distant nucleotide U2585 in the PTC active site	52

## **LIST OF FIGURES (continued)**

2.10	Molecular dynamics (MD) simulations illuminate the existence of a structural link between the nascent peptide exit tunnel (NPET) and the peptidyl transferase center (PTC)	53
2.11	MD simulations substantiate the allosteric effect of the NPET-bound ERY on the distant PTC nucleotides U2585 and A2602	54
2.12	Equilibration of the ribosome structure and conformations of U2585 and A2602 rRNA residues during MD simulations	55
2.13	ERY is stably bound in the tunnel	56
3.1	ERY dependent translation arrest in the MRLR ORF is not dependent on the mRNA structure or the nature of its tRNA decoders	78
3.2	Amino acid residues critical for ERY dependent translation arrest in MRLR ORF	81
3.3	ERY dependent translation arrest in mutants of the MRLR sequence	82
3.4	ERY-mediated translation arrest is supported by the MKXXK sequence regardless of the identity of the codon 3 of the ORF	83
3.5	Translation arrest triggered by diverse macrolides is similarly affected by alanine mutations of the MRLR sequence	84
3.6	Arg and Lys are poor acceptors of the MRL-peptide in the stalled ribosome	88
3.7	Reactivity of substrate analogs reveals the charge of the amino acid side chain as the predominant factor of slow peptide bond formation	90
3.8	Reaction of model A-site substrates with the MRL peptide in the absence of ERY	91
3.9	Arg- and Lys- substrates are good acceptors of the non-stalling MAL- peptide in spite of the presence of ERY	93
3.10	Reaction of MAL peptide with model A-site substrates in the absence of ERY	94
3.11	Drug dependent translation arrest is not efficient when the PTC donor and acceptor substrates are negatively charged	96

## **LIST OF FIGURES (continued)**

4.1	Translation is not implicitly arrested at ‘RLR’ always in the presence of ERY	110
4.2	Changing the amino acid sequence of the N-terminal segment of ErmDL abrogates translation arrest	115
4.3	Ala substitutions of the N-terminal amino acids of ErmDL do not significantly affect ERY-dependent translation arrest at the RLR motif	116
4.4	Integrity of the N-terminal segment of ErmDL is required for efficient antibiotic dependent translation arrest	117
4.5	ERY remains bound to ribosomes that do not get arrested at ‘RLR’ while translating the nonstalling peptide	120
4.6	Antibiotic-mediated late translation arrest at internal ‘RLR’ sequences is also context specific	122
4.7	The N-terminal segment of ErmDL can support translation arrest even when its arrest motif is altered	124
4.8	Altering the arrest sequence abolishes ribosome stalling when there is no preceding n-terminal sequence	125
4.9	The ‘RLR’ arrest motif is more important for antibiotic mediated late translation arrest	126
4.10	Cartoon representation of the effect of N-terminal sequence of the peptide on the C-terminal arrest motif in the exit tunnel of the antibiotic bound ribosome	129

## LIST OF TABLES

<u>Table</u>		<u>Page</u>
2.1	Primers used in this study	34
2.2	Putative RLR leader peptides of the macrolide resistance genes	36
3.1	Primers used in this study	73
3.2	Peptidyl transfer reaction with model A site substrates	86
4.1	Primers used in this study	111

## LIST OF ABBREVIATIONS

PTC	Peptidyl transferase center
rRNA	Ribosomal RNA
NPET	Nascent peptide exit tunnel
ORF	Open reading frame
uORF	Upstream open reading frame
RNA	Ribonucleic acid
tRNA	Transfer RNA
mRNA	Messenger RNA
Erm	Erythromycin resistance methyltransferase
PCR	Polymerase chain reaction
C3	Carbon 3
C5	Carbon 5
cDNA	Complementary deoxyribonucleic acid
DNA	Deoxyribonucleic acid
ERY	Erythromycin
TEL	Telithromycin
SOL	Solithromycin
AZI	Azithromycin
SDS	Sodium dodecyl sulfate
SDS-PAGE	Sodium dodecyl sulfate-polyacrylamide gel electrophoresis
PDB	Protein data bank

## **AUTHOR CONTRIBUTIONS**

### **Chapter 1**

The bioinformatic analysis of the Erm leader peptides was contributed by Gemma Catherine Atkinson, Age Brauer and Mairo Remm in collaboration with the laboratory of Prof. Tanel Tenson at Institute of Technology, University of Tartu, 50411 Tartu, Estonia

The MD simulations of the empty and drug bound ribosomes was done by Bo Liu and Wei Han in collaboration with the laboratory of Prof. Klaus Schulten at Beckman Institute and Center for Biophysics and Computational Biology, University of Illinois at Urbana-Champaign, Urbana, IL 61801

### **Chapter 2**

The model A site substrates used in this part of the study was synthesized by Lukas rigger and Sandro Neuner in collaboration with the laboratory of Prof. Ronald Micura at Institute of Organic Chemistry and Center for Molecular Biosciences (CMBI) Leopold-Franzens University, Innrain 80-82, 6020 Innsbruck (Austria)

## SUMMARY

Nascent peptide-dependent programmed translation arrest serves as an important mode of gene control. Ribosome stalling at regulatory open reading frames (ORFs) has been implicated in controlling expression of genes involved in protein secretion (*secM* and *mifM*), amino acid metabolism (*tnaC*), antibiotic resistance (*erm* genes), among others. Programmed translation arrest is tuned by cellular cues. In many cases, stalling occurs in response to presence of small molecules, such as amino acids, polyamines, or antibiotics. Among the most medically important genes whose expression is regulated through nascent peptide-and cofactor-dependent translation arrest are those involved in conferring resistance to antibiotics that target the ribosome.

Macrolide antibiotics are important drugs used to treat serious bacterial infections. They bind in the exit tunnel of the ribosome. The mechanism to induce macrolide resistance genes includes nascent peptide-and drug-dependent stalling of the ribosome at their upstream regulatory ORFs. The plausible models for antibiotic-mediated translation arrest, which stemmed from the studies with several regulatory peptides, implicated that direct interactions between the nascent chain and the cofactor molecule in the ribosomal exit tunnel were the necessary pre-requisite for stalling. For this mechanism to operate, a key element is the juxtaposition of the peptide alongside the antibiotic molecule bound in the tunnel. However, we discovered that a nascent peptide as short as three amino acids ('MRL'), that can barely reach the site where the antibiotic is bound, can promote ribosome arrest. By exploring the unique properties of our minimalistic stalling system, we found that the binding of macrolide antibiotics to the exit tunnel of the ribosome

## **SUMMARY (continued)**

allosterically change the conformation of the peptidyl transferase catalytic center. These alterations may predispose the ribosome for stalling polymerization of specific sequences. We demonstrate that macrolide bound ribosomes are unable to synthesize peptides containing the 'Arg/Lys-X-Arg/Lys (R/K-X-R/K, where X corresponds to any amino acid) sequence. The presence of the drug in the exit tunnel prevents peptide bond formation between a M-R/K-X peptidyl donor and a R/K aminoacyl acceptor. By genetically and biochemically manipulating the nature of the donor and acceptor substrates, we found that the positive charge in both, the amino acid in the penultimate position of the peptide and the incoming amino acid, is the major factor that makes the sequence R/K-X-R/K arduous for the drug bound ribosome. We also found that the size of the amino acid side chains in the critical position of the motif is an additional obstacle that makes peptide bond formation less efficient.

Examination of ribosome profiling data obtained from cells treated with macrolides revealed that while the R/K-X-R/K sequence is one of the major motifs for macrolide-dependent translation arrest, in several instances continuation of translation persists. This observation made it evident that besides the presence of the arrest sequence, other elements of the peptide being elongated could contribute to stalling the drug-bound ribosome. Using the regulatory peptide ErmDL, that contains the 'R/K-X-R/K' motif, we demonstrated that the nature of the amino acid sequence preceding the problematic motif determines whether drug bound ribosomes get arrested or continue translation upon reaching this sequence.

### **SUMMARY (continued)**

In conclusion, our studies expand the understanding of the mechanism of nascent peptide- and small molecule- mediated translation arrest. In addition to gaining novel insights into the mode of action of macrolide antibiotics, this work has extended our understanding of fundamental properties of the ribosome. Further, our findings may contribute to develop better antibiotics and avoid resistance.

## 1. Introduction

### 1.1 Ribosome: the protein synthesis factory

The information encoded in the messenger RNA is translated into proteins by the ribosome. The ribosome is the largest ribonucleoprotein complex in the cell. It is composed of two subunits. In bacteria, the small subunit, 30S, is built of ~ 1500 nt-long 16S rRNA and 21 proteins. The large subunit, 50S, contains a ~ 3000 nt-long 23S rRNA, 120 nt-long 5S rRNA and 36 proteins. There is a clear division of functions between the two subunits. The 30S subunit decodes the genetic information written as a sequence of mRNA codons. The 50S subunit is in charge of catalyzing formation of peptide bonds between the amino acids determined by the mRNA sequence (reviewed in (Ramakrishnan, 2002 and Schmeing et al., 2009); Ban et al., 2000) (Figure 1.1). The adaptor tRNA molecules interact with the three ribosomal sites, A, P and E, contributing to decode the mRNA message and transfer the appropriate amino acid into the growing polypeptide. The assembly of the protein chain takes place at the peptidyl transferase center (PTC) of the large subunit, where the peptidyl moiety of the peptidyl-tRNA (p-tRNA) in the P-site is transferred into the amino acid residue of the aminoacyl-tRNA (aa-tRNA) in the A-site, forming a peptide bond. In simplistic terms, the peptidyl transfer reaction involves aminolysis of the ester bond of the p-tRNA by a nucleophilic attack of the  $\alpha$ -amino group of the aa-tRNA. Although, mechanistic details of the chemical catalysis of peptidyl transferase reaction (Polikanov et al., 2014; reviewed in Rodnina, 2011) is a debate in the field, in general, the ribosome accelerates this reaction over  $10^7$

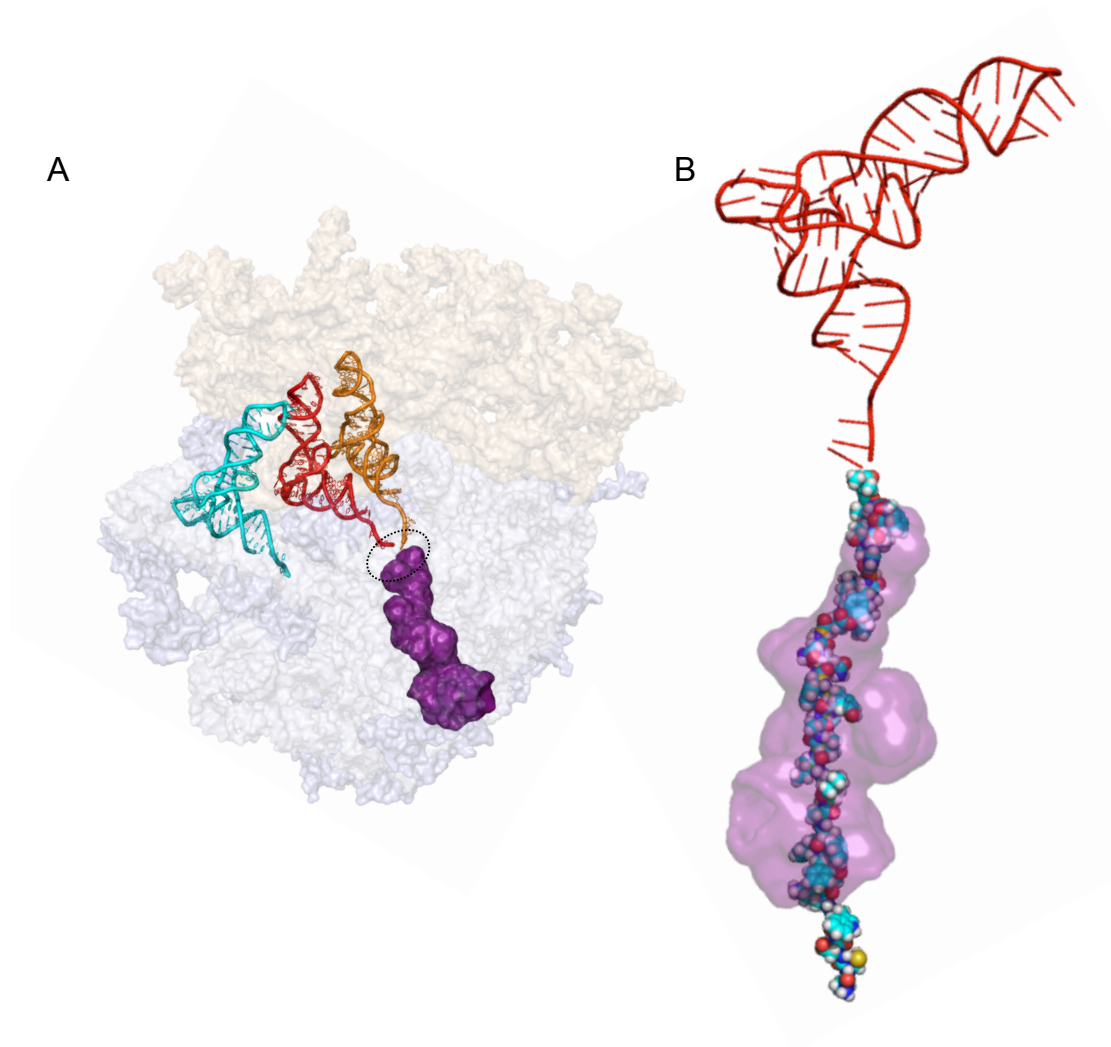


**Figure 1.1. The ribosome and its exit tunnel.** (A) The bacterial ribosome with tRNAs in the A- (orange), P- (red) and E- (cyan) sites. The 30S subunit is light yellow and the 50S is in grey. The peptidyl transferase center (PTC) is circled and the nascent peptide exit tunnel (NPET) is highlighted in purple. (B) The contour of NPET containing a nascent peptide esterified to the P site tRNA.

fold compared to the rate of reaction between substrates in solution (Sievers et al., 2004), by orienting the catalytic substrates in a conformation that is conducive for peptide bond formation.

The synthesized peptide leaves the ribosome through a narrow passage called the nascent peptide exit tunnel (NPET) (Figure 1.1) (Milligan and Unwin, 1986; Yonath et al., 1987; Frank et al., 1995). The NPET is approximately 10-20 Å wide and 100 Å long. It starts at the PTC, traverses the body of the large ribosomal subunit, and opens on the solvent side (Jenni and Ban, 2003; Voss et al., 2006). Its walls are predominantly composed of 23S rRNA nucleotides, although protrusions of proteins L4 and L22 are exposed in the lumen of the NPET ca. 30 Å away from the PTC, and an arm of protein L23 extends near the exit. In addition to serving as a passage for the elongating peptides (which, as we will describe in the work presented here, is a highly regulated process), the NPET facilitates folding, processing and targeting of newly synthesized proteins (Zhang et al., 2009; Nilsson et al., 2015; reviewed in Kramer et al., 2009), cofactor recruitment, and degradation of misfolded proteins (reviewed in Pechmann et al., 2013). The three chapters of this dissertation illustrate how nascent peptides (NPs) and small molecules hosted in the NPET cooperate in translation regulation.

## **1.2 Ribosome stalling and regulation of gene expression**

Due to the intrinsic ability of the ribosome to synthesize a broad spectrum of protein sequences, it had been assumed that the role of the exit tunnel was merely to serve as a passive conduit for the peptides assembled in the PTC. However, it is now well

established that the ribosome is not indifferent towards the proteins it makes. The synthesized polypeptides apparently undergo constant surveillance by the NPET, which senses the composition of the elongating chain and causes the ribosome to appropriately tune its catalytic functions. In extreme cases, specific peptide sequences bring the ribosome to a complete translation halt. This phenomenon, called programmed ribosome stalling, plays a crucial role in the regulation of a variety of cellular genes, whose functions range from protein secretion, to amino acid metabolism, to antibiotic resistance, and many others (reviewed in Ito and Chiba, 2013). Thus, the events that take place between the ribosome and the nascent chain in the NPET are highly significant for cell physiology, survival and proliferation.

Programmed translation arrest mediated by the NPs encoded in regulatory ORFs usually regulates the expression of the downstream genes in both bacteria and eukaryotes (reviewed in Ito and Chiba et al., 2013). The well characterized examples of NP-mediated translation arrest in bacteria take place at: i) the *secM* ORF that is involved in controlling the expression of the *secA* gene by monitoring protein secretion (Nakatogawa and Ito, 2002; Oliver et al., 1998), ii) the *mifM* ORF that regulates expression of the protein YidC2 involved in membrane protein insertion and folding (Chiba and Ito, 2012; Chiba et al., 2009), iii) the *tnaC* ORF, which regulates expression of genes involved in tryptophan catabolism (Gollnick and Yanofsky, 1990; Gong and Yanofsky, 2003), and iv) the leader ORFs of the erythromycin resistance genes, including the *erm* genes encoding Erm rRNA methyltransferases. This latter class is of particular medical interest because the *erm* genes are responsible for resistance to clinically important antibiotics such as

macrolides, ketolides, lincosamides and streptogramin B (reviewed in Ramu et al., 2009 and Subramanian et al., 2012).

There are numerous ways by which NP-mediated ribosome stalling leads to activation of gene expression. For example, in one of the first characterized examples of this class, the ribosome that stalls at the *tnaC* ORF when the concentration of L-tryptophan in the cell is high, occludes the rho-dependent transcription termination site, allowing continuation of transcription of the *tnaA* and *tnaB* genes and activation of the catabolic operon (Yanofsky, 1981; Gong and Yanofsky, 2002; Cruz-Vera and Yanofsky, 2008). In fungal systems, ribosomes respond to high concentrations of arginine by halting at the arginine attenuator peptide (AAP) uORF, disrupting the ribosome scanning required for initiation of the downstream genes involved in arginine biosynthesis (Luo and Sachs, 1996). Also in eukaryotic systems, including mammals and fungi, ribosomes pause at the *oaz1* ORF and prevent ribosomal frameshifting required for regulation of polyamine biosynthesis (Kurian et al., 2011). Ribosomes stopped in the *cgs1* ORF of *Arabidopsis* lead to endonucleolytic cleavage of mRNA resulting in regulation of methionine biosynthesis genes (Onouchi, 2005). However, the most common mode of gene activation by NP-mediated ribosome stalling is translation attenuation. In bacteria, in the non-induced conditions, the expression of the regulated gene is repressed due sequestration of its Shine-Dalgarno (SD) region in mRNA secondary structure. The gene is activated when ribosomes, stalled under specific conditions at the regulatory ORF, disrupt the secondary structure of the mRNA intergenic region. The conformational change of the mRNA releases the previously sequestered ribosome-binding site, leading to activation of translation of the downstream cistron. Such mechanism operates during

activation of the *E. coli secA* gene regulated by arrest at the *secM* ORF (Nakatogawa and Ito, 2002; Oliver et al., 1998). A similar mechanism is also responsible for the induction of the *erm* resistance genes in antibiotic producers and in clinical pathogens (Horinouchi and Weisblum, 1980; Narayanan and Dubnau, 1985; Almutairi et al, 2015). The central question in all these scenarios is what causes the ribosomes to halt translation of specific nascent peptides?

### **1.3 Nascent peptide and small molecule mediated regulation of translation**

The nature of the nascent peptide is a prime component of the programmed translation arrest. The studied regulatory NPs are characterized by the presence of specific sequences of amino acids, known as the ‘arrest sequence’ or the ‘stalling motif’, which are recognized by the ribosome as signals for halting translation (Figure 1.2). However, the mere placement of the arrest sequence in the NPET is often not sufficient for stalling, which occurs only when a specific environmental cue is received by the ribosome. The proper cue often comes in the form of a small molecule that serves as the cofactor for NP-mediated ribosome stalling. Hence, NP controlled programmed translation arrest can be classified into two distinct categories based on the cofactor requirements. For the intrinsic stalling, the presence of the proper NP sequence (for example, SecM, MifM) in the NPET is sufficient for arresting translation. In these cases, the arrest is relieved by additional factors, e.g. active secretion of the nascent regulatory peptide (Nakatogawa and Ito, 2002; Oliver et al., 1998, Chiba and Ito, 2012; Chiba et al., 2009.). The inducible systems rely on the presence of small molecular weight cofactors,

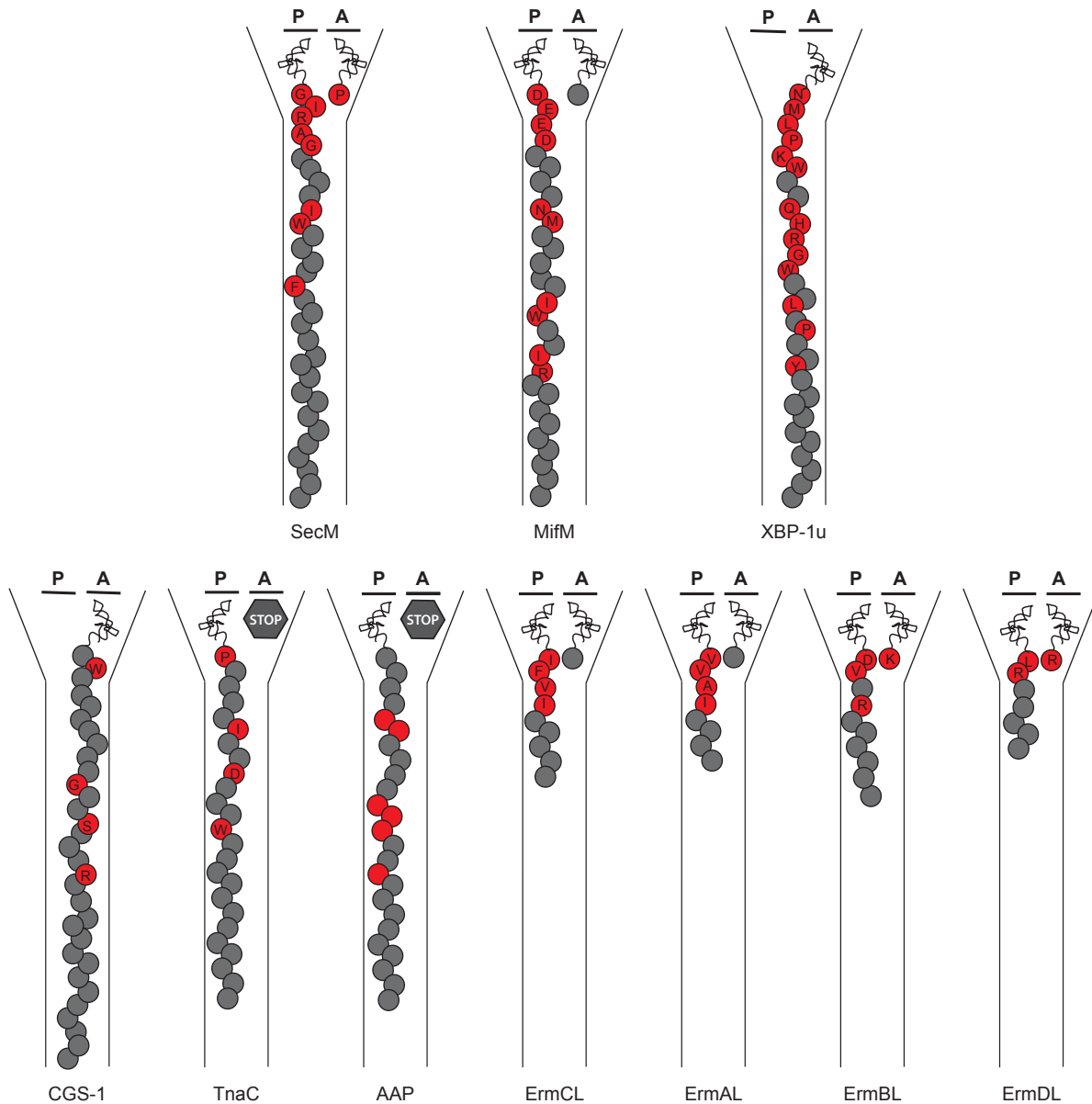


**Figure 1.2. Examples of regulatory nascent peptides and their arrest sequences.** (Top) Stalling NPs of the intrinsic class and (Bottom) peptides requiring cofactors for inducing translation arrest. The amino acid residues whose identities are critical for stalling are represented by red circles. The PTC P- and the A-sites are indicated.

such as an antibiotic (e.g. macrolides in the case of the Erm leader peptides) or an amino acid (tryptophan for TnaC or arginine for AAP).

Elucidation of the mechanistic details of ribosome stalling has been limited partly by the complexity of the available systems, because in most cases, the stalling nascent peptides are fairly long, and, on the other hand, by the lack of knowledge of the ribosomal binding site of the small cofactors. An important advantage of studying programmed ribosome stalling that relies on ribosomal antibiotics is that the binding site of these small molecule cofactors in the NPET is well characterized, both biochemically (reviewed in Gaynor and Mankin, 2003) and structurally (Tu et al., 2005; Bulkley et al., 2010; Dunkle et al., 2010). This understanding greatly facilitates the elucidation of the molecular details of ribosome stalling induced by the coordinated action of nascent peptides and small molecules.

#### **1.4 Antibiotic- and nascent peptide- dependent ribosome stalling and inducible expression of resistance genes**

Among the best-studied examples of NP-mediated programmed ribosome stalling are those involving antibiotics as stalling cofactors. In particular, the antibiotics that trigger translation arrest of the Erm leader peptides (briefly described in section 1.2) belong to the macrolides family. Hence, prior to discussing how the concerted action of NP and antibiotics lead to activation of antibiotic resistance genes, we will summarize few structural and functional aspects pertaining to the macrolide antibiotics.

The prototype of the macrolide antibiotic class, erythromycin (ERY), contains a 14-membered-macrolactone ring appended by two sugars, cladinose linked at position C3 of the macrolactone ring, and desosamine at position C5. In the drugs of the newest class, called ketolides, e.g. solithromycin (SOL) or telithromycin (TEL), C3 cladinose is replaced with a keto group. In addition, ketolides contain C11, C12 cyclic carbamate, and an extended alkyl-aryl side chain (Figure 1.3A). All macrolide antibiotics bind to the same site of the ribosomal NPET at a distance of ca. 8Å away from the peptidyl transferase center (PTC) (Tu et al., 2005, Bulkley et al., 2010; Dunkle et al., 2010)(Figure 1.3B). The macrolactone ring of macrolides makes hydrophobic interactions with 23S rRNA residues A2057, U2611, and A2058 (*E. coli* numbering) in the exit tunnel. Desosamine sugar extends into the cleft between residues A2058 and A2059, forming interactions that are absolutely crucial for the high-affinity binding of these drugs to the ribosome (Bulkley et al., 2010; Dunkle et al., 2010). The Erm resistance enzymes (erythromycin resistance rRNA methyltransferases), whose expression often depends on the macrolide-mediated translation arrest (as we briefly mentioned above), specifically methylate residue A2058. The modification of this sole residue is sufficient to hinder the binding of macrolides to the ribosome (Vester and Garrett, 1987; Weisblum, 1995).

When macrolide antibiotics bind in the NPET, they partially obstruct it, thereby complicating the passage of the NPs through the ribosome (Figure 1.3B). The narrowing of the tunnel caused by the presence of the antibiotic leads, in general, to inhibition of protein synthesis during the early rounds of translation. When the NP grows to the size of 5-8 amino acids, it reaches the site where the antibiotic is bound and at this point, its

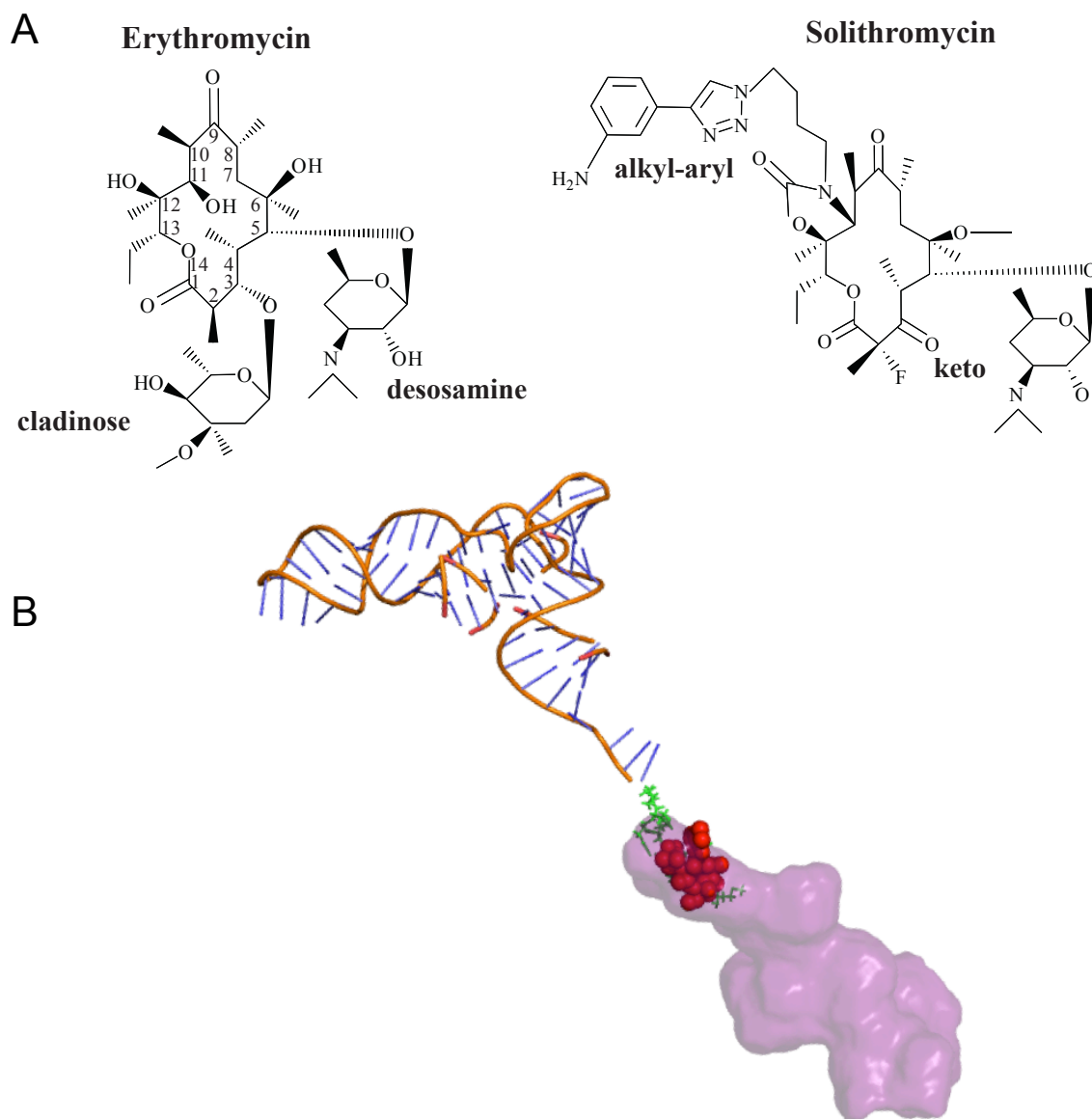


**Figure 1.3. Structure of macrolide antibiotics and their binding site in the ribosomal exit tunnel. (A)** The prototype macrolide, ERY, and the newest generation ketolide SOL. Specific chemical features of the antibiotics are indicated. **(B)** ERY bound in the exit tunnel. A short nascent peptide (in green) linked to tRNA is shown for reference.

passage through the obstructed tunnel could be hindered, often causing premature drop off of the peptidyl-tRNA (Vazquez, 1975; Menninger, 1995; Tenson et al., 2003). Importantly, however, experimental evidence from our laboratory and other groups, has shown that peptidyl-tRNA drop off is not the only mode of macrolide action. Depending on the amino acid sequence of the nascent chain, certain peptides are able to bypass the antibiotic bound in the NPET. Translation of such proteins may continue to its completion (Starosta et al., 2010; Kannan et al., 2012). However, some peptides could trigger the formation of ribosome-antibiotic-nascent peptide stalled complexes (reviewed in Vazquez-Laslop and Mankin, 2014). The fate of translation in the presence of macrolide antibiotics is thus determined by the interplay between the antibiotic in the NPET, the peptide being synthesized, and the ribosome.

Antibiotic- and NP- mediated ribosome stalling is one of the favorite mechanisms exploited by antibiotic producing bacteria and clinical pathogenic strains to regulate the expression of their resistance genes. Ribosomes bound by the antibiotic are arrested during translation of leader peptides, such as ErmCL, ErmAL, ErmBL, or ErmDL, encoded in the short regulatory uORFs that precede *erm* resistance genes (Figure 1.4). The ribosome stalled at a specific codon of the regulatory ORF, triggers isomerization of the mRNA secondary structure, exposing the previously occluded initiation region of the downstream ORF, thus allowing expression of the resistance cistron (Horinouchi and Weisblum, 1980; Narayanan and Dubnau, 1985; reviewed in Ramu et al., 2009; Subramanian et al., 2012) (Figure 1.5). For a long time it was unknown why bacteria favors *erm* genes to be inducible, instead of shielding their ribosomes from antibiotic

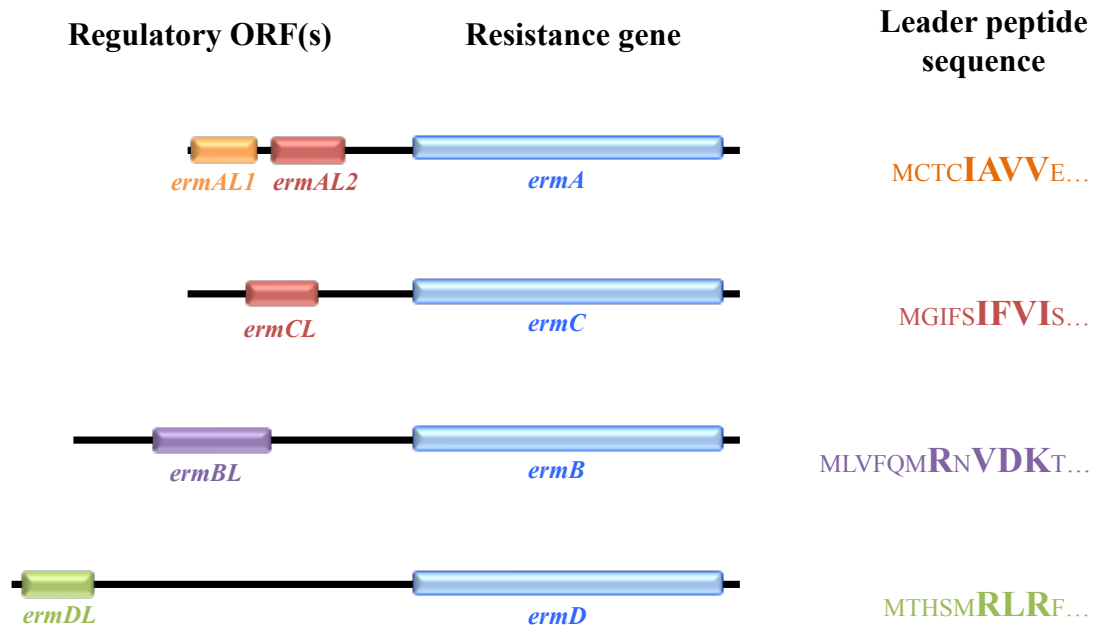


**Figure 1.4. The regulatory uORFs and the encoded leader peptides of representative macrolide resistance genes.** Schematic representation of several *erm* resistance operons. Expression of the resistance gene (light blue) is regulated by programmed translation arrest at the regulatory uORFs (colors). The leader peptide sequence encoded in the uORFs is shown and the amino acid sequences critical for the arrest are highlighted in bold.

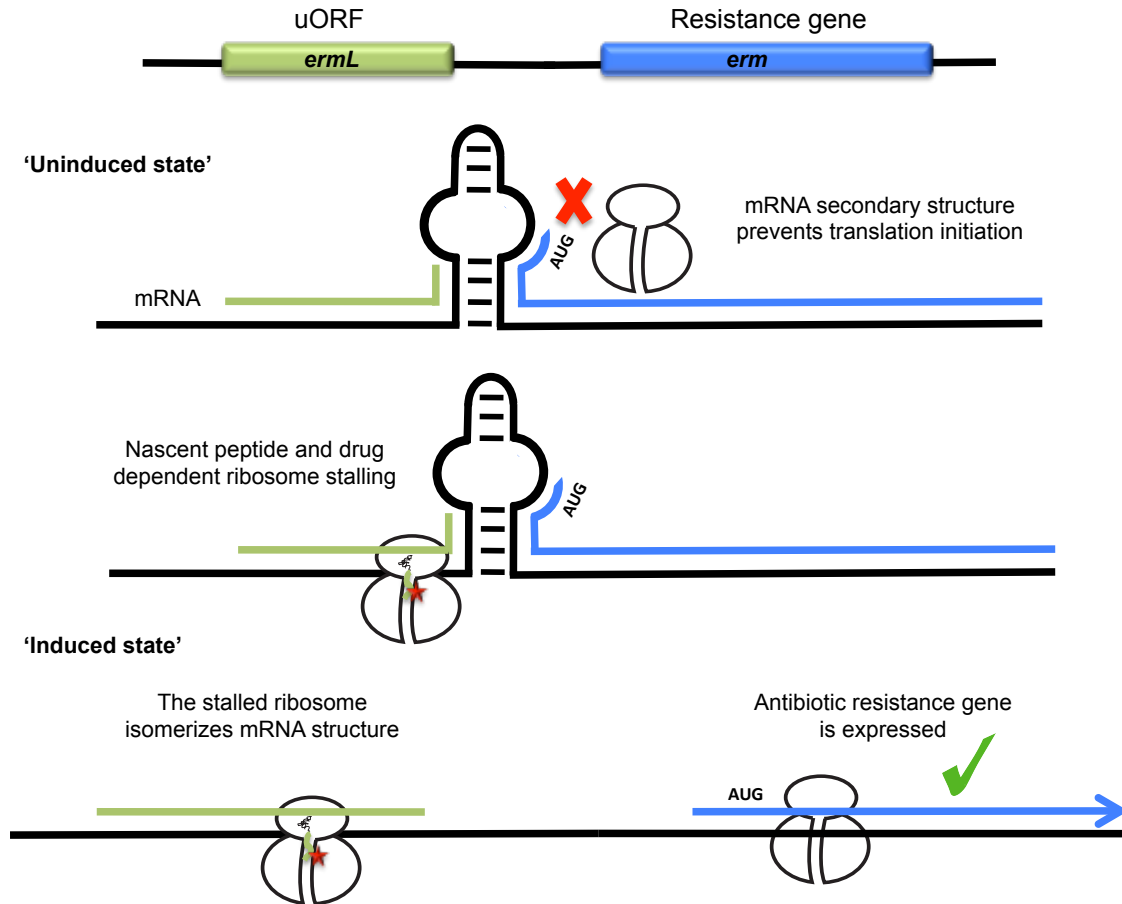


**Figure 1.5. Inducible expression of antibiotic resistance by programmed translation arrest.** A generalized scheme for induction of antibiotic resistance, where antibiotic dependent ribosome stalling at the uORF (green) causes alteration in the mRNA structure allowing the downstream resistance gene (blue) to be translated.

binding by having the NPET residue A2058 constitutively methylated. The answer came from our work, where we showed that constitutive expression of ErmC comes at a significant cost of fitness, because the modification of this adenine alters translation of some proteins leading to disbalance of the cellular proteome (Gupta et al., 2013). (I participated in this project while performing my rotation in the Mankin lab and co-authored the publication. For this reason the article Gupta et al., 2013 is included in Appendix A). Therefore, bacteria prefer to express the resistance genes only when they are challenged by the presence of the antibiotic. However, the molecular details that determine the formation of the stalled ribosomal complexes, which depends on the nature of the regulatory NP and the presence of the antibiotic, are far from being understood. Therefore, the general goal of my research was to advance the understanding of how the coordinated action of the antibiotic and the nascent peptide affects the ribosome and induce the stalled state.

One of the main questions about the mechanism of translation arrest is why the sequence of the nascent peptide affects formation of the stalled ribosomal complex. Previous studies showed that the sequences of the leader peptides encoded in the regulatory regions of antibiotic resistance genes are highly heterogeneous (Gryczan et al., 1980; Horinouchi and Weisblum, 1980; Ramu et al., 2009; Subramanian et al., 2012). Analysis of the sequences of the regulatory uORFs of resistance genes in a wide range of bacterial species, led to the classification of the leader peptides into several major categories. This classification was based on the conservation of the arrest sequences (i.e., the segment of the leader peptide sequence critical to support the halting of translation)

namely, 'IFVI', 'IAVV', 'RLR', and one more category that included miscellaneous peptides, where preservation of the arrest sequence was not clearly defined (reviewed in Ramu et al., 2009 and Subramanian et al., 2012). Whether the different leader peptides, along with the antibiotic cofactor, use unique or diverse strategies to arrest translation conducting to expression of resistance remained unknown.

The first model for antibiotic dependent formation of stalled ribosomal complexes emerged from the studies based on the 8 amino acid long ErmAL (MCTSI**IAVV**) and the 9 amino acid long ErmCL (MGIFS**IFVI**) arrest peptides (Vazquez-Laslop et al., 2008, 2010 and 2011; Ramu et al., 2011). This model proposed that both, the antibiotic cofactor and the NP generate the arrest signal by establishing unique interactions in the exit tunnel of the ribosome. In response to this composite 'antibiotic-NP' signal the functions of the ribosomal catalytic center are halted (Vazquez-Laslop et al., 2008, 2010 and 2011; Ramu et al., 2011; Arenz et al., 2014a; Arenz et al., 2014b). A crucial aspect of this model is that the NP has to be long enough to be placed alongside the antibiotic molecule in the NPET in order to establish the arrest-promoting interactions. Indeed, the stalling nascent chains of ErmAL and ErmCL (8 and 9 residues long, respectively) are long enough to reach and even bypass the site in the NPET where the antibiotic is bound (Figure 1.6). Biochemical and structural studies with IFVI (ErmCL) and IAVV (ErmAL1) leader peptides supported the role of specific amino acid residues of the nascent chain in ribosome stalling and the importance of the placement of the stalling sequence within the NP (Vazquez-Laslop et al., 2008; Ramu et al., 2011; Arenz et al., 2014a). Consistent with this view, removal of one or several N-terminal amino acids of the ErmCL peptide

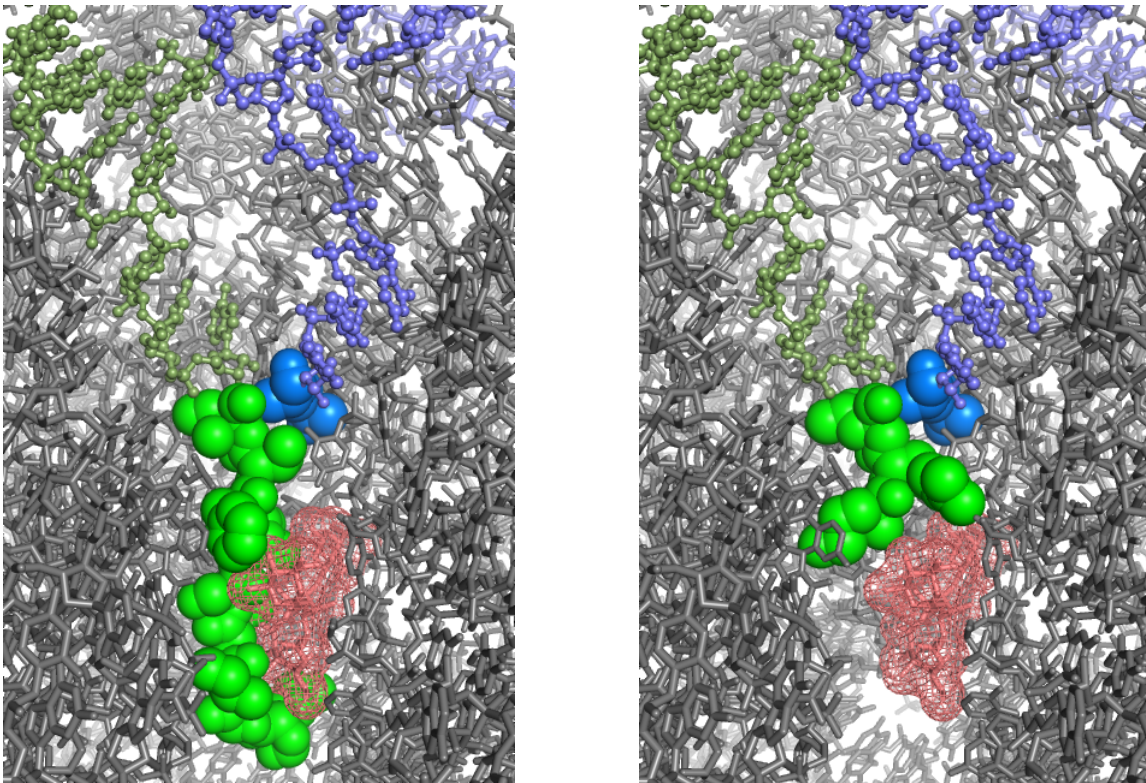


**Figure 1.6. Models of leader peptides in the drug bound exit tunnel.** ErmCL peptide (MGIFSIFVI) (left) and MRL peptide (right) in the exit tunnel of drug bound ribosome. Peptides attached to p-tRNA are shown in green, aa-tRNA is in blue, ERY is in salmon and 23S rRNA nucleotides lining the exit tunnel are in gray. (Figure courtesy of A. Mankin).

negatively affects formation of the stalled complex (Vazquez-Laslop et al., 2008; Sothiselvam et al., 2014). Furthermore, position of the IAVV and IFVI motifs among the peptides of this class is highly conserved and the identity of the N-terminal amino acids is fairly invariant (Ramu et al., 2009, Subramanian et al., 2012). In stark contrast, analysis of the N-terminal sequences of the leader peptides of the RLR class showed that the position of the conserved RLR motif is remarkably heterogeneous and that the N-terminal sequences do not show any conservation (Ramu et al., 2009, Sothiselvam et al., 2014). The difference in the length and sequences of the regulatory peptides of the RLR class made us wonder whether these leader peptides exploit the ‘antibiotic-NP’ composite mechanism proposed for the IAVV and IFVI stalling peptides. Therefore, we initiated the investigation of antibiotic dependent arrest mediated by RLR peptides, because these studies could reveal novel aspects of the mechanisms of formation of stalled ribosomal complexes and could even unveil entirely different strategies for the onset of translation arrest.

#### **1.4.1 Macrolide antibiotics allosterically predispose the ribosome for translation arrest**

Because the length and composition of the amino acid sequences preceding the conserved motif in the leader peptides of the RLR class is heterogeneous (Ramu et al., 2009), we decided to investigate whether the N-terminal segment of these peptides was important for antibiotic-mediated arrest. For these experiments, we used ErmDL, the leader peptide controlling expression of the *ermD* methyltransferase gene (Kwon et al.,

2006; Hue, 1992; Vazquez-Laslop et al., 2010) (Figure. 1.4). Intriguingly, and in stark contrast with the ErmCL stalled complex, we found that progressive shortening of the ErmDL from the original MTHSMRLR down to the mere MRLR sequence did not hinder its ability to support macrolide-mediated translation arrest (Sothiselvam et al., 2014). We further demonstrated that the complex with the minimal ErmDL carries the short MRL nascent chain (because arginine encoded in the 4<sup>th</sup> codon of the mini-ORF is not incorporated into the nascent peptide). Such a short peptide (only three amino acids long) can barely reach the binding site of the antibiotic in the exit tunnel (Figure 1.6). Therefore, this result revealed that the mechanism of arrest proposed for the longer ErmAL and ErmCL peptides, which relied on placement of the nascent chain along the antibiotic molecule in the NPET, could not possibly be applied for the minimal ErmDL. The ability of a peptide as short as MRL to trigger drug dependent translation arrest, indicated that stalling of the ribosome could be promoted by a fundamentally different mechanism. Our subsequent experiments highlighted the existence of an allosteric link between the drug-binding site in the exit tunnel and the peptidyl transferase center of the ribosome. The model that emerged from this work illuminated a new mode of drug-dependent translation arrest, which does not need direct interactions between the peptide and the antibiotic in the exit tunnel. An interesting implication of this model is that the antibiotic, upon binding to the NPET, predisposes the ribosome to functionally respond to specific nascent peptides.

The study of translation arrest promoted by the MRL peptide lacking extensive interactions with the antibiotic molecule in the NPET are described in our published work (Sothiselvam et al., 2014) and included in Chapter 2 of this thesis.

### **1.4.2 Ribosome can discriminate its catalytic substrates based on their charge and size**

Ribosome profiling analysis, that reports on the distribution of translating ribosomes along mRNAs (Ingolia et al., 2009), showed that one of the most problematic sequences for the macrolide bound ribosomes is the ‘R/K-X-R/K’ motif (Kannan et al., 2014; Davis et al., 2014). Since, as we already described, the R/K-X-R/K motif is widely prevalent among the leader peptides encoded in the regulatory ORFs of the resistance genes (Ramu et al., 2009; Subramanian et al., 2012; Sothiselvam et al., 2014; Almutairi et al., 2015), we asked why this particular sequence is so difficult for the antibiotic-bound ribosome to polymerize. The salient features of arginine and lysine are that the side chains of these two residues are positively charged and are the longest among the 20 natural amino acids. Conceivably, the charge, the size, or both of these characteristics of the side chain could constitute the main obstacle for the ribosome to elongate past the R/K-X-R/K motif in the presence of macrolides. Therefore, the aim of the second project was to unravel the contribution of the charge and size of the amino acid side chains to antibiotic-dependent ribosome stalling at the model MRLR sequence. We carried an extensive mutational analysis to demonstrate that only Arg or Lys residues at the first and last positions of the motif are conducive to stalling. We then rationally selected and tested the acceptor capacity of model substrates carrying amino acids with specific variations in the size and charge of their side chains. (These substrates were synthesized by the group of our collaborator, Prof. Ronald Micura of the University of Innsbruck-Austria). We found that the positive charge of arginine and lysine in the A-site is the predominant

factor that makes them ‘bad’ acceptors of a nascent tripeptide, whose penultimate amino acid is also an arginine or a lysine. The size of the side chain was also a contributing factor but played only a secondary role. Unexpectedly, we found that the ribosome could only slowly catalyze the transfer of the MRL peptide to the positively charged acceptors even in the absence of the antibiotic. This result suggested that binding of a macrolides in the NPET exacerbates the problem of intrinsically difficult ribosomal substrates, making peptidyl transfer highly inefficient. Therefore, this work revealed not only important mechanistic aspects of antibiotic-dependent protein synthesis arrest, but also illuminated previously unknown properties of the ribosomal catalytic center.

This work has been prepared as a manuscript to be submitted to Molecular Cell and it constitutes Chapter 3 of this thesis.

### **1.4.3 Context specific translation arrest mediated by macrolide antibiotics**

A conclusion that could be drawn from our previous findings is that, a macrolide-bound ribosome would halt translation whenever it encounters the ‘R/K-X-R/K’ sequence. However, closer examination of the ribosome profiling data of cells treated with macrolides (Kannan et al., 2014) revealed that, in several instances, translation actively proceeded beyond the ‘R/K-X-R/K’ sequences. This simple observation made evident that, besides the presence of the arrest sequence, additional elements can modulate translation arrest. The work presented in Chapter 4 (also included in the form of a manuscript prepared for submission to Nucleic Acids Research), investigates the elements of the nascent peptide, specifically the nature of the amino acids that precede

the stalling motif, that determine whether translation elongation proceeds or halts when the ribosome with antibiotic encounters the R/K-X-R/K sequence. Using this time the full 7 amino acid long ErmDL stalling peptide as a model, we altered the residues 2 to 5 constituting its N-terminal segment (MTHSM) (Figure. 1.4), without altering the arrest domain, and analyzed the effects of these mutations on ribosome stalling at the RLR sequence. We found that mutating the wt ErmDL N- terminal sequence to MDTLN completely abrogated stalling at the RLR sequence. This result suggested that the N-terminal sequence of ErmDL preceding the true stalling motif has also been evolutionary selected to support programmed translation arrest. Furthermore, the wt MTHSM sequence was able to direct efficient stalling even when the conventional arrest sequence RLR was mutated, indicating that the N-terminal module of ErmDL has its independent stalling capacity. Altogether, these results highlighted that the arrest sequences are not the only determinants for antibiotic dependent ribosome stalling: the amino acid context of the nascent peptide preceding the arrest motif can greatly influence the fate of the protein synthesized by the drug-bound ribosome.

In summary, the work presented in this thesis expands our knowledge and provides new insights into antibiotic-controlled programmed translation arrest. Studying nascent peptides belonging to the R/K-X-R/K category allowed the elucidation of novel mechanisms of translation arrest and modes of action of ribosomal antibiotics. The newly gained understanding of the mechanism of inducible expression of resistance genes via antibiotic-dependent translation arrest illuminates fundamental yet poorly understood properties of the ribosome.

## 1.5 Cited Literature

Almutairi, M.M., Park, S.R., Rose, S., Hansen, D.A., Vazquez-Laslop, N., Douthwaite, S., Sherman, D.H., and Mankin, A.S. (2015). Resistance to ketolide antibiotics by coordinated expression of rRNA methyltransferases in a bacterial producer of natural ketolides. *Proceedings of the National Academy of Sciences of the United States of America* 112, 12956-12961.

Arenz, S., Meydan, S., Starosta, A.L., Berninghausen, O., Beckmann, R., Vazquez-Laslop, N., and Wilson, D.N. (2014a). Drug sensing by the ribosome induces translational arrest via active site perturbation. *Molecular cell* 56, 446-452.

Arenz, S., Ramu, H., Gupta, P., Berninghausen, O., Beckmann, R., Vazquez-Laslop, N., Mankin, A.S., and Wilson, D.N. (2014b). Molecular basis for erythromycin-dependent ribosome stalling during translation of the ErmBL leader peptide. *Nature communications* 5, 3501.

Bulkley, D., Innis, C.A., Blaha, G., and Steitz, T.A. (2010). Revisiting the structures of several antibiotics bound to the bacterial ribosome. *Proceedings of the National Academy of Sciences of the United States of America* 107, 17158-17163.

Chiba, S., and Ito, K. (2012). Multisite ribosomal stalling: a unique mode of regulatory nascent chain action revealed for MifM. *Molecular cell* 47, 863-872.

Chiba, S., Lamsa, A., and Pogliano, K. (2009). A ribosome-nascent chain sensor of membrane protein biogenesis in *Bacillus subtilis*. *The EMBO journal* 28, 3461-3475.

Cruz-Vera, L.R., and Yanofsky, C. (2008). Conserved residues Asp16 and Pro24 of TnaC-tRNA<sup>Pro</sup> participate in tryptophan induction of Tna operon expression. *Journal of bacteriology* 190, 4791-4797.

Davis, A.R., Gohara, D.W., and Yap, M.N. (2014). Sequence selectivity of macrolide-induced translational attenuation. *Proceedings of the National Academy of Sciences of the United States of America* 111, 15379-15384.

Dunkle, J.A., Xiong, L., Mankin, A.S., and Cate, J.H. (2010). Structures of the *Escherichia coli* ribosome with antibiotics bound near the peptidyl transferase center explain spectra of drug action. *Proceedings of the National Academy of Sciences of the United States of America* 107, 17152-17157.

Frank, J., Zhu, J., Penczek, P., Li, Y., Srivastava, S., Verschoor, A., Radermacher, M., Grassucci, R., Lata, R.K., and Agrawal, R.K. (1995). A model of protein synthesis based on cryo-electron microscopy of the *E. coli* ribosome. *Nature* 376, 441-444.

Gaynor, M., and Mankin, A.S. (2003). Macrolide antibiotics: binding site, mechanism of action, resistance. *Current topics in medicinal chemistry* 3, 949-961.

Gollnick, P., and Yanofsky, C. (1990). tRNA(Trp) translation of leader peptide codon 12 and other factors that regulate expression of the tryptophanase operon. *Journal of bacteriology* 172, 3100-3107.

Gong, F., and Yanofsky, C. (2003). A transcriptional pause synchronizes translation with transcription in the tryptophanase operon leader region. *Journal of bacteriology* 185, 6472-6476.

Gryczan, T.J., Grandi, G., Hahn, J., Grandi, R., and Dubnau, D. (1980). Conformational alteration of mRNA structure and the posttranscriptional regulation of erythromycin-induced drug resistance. *Nucleic acids research* 8, 6081-6097.

Gupta, P., Sothiselvam, S., Vazquez-Laslop, N., and Mankin, A.S. (2013). Deregulation of translation due to post-transcriptional modification of rRNA explains why erm genes are inducible. *Nature communications* 4, 1984.

Horinouchi, S., and Weisblum, B. (1980). Posttranscriptional modification of mRNA conformation: mechanism that regulates erythromycin-induced resistance. *Proceedings of the National Academy of Sciences of the United States of America* 77, 7079-7083.

Hue, K.K., and Bechhofer, D.H. (1992). Regulation of the macrolide-lincosamide-streptogramin B resistance gene ermD. *Journal of bacteriology* 174, 5860-5868.

Ito, K., and Chiba, S. (2013). Arrest peptides: cis-acting modulators of translation. *Annual review of biochemistry* 82, 171-202.

Jenni, S., and Ban, N. (2003). The chemistry of protein synthesis and voyage through the ribosomal tunnel. *Current opinion in structural biology* 13, 212-219.

Jenni, S., and Ban, N. (2003). The chemistry of protein synthesis and voyage through the ribosomal tunnel. *Current opinion in structural biology* 13, 212-219.

Kannan, K., Vazquez-Laslop, N., and Mankin, A.S. (2012). Selective protein synthesis by ribosomes with a drug-obstructed exit tunnel. *Cell* 151, 508-520.

Kannan, K., Kanabar, P., Schryer, D., Florin, T., Oh, E., Bahroos, N., Tenson, T., Weissman, J.S., and Mankin, A.S. (2014). The general mode of translation inhibition by macrolide antibiotics. *Proceedings of the National Academy of Sciences of the United States of America* 111, 15958-15963.

Kramer, G., Boehringer, D., Ban, N., and Bukau, B. (2009). The ribosome as a platform for co-translational processing, folding and targeting of newly synthesized proteins. *Nature structural & molecular biology* 16, 589-597.

Kurian, L., Palanimurugan, R., Godderz, D., and Dohmen, R.J. (2011). Polyamine sensing by nascent ornithine decarboxylase antizyme stimulates decoding of its mRNA. *Nature* 477, 490-494.

Kwon, A.R., Min, Y.H., Yoon, E.J., Kim, J.A., Shim, M.J., and Choi, E.C. (2006). ErmK leader peptide : amino acid sequence critical for induction by erythromycin. *Archives of pharmacal research* 29, 1154-1157.

Luo, Z., and Sachs, M.S. (1996). Role of an upstream open reading frame in mediating arginine-specific translational control in *Neurospora crassa*. *Journal of bacteriology* 178, 2172-2177.

Menninger, J.R. (1995). Mechanism of inhibition of protein synthesis by macrolide and lincosamide antibiotics. *Journal of basic and clinical physiology and pharmacology* 6, 229-250.

Milligan, R.A., and Unwin, P.N. (1986). Location of exit channel for nascent protein in 80S ribosome. *Nature* 319, 693-695.

Nakatogawa, H., and Ito, K. (2002). The ribosomal exit tunnel functions as a discriminating gate. *Cell* 108, 629-636.

Narayanan, C.S., and Dubnau, D. (1985). Evidence for the translational attenuation model: ribosome-binding studies and structural analysis with an in vitro run-off transcript of *ermC*. *Nucleic acids research* 13, 7307-7326.

Nilsson, O.B., Hedman, R., Marino, J., Wickles, S., Bischoff, L., Johansson, M., Muller-Lucks, A., Trovato, F., Puglisi, J.D., O'Brien, E.P., et al. (2015). Cotranslational Protein Folding inside the Ribosome Exit Tunnel. *Cell reports* 12, 1533-1540.

Nissen, P., Hansen, J., Ban, N., Moore, P.B., and Steitz, T.A. (2000). The structural basis of ribosome activity in peptide bond synthesis. *Science* 289, 920-930.

Oliver, D., Norman, J., and Sarker, S. (1998). Regulation of *Escherichia coli* *secA* by cellular protein secretion proficiency requires an intact gene X signal sequence and an active translocon. *Journal of bacteriology* 180, 5240-5242.

Onouchi, H., Nagami, Y., Haraguchi, Y., Nakamoto, M., Nishimura, Y., Sakurai, R., Nagao, N., Kawasaki, D., Kadokura, Y., and Naito, S. (2005). Nascent peptide-mediated translation elongation arrest coupled with mRNA degradation in the *CGS1* gene of *Arabidopsis*. *Genes & development* 19, 1799-1810.

Onouchi, H., Nagami, Y., Haraguchi, Y., Nakamoto, M., Nishimura, Y., Sakurai, R., Nagao, N., Kawasaki, D., Kadokura, Y., and Naito, S. (2005). Nascent peptide-mediated translation elongation arrest coupled with mRNA degradation in the *CGS1* gene of *Arabidopsis*. *Genes & development* 19, 1799-1810.

Pechmann, S., Willmund, F., and Frydman, J. (2013). The ribosome as a hub for protein quality control. *Molecular cell* 49, 411-421.

Polikanov, Y.S., Steitz, T.A., and Innis, C.A. (2014). A proton wire to couple aminoacyl-tRNA accommodation and peptide-bond formation on the ribosome. *Nature structural & molecular biology* 21, 787-793.

Ramakrishnan, V. (2002). Ribosome structure and the mechanism of translation. *Cell* 108, 557-572.

Ramu, H., Mankin, A., and Vazquez-Laslop, N. (2009). Programmed drug-dependent ribosome stalling. *Molecular microbiology* 71, 811-824.

Ramu, H., Vazquez-Laslop, N., Klepacki, D., Dai, Q., Piccirilli, J., Micura, R., and Mankin, A.S. (2011). Nascent peptide in the ribosome exit tunnel affects functional properties of the A-site of the peptidyl transferase center. *Molecular cell* 41, 321-330.

Rodnina, M.V. (2011). Mechanisms of decoding and peptide bond formation. *Ribosomes Structure Function and Dynamics* 1, 199-213.

Schmeing, T.M., and Ramakrishnan, V. (2009). What recent ribosome structures have revealed about the mechanism of translation. *Nature* 461, 1234-1242.

Sievers, A., Beringer, M., Rodnina, M.V., and Wolfenden, R. (2004). The ribosome as an entropy trap. *Proceedings of the National Academy of Sciences of the United States of America* 101, 7897-7901.

Sothiselvam, S., Liu, B., Han, W., Ramu, H., Klepacki, D., Atkinson, G.C., Brauer, A., Remm, M., Tenson, T., Schulten, K., et al. (2014). Macrolide antibiotics allosterically predispose the ribosome for translation arrest. *Proceedings of the National Academy of Sciences of the United States of America* 111, 9804-9809.

Starosta, A.L., Karpenko, V.V., Shishkina, A.V., Mikolajka, A., Sumbatyan, N.V., Schlunzen, F., Korshunova, G.A., Bogdanov, A.A., and Wilson, D.N. (2010). Interplay between the ribosomal tunnel, nascent chain, and macrolides influences drug inhibition. *Chemistry & biology* 17, 504-514.

Subramanian SL, Ramu H, Mankin AS. Inducible resistance to macrolide antibiotics. In: Dougherty TJ, Pucci, M. J. , editor. *Antibiotic Drug Discovery and Development*. New York, NY: Springer Publishing Company; 2011.

Tenson, T., Lovmar, M., and Ehrenberg, M. (2003). The mechanism of action of macrolides, lincosamides and streptogramin B reveals the nascent peptide exit path in the ribosome. *Journal of molecular biology* 330, 1005-1014.

Tu D, Blaha G, Moore PB, Steitz TA (2005) Structures of MLSBK antibiotics bound to mutated large ribosomal subunits provide a structural explanation for resistance. *Cell* 121(2), 257–270.

Vazquez D (1975) The macrolide antibiotics. *Antibiotics III. Mechanism of Action of Antimicrobial and Antitumor Agents*, eds Corcoran JW, Hahn FE (Springer, New York), 459–479.

Vazquez-Laslop, N., Klepacki, D., Mulhearn, D.C., Ramu, H., Krasnykh, O., Franzblau, S., and Mankin, A.S. (2011). Role of antibiotic ligand in nascent peptide-dependent ribosome stalling. *Proceedings of the National Academy of Sciences of the United States of America* 108, 10496-10501.

Vazquez-Laslop, N., Thum, C., and Mankin, A.S. (2008). Molecular mechanism of drug-dependent ribosome stalling. *Molecular cell* 30, 190-202.

Vázquez-Laslop N, Ramu H, Klepacki D, Kannan K, Mankin AS (2010) The key function of a conserved and modified rRNA residue in the ribosomal response to the nascent peptide. *EMBO J* 29(18):3108–3117.

Vázquez-Laslop N, Mankin AS (2014) Triggering peptide-dependent translation arrest by small molecules: ribosome stalling modulated by antibiotics. *Regulatory Nascent Polypeptides*, ed Ito K (Springer, New York).

Vester, B., and Garrett, R.A. (1987). A plasmid-coded and site-directed mutation in *Escherichia coli* 23S RNA that confers resistance to erythromycin: implications for the mechanism of action of erythromycin. *Biochimie* 69, 891-900.

Weisblum, B. (1995). Erythromycin resistance by ribosome modification. *Antimicrobial agents and chemotherapy* 39, 577-585.

Yanofsky, C. (1981). Attenuation in the control of expression of bacterial operons. *Nature* 289, 751-758.

Yonath, A., Leonard, K.R., and Wittmann, H.G. (1987). A tunnel in the large ribosomal subunit revealed by three-dimensional image reconstruction. *Science* 236, 813-816.

Zhang, G., Hubalewska, M., and Ignatova, Z. (2009). Transient ribosomal attenuation coordinates protein synthesis and co-translational folding. *Nature structural & molecular biology* 16, 274-280.

## **2. Macrolide antibiotics allosterically predispose the ribosome for translation arrest**

### **2.1 Introduction and rationale**

Expression of several bacterial and eukaryotic genes is controlled by nascent peptide-dependent programmed translation arrest. In the general scenario, ribosome stalling at an upstream regulatory ORF (uORF) triggers isomerization of the mRNA structure, leading to activation of expression of downstream cistron(s). Translation arrest ensues when a distinctive amino acid sequence (the “stalling domain”) of the growing chain assembled in the ribosomal peptidyl transferase center (PTC) is placed in the nascent peptide exit tunnel (NPET). Ribosome stalling may require additional signals, thereby making this gene control mechanism sensitive to the physiological state of the cell or to the chemical composition of the environment. Often the external signal is a small molecule whose binding to the ribosome renders translation responsive to specific nascent peptides (reviewed in (Vazquez-Laslop and Mankin, 2014, Ito and Chiba, 2013)). In most of the examined cases of cofactor and nascent peptide-dependent translation arrest, the binding site of the cofactor in the ribosome is unknown, which hampers understanding of the interplay among the cofactor, the nascent peptide, and the ribosome. The exception is the inducible antibiotic resistance, in which ribosome stalling and gene activation rely on binding of an antibiotic to a well-defined site in the ribosome.

Expression of macrolide resistance genes is triggered by drug-induced ribosome stalling at a defined codon of the uORF (reviewed in (Weisblum, 1995, Ramu et al. 2009, Subramanian et al., 2011)). Macrolides, from the prototype erythromycin (ERY) to the newest macrolide derivatives—ketolides, e.g., solithromycin (SOL)—bind in the NPET at a short distance from the PTC (Schlunzen et al., 2001, Tu et al., 2005, Dunkle et al.,

2010, Bulkley et al., 2010) (Figure 2.1A). When a nascent peptide grows to 4–7 amino acids, it reaches the site of antibiotic binding and has to negotiate the drug obstructed NPET aperture. Subsequent events depend on the properties of the nascent chain (Weisblum, 1995, Vazquez, 1975, Kannan et al., 2012). Although for many proteins the encounter of the peptide with the antibiotic results in peptidyl-tRNA drop-off, the N-termini of certain nascent peptides can bypass the antibiotic. Translation of some of such proteins can be arrested at specific sites within the gene, resulting in formation of a stable stalled complex (Kannan et al., 2012). Such translation arrest defines the role of macrolides as cofactors of programmed ribosome stalling (Weisblum, 1995, Vazquez, 1975, Kannan et al., 2012, Vazquez-Laslop et al., 2008).

The regulatory leader peptides of macrolide resistance genes have been classified by the structure of their known or presumed stalling domains (Ramu et al., 2009, Subramanian et al., 2011). Translation of ErmAL1 and ErmCL peptides is arrested after the ribosome has polymerized the 8-aa (ErmAL1) or 9-aa (ErmCL) long nascent chains that carry the C-terminal stalling domains Ile-Ala-Val-Val (IAVV) and Ile-Phe-Val-Ile (IFVI), respectively (Vazquez-Laslop et al., 2008, Ramu et al., 2011, Mayford et al., 1989). The drug-bound ribosome stalls because it cannot catalyze transfer of the peptide from the P-site peptidyl-tRNA to the A-site aminoacyl-tRNA (Vazquez-Laslop et al., 2008, Ramu et al., 2011). Importantly, although the N-terminal sequences of these peptides are not critical, the N-terminal segments are required for translation arrest (Vazquez-Laslop et al., 2008). The conservation of the distance of the stalling domain from the N-terminus among peptides of these classes (Ramu et al., 2009) corroborates the importance of the nascent chain length for the arrest. The 8–9-aa long ErmAL1 or

ErmCL stalling peptides reach far into the NPET and must be juxtaposed with the antibiotic molecule in the NPET; such apposition has been suggested to play a key role in the mechanism of arrest (Vazquez-Laslop et al., 2008) (Figure 2.1B). This view agrees with the strict structural requirements of the macrolide cofactor in which removal or modification of the C3 cladinose abolishes stalling, possibly by disrupting drug-peptide interactions (Vazquez-Laslop et al., 2011).

The resistance leader peptides of the third major class have been studied to a much lesser extent (Gryczan et al., 1984, Hue and Bechhofer, 1992, Kwon et al., 2006). These peptides were grouped together based on the presence of the Arg-Leu-Arg (RLR) motif in their sequence (Ramu et al., 2009) (Table 2.2), although the role of this motif in programmed arrest has not been verified. Intriguingly, in striking contrast to the IAVV and IFVI classes, the placement of the RLR motif within these peptides is highly variable (Ramu et al., 2009).

By analyzing translation arrest controlled by the RLR peptides, we discovered that the N-terminus is dispensable and macrolide antibiotic can block peptide bond formation and halt translation when the nascent chain is only 3-aa long and barely reaches the antibiotic in the NPET. Structural probing and molecular dynamics (MD) modeling showed the existence of an allosteric link between the NPET and the PTC, illuminating how binding of an antibiotic in the NPET predisposes the ribosome for stalling when translating specific amino acid sequences.

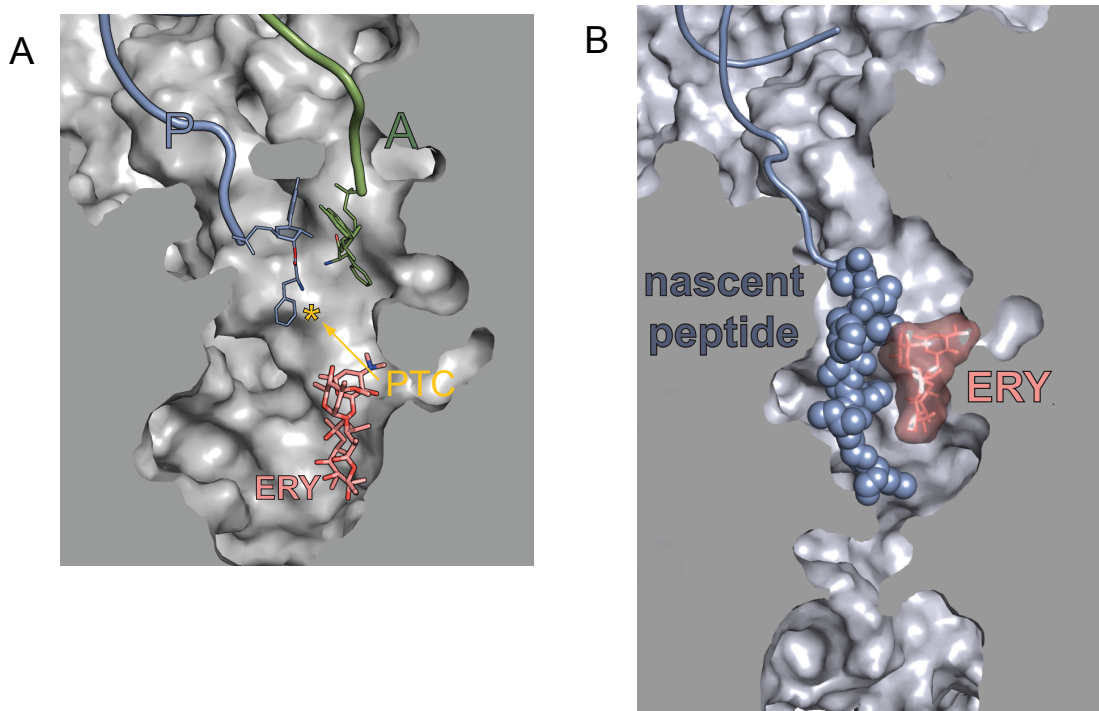


**Figure 2.1. Antibiotic and nascent peptide in the ribosomal exit tunnel.** (A) The relative locations of the macrolide binding site in the NPET and the PTC active site were rendered by aligning crystallographic structures of *Thermus thermophilus* 70S ribosome complexed with aminoacylated donor and acceptor tRNA substrates [Protein Data Bank (PDB) ID codes 2WDK, 2WDL (Voorhees et al., 2009)] and the vacant ribosome complexed with ERY [PDB ID codes 3OHC, 3OHJ (Bulkley et al., 2010)]. The PTC active site, defined as the mid-distance between the attacking amino group of the acceptor substrate and the carbonyl carbon atom of the donor, is marked by an asterisk. (B) The modeled position of the 9-aa-long ErmCL nascent peptide in the ribosomal tunnel obstructed by ERY (Vazquez-Laslop et al., 2010). In the stalled complex, ErmCL is juxtaposed with the antibiotic in the tunnel.

## 2.2 Materials and Methods

### **Preparation of *E. coli* ribosomes and cell-free translation.**

Cell-free translation and toeprinting analyses were carried out as described (Vazquez-Laslop et al., 2008). Linear DNA templates (0.5–1 pmol) encoding the ORF of interest preceded by the T7 promoter were generated by PCR using primers shown in Table 2.1. The templates were used to direct transcription–translation in the  $\Delta$ ribosome PURExpress cell-free system (New England Biolabs). The reactions were supplemented with antibiotics and with wild type or mutant ribosomes prepared as described in (Vazquez-Laslop et al., 2008 and 2011, Ohashi et al., 2007) in a total volume of 5  $\mu$ L. The reactions were incubated for 10 min at 37 °C followed by a 5-min primer extension initiated by addition of reverse transcriptase. cDNA products were separated in a 6% sequencing gel and visualized with a Typhoon imager (GE).

### **Foot-printing analysis of 23S rRNA.**

Chemical probing of rRNA was performed using ribosomes prepared according to Ohashi et al., 2007. The 50- $\mu$ L reactions containing 80 mM K-Hepes, 10 mM MgCl<sub>2</sub>, 100 mM NH<sub>4</sub>Cl and 200 nM ribosomes were preincubated for 5 min at 42 °C. After addition of antibiotic to a final concentration of 50  $\mu$ M, reactions were incubated for 10 min at 37 °C and 10 min at room temperature. 1-Methyl-7-nitroisatoic anhydride reagent (1M7) (Merino et al., 2005) was added to a final concentration of 16 mM; after incubation for 1.25 min at 37 °C and 1 min at room temperature, reactions were quenched by addition of stop buffer containing 3 M NaOAc and 0.5 M K-borate. As described

previously (Merryman and Noller, 1998), 1M7-modified RNA was extracted and analyzed by primer extension.

### **Cell-free translation and analysis of peptidyl-tRNA.**

For peptidyl-tRNA analysis, PURExpress translation reactions were supplemented with 0.5  $\mu\text{Ci}$  of  $[^{14}\text{C}]$ -Leu (specific activity 306 Ci/mol) or 0.5  $\mu\text{Ci}$  of  $[^{14}\text{C}]$ -Lys (specific activity 250 Ci/mol) (American Radiolabeled Chemicals). The products were analyzed in Bis-Tris polyacrylamide gels (Vazquez-Laslop et al., 2008).

### **Molecular Dynamics Simulations.**

The complete atomic models of the E. coli ribosome with ERY bound (the ERY model) and without the compound (drug-free model) are based on X-ray crystal structures 3OFO/3OFR and 2AVY/2AW4, respectively (Dunkle et al., 2010, Schuwirth et al., 2006). The systems were prepared as described (Trabuco et al., 2010). The final dimensions of both simulation systems were  $\sim 280 \times 340 \times 340 \text{ \AA}$ . All simulations were performed using NAMD 2.9 (Phillips et al., 2005) with the AMBER99SB force field (Hornak et al., 2006, Cornell et al., 1995), which includes parameters for modified nucleosides (Aduri et al., 2007). Modeling and analysis also used the program VMD (Humphrey et al., 1996). The equations of motion were integrated with a 1-fs time step and bonded interactions, nonbonded short-range interactions, and nonbonded long-range interactions were calculated every one, two, and four time steps, respectively. The particle mesh Ewald method (Darden et al., 1993, Essmann et al., 1995) was used to evaluate the nonbonded long-range electrostatic interactions. All simulations were carried

out in the NpT ensemble at  $T = 310$  K and  $P = 1$  atm with the following protocol: water and ions were first equilibrated for 2 ns with the remainder of the simulation system restrained, after which side chains of proteins and bases of nucleotides were allowed to move for another 5 ns. Finally, all restraints were released for an equilibration of an additional 10 ns. After these first 17-ns initial equilibrations, production simulations were performed for each system (Figure 2.12D). All analyses were carried out using only the production simulation data. The force-field parameters of erythromycin were optimized in two steps. In the first step, the parameterization of partial charges of atoms followed the standard procedure for AMBER, fitting restricted electrostatic potentials generated from quantum mechanics calculations at the RHF/6-31G\* level (Bayly et al., 1993). The calculations and fitting were performed using Gaussian (Frisch et al., 2004) and Antechamber (Wang et al., 2005), respectively. In the second step, all the bonded terms were deduced based on analogous bonded types available in the AMBER99SB force field (Hornak et al., 2006, Cornell et al., 1995), except for the length of bonds and the values of angles involving heavy atoms, which were taken directly from the crystal structures. The resulting parameter files and the associated topology files needed for simulations with NAMD are available at <http://www.ks.uiuc.edu/~boliu/eryAMBER/>

**Table 2.1: Primers used in this study**

<b>Primer Name</b>	<b>Primer sequence (5' to 3')</b>
T7	TAATACGACTCACTATAGGG
NV1	GGTTATAATGAATTTTGCTTATTAAC
ERMD-I-F	TATACGACTCACTATAGGGCTTAAGTATAAGGAGGAAAAAATATG ACACACTCAATGAGACTTCGTTTCCCAATTACTTTGAACCAG
S6DL-I-F	TAATACGACTCACTATAGGGCTTAAGTATAAGGAGGAAAAAATAT GCACTCAATGAGACTTCGTTTCCCAATTACTTTGAACCAG
S5DL-I-F	TAATACGACTCACTATAGGGCTTAAGTATAAGGAGGAAAAAATAT GTCAATGAGACTTCGTTTCCCAATTACTTTGAACCAG
S4DL-I-F	TAATACGACTCACTATAGGGCTTAAGTATAAGGAGGAAAAAATAT GATGAGACTTCGTTTCCCAATTACTTTGAACCAG
S3DL-I-F	TAATACGACTCACTATAGGGCTTAAGTATAAGGAGGAAAAAATAT GAGACTTCGTTTCCCAATTACTTTGAACCAGTAAGTGATAG
S2DL-I-F	TAATACGACTCACTATAGGGCTTAAGTATAAGGAGGAAAAAATAT GCTTCGTTTCCCAATTACTTTGAACCAG
ERMDL-I-R	GGTTATAATGAATTTTGCTTATTAACGATAGAATTCTATCACTTAC TGGTTCAAAGTAATTGGG
MUT-R	GGTTATAATGAATTTTGCTTATTAACGATAGAATTCTATCACTTAC TGGTTCAA
MRLK-I-F	TAATACGACTCACTATAGGGCTTAAGTATAAGGAGGAAAAAATAT GAGACTTAAATTCCCAATTACTTTGAACCAGTAAGTGATAG
S3DL-R4K- STOP-FWD	TAATACGACTCACTATAGGGCTTAAGTATAAGGAGGAAAAAATAT GAGACTTAAATAAGTGATAGAATTCTATC
S3DL-R4K- STOP-REV	GGTTATAATGAATTTTGCTTATTAACGATAGAATTCTATCACTTA
L2667	GGTCCTCTCGTACTAGGAGCAG
S8CL-W-F	AATACGACTCACTATAGGGCTTAAGTATAAGGAGGAAAAAATATG GGCATTTTTAGTATTTTGTAATCAGCACATGGGTTTCATTAT
S7CL-W-F	TAATACGACTCACTATAGGGCTTAAGTATAAGGAGGAAAAAATAT GATTTTAGTATTTTGTAATCAGCACATGGGTTTCATTAT
S6CL-W-F	TAATACGACTCACTATAGGGCTTAAGTATAAGGAGGAAAAAATAT GTTTAGTATTTTGTAATCAGCACATGGGTTTCATTAT
S5CL-W-F	TAATACGACTCACTATAGGGCTTAAGTATAAGGAGGAAAAAATAT GAGTATTTTGTAATCAGCACATGGGTTTCATTAT
S4CL-W-F	TAATACGACTCACTATAGGGCTTAAGTATAAGGAGGAAAAAATAT GATTTTGTAATCAGCACATGGGTTTCATTAT
ERMCL-R	GGTTATAATGAATTTTGCTTATTAACGATAGAATTCTATCACTTATT GATAATGAACCCATGTGCTGA
MRLR-I-F	TAATACGACTCACTATAGGGCTTAAGTATAAGGAGGAAAAAATAT GAGACTTCGATTTTCCCAACTTTGAACCAG

ERMDL-NEW MUP-R	GGTTATAATGAATTTTGCTTATTAACGATAGAATTCTATCACTTAC TGGTTCAAAGTTGGGAA
MSR-C-F	TAATACGACTCACTATAGGGCTTAAGTATAAGGAGGAAAAAATAT GACTGCATCGATGAAATTACGTTTCGAACTTTTGAATA
MSR-C-R	GGTTATAATGAATTTTGCTTATTAACGATAGAATTCTATCACTTAG TTGTTATTCAAAGTTTCGAAACGTAAT
MSR-SA-F	TAATACGACTCACTATAGGGCTTAAGTATAAGGAGGAAAAAATAT GACAGCTTCTATGAGACTCAAATAA
MSR-SA-R	GGTTATAATGAATTTTGCTTATTAACGATAGAATTCTATCACTTATT TGAGTCTCATAGAAGCTGTC
ERMDL(1)*-F	TAATACGACTCACTATAGGGCTTAAGTATAAGGAGGAAAAAATAT GCATTTCATAAGATTGCGTTTTCTCGTTTTG
ERMDL(1)*-R	GGTTATAATGAATTTTGCTTATTAACGATAGAATTCTATCACTTAC TTGTTCAAACGAGAAAACGCAATC
ERM39*-F	TAATACGACTCACTATAGGGCTTAAGTATAAGGAGGAAAAAATAT GGCTCCATGTTCGGTGACCTACATCCGCTTGCGCATCAGGTAA
ERM39*-R	GGTTATAATGAATTTTGCTTATTAACGATAGAATTCTATCACTTAC CTGATGCGCAAGC
ERMDL(2)*-F	TAATACGACTCACTATAGGGCTTAAGTATAAGGAGGAAAAAATAT GATCAAGAGAAACGCCTTTGGCTTTCGGCGTTATGATCGCCTACG
ERMDL(2)*-R	GGTTATAATGAATTTTGCTTATTAACGATAGAATTCTATCACTTAT AATAGAATACGGTTTCGTAGGCGATCATAACGCC
ERMUL-F	TAATACGACTCACTATAGGGCTTAAGTATAAGGAGGAAAAAATAT GACACCCTCGTTCCCGCCGTACAGCCACATAAATGACGGGAAGAT
ERMUL-R	GGTTATAATGAATTTTGCTTATTAACGATAGAATTCTATCACTTAA CGGAGCCTAGCAAGGGCGCGCTGGATCTTCCCGTCATTTATGT
ERMXL*-F	TAATACGACTCACTATAGGGCTTAAGTATAAGGAGGAAAAAATAT GTTGATTTACAGGTACCGCTTCTTTCGGTTGCGCAC
ERMXL*-R	GGTTATAATGAATTTTGCTTATTAACGATAGAATTCTATCACCTAC GGGGTAGGAAACGCCTTACGGTTGGTGCGCAACCGCAAGAAAG
ERMQL*-F	TAATACGACTCACTATAGGGCTTAAGTATAAGGAGGAAAAAATAT GAATGGTGAATAGCGTCAATAAGATTAAGAAGAT
ERMQL*-R	GGTTATAATGAATTTTGCTTATTAACGATAGAATTCTATCACCTAT CTTCTTAATCTTATTGAC

Table 2.2: Putative RLR leader peptides of the macrolide resistance genes <sup>a)</sup>

Gene <sup>b)</sup>	Species	Putative Leader Peptide <sup>c)</sup>	Genbank PID	GenBank GID	SD Score <sup>d)</sup>
erm37	<i>Kribbella flavida</i>	MGRRLRP (28AA)	284033869	284027999	5
ermZ*	<i>Streptomyces caelestis</i> <sup>e)</sup>	MGPRLRR (8AA)	284518868	284518867	4
ermB	<i>Lactobacillus crispatus</i>	MEIRLRS (18AA)	33243437	33243436	5
ermT*	<i>Lactobacillus fermentum</i>	MEIRLRS (18AA)	28373207	28373195	5
ermB	<i>Lactobacillus reuteri</i>	MEIRLRS (18AA)	2623780	2623778	5
ermB	<i>Streptococcus pneumoniae</i> <sup>e)</sup>	MEIRLRS (18AA)	182684297	182682970	5
ermB	<i>Enterococcus faecium</i> <sup>e)</sup>	MEIRLRS (18AA)	32470479	32470458	5
ermB	<i>Lactococcus garvieae</i>	MEIRLRS (18AA)	187729640	187729634	5
ermB	<i>Enterococcus faecalis</i> <sup>e)</sup>	MEIRLRS (18AA)	256965588	242362021	5
ermB	<i>Enterococcus faecalis</i> <sup>e)</sup>	MEIRLRS (18AA)	305678698	305678685	5
ermB	<i>Pediococcus acidilactici</i>	MEIRLRS (18AA)	190410490	190410480	5
ermB	<i>Streptococcus pneumoniae</i> <sup>e)</sup>	MEIRLRS (18AA)	138752661	138752654	5
ermD*	<i>Bacillus clausii</i> <sup>e)</sup>	MYFIRLRF (5AA)	56965270	56961782	6
ermD*	<i>Bacillus clausii</i> <sup>e)</sup>	MHFIRLRF (5AA)	37359459	37359457	6
ermG	<i>Bacteroides coprophilus</i>	MYWTRIRY (16AA)	224026271	221217255	5
ermD	<i>Bacillus Licheniformis</i>	MTHSMRLRF (6AA)	143201	511060863	6,6
ermJ	<i>Bacillus Anthracis</i>	MTHSMRLRF (6AA)	730032	143196	6,6
msrSA	<i>Staphylococcus aureus</i> <sup>e)</sup>	MTASMLRL	6594277	486222549	7
ermD*	<i>Desmospora sp.</i>	MLVYIRLRF (5AA)	333373800	333373795	7,6
ermZ*	<i>Streptomyces caelestis</i> <sup>e)</sup>	MTQSTRLRG (82AA)	284518868	284518867	5
ermD*	<i>Paenibacillus sp.</i> <sup>e)</sup>	MRGVCRI RT (28AA)	261405179	261403876	4
ermD*	<i>Paenibacillus sp.</i> <sup>e)</sup>	MRGVRRI RT (28AA)	329930026	329930019	4
ermB	<i>Streptococcus suis</i>	MI VDDKIRI (6AA)	223932186	223932093	6
erm36*	<i>Alkaliphilus oremlandii</i>	MGIASIRIRN (4AA)	158321869	158319059	6
ermB	<i>Enterococcus gallinarum</i>	MWIWKVKIKY (15AA)	257869905	239633765	5,8
ermD*	<i>Paenibacillus sp.</i> <sup>e)</sup>	MCCIAFIRIR	261405179	261403876	7
ermU*	<i>Tsukamurella paurometabola</i>	MEPHRYLRIRF (5AA)	296138265	296137750	7
ermU*	<i>Microclunatus phosphovorus</i>	MGIFATIRIRG (1AA)	336117971	336115651	6
erm39*	<i>Mycobacterium boenickei</i>	MAAMSVTHLRRI (1AA)	73486998	73486996	6,5,5
erm39*	<i>Mycobacterium neworleansense</i>	MASMSVTYIRLRI (1AA)	73487011	73487010	5,5,5
erm39*	<i>Mycobacterium houstonense</i>	MASMSVTYIRLRI (1AA)	73487007	73487005	5,7,7
ermX*	<i>Arcanobacterium pyogenes</i>	MLISGTAFLRLRS (2AA)	38261101	38261095	6
ermX*	<i>Corynebacterium glucuronolyticum</i>	MLISGTAFLRLRT (2AA)	227487333	209951644	6
ermX*	<i>Actinomyces sp.</i>	MLVLGTASLRRT (1AA)	329944089	329944073	5
ermB	<i>Enterococcus faecium</i> <sup>e)</sup>	MVNPKVMEIRLRS (18AA)	294617740	294617735	6,5
ermB	<i>Lactobacillus acidophilus</i>	MVNPKVMEIRLRS (18AA)	325955700	325955697	6,5
ermB	<i>Lactobacillus plantarum</i>	MVNPKVMEIRLRS (18AA)	228860921	228860919	6,5
ermB	<i>Streptococcus pyogenes</i> <sup>e)</sup>	MVNPKVMEIRLRS (18AA)	63022016	63021982	6,5
ermS*	<i>Streptomyces violaceusniger</i> <sup>e)</sup>	MPGWRVRASRLRL (20AA)	307329006	307328957	3,6
erm39*	<i>Mycobacterium porcinum</i>	MTAMSVTYLRRT (1AA)	90901924	90901922	4,4,4
ermQ	<i>Clostridium bartlettii</i> <sup>e)</sup>	MI MNGGIASIRLR	164687690	163813840	8,8
erm39*	<i>Mycobacterium wolinskyi</i>	MAAMSAATFFIRIRI (3AA)	73487015	73487013	4,5
ermB	<i>Streptococcus agalactiae</i>	MAEIVKEVMEIRLRS (18AA)	392560	392558	5,5
ermU*	<i>Streptomyces sp.</i>	MGATFAAYALIRLN (1AA)	302527546	224581096	5
erm39*	<i>Mycobacterium mageritense</i> <sup>e)</sup>	MTDVHNGSPTGLRS (22AA)	45758647	45758644	5
erm39*	<i>Mycobacterium mageritense</i> <sup>e)</sup>	MVMSAACFFIRIRI (1AA)	45758647	45758644	6,6,8
ermX*	<i>Kytococcus sedentarius</i> <sup>e)</sup>	MITAGRLFORALRH (14AA)	256825598	256823905	7
ermD*	<i>Bacillus halodurans</i>	MIKRNAGFRYDRLRN (16AA)	15612943	57596592	5
ermX*	<i>Bifidobacterium thermophilum</i> <sup>e)</sup>	MDIIRPMLISGTAFLRLRT (2AA)	188593347	188593344	4,7
ermX*	<i>Bifidobacterium thermophilum</i> <sup>e)</sup>	MDIIRPMLISGTAFLRLRT (2AA)	188593350	188593348	4,7
ermX*	<i>Corynebacterium diphtheriae</i>	MDIIRPMLISGTAFLRLRT (2AA)	32470494	32470491	4,7
ermX*	<i>Corynebacterium jeikeium</i>	MDIIRPMLISGTAFLRLRT (2AA)	13517628	13517627	4,7
ermX*	<i>Corynebacterium striatum</i>	MDIIRPMLISGTAFLRLRT (2AA)	32479370	32479367	4,7
ermQ	<i>Clostridium bartlettii</i> <sup>e)</sup>	MKGVVVMKNLYIMLNKLRK (10AA)	164687690	163813840	5,8,5
msrC	<i>Enterococcus faecium</i> <sup>e)</sup>	MCGNLIKKEVGRMTASMLRF (6AA)	10442770	552941973	4,8,7
erm36*	<i>Gordonia bronchialis</i>	MGTLYSAPSSARNTNMGRLRR (1AA)	262203305	262200046	4,5
ermU*	<i>Pseudonocardia sp.</i>	MRGRHPANVRAVAAFMLRLV (1AA)	324998303	324330628	6,5,5
ermA	<i>Streptococcus pyogenes</i> <sup>e)</sup>	MYMYCSSRYFFISFIMKRIK (22AA)	338795795	338795780	9,7,6
ermA	<i>Streptococcus pyogenes</i> <sup>e)</sup>	MYMYCSSRYFFISFIMKRIK (22AA)	94995100	94993396	9,7,6
ermX*	<i>Kytococcus sedentarius</i> <sup>e)</sup>	MAVGSPTLVGMVYGTAFLRLRS (1AA)	256825598	256823905	6,6,6
ermD*	<i>Bacillus clausii</i> <sup>e)</sup>	MKCASGVFLFSFTLSRRRFRLRL (4AA)	56965270	56961782	5

<sup>a)</sup> Methyltransferase proteins of the Erm class were searched in the National Center for Biotechnology Information “nr” database with PSI-BLAST using *Streptomyces venezuelae* PikR1 (GenInfo Identifier number 3800833) as the query. The sequences were aligned with MAFFT (Katoh et al., 2005), and after ambiguously aligned regions were removed, phylogenetic analysis was carried out with RaxML (Stamatakis et al., 2006) to classify the sequences into the various subgroups of Erm methyltransferases.

The reconstructed phylogenetic tree is available upon request from G.C.A. (gemma.atkinson@gmail.com) or T.T. (tanel.tenson@ut.ee). Search for upstream ORFs were performed within 500 bps upstream from the start of Erm-like methyltransferase genes. Several macrolide efflux pump genes known to be controlled by the leader ORFs were added to the table. The upstream sequences were translated in all three reading frames and scanned for ORFs starting with AUG or GUG codons and containing at least five codons. The ORFs encoding peptides containing the (R/K)(L/I)(R/K) motifs were selected, and the putative Shine–Dalgarno sequences within 21 bp upstream from a possible start codon were identified.

b) The names of the *erm* genes previously assigned to a specific erm class are shown without asterisks. Genes whose class assignment is based on the proximity in the phylogenetic tree are indicated by asterisks. Leader ORFs at which ribosome stalling was assessed experimentally (Figure 2.2) are highlighted in yellow. The *ermDL* ORF, which was subjected to truncation mutagenesis and detailed biochemical analysis, is highlighted in cyan.

c) The peptides with the initiator site within 25 codons upstream from the conserved motif are shown. Alternative potential initiation sites (corresponding to in-frame AUG or GUG codons) are indicated by boldface characters.

d) Shine-Dalgarno scores of all potential initiation sites within the putative leader ORFs were assigned on the basis of direct match to the sequence AAGGAGGTGATC in the 20 nt region preceding a possible initiation codon. When the first initiator codon was within less than 12 nt from the beginning of the available sequence, SD score was not determined ('nd').

e) Same species, different strains; <sup>f)</sup> No single closely homologous *erm* gene

## 2.3 Results

### 2.3.1 The Position of the Conserved RLR Motif Varies in the Leader Peptides of Macrolide Resistance Genes.

Puzzled by the variable distance of the RLR motif from the N-termini of the leader peptides of macrolide resistance genes (Table 2.2), we first tested whether the RLR sequence is relevant for programmed translation arrest. Several of the known or putative uORFs with varying placement of the RLR motif were generated by PCR and translated in a cell-free system, and antibiotic-dependent ribosome stalling was assayed by toeprinting. The analysis showed that irrespective of the distance of the RLR motif from the N-terminus, the drug bound ribosome halts translation upon entrance of the Leu codon of the RLR-coding sequence into the ribosomal P site (Figure 2.2). This result not only demonstrated the importance of the RLR motif for translation arrest, but also clearly indicated that for these peptides, the length of the N-terminal region preceding the stalling sequence is not as critical as it is for the IAVV and IFVI regulatory peptides (Ramu et al., 2009, Subramanian et al., 2011). This observation was strengthened further by the variability of the amino acid sequences preceding the RLR domain (Table 2.2), made us wonder whether the N-terminal segment is even required for antibiotic-dependent arrest. Therefore, we introduced progressive truncations in the *ermDL* regulatory ORF that controls expression of the resistance methyltransferase ErmD. In the presence of ERY, translation of the wild-type 14-aa-long ErmDL peptide is arrested at the Leu (L7) codon, sandwiched between two Arg codons (R6 and R8) (Kwon et al., 2006, Vazquez-Laslop et al., 2010) (wt in Figure 2.3). Remarkably, deletion of one, two,

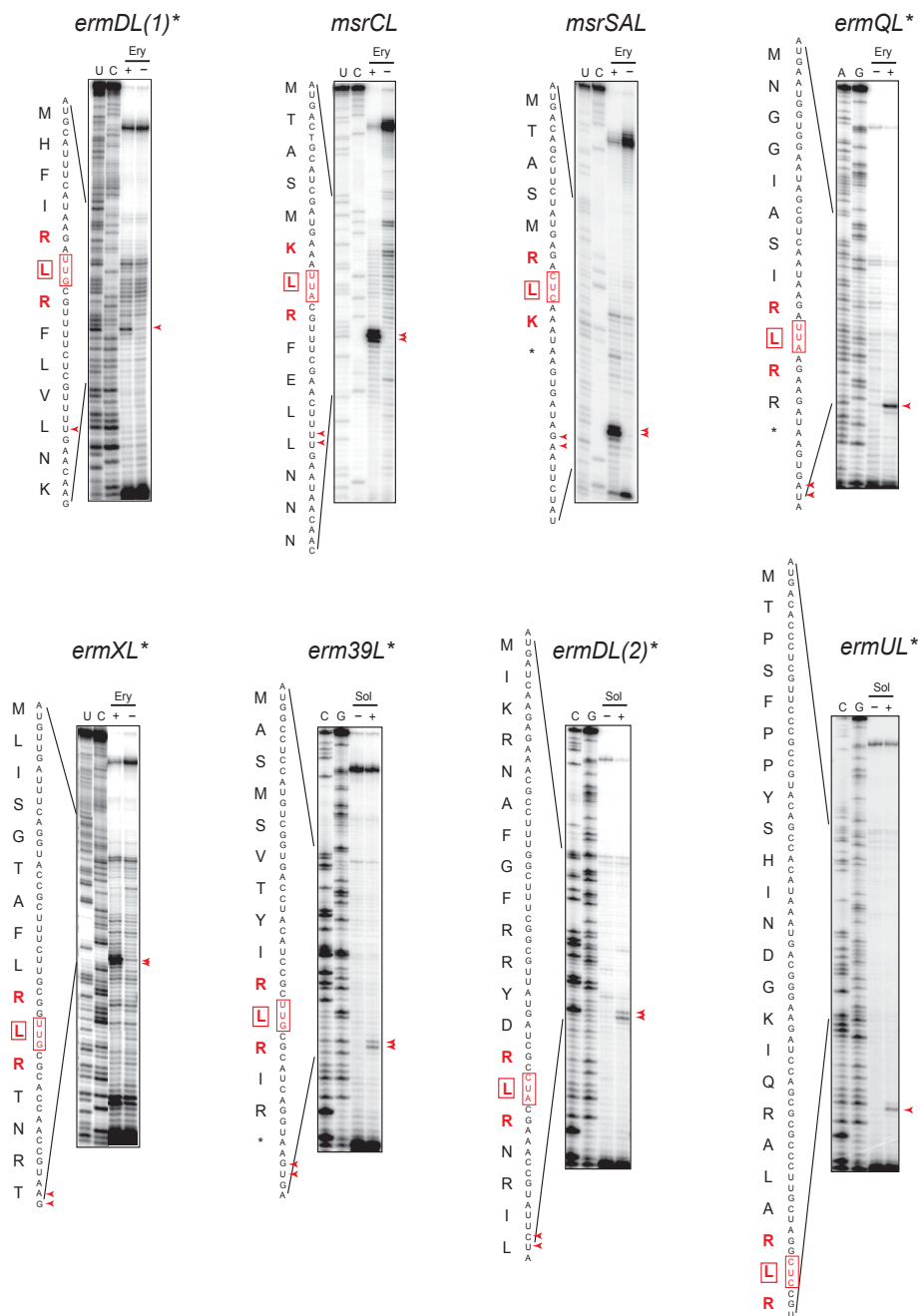


**Figure 2.2. Antibiotic-dependent ribosome stalling occurs at the R/K-L-R/K motif of leader peptides with heterogeneous N-termini.** Erm leader peptides containing the Arg-Leu-Arg (RLR) motif (Table 2.1) at varying positions were translated in the cell-free system with no antibiotic (–) or with 50  $\mu$ M of either erythromycin (ERY) or solithromycin (SOL) and analyzed by toe-printing as described in Materials and Methods (2.2). Arrows indicate the drug-dependent toeprinting signal. The corresponding codon occupying the P-site of the stalled ribosome is boxed on the sequences of the leader ORFs shown on the left of each gel.

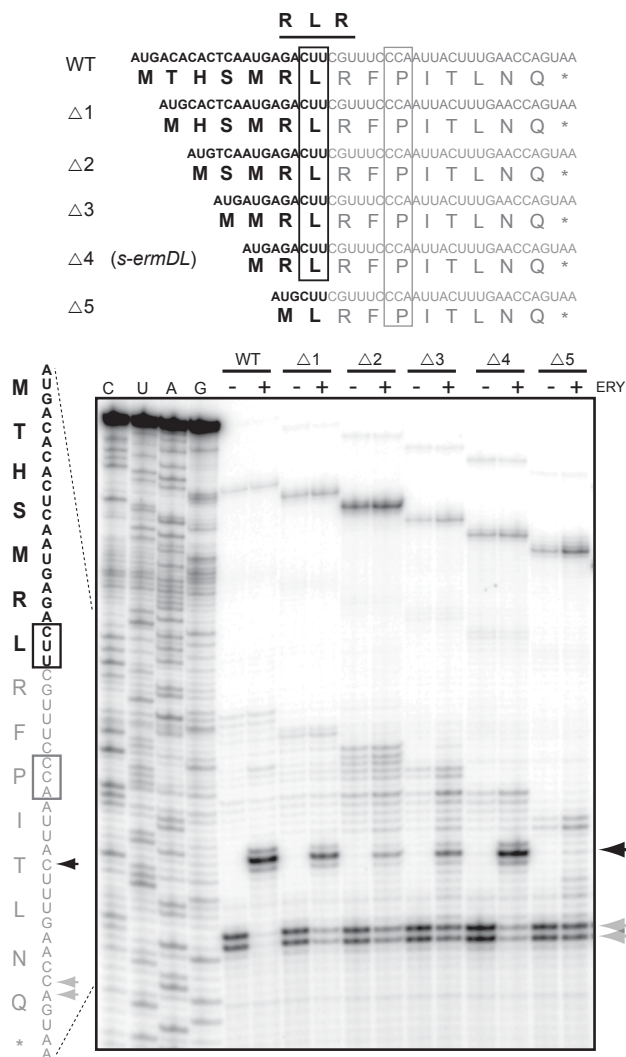


**Figure 2.3. The N-terminal segment preceding the RLR motif is dispensable for antibiotic-mediated translation arrest.** (Upper) Amino acid sequences of ErmDL peptide (WT) and its N-terminally truncated mutants ( $\Delta 1$ – $\Delta 5$ ) (the corresponding ORFs are shown above the peptide sequences). (Lower) Toeprinting analysis of ERY-dependent ribosome stalling during cell-free translation of the wild-type and truncated ermDL ORFs. Black arrowheads and box indicate the ERY-induced toe print signal corresponding to the arrest with the Leu codon in the P site. The nonstalled ribosomes are captured at the downstream Pro codon (gray box and arrowheads) as a result of the presence of mupirocin, an IleRS inhibitor.

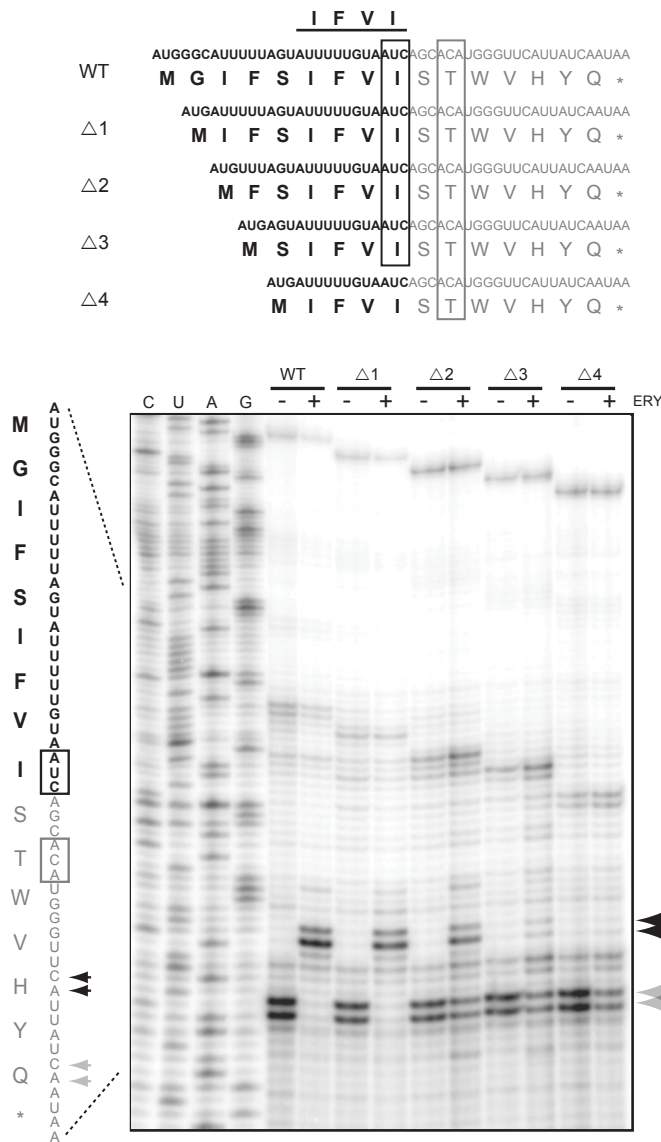


**Figure 2.4. Drug-dependent ribosome stalling is abolished by the N-terminal truncations of ErmCL.** The codons preceding the Ile-Phe-Val-Ile (IFVI) stalling domain of ermCL were deleted sequentially to generate truncations Δ1–Δ4. Toeprinting analysis shows reduced ERY-dependent ribosome stalling at the last Ile codon of the IFVI domain (black arrowheads and box). Gray arrows and box show the ERY-independent ribosome capture at the downstream Thr codon due to the lack of Trp-tRNA<sup>Trp</sup> in the translation reactions depleted by addition of the TrpRS inhibitor indolmycin.

three, or even four codons preceding the *ermDL* stall site did not prevent drug-dependent ribosome arrest at the Leu codon of the RLR motif (Figure 2.3). Although the stalling efficiency was reduced slightly when two or three codons were deleted, the four-codon deletion, resulting in a truncated ORF starting with the sequence Met-Arg-Leu-Arg (MRLR), directed arrest nearly as efficiently as the wild type *ermDL* (*s-ermDL* in Figure 2.3). However, when the truncation encompassed the first Arg codon of RLR, arrest essentially was abolished (Figure 2.3, two right lanes). These results show that the N-terminal segment of the RLR peptides is dispensable for drug-dependent stalling and that binding of ERY to the NPET can trigger arrest when the nascent chain is only 4-aa (MRLR) or perhaps even 3-aa (MRL) long. In contrast to ErmDL, and consistent with our previous observations (Vazquez-Laslop et al., 2008), removal of the N-terminal segments preceding the IFVI or IAVV domains of the ErmAL1 or ErmCL peptides significantly reduced the efficiency of drug-dependent arrest (Figure 2.4), suggesting that the mechanism of ribosome stalling directed by the RLR peptides significantly deviates from that proposed for the regulatory peptides of other classes.

### **2.3.2 Tunnel-Bound Antibiotic Inhibits Formation of Peptide Bond Between MRL Peptide and the Incoming Aminoacyl-tRNA.**

The ribosome arrested at the L3 codon of the truncated *s-ermDL* ORF might carry either the tripeptide MRL esterified to the P-site tRNA<sup>Leu</sup> (if catalysis of peptide bond formation is impaired) or the tetrapeptide MRLR linked to the A-site tRNA<sup>Arg</sup> (if translocation is inhibited) (Figure 2.5B). To distinguish between these scenarios and,

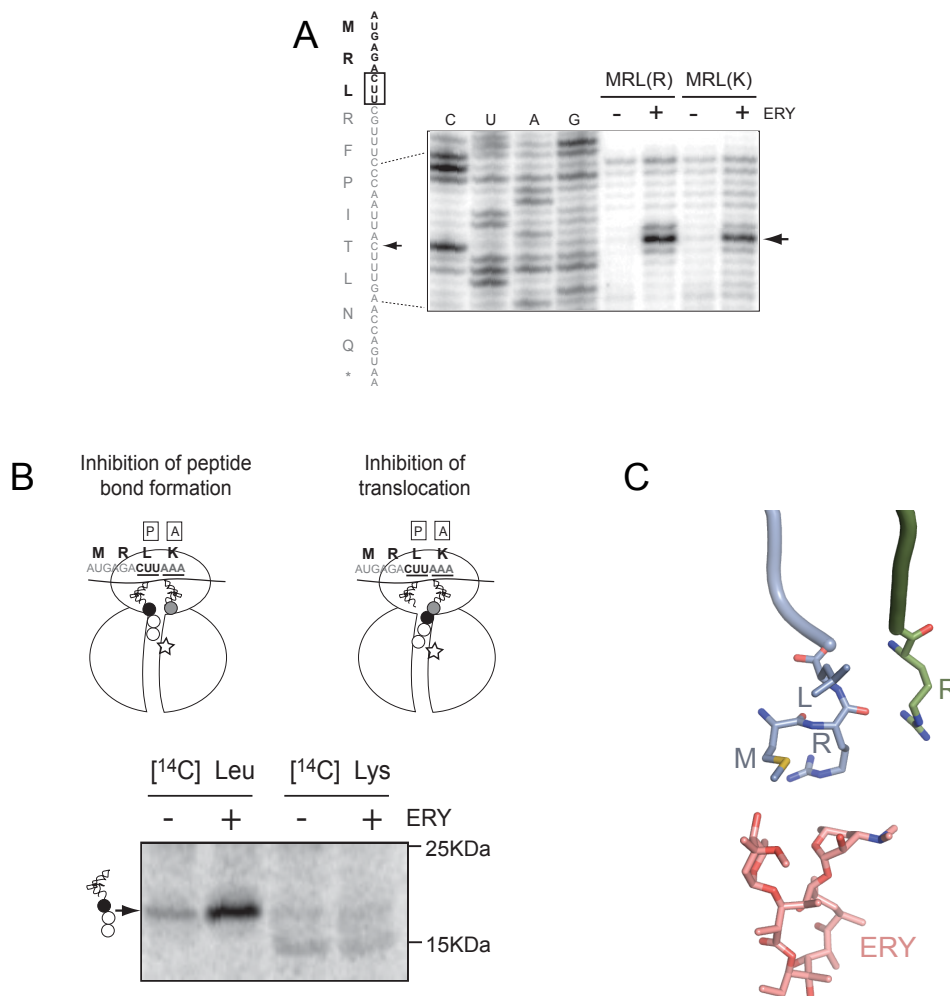


**Figure 2.5.** Antibiotic inhibits the ability of the ribosome carrying the MRL nascent peptide to catalyze peptidyl transfer. **(A)** Toeprinting analysis of ERY mediated stalling during translation of *s-ermDL* (MRLR) or *s-ermDL* (MRLK) ORFs. Sequencing reactions represent the *s-ermDL* (MRLR) template. Arrowheads show the toe print of ribosomes stalled at the Leu codon (boxed). **(B, upper)** The ribosome stalled at the Leu codon of *s-ermDL* (MRLK) can carry either MRL tripeptide at the P-site tRNA<sup>Leu</sup> or MRLK tetrapeptide at the A-site tRNA<sup>Lys</sup>. The Leu-3 and Lys-4 of the peptide are shown as black and gray circles, respectively. The codons in the P and A-sites of the stalled ribosome are underlined. ERY is shown by a star. **(lower)** Gel electrophoresis analysis of peptidyl-tRNA accumulated during translation of the *s-ermDL* (MRLK) ORF in the presence of the indicated radiolabeled amino acids. Migration of markers is indicated on the right. **(C)** The nascent MRL tripeptide barely reaches the antibiotic in the NPET and cannot be juxtaposed with it. The P-site MRL-tRNA<sup>Leu</sup> (blue) and A-site Arg-tRNA<sup>Arg</sup> (green) were modeled into the structure of the *E. coli* ribosome-ERY complex and subjected to 2 ns equilibration to avoid immediate structural clashes.

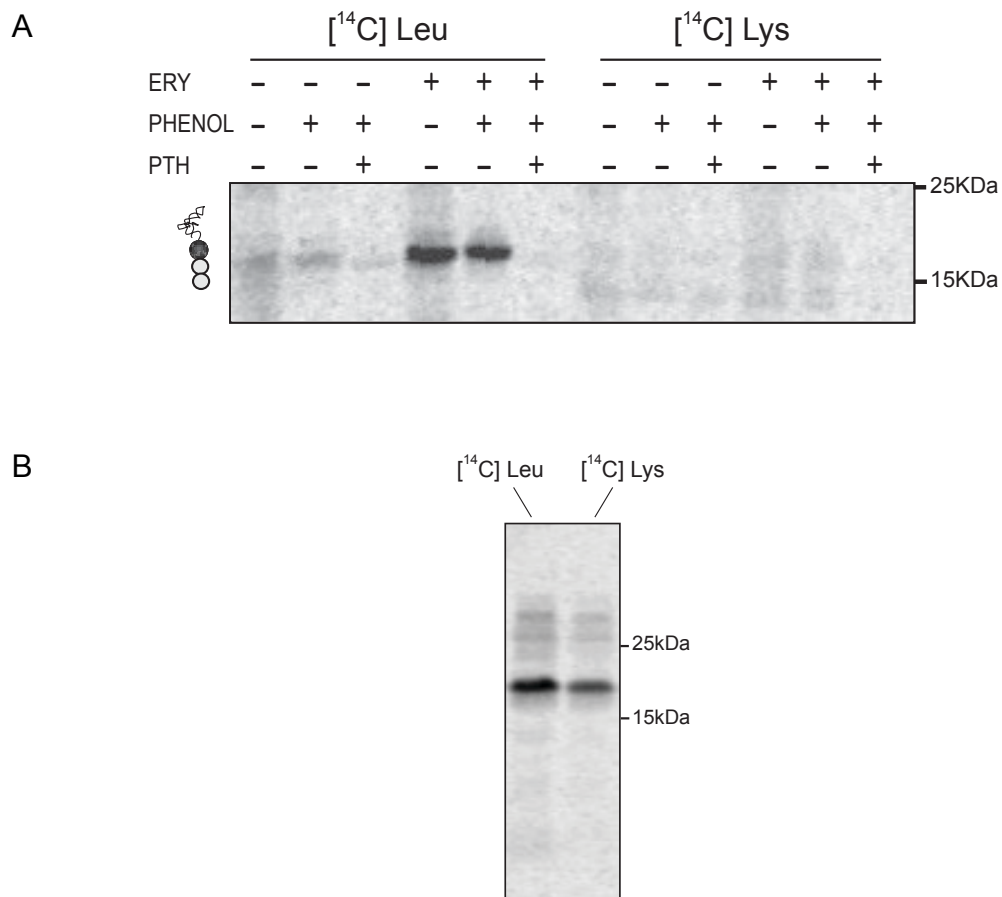


**Figure 2.6. Characterization of peptidyl-tRNA in the stalled complex.** **(A)** Electrophoresis analysis in the Bis-Tris gel system of the  $[^{14}\text{C}]$ -radiolabeled peptidyl-tRNA accumulating in the course of cell-free translation of the *s-ermDL* (MRLK) template in the absence or presence of ERY. The product, which incorporates  $[^{14}\text{C}]$ -Leu but not  $[^{14}\text{C}]$ -Lys, partitions into aqueous phase upon phenol extraction of the reaction and is sensitive to treatment with peptidyl-tRNA hydrolase (PTH). This confirms the peptidyl-tRNA nature of the product represented by strong bands observed in the  $[^{14}\text{C}]$ -Leu/ERY sample. **(B)** Translation of the control dihydrofolate reductase protein in the cell-free system in the presence of  $[^{14}\text{C}]$ -Leu or  $[^{14}\text{C}]$ -Lys, showing that both radioactive amino acids are incorporated efficiently in the protein product.

thus, deduce the exact length of the stalling peptide, we took advantage of the fact that the RLR peptides seem to tolerate Arg-to-Lys substitutions within the motif (Table 2.2). Indeed, ERY directed ribosome stalling at the L3 codon of the s-ermDL mRNA regardless of whether it was followed by an Arg (R4) or a Lys (K4) codon (Figure 2.5A and Figure 2.6). Thus, we used template s-ermDL (MRLK) to determine whether the fourth amino acid (K) is incorporated into the peptidyl-tRNA of the stalled ribosome. In the cell-free translation reaction, incorporation of [14C]- Leu in peptidyl-tRNA was stimulated greatly by ERY (Figure 2.5B, lanes 1 and 2), whereas incorporation of [14C]-Lys remained negligible (Figure 2.5B, lanes 3 and 4). Therefore, ERY arrests translation of the s-ermDL (MRLK) by blocking the transfer of the P-site tripeptide MRL to the incoming Arg or Lys aminoacyl-tRNA. This result implies that the presence of the drug in the NPET alters the catalytic properties of the PTC when the nascent chain is only three amino acid residues long (Figure 2.5C).

### **2.3.3 Known Nascent Peptide Ribosomal Sensors Are Not Involved in Drug Induced Stalling with the MRL Peptide.**

Juxtaposition of 8–9-aa long IAVV and IFVI stalling peptides with the antibiotic in the tunnel brings the peptide in contact with specific rRNA sensors in the NPET that help recognize the nascent chains and relay the arrest signal to the PTC. Mutations of such 23S rRNA residues (A2062, A2503, U1782, C2610) dramatically reduce the efficiency of stalling with ErmAL1 or ErmCL (Vazquez-Laslop et al., 2010 and 2011). Strikingly, neither these mutations nor changes of residues involved in recognition of other stalling peptides (G2583, U2584, U2586, A2587, and U2609) (Nakatogawa and Ito,

2002, Cruz-Vera et al., 2005, Yang et al., 2009) significantly affected arrest with the MRL peptide (Figure 2.7). Although the search for potential MRL sensors has not been exhaustive, the available data are compatible with the possibility that it is the presence of the tunnel-bound antibiotic *per se* rather than the drug-imposed interaction of the nascent peptide with the tunnel sensors that is critical for the arrest of the ribosome carrying the MRL peptide.

#### **2.3.4 Structurally Diverse Antibiotics Promote Ribosome Stalling with RLR Peptides.**

The antibiotic structure is essential for ribosome stalling directed by IAVV or IFVI peptides (Vazquez-Laslop et al., 2008). Removal or modification of the C3 cladinose sugar of ERY abolishes arrest, possibly by disrupting specific interactions between the antibiotic and the 8–9 amino acid long nascent chain (Vazquez-Laslop et al., 2011). The MRL peptide, however, is too short to make extensive contact with the antibiotic (Figure 2.5C), suggesting that the drug–peptide interface may not play any role in the arrest mechanism. Consistently, we found that stalling with MRL is triggered not only by cladinose-containing ERY, but also by azalide azithromycin (AZI) and even cladinose-lacking ketolide SOL (Figure 2.8), which fails to induce arrest with IAVV or IFVI peptides. The high tolerance of MRL-dependent stalling to alterations in the antibiotic structure supports the possibility that the sole presence of the drug in the NPET, rather than its interaction with the nascent chain, is sufficient for stalling at the *s-ermDL* ORF.



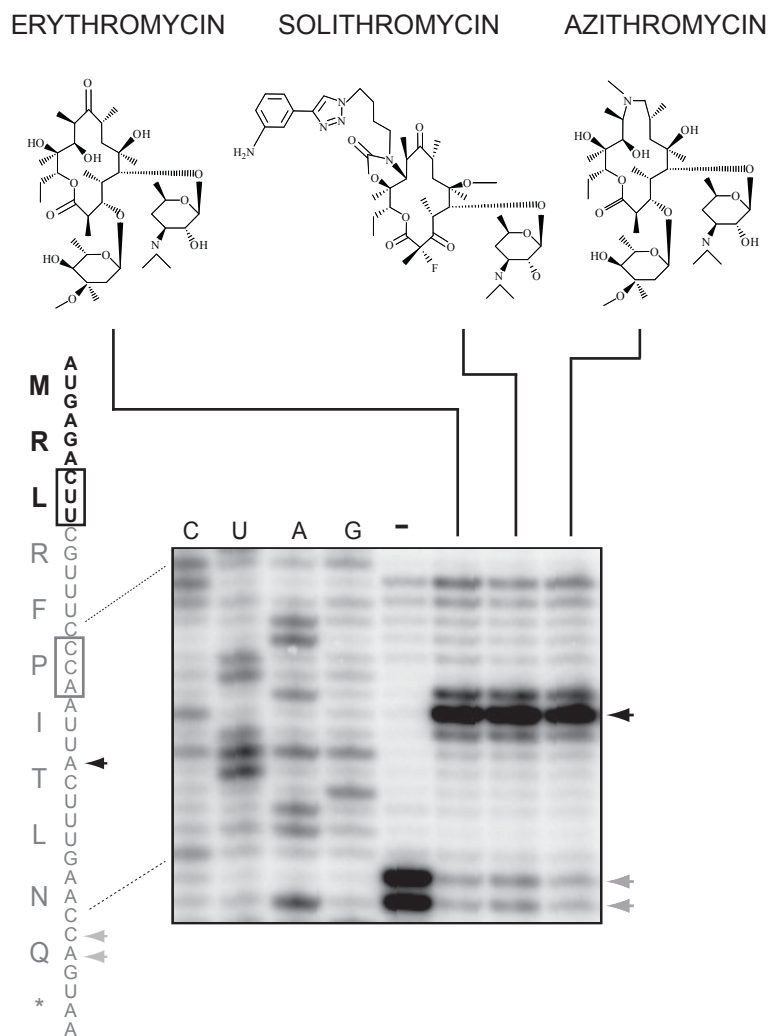


**Figure 2.8. Diverse macrolides induce ribosome stalling with the MRL nascent peptide.** Toeprinting analysis of ribosomes stalled during translation of the *s-ermDL* ORF induced by macrolide ERY, ketolide SOL, or azalide AZI. Drug induced toe print representing arrest at the Leu codon (black box) is indicated by a black arrowhead. Gray arrowheads and box indicate macrolide independent translation arrest at the Pro codon due to the presence of mupirocin, which depletes Ile-tRNA in the reaction.

### **2.3.5 Binding of Antibiotics in the NPET Allosterically Alters the Conformation of the PTC.**

A distance of more than 11 Å separates the nearest atom of the tunnel-bound antibiotic (ERY, AZI, or SOL) from the PTC active site (Dunkle et al., 2010, Bulkley et al., 2010). Hence, macrolides cannot prevent peptide bond formation by direct steric hindrance unless the peptide induces relocation of the drug to the PTC, which we view as an implausible scenario. Furthermore, the short length of the MRL peptide makes it unlikely that the drug forces it into a nonproductive conformation, as was proposed for the longer stalling peptides (Vazquez-Laslop et al., 2008 and 2011). Therefore, we hypothesized that binding of the drug in the NPET may allosterically influence the structure, and hence the function, of the PTC.

When drug-free or ERY-bound ribosomes were treated with 1-methyl-7-nitroisatoic anhydride (1M7), the reagent used for selective 2'-hydroxyl acylation analyzed by primer extension (SHAPE) (Merino et al., 2005), modification of several rRNA residues was reduced in the presence of antibiotic. Protections of some nucleotides (e.g., A2058 and A2059) were expected because these residues interact directly with the drug. Strikingly, however, modification of the distant U2585 in the PTC also was reduced significantly in response to ERY binding (Figure 2.9B). Other macrolide inducers of MRL-dependent arrest (AZI and SOL) had a similar effect on the U2585 reactivity (Figure 2.9B). Importantly, U2585 is located in the PTC active site and is critically involved in catalysis of peptide bond formation (Schmeing et al., 2005, Voorhees et al., 2009). These results clearly established that the structure of the PTC and, thus, likely its

catalytic properties are sensitive to the presence of the antibiotic in the NPET, thereby revealing the existence of an allosteric and functional link between the exit tunnel and the catalytic center.

### **2.3.6 MD Simulations Substantiate the Existence of a Structural Link Between the NPET and the PTC.**

To gain independent evidence for the drug-dependent structural link between the NPET and PTC, we carried out all-atom MD simulations of the drug free and ERY-bound *Escherichia coli* ribosome on the bases of the corresponding crystallographic structures (Dunkle et al., 2010, Schuwirth et al., 2005). Six independent simulations, three with the drug-free and three with the ERY-bound structure, were performed for the entire ribosome (about 3 million atoms), with production simulation time in each run ranging from 70 to 273 ns. After the preproduction equilibrations, the starting structures of both models show very similar conformations at the PTC region (Figure 2.10A). Consistent with the crystal structures (Bulkley et al., 2010), MD simulations showed that the presence of ERY affects the placement of its immediate neighbor A2062 (Figure 2.10B). Most notably, the presence of antibiotic also affects two remote sites in the PTC (Figure 2.11 A, C and D). In excellent agreement with the results of chemical probing, the drug promotes a dramatic reorientation of U2585. Although in the absence of antibiotic the nucleotide stably populates a “looped out” configuration, ERY prompts rotation of the U2585 base by  $\sim 100^\circ$  (Figure 2.11B, Figure 2.10B and Figure 2.12A, and Movie 2.1(present in the online version of the paper)) This new “folded-in” state of U2585 is stabilized by its stacking interaction with U2584. In two of the three

simulations of the drug bound ribosome, U2585 rotation occurred within 50 ns after the start of the production simulation and remained in this orientation most of the time thereafter (Figure 2.12A and Movie 2.1). In the third simulation, the folded-in state of U2585 was not fully achieved, but the U2585 base had rotated toward the folded-in position on average by  $10^\circ$  (Figure 2.12 A and C) In contrast, in three simulations of the drug-free ribosome, the U2585 base barely visited the folded-in state (a total of 418 ns of the combined simulation time) and instead populated the looped out conformation (Figure 2.11B, Figure 2.12A and C, and Movie 2.1).

A second, even more distant PTC residue, A2602, was also sensitive to the binding of ERY. The preferred orientations of the A2602 base in drug-free and ERY-bound states differ by  $\sim 110^\circ$  (Figure 2.11A). Although in the absence of the drug A2602 is in a looped-out state away from helix 93 of 23S rRNA, the antibiotic provokes insertion of the base into the helix concomitant with its local distortion (Figure 2.11C, Figure 2.12 B and C, and Movie 2.1). Taken together, the results of the whole-ribosome MD simulations provide independent support for communication between the NPET and the PTC active site.

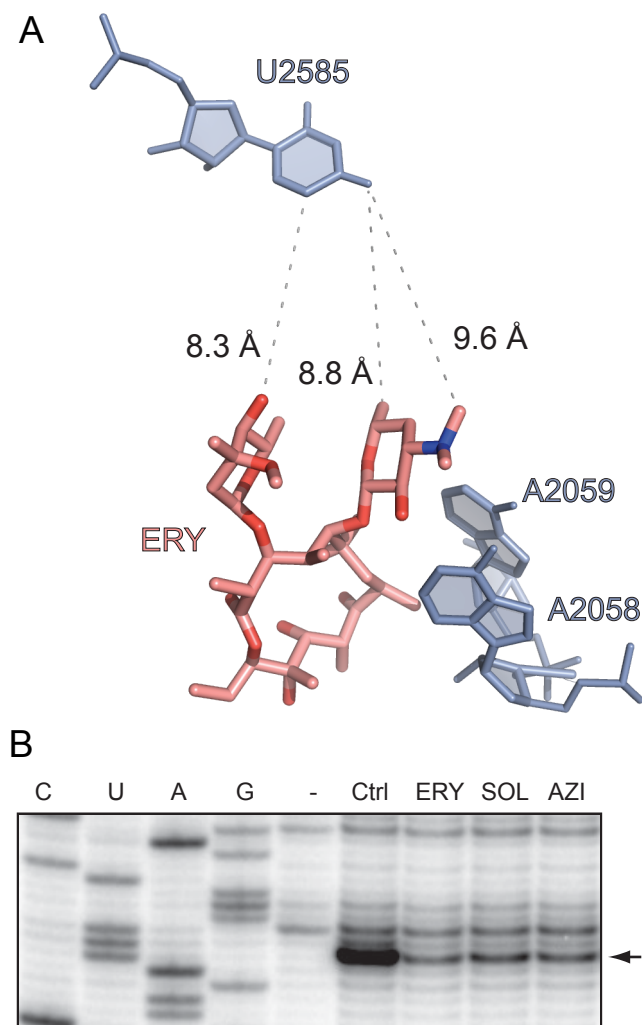


**Figure 2.9. Binding of antibiotics in the NPET affect the distant nucleotide U2585 in the PTC active site.** (A) The relative placement of ERY in the NPET and U2585 in the PTC in the crystallographic structure of the *E. coli* ribosome–ERY complex (Dunkle et al., 2010) (PDB ID code 3OFR). Residues A2058 and A2059 in the ERY binding site are also shown. (B) Chemical probing of ribosome–antibiotic complexes with the SHAPE reagent 1M7. Ribosomes were incubated with no antibiotic (Ctrl) or with 50  $\mu$ M of ERY, SOL, or AZI (see their structures in Figure. 2.8) and modified with 1M7. The state of modification of U2585 (arrowhead) was assessed by primer extension.

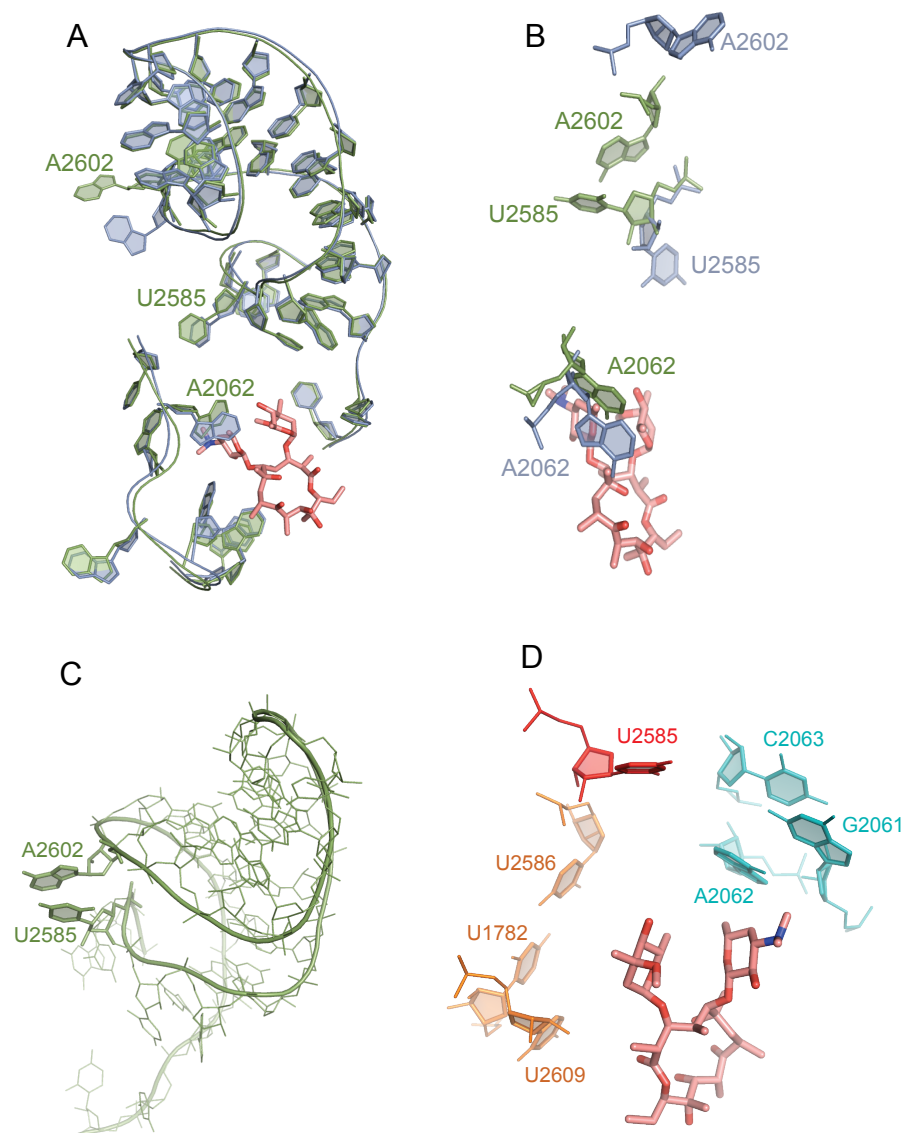


**Figure 2.10. Molecular dynamics (MD) simulations illuminate the existence of a structural link between the nascent peptide exit tunnel (NPET) and the peptidyl transferase center (PTC).** (A) The conformation of the NPET and PTC rRNA residues of drug-free (green) and ERY-bound (blue) ribosomes are similar after the initial preproduction equilibration. (B) During production simulations, the ERY-proximal A2062 in the NPET and distant U2585 and A2602 in the PTC tend to adopt different conformations. The figure shows the “last-frame” position of the nucleotides averaged over three independent simulations. Green, drug-free ribosome; blue, ERY-bound ribosome. (C) The looped-out conformation of U2585 and A2602 in the drug-free ribosome sometimes can be stabilized by possible stacking interactions between the two residues. (D) Possible conformational relay routes connecting the macrolide molecule in the NPET to the PTC. The pathway initiated at A2062 is shown in cyan, and the one starting at U2609 is orange. U2585 in the PTC active site is red. The mutations of A2062, U2609, U2586, or U1782 do not abrogate translation arrest controlled by antibiotic and the MRL peptide.

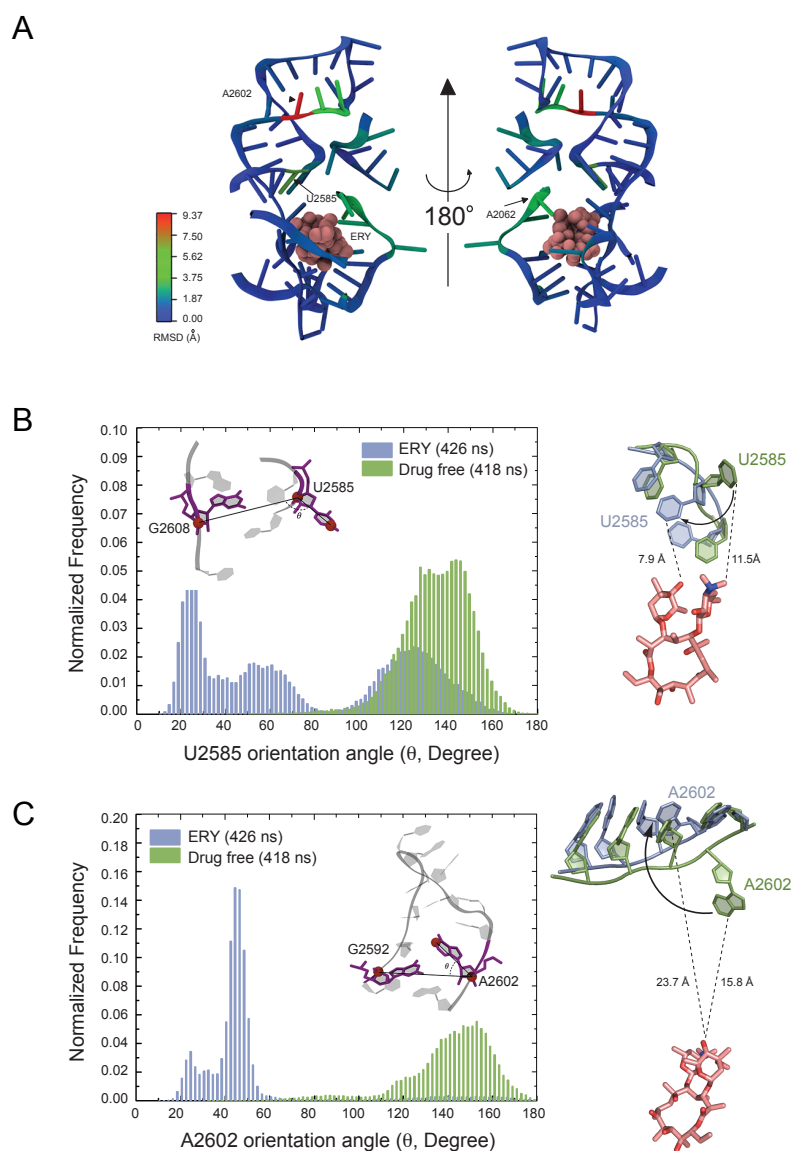


**Figure 2.11. MD simulations substantiate the allosteric effect of the NPET-bound ERY on the distant PTC nucleotides U2585 and A2602.** (A) Root mean square deviation (rmsd) of the preferred positions of rRNA residues in drug-free and ERY-bound ribosome. The rmsd was calculated by averaging the “lastframe” coordinates of the residues in three independent simulations of drug-free and ERY-bound ribosome. (B, Left) The frequency of visiting various conformations by U2585 in the course of MD simulations of drug-free (green) or ERY-bound (blue) ribosome [presented as angles between vectors linking atoms U2585 (C3’)/U2585 (C4) and U2585 C3’/G2608 C3’ (Inset)]. (Right) Placement of U2585 in drug-free (green) and drug-bound (blue) ribosomes. The averaged last-frame positions of the residues are shown. The shortest distances between the drug and U2585 base in two states are indicated. (C) Same as (B) but for the residue A2602.

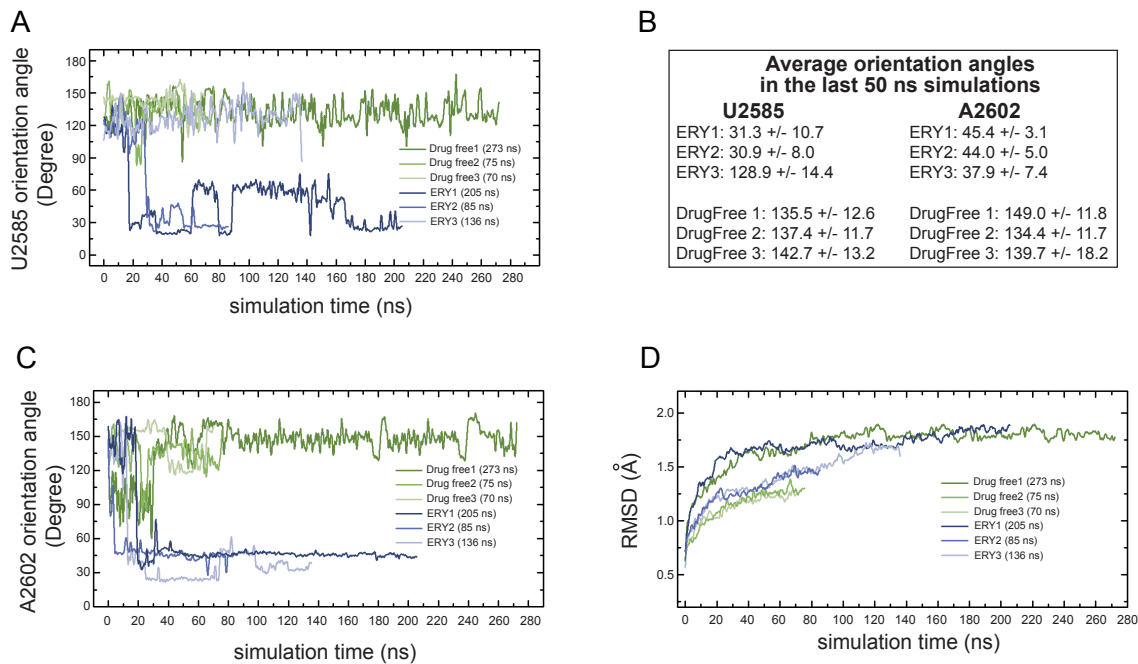


**Figure 2.12. Equilibration of the ribosome structure and conformations of U2585 and A2602 rRNA residues during MD simulations.** (A) The changes in the orientation angle of U2585 over simulation time. The orientation angle is defined as in Figure 2.11B. ERY1, ERY2, and ERY3 are independent simulations of the ERY bound ribosome. Drug free1, Drug free2, and Drug free3 are independent simulations of the drug-free ribosome. (B) Same as A, but for A2602. (C) Average orientation angles of U2585 and A2602 during the last 50-ns simulations ( $\pm$  SD). (D) The rmsd-vs-time plot for nonhydrogen atoms shows the progress of reaching stable equilibrium during the all-atom ribosome MD simulations. Drug-free and ERY-bound ribosome structures were aligned to reference crystallographic structures 2AVY/2AW4 and 3OFO/3OFR, respectively, and rmsd values were calculated between simulation frames and the corresponding reference structures [2AVY/2AW4 (Schuwirth et al., 2005) for the drug-free ribosome and 3OFO/3OFR (Dunkle et al., 2010) for the ERY-bound ribosome]. All nonhydrogen atoms within 40 Å of U2585 in each system were considered in the rmsd calculations.

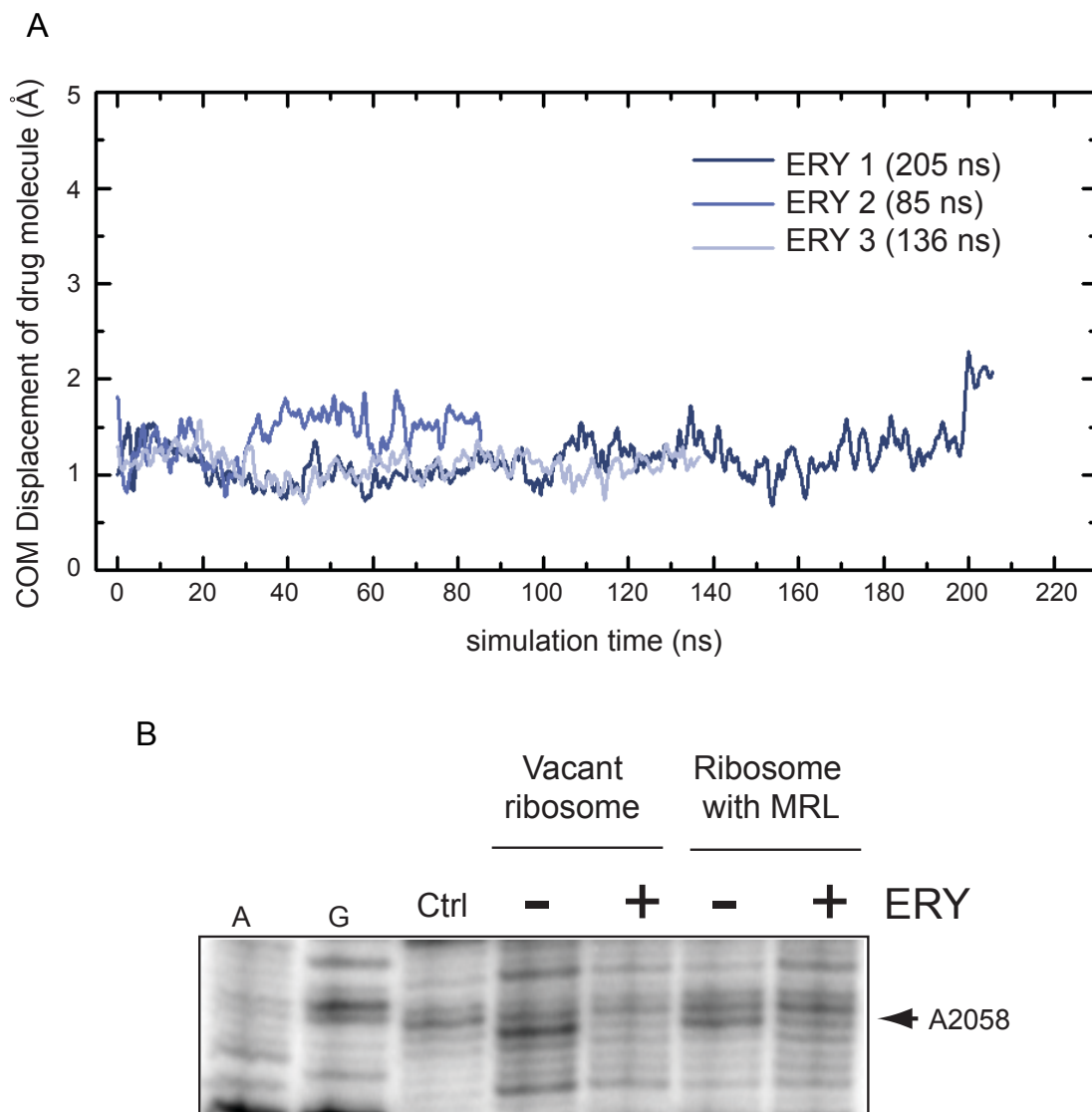


**Figure 2.13. ERY is stably bound in the tunnel.** (a) Center-of-mass (COM) displacement plots for the ERY molecule in the tRNA-free ribosome during three independent simulation runs show no tendency for the antibiotic to relocate from its tunnel site. The COM displacement is measured between the COM of ERY in MD simulations and its COM in the crystallographic structure with the Protein Data Bank ID code 3OFR. (b) Selective 2'-hydroxyl acylation analyzed by primer extension (SHAPE) probing of the accessibility of A2058 in the ERY binding site in the vacant ribosome or in the ribosome that has synthesized the MRL tripeptide in the cell-free translation system. Note that A2058, which is modified readily by the 1M7 reagent in the absence of ERY, is similarly protected by the antibiotic in the vacant or in the MRL-stalled ribosome.

## 2.4 Discussion

The common view of the mechanism of antibiotic- and nascent peptide-controlled translation arrest presumes the key role of molecular interactions at the interface of the drug and the nascent chain. The juxtaposition of the peptide and antibiotic brings the stalling domain into contact with tunnel sensors, which relay the signal to the PTC, impairing its functions (Vazquez-Laslop et al., 2008 and 2010, Ramu et al. 2011, Arenz et al., 2014). Although such a view is sufficient to rationalize the mechanism of arrest with long regulatory peptides, it fails to explain how an antibiotic can promote arrest with the only 3-aa-long MRL peptide. Furthermore, the tolerance of such arrest to alterations in antibiotic structure or to the mutations of the known nascent peptide sensors does not fit with the conventional view.

Our findings, however, may be reconciled within the framework of an alternative, potentially complementary model whose centerpiece is the allosteric link between the tunnel and the PTC. Binding of antibiotic in the tunnel alters properties of the PTC and inhibits peptidyl transfer catalysis between certain donor and acceptor substrates. Therefore, the tunnel-bound small molecule predisposes the ribosome for stalling when such combinations of substrates are encountered during translation.

The results of our biochemical testing and MD simulations clearly show that the binding of an antibiotic in the NPET alters the structural and thus likely functional features of the PTC. The data are most consistent in regard to U2585, a key residue in the PTC active site (Schmeing et al., 2005, Voorhees et al., 2009). The reactivity of this residue to the SHAPE reagent is altered when the antibiotic is bound in the tunnel (Figure

2.9). It also is one of the PTC residues that in the MD simulations reorients most dramatically in response to ERY binding and adopts a conformation rarely visited in the drug-free ribosome. The movement of U2585 seemed to be accompanied by repositioning of A2602 (Figure 2.10). Although chemical probing did not provide additional evidence for rearrangements of A2602, its ERY-induced movement is supported by crystallographic structures of antibiotic-containing complexes, in which it was modeled in a conformation different from that in the drug-free ribosome (Schlünzen et al., 2001, Bulkley et al., 2010). In the absence of antibiotic, both U2585 and A2602 prefer the looped-out configuration, often stabilized by a stacking interaction between their bases (Figure 2.10C and Movie 2.1). Drug-induced rotation of one of the residues would release the restriction and favor the repositioning of the other base as well. Because simulations of drug-free and ERY-bound ribosomes start from comparable states of the PTC, in which both residues are in looped-out conformation, their ERY-induced reorientation is compatible with either lowering the transition barrier or changing the free energy balance between the folded-in and looped-out states. Because of the limited sampling time, the available data are insufficient to distinguish between these scenarios.

Presently, we can only hypothesize how the antibiotic can promote reorientation of the distal PTC residues. Although hypothetically relocation of the antibiotic from its binding site in the NPET to the PTC is possible, neither the published crystal structures (Dunkle et al., 2010, Bulkley et al., 2010) nor our MD simulations, in which binding of ERY in its tunnel site was extremely stable (Figure 2.13A), support this scenario. Furthermore, RNA probing experiments suggest that the drug does not move from its conventional site when MRL peptide is placed in the tunnel (Figure 2.13B). Therefore,

we favor the model that the NPET-bound antibiotic induces changes in the PTC allosterically. One possibility is that a conformational relay could be initiated by rotation of the A2062 base located in the immediate vicinity of the drug-binding site in the NPET (Figure 2.10B) and connected to the PTC through its immediate neighbors, G2061 and C2063 (Seidelt et al., 2009, Gumbart et al., 2012) (Figure 2.10D). A possible alternative route might start at U2609 on the NPET wall opposite ERY. This highly flexible nucleotide is linked to the PTC via U1782 and U2586 (Figure 2.10D). However, the mutations of rRNA residues in both these pathways (e.g., A2062, U2609, U2586, U1782) have either no or only a marginal effect upon ERY- and MRL peptide- dependent stalling (Figure 2.7), suggesting that either the identity of these nucleotides is not critical for signal relay or other pathways are involved. In this regard, it should be noted that although biochemical and computational data clearly identified the PTC as a site sensitive to binding of antibiotic in the NPET, our MD analysis, which was performed with the tRNA free ribosome, cannot accurately describe the placement of the PTC or NPET residues in the translating ribosome.

Although the presence of the antibiotic in the NPET is strictly required for inhibition of peptide bond formation between MRL and the incoming Arg- (or Lys-) tRNA, the requirements for drug structure are far less restrictive than those with the longer stalling peptides. Not only cladinose-containing macrolides that induce translation arrest with IAVV and IFVI peptides, but also azalides and ketolides can promote stalling after polymerization of the MRL tripeptide (Figure 2.8). These results indicate that different antibiotics in the NPET can induce functionally similar changes in the PTC and

reinforce our notion that specific drug–peptide interactions are inconsequential for stalling with short peptides.

The mere presence of the macrolide in the NPET does not indiscriminately inhibit catalysis of peptidyl transfer, but instead interferes with peptidyl transfer between specific substrates. The ribosome can reach the RLR motif in the full-size ErmDL and other RLR-type peptides without being arrested near the start of the leader ORFs (Table 2.2), clearly showing that only specific combinations of PTC donors and acceptors are problematic for the drug-bound ribosome. Thus, the antibiotic predisposes the ribosome for response to specific peptide sequences encoded in the uORFs. Importantly, the short size of the MRL peptide shows that the critical amino acid residues are those located in the PTC rather than in the tunnel. A similar trend is observed even with the longer stalling peptides in which residues critical for stalling are confined to the nascent chain C-terminus and the acceptor substrate (Vazquez-Laslop et al., 2008, Ramu et al., 2011, Arenz et al., 2014). Even in the absence of antibiotic, the ribosomal catalytic center exhibits a considerable degree of selectivity. The rate of catalysis of peptide bond formation depends on the nature of the substrates and when peptidyl transfer becomes rate limiting, it may be manifested as context-specific ribosome stalling (Woolstenhulme et al., 2013, Peil et al., 2013). Importantly, the presence of the NPET bound antibiotic does not seem to exacerbate the problem of the intrinsically problematic PTC substrates, but rather the macrolide induced restrictive selectivity of the PTC makes some otherwise “normal” substrate pairs particularly difficult.

Although our findings suggest a previously unknown role of the antibiotic in the mechanism of translation arrest, they do not dismiss the importance of the drug–peptide

contacts proposed previously. Conceivably, the drug may play a dual role with the longer stalling peptides: not only does it corrupt the PTC, but it may coerce the nascent chain to adopt a nonproductive conformation. Thus, the role of the cofactor in programmed translation arrest may differ depending on the nature of the peptide. With some nascent chains, the interaction between the drug and the growing protein may be absolutely critical for the arrest, which would explain why truncations of ErmCL or ErmAL1 prevent stalling. With other peptides, in which direct contacts between the antibiotic molecule and the nascent chain in the tunnel are minimal [e.g., ErmBL (Arenz et al., 2014)], the allosterically altered PTC is sufficient to prevent peptide bond formation between certain donor–acceptor combinations. Such a role of the cofactor in programmed translation arrest may apply not only to antibiotics but also to other ligands that assist a broad array of peptides in halting translation (Ito and Chiba, 2013, Cruz-Vera et al., 2006).

## 2.5 Cited Literature

Aduri R, *et al.* (2007) AMBER Force Field Parameters for the Naturally Occurring Modified Nucleosides in RNA. *J Chem Theory Comput* 3:1464–1475.

Arenz S, Ramu, H., Gupta, P., Berninghausen, O., Beckmann, R., Vázquez-Laslop, N., Mankin, A.S., Wilson, D.N. (2014) Molecular basis for drug- and nascent polypeptide-mediated translation arrest. *Nat Commun* (In press).

Bayly CI, Cieplak P, Cornell WD, & Kollman PA (1993) A Well-Behaved Electrostatic Potential Based Method Using Charge Restraints for Deriving Atomic Charges - the Resp Model. *J Phys Chem B* 97(40):10269-10280.

Bulkley D, Innis CA, Blaha G, & Steitz TA (2010) Revisiting the structures of several antibiotics bound to the bacterial ribosome. *Proc Natl Acad Sci USA* 107(40):17158-17163.

Cornell WD, *et al.* (1995) A Second Generation Force Field for the Simulation of Proteins, Nucleic Acids, and Organic Molecules. *J Am Chem Soc* 117:5179–5197.

Cruz-Vera LR, Gong M, & Yanofsky C (2006) Changes produced by bound tryptophan in the ribosome peptidyl transferase center in response to TnaC, a nascent leader peptide. *Proc Natl Acad Sci USA* 103(10):3598-3603.

Cruz-Vera LR, Rajagopal S, Squires C, & Yanofsky C (2005) Features of ribosome-peptidyl-tRNA interactions essential for tryptophan induction of tna operon expression. *Mol Cell* 19(3):333-343.

Darden Y, York D, & Pedersen L (1993) Particle mesh Ewald: An N·log(N) method for Ewald sums in large systems. *J Chem Phys* 98:10089-10092.

Dunkle JA, Xiong L, Mankin AS, & Cate JH (2010) Structures of the Escherichia coli ribosome with antibiotics bound near the peptidyl transferase center explain spectra of drug action. *Proc Natl Acad Sci USA* 107(40):17152-17157.

Essmann U, *et al.* (1995) A smooth particle mesh ewald method. *J Chem Phys* 103:8577-8593.

Frisch MJT, *et al.* (2004) Gaussian 03, Revision C.02. *Gaussian, Inc., Wallingford CT.*

Gryczan T, Israeli-Reches M, Del Bue M, & Dubnau D (1984) DNA sequence and regulation of ermD, a macrolide-lincosamide-streptogramin B resistance element from Bacillus licheniformis. *Mol Gen Genet* 194(3):349-356.

Gumbart J, Schreiner E, Wilson DN, Beckmann R, & Schulten K (2012) Mechanisms of SecM-mediated stalling in the ribosome. *Biophys J* 103(2):331-341.

- Hornak V, *et al.* (2006) Comparison of multiple Amber force fields and development of improved protein backbone parameters. *Proteins* 65(3):712-725.
- Hue KK & Bechhofer DH (1992) Regulation of the macrolide-lincosamide-streptogramin B resistance gene *ermD*. *J Bacteriol* 174:5860-5868.
- Humphrey W, Dalke A, & Schulten K (1996) VMD: visual molecular dynamics. *J Mol Graphics Modell* 14(1):33-38, 27-38.
- Ito K & Chiba S (2013) Arrest peptides: cis-acting modulators of translation. *Annu Rev Biochem* 82:171-202.
- Kannan K, Vazquez-Laslop N, & Mankin AS (2012) Selective protein synthesis by ribosomes with a drug-obstructed exit tunnel. *Cell* 151(3):508-520.
- Katoh K, Kuma K, Toh H, & Miyata T (2005) MAFFT version 5: improvement in accuracy of multiple sequence alignment. *Nucleic Acids Res* 33(2):511-518.
- Kwon AR, *et al.* (2006) ErmK leader peptide : amino acid sequence critical for induction by erythromycin. *Archives of pharmacal research* 29(12):1154-1157.
- Mayford M & Weisblum B (1989) *ermC* leader peptide. Amino acid sequence critical for induction by translational attenuation. *J Mol Biol* 206(1):69-79.
- Merino EJ, Wilkinson KA, Coughlan JL, & Weeks KM (2005) RNA structure analysis at single nucleotide resolution by selective 2'-hydroxyl acylation and primer extension (SHAPE). *J Am Chem Soc* 127(12):4223-4231.
- Merryman C & Noller HF (1998) Footprinting and modification-interference analysis of binding sites on RNA. *RNA:Protein Interactions, A Practical Approach*, ed Smith CWJ (Oxford University Press, Oxford), pp 237-253.
- Nakatogawa H & Ito K (2002) The ribosomal exit tunnel functions as a discriminating gate. *Cell* 108:629-636.
- Ohashi H, Shimizu Y, Ying BW, & Ueda T (2007) Efficient protein selection based on ribosome display system with purified components. *Biochem Biophys Res Commun* 352(1):270-276.
- Onouchi H, *et al.* (2005) Nascent peptide-mediated translation elongation arrest coupled with mRNA degradation in the *CGS1* gene of *Arabidopsis*. *Genes Dev* 19(15):1799-1810.

Peil L, *et al.* (2013) Distinct XPPX sequence motifs induce ribosome stalling, which is rescued by the translation elongation factor EF-P. *Proc Natl Acad Sci USA* 110(38):15265-15270.

Phillips JC, *et al.* (2005) Scalable molecular dynamics with NAMD. *J Comput Chem* 26(16):1781-1802.

Ramu H, *et al.* (2011) Nascent peptide in the ribosome exit tunnel affects functional properties of the A-site of the peptidyl transferase center. *Mol Cell* 41:321-330.

Ramu H, Mankin A, & Vazquez-Laslop N (2009) Programmed drug-dependent ribosome stalling. *Mol Microbiol* 71(4):811-824.

Schlunzen F, *et al.* (2001) Structural basis for the interaction of antibiotics with the peptidyl transferase centre in eubacteria. *Nature* 413(6858):814-821.

Schmeing TM, Huang KS, Strobel SA, & Steitz TA (2005) An induced-fit mechanism to promote peptide bond formation and exclude hydrolysis of peptidyl-tRNA. *Nature* 438(7067):520-524.

Schuwirth BS, *et al.* (2005) Structures of the bacterial ribosome at 3.5 Å resolution. *Science* 310(5749):827-834.

Seidelt B, *et al.* (2009) Structural insight into nascent polypeptide chain-mediated translational stalling. *Science* 326(5958):1412-1415.

Stamatakis A (2006) RAxML-VI-HPC: maximum likelihood-based phylogenetic analyses with thousands of taxa and mixed models. *Bioinformatics (Oxford, England)* 22(21):2688-2690.

Subramanian SL, Ramu H, & Mankin AS (2011) Inducible resistance to macrolide antibiotics. *Antibiotic Drug Discovery and Development*, ed Dougherty TJ, Pucci, M. J. (Springer Publishing Company, New York, NY).

Trabuco LG, *et al.* (2010) The role of L1 stalk-tRNA interaction in the ribosome elongation cycle. *J Mol Biol* 402(4):741-760.

Tu D, Blaha G, Moore PB, & Steitz TA (2005) Structures of MLSBK antibiotics bound to mutated large ribosomal subunits provide a structural explanation for resistance. *Cell* 121(2):257-270.

Vazquez D (1975) The Macrolide Antibiotics. *Antibiotics III. Mechanism of action of antimicrobial and antitumor agents.*, eds Corcoran JW & Hahn FE (Springer-Verlag, New York, Heidelberg, Berlin), pp 459-479.

Vázquez-Laslop N & Mankin AS (2014) Triggering peptide-dependent translation arrest by small molecules: ribosome stalling modulated by antibiotics. *Regulatory Nascent Polypeptides*, ed Ito K (Springer, New York).

Vazquez-Laslop N, *et al.* (2011) Role of antibiotic ligand in nascent peptide-dependent ribosome stalling. *Proc Natl Acad Sci USA* 108(26):10496-10501.

Vazquez-Laslop N, Ramu, H., Klepacki, D., Kannan, K., Mankin, A. S. (2010) The key role of a conserved and modified rRNA residue in the ribosomal response to the nascent peptide. *EMBO J.* 29:3108-3117.

Vazquez-Laslop N, Thum C, & Mankin AS (2008) Molecular mechanism of drug-dependent ribosome stalling. *Mol Cell* 30(2):190-202.

Voorhees RM, Weixlbaumer A, Loakes D, Kelley AC, & Ramakrishnan V (2009) Insights into substrate stabilization from snapshots of the peptidyl transferase center of the intact 70S ribosome. *Nat Struct Mol Biol* 16(5):528-533.

Wang JM, W. W, Kollman P, & Case DA (2005) Antechamber: An accessory software package for molecular mechanical calculations. *J Comput Chem* 25:1157-1174.

Weisblum B (1995) Erythromycin resistance by ribosome modification. *Antimicrob Agents Chemother* 39(3):577-585.

Woolstenhulme CJ, *et al.* (2013) Nascent peptides that block protein synthesis in bacteria. *Proc Natl Acad Sci USA* 110(10):E878-887.

Yang R, Cruz-Vera LR, & Yanofsky C (2009) 23S rRNA nucleotides in the peptidyl transferase center are essential for tryptophanase operon induction. *J Bacteriol* 191(11):3445-3450.

### **3. Antibiotic bound ribosome discriminates its catalytic substrates based on charge**

#### **3.1 Introduction and rationale**

The ribosome is an incredibly complex and sophisticated protein synthesis machine, which represents one of the major antibiotic targets in the bacterial cells. While many protein synthesis inhibitors completely abolish protein synthesis, some antibiotics interfere with translation in a context-specific manner. Macrolides, such as erythromycin (ERY), and its newer derivatives represent the best-studied examples of the inhibitors whose action critically depends on the amino acid sequence of the protein synthesized by the ribosome (Kannan et al., 2012, Starosta et al., 2010). Depending on the nature of the nascent protein chain and the structure of the drug, synthesis of the polypeptide can be arrested at its very early rounds, at the later stages of translation elongation, or it can be completely refractory to the action of the inhibitor. Although understanding the mode of action plays the central role in the optimizing clinical outcomes of the antibiotic treatment, the mechanistic explanation for the context specificity of macrolides is essentially lacking.

The site of action of macrolide antibiotics is located in the large ribosomal subunit. The drugs bind in the nascent peptide exit tunnel (NPET), at a short distance from the peptidyl transferase center (PTC) where catalysis of peptide bond formation takes place. Binding of the antibiotic obstructs the NPET and restricts placement of the nascent chain in the tunnel and its progression from the PTC to the tunnel exit. When the newly initiated peptide chain grows to the size of ca. 4 amino acids, it reaches the site of antibiotic binding (Arenz et al., 2014a, Arenz et al., 2014b). Synthesis of some proteins

by the drug-bound ribosome is interrupted at this stage especially if the drug, like ERY, contains a 3' cladinose sugar that protrudes into the lumen of the tunnel cavity (Dunkle et al., 2010, Bulkley et al., 2010, Schlunzen et al., 2001). However, some nascent peptides are able to bypass the antibiotic and their synthesis continues in spite of the presence of a bulky drug molecule in the NPET. Ketolide drugs, which lack C3 cladinose, are much less prone to inhibit translation at the early stages and synthesis of many proteins continues past the initial rounds of peptide bond formation (Kannan et al., 2012).

Even though macrolides do not inhibit synthesis of many proteins at the early rounds, translation of the majority of polypeptides by the drug-bound ribosome is eventually interrupted at the later stages of elongation. Strikingly, abrogation of translation does not occur randomly but, instead, drug-bound ribosomes get arrested at specific, well-defined mRNA sites. Ribosome profiling analysis carried out in Gram positive and Gram negative bacteria treated with macrolides helped to identify the major sites of such 'late' translation arrest and allowed for initial classification of the problematic sequences (Davis et al., 2014, Kannan et al., 2014). The most prevalent consensus motif for macrolide-induced arrest that emerged from these studies is the sequence R/K-X-R/K, where R and K represent arginine and lysine, respectively, and 'X' represents any amino acid. The *in vitro* biochemical testing supported the conclusion drawn from the ribosome profiling analysis that the ribosome stalls when the codon specifying the middle amino acid (X) of the motif enters the P site. Accordingly, the first residue of the consensus (R or K) represents the penultimate amino acid of the nascent peptide chain and the last consensus residue (also R or K) corresponds to the A site bound aminoacyl-tRNA (Kannan et al., 2014, Davis et al., 2014).

Importantly, the context specificity of antibiotic action is exploited by macrolide producing microorganisms as well as by bacterial pathogens for regulation of expression of the resistance genes (reviewed in Weisblum, 1995, Ramu et al., 2009, Subramanian et al., 2011). The inducible macrolide-resistance genes remain silent in the absence of antibiotic, but are activated when the inhibitor appears in the environment. Activation relies on programmed ribosome stalling at a precise, evolutionarily defined site of the regulatory upstream ORF (uORF) that precedes the resistance gene. Translation arrest of uORF translation leads to isomerization of the mRNA structure, which triggers the expression of the downstream resistance cistron. The antibiotic structure and the sequence of the leader peptide encoded in the uORF are the two main factors that determine the site of programmed translation arrest (Horinouchi et al., 1980, Gryczan et al., 1980, Vazquez-Laslop et al., 2010, Vazquez-Laslop et al., 2008, Ramu et al., 2011, Arenz et al., 2014a, Arenz et al., 2014b). Strikingly, the R/K-X-R/K sequence, identified as the major site of macrolide-induced translation arrest in cellular genes (Davis et al., 2014, Kannan et al., 2014), can be found in many regulatory uORFs of macrolide resistance genes, including the well-studied *ermDL* ORF that controls expression of the *ermD* gene (Kwak et al., 1991, Kwon et al., 2006, Hue et al., 1992, Sothiselvam et al., 2014). Genetic and biochemical analysis showed that in all the tested regulatory uORFs with the R/K-X-R/K sequence the ribosome stalls, just as it was determined for the cellular genes, when the second codon of the consensus enters the ribosomal P site (Sothiselvam et al., 2014, Almutairi et al., 2015).

One of the most unexpected aspects of the R/K-X-R/K consensus is the placement of the encoded arrest peptide segment within the ribosome. Rather than being in the

immediate vicinity of the antibiotic molecule in the NPET, the amino acid residues of the R/K-X-R/K motif are located right at the PTC active site, at a considerable distance (~8-10 Å) from the antibiotic molecule. Similarly, other stalling motifs identified in ribosome profiling experiments were also confined to the C-terminal residues of the nascent chain and the incoming amino acid (Davis et al., 2014, Kannan et al., 2014). This observation led to the unexpected conclusion that at least at the ‘late’ elongation stage, macrolides act not as ‘NPET blockers’, but rather as selective ‘PTC disrupters’ (Kannan et al., 2014). Indeed, RNA chemical probing showed that binding of macrolides to the NPET of the vacant ribosome was sufficient to allosterically induce structural changes in the PTC (Sothiselvam et al., 2014). In agreement with this view, translation of the 5'-terminally truncated *ermDL* ORF, that specifies the peptide starting with the MRLR sequence, was efficiently arrested by macrolides at the Leu3 codon, when the nascent chain was only three amino acids long, too short to reach the drug in its NPET binding site. It became clear that inhibition of translation elongation does not necessarily originate from the interactions between the nascent chain and the macrolide molecule in the NPET but rather binding of the antibiotic prompts the PTC to become more restrictive to its substrates, thus predisposing the ribosome for translation arrest when certain combinations of donor and acceptor substrates meet in the catalytic center.

While these new data called for a re-evaluation of the conventional textbook view of macrolides as indiscriminate NPET blockers, the molecular mechanisms underlying their specificity remain obscure. It is poorly understood why certain combinations of donor-acceptor substrates, defined by the identified consensus sequences, are troublesome for the drug-bound ribosome. It is also unclear, whether the changes in the

PTC induced by macrolide antibiotics exacerbate the ribosome struggle in dealing with the intrinsically problematic substrates or if, alternatively, peptide bond formation between 'easy' substrates becomes tortuous for the drug-corrupted ribosome.

In the current work, in order to gain mechanistic insights into the mode of action of macrolide antibiotics, we investigated the functional properties of the catalytic center of the drug-bound ribosome carrying the short stalled nascent MRL peptide. The lack of an extended nascent chain in this stalled complex, allowed us to dissociate the direct effects of macrolides on the PTC from those that could be triggered by direct drug-nascent peptide interactions. Reacting the ribosome-antibiotic complex carrying the minimal stalling peptide with a series of strategically designed synthetic acceptor analogs, we examined how the chemical nature of PTC substrates affects the efficiency of peptide bond formation in the macrolide-bound ribosome. We found that the size of the side chains of the amino acid residues in the donor and acceptor substrates is a contributing factor for the macrolide-induced arrest, however, it is their positive charge which is the major element rendering the consensus sequence R/K-X-R/K burdensome for the drug bound ribosome. Interestingly, we found that the model substrates that react extremely slowly in the presence of antibiotic appear to be problematic donor-acceptor pairs even for the drug-free ribosome.

### 3.2 Materials and Methods

#### **Toeprinting assay.**

Linear DNA templates (0.5–1 pmol) encoding the ORF of interest preceded by the T7 promoter sequence were generated by PCR using primers indicated in Table 3.1. The resulting templates were used to direct coupled transcription–translation in the PURExpress cell-free system (New England Biolabs). The reactions were carried out in a total volume of 5  $\mu$ L and, where indicated, were supplemented with antibiotics (50  $\mu$ M final concentration). Following 10 min incubation at 37 °C, a 5-min primer extension initiated by addition of reverse primer NV1 (Table 3.1) and 3 U of reverse transcriptase (Roche Applied Science). The cDNA products along with sequencing reactions were separated in a 6% sequencing gel and visualized with a Typhoon imager (GE).

#### ***In vitro* peptidyl transfer reaction.**

Commercially synthesized (Thermo Fisher) mRNAs encoding MRL (ATAAGGAGGAAAAAATATGAGACUU) or MAL (ATAAGGAGGAAAAAATATGGCACUU) were used for *in vitro* translation in the PURE system. The reactions containing 75 pmoles of template were supplemented with erythromycin at a final concentration of 50  $\mu$ M and with 1  $\mu$ Ci [<sup>35</sup>S]-methionine (specific activity 1175 Ci/mmol). Following 7 min incubation at 37 °C, thiostrepton was added to 50  $\mu$ M to prevent further rounds of translation. Samples were then reacted with 0.7 mM of the model ACCA-N-amino acid substrates (Table 3.2). Aliquots (5  $\mu$ l) were taken at different times and mixed with an equal volume of tricine sample buffer (Bio-Rad Laboratories). Reaction products were resolved using 16% Bis-Tris polyacrylamide gel

(Vazquez-Laslop et al., 2008 and as described in [http://openwetware.org/Sauer:bis-Tris\\_SDS\\_PAGE](http://openwetware.org/Sauer:bis-Tris_SDS_PAGE) based on US patent 6,162,338) and visualized with a Typhoon imager. Quantification of the peptidyl-tRNA bands was done using ImageJ.

### **Chemical synthesis of ACCA-amino acid conjugates.**

The synthesis of all the ACCA model substrates used in this study were done by Lukas Rigger and Sandro Neuner in collaboration with the laboratory of Dr. Ronald Micura. The description of the synthesis is detailed in Appendix C of this thesis.

**Table 3.1: Primers used in this study**

<b>Primer name</b>	<b>Primer sequence (5' to 3')</b>
T7	TAATACGACTCACTATAGGG
NV1	GGTTATAATGAATTTTGCTTATTAAC
MRLR-I-fwd	TAATACGACTCACTATAGGGCTTAAGTATAAGGAGGAAAAAATA TGAGACTTCGTTTCCCAATTACTTTGAACCAGTAAGTGATAG
MALR –I-fwd	TAATACGACTCACTATAGGGCTTAAGTATAAGGAGGAAAAAATA TGGCACTTCGTTTCCCAATTACTTTGAACCAGTAAGTGATAG
MCLR –I-fwd	TAATACGACTCACTATAGGGCTTAAGTATAAGGAGGAAAAAATA TGTGCCTTCGTTTCCCAATTACTTTGAACCAGTAAGTGATAG
MDLR –I-fwd	TAATACGACTCACTATAGGGCTTAAGTATAAGGAGGAAAAAATAT GGATCTTCGTTTCCCAATTACTTTGAACCAGTAAGTGATAG
MELR –I-fwd	TAATACGACTCACTATAGGGCTTAAGTATAAGGAGGAAAAAATAT GGAACCTTCGTTTCCCAATTACTTTGAACCAGTAAGTGATAG
MFLR –I-fwd	TAATACGACTCACTATAGGGCTTAAGTATAAGGAGGAAAAAATA TGTTTCTTCGTTTCCCAATTACTTTGAACCAGTAAGTGATAG
MGLR –I-fwd	TAATACGACTCACTATAGGGCTTAAGTATAAGGAGGAAAAAATAT GGGTCTTCGTTTCCCAATTACTTTGAACCAGTAAGTGATAG
MHLR –I-fwd	TAATACGACTCACTATAGGGCTTAAGTATAAGGAGGAAAAAATA TGCACCTTCGTTTCCCAATTACTTTGAACCAGTAAGTGATAG
MILR –W-fwd	TAATACGACTCACTATAGGGCTTAAGTATAAGGAGGAAAAAATAT GATTCTTCGTTTCCCAATTACTTTGAACCAGTAAGTGATAG
MKLR –I-fwd	TAATACGACTCACTATAGGGCTTAAGTATAAGGAGGAAAAAATAT GAAACTTCGTTTCCCAATTACTTTGAACCAGTAAGTGATAG
MLLR –I-fwd	TAATACGACTCACTATAGGGCTTAAGTATAAGGAGGAAAAAATA TGCTTCTTCGTTTCCCAATTACTTTGAACCAGTAAGTGATAG
MMLR –I-fwd	TAATACGACTCACTATAGGGCTTAAGTATAAGGAGGAAAAAATAT GATGCTTCGTTTCCCAATTACTTTGAACCAGTAAGTGATAG
MNLR –I-fwd	TAATACGACTCACTATAGGGCTTAAGTATAAGGAGGAAAAAATAT GAACCTTCGTTTCCCAATTACTTTGAACCAGTAAGTGATAG
MPLR –I-fwd	TAATACGACTCACTATAGGGCTTAAGTATAAGGAGGAAAAAATA TGCCACTTCGTTTCCCAATTACTTTGAACCAGTAAGTGATAG
MQLR –I-fwd	TAATACGACTCACTATAGGGCTTAAGTATAAGGAGGAAAAAATAT GCAGCTTCGTTTCCCAATTACTTTGAACCAGTAAGTGATAG
MSLR –I-fwd	TAATACGACTCACTATAGGGCTTAAGTATAAGGAGGAAAAAATA TGCACTTCGTTTCCCAATTACTTTGAACCAGTAAGTGATAG
MTLR –I-fwd	TAATACGACTCACTATAGGGCTTAAGTATAAGGAGGAAAAAATAT GACACTTCGTTTCCCAATTACTTTGAACCAGTAAGTGATAG
MVLR –I-fwd	TAATACGACTCACTATAGGGCTTAAGTATAAGGAGGAAAAAATAT GGTACTTCGTTTCCCAATTACTTTGAACCAGTAAGTGATAG
MWLR –I-fwd	TAATACGACTCACTATAGGGCTTAAGTATAAGGAGGAAAAAATAT GTGGCTTCGTTTCCCAATTACTTTGAACCAGTAAGTGATAG
MYLR –I-fwd	TAATACGACTCACTATAGGGCTTAAGTATAAGGAGGAAAAAATA TGTATCTTCGTTTCCCAATTACTTTGAACCAGTAAGTGATAG
MRAR-I-fwd	TAATACGACTCACTATAGGGCTTAAGTATAAGGAGGAAAAAATAT GAGAGCACGTTTCCCAATTACTTTGAACCAGTAAGTGATAG
MRCR-I-fwd	TAATACGACTCACTATAGGGCTTAAGTATAAGGAGGAAAAAATAT GAGATGCCGTTTCCCAATTACTTTGAACCAGTAAGTGATAG
MRDR-I-fwd	TAATACGACTCACTATAGGGCTTAAGTATAAGGAGGAAAAAATAT

	GAGAGATCGTTTCCCAATTACTTTGAACCAGTAAGTGATAG
MRER-I-fwd	TAATACGACTCACTATAGGGCTTAAGTATAAGGAGGAAAAAATAT GAGAGAACGTTTCCCAATTACTTTGAACCAGTAAGTGATAG
MRFR-I-fwd	TAATACGACTCACTATAGGGCTTAAGTATAAGGAGGAAAAAATAT GAGATTTTCGTTTCCCAATTACTTTGAACCAGTAAGTGATAG
MRGR-I-fwd	TAATACGACTCACTATAGGGCTTAAGTATAAGGAGGAAAAAATAT GAGAGGTCGTTTCCCAATTACTTTGAACCAGTAAGTGATAG
MRHR-I-fwd	TAATACGACTCACTATAGGGCTTAAGTATAAGGAGGAAAAAATAT GAGACACCGTTTCCCAATTACTTTGAACCAGTAAGTGATAG
MRIR-W-fwd	TAATACGACTCACTATAGGGCTTAAGTATAAGGAGGAAAAAATAT GAGAATTCGTTTCCCATGGACTTTGAACCAGTAAGTGATAG
MRKR-I-fwd	TAATACGACTCACTATAGGGCTTAAGTATAAGGAGGAAAAAATAT GAGAAAACGTTTCCCAATTACTTTGAACCAGTAAGTGATAG
MRMR-I-fwd	TAATACGACTCACTATAGGGCTTAAGTATAAGGAGGAAAAAATAT GAGAATGCGTTTCCCAATTACTTTGAACCAGTAAGTGATAG
MRNR-I-fwd	TAATACGACTCACTATAGGGCTTAAGTATAAGGAGGAAAAAATAT GAGAAACCGTTTCCCAATTACTTTGAACCAGTAAGTGATAG
MRPR-I-fwd	TAATACGACTCACTATAGGGCTTAAGTATAAGGAGGAAAAAATAT GAGACCACGTTTCCCAATTACTTTGAACCAGTAAGTGATAG
MRQR-I-fwd	TAATACGACTCACTATAGGGCTTAAGTATAAGGAGGAAAAAATAT GAGACAGCGTTTCCCAATTACTTTGAACCAGTAAGTGATAG
MRRR-I-fwd	TAATACGACTCACTATAGGGCTTAAGTATAAGGAGGAAAAAATAT GAGACGGCGTTTCCCAATTACTTTGAACCAGTAAGTGATAG
MRSR-I-fwd	TAATACGACTCACTATAGGGCTTAAGTATAAGGAGGAAAAAATAT GAGATCACGTTTCCCAATTACTTTGAACCAGTAAGTGATAG
MRTR-I-fwd	TAATACGACTCACTATAGGGCTTAAGTATAAGGAGGAAAAAATAT GAGAACACGTTTCCCAATTACTTTGAACCAGTAAGTGATAG
MRVR-I-fwd	TAATACGACTCACTATAGGGCTTAAGTATAAGGAGGAAAAAATAT GAGAGTACGTTTCCCAATTACTTTGAACCAGTAAGTGATAG
MRWR-I-fwd	TAATACGACTCACTATAGGGCTTAAGTATAAGGAGGAAAAAATAT GAGATGGCGTTTCCCAATTACTTTGAACCAGTAAGTGATAG
MRYR-I-fwd	TAATACGACTCACTATAGGGCTTAAGTATAAGGAGGAAAAAATAT GAGATATCGTTTCCCAATTACTTTGAACCAGTAAGTGATAG
MRLA-I-fwd	TAATACGACTCACTATAGGGCTTAAGTATAAGGAGGAAAAAATAT GAGACTTGCATTCCCAATTACTTTGAACCAGTAAGTGATAG
MRLC-I-fwd	TAATACGACTCACTATAGGGCTTAAGTATAAGGAGGAAAAAATAT GAGACTTTGCTTCCCAATTACTTTGAACCAGTAAGTGATAG
MRLD-I-fwd	TAATACGACTCACTATAGGGCTTAAGTATAAGGAGGAAAAAATAT GAGACTTGATTTCCCAATTACTTTGAACCAGTAAGTGATAG
MRL E-I-fwd	TAATACGACTCACTATAGGGCTTAAGTATAAGGAGGAAAAAATAT GAGACTTGAATTTCCCAATTACTTTGAACCAGTAAGTGATAG
MRLF-I-fwd	TAATACGACTCACTATAGGGCTTAAGTATAAGGAGGAAAAAATAT GAGACTTTTTTTTCCCAATTACTTTGAACCAGTAAGTGATAG
MRLG-I-fwd	TAATACGACTCACTATAGGGCTTAAGTATAAGGAGGAAAAAATAT GAGACTTGGTTTCCCAATTACTTTGAACCAGTAAGTGATAG
MRLH-I-fwd	TAATACGACTCACTATAGGGCTTAAGTATAAGGAGGAAAAAATAT GAGACTTCACTTCCCAATTACTTTGAACCAGTAAGTGATAG
MRLI-W-fwd	TAATACGACTCACTATAGGGCTTAAGTATAAGGAGGAAAAAATAT GAGACTTATTTTCCCATGGACTTTGAACCAGTAAGTGATAG
MRLK-I-fwd	TAATACGACTCACTATAGGGCTTAAGTATAAGGAGGAAAAAATAT GAGACTTAAATTTCCCAATTACTTTGAACCAGTAAGTGATAG
MRL L-I-fwd	TAATACGACTCACTATAGGGCTTAAGTATAAGGAGGAAAAAATAT GAGACTTCTTTTCCCAATTACTTTGAACCAGTAAGTGATAG
MRLM-I-fwd	TAATACGACTCACTATAGGGCTTAAGTATAAGGAGGAAAAAATAT GAGACTTATGTTCCCAATTACTTTGAACCAGTAAGTGATAG

MRLN-I-fwd	TAATACGACTCACTATAGGGCTTAAGTATAAGGAGGAAAAAATAT GAGACTTAACTTCCCAATTACTTTGAACCAGTAAGTGATAG
MRLP-I-fwd	TAATACGACTCACTATAGGGCTTAAGTATAAGGAGGAAAAAATAT GAGACTTCCATTCCCAATTACTTTGAACCAGTAAGTGATAG
MRLQ-I-fwd	TAATACGACTCACTATAGGGCTTAAGTATAAGGAGGAAAAAATAT GAGACTTCAGTTCCCAATTACTTTGAACCAGTAAGTGATAG
MRLS-I-fwd	TAATACGACTCACTATAGGGCTTAAGTATAAGGAGGAAAAAATAT GAGACTTTCATTCCCAATTACTTTGAACCAGTAAGTGATAG
MRLT-I-fwd	TAATACGACTCACTATAGGGCTTAAGTATAAGGAGGAAAAAATAT GAGACTTACATTCCCAATTACTTTGAACCAGTAAGTGATAG
MRLV-I-fwd	TAATACGACTCACTATAGGGCTTAAGTATAAGGAGGAAAAAATAT GAGACTTGTATTCCCAATTACTTTGAACCAGTAAGTGATAG
MRLW-I-fwd	TAATACGACTCACTATAGGGCTTAAGTATAAGGAGGAAAAAATAT GAGACTTTGGTTCCCAATTACTTTGAACCAGTAAGTGATAG
MRLY-I-fwd	TAATACGACTCACTATAGGGCTTAAGTATAAGGAGGAAAAAATAT GAGACTTTATTCCCAATTACTTTGAACCAGTAAGTGATAG
MRLR-Mut-rev	GGTTATAATGAATTTTGCTTATTAACGATAGAATTCTATCACTTAC TGGTTCAA
MDLD-I-fwd	TAATACGACTCACTATAGGGCTTAAGTATAAGGAGGAAAAAATAT GGATCTTGATTTCCTCAATTACTTTGAACCAGTAAGTGATAG
MELE-I-fwd	TAATACGACTCACTATAGGGCTTAAGTATAAGGAGGAAAAAATAT GGAACTTGAATTCCCAATTACTTTGAACCAGTAAGTGATAG
RLR-V1-fwd	TAATACGACTCACTATAGGGCTTAAGTATAAGGAGGAAAAAATAT GCGCCTGCGATTCCCAATTACTTTGAACCAGTAAGTGATAG
RLR-V2-fwd	TAATACGACTCACTATAGGGCTTAAGTATAAGGAGGAAAAAATAT GCGACTACGCTTCCCAATTACTTTGAACCAGTAAGTGATAG
RLR-V3-fwd	TAATACGACTCACTATAGGGCTTAAGTATAAGGAGGAAAAAATAT GAGGTTGCGGTTCCCAATTACTTTGAACCAGTAAGTGATAG
MKAK-I-fwd	TAATACGACTCACTATAGGGCTTAAGTATAAGGAGGAAAAAATAT GAAGGCAAATTCCTCAATTACTTTGAACCAGTAAGTGATAG
MKCK-I-fwd	TAATACGACTCACTATAGGGCTTAAGTATAAGGAGGAAAAAATAT GAAGTGCAAATTCCTCAATTACTTTGAACCAGTAAGTGATAG
MKDK-I-fwd	TAATACGACTCACTATAGGGCTTAAGTATAAGGAGGAAAAAATAT GAAGGATAAATTCCTCAATTACTTTGAACCAGTAAGTGATAG
MKEK-I-fwd	TAATACGACTCACTATAGGGCTTAAGTATAAGGAGGAAAAAATAT GAAGGAAAAATTCCTCAATTACTTTGAACCAGTAAGTGATAG
MKFK-I-fwd	TAATACGACTCACTATAGGGCTTAAGTATAAGGAGGAAAAAATAT GAAGTTAAATTCCTCAATTACTTTGAACCAGTAAGTGATAG
MKGG-I-fwd	TAATACGACTCACTATAGGGCTTAAGTATAAGGAGGAAAAAATAT GAAGGGTAAATTCCTCAATTACTTTGAACCAGTAAGTGATAG
MKHK-I-fwd	TAATACGACTCACTATAGGGCTTAAGTATAAGGAGGAAAAAATAT GAAGCACAAATTCCTCAATTACTTTGAACCAGTAAGTGATAG
MKIK-W-fwd	TAATACGACTCACTATAGGGCTTAAGTATAAGGAGGAAAAAATAT GAAGATTAATTCCTCATGGACTTTGAACCAGTAAGTGATAG
MKKK-I-fwd	TAATACGACTCACTATAGGGCTTAAGTATAAGGAGGAAAAAATAT GAAGAAGAAATTCCTCAATTACTTTGAACCAGTAAGTGATAG
MKLL-I-fwd	TAATACGACTCACTATAGGGCTTAAGTATAAGGAGGAAAAAATAT GAAGCTTAAATTCCTCAATTACTTTGAACCAGTAAGTGATAG
MKMK-I-fwd	TAATACGACTCACTATAGGGCTTAAGTATAAGGAGGAAAAAATAT GAAGATGAAATTCCTCAATTACTTTGAACCAGTAAGTGATAG
MKNK-I-fwd	TAATACGACTCACTATAGGGCTTAAGTATAAGGAGGAAAAAATAT GAAGAACAATTCCTCAATTACTTTGAACCAGTAAGTGATAG
MKPK-I-fwd	TAATACGACTCACTATAGGGCTTAAGTATAAGGAGGAAAAAATAT GAAGCCAAATTCCTCAATTACTTTGAACCAGTAAGTGATAG

MKQK-I-fwd	TAATACGACTCACTATAGGGCTTAAGTATAAGGAGGAAAAAATAT GAAGCAGAAATTCCCAATTACTTTGAACCAGTAAGTGATAG
MKRK-I-fwd	TAATACGACTCACTATAGGGCTTAAGTATAAGGAGGAAAAAATAT GAAGCGTAAATTCCCAATTACTTTGAACCAGTAAGTGATAG
MKSK-I-fwd	TAATACGACTCACTATAGGGCTTAAGTATAAGGAGGAAAAAATAT GAAGTCAAAATTCCCAATTACTTTGAACCAGTAAGTGATAG
MKTK-I-fwd	TAATACGACTCACTATAGGGCTTAAGTATAAGGAGGAAAAAATAT GAAGACAAAATTCCCAATTACTTTGAACCAGTAAGTGATAG
MKVK-I-fwd	TAATACGACTCACTATAGGGCTTAAGTATAAGGAGGAAAAAATAT GAAGGTAAAATTCCCAATTACTTTGAACCAGTAAGTGATAG
MKWK-I-fwd	TAATACGACTCACTATAGGGCTTAAGTATAAGGAGGAAAAAATAT GAAGTGAAAATTCCCAATTACTTTGAACCAGTAAGTGATAG
MKYK-I-fwd	TAATACGACTCACTATAGGGCTTAAGTATAAGGAGGAAAAAATAT GAAGTATAAATTCCCAATTACTTTGAACCAGTAAGTGATAG

### 3.3 **Results**

#### 3.3.1 **Antibiotic-mediated translation arrest at the MRLR ORF is independent of the mRNA sequence and tRNA structure.**

Our previous experiments showed that macrolide antibiotics arrest translation of the truncated *ermDL* gene (MRLR...), when the Leu<sub>3</sub> codon is placed in the ribosomal P site and Arg<sub>4</sub> codon enters the decoding (A) site (Sothiselvam et al., 2014). In order to test whether macrolide-induced ribosome stalling is influenced by the structures of mRNA or tRNA, we changed codons 2-4 of this truncated *ermDL* template to several different combinations of synonymous triplets, that not only alter the mRNA sequence, but also direct binding of different aminoacyl-tRNAs isoacceptors (Figure. 3.1). Toeprinting analysis showed that these alterations in mRNA sequence had minimal effect on the efficiency of the ERY-directed arrest (Figure. 3.1). Therefore, neither precise mRNA sequence, nor the structure of the tRNA body affect macrolide-dependent ribosome stalling at the truncated *ermDL* ORF, leaving the nature of the nascent peptide sequence as the likely primary determinant of the translation arrest.

#### 3.3.2 **Only the templates encoding Arg or Lys in the second and fourth codons are conducive to ERY-induced translation arrest.**

In the ribosome stalled at the truncated *ermDL* template, the MRL tripeptide esterifies the P site tRNA<sup>Leu</sup> and the A site codon specifies for Arg-tRNA. We wanted to understand how the chemical nature of the peptidyl donor and aminoacyl acceptor affects

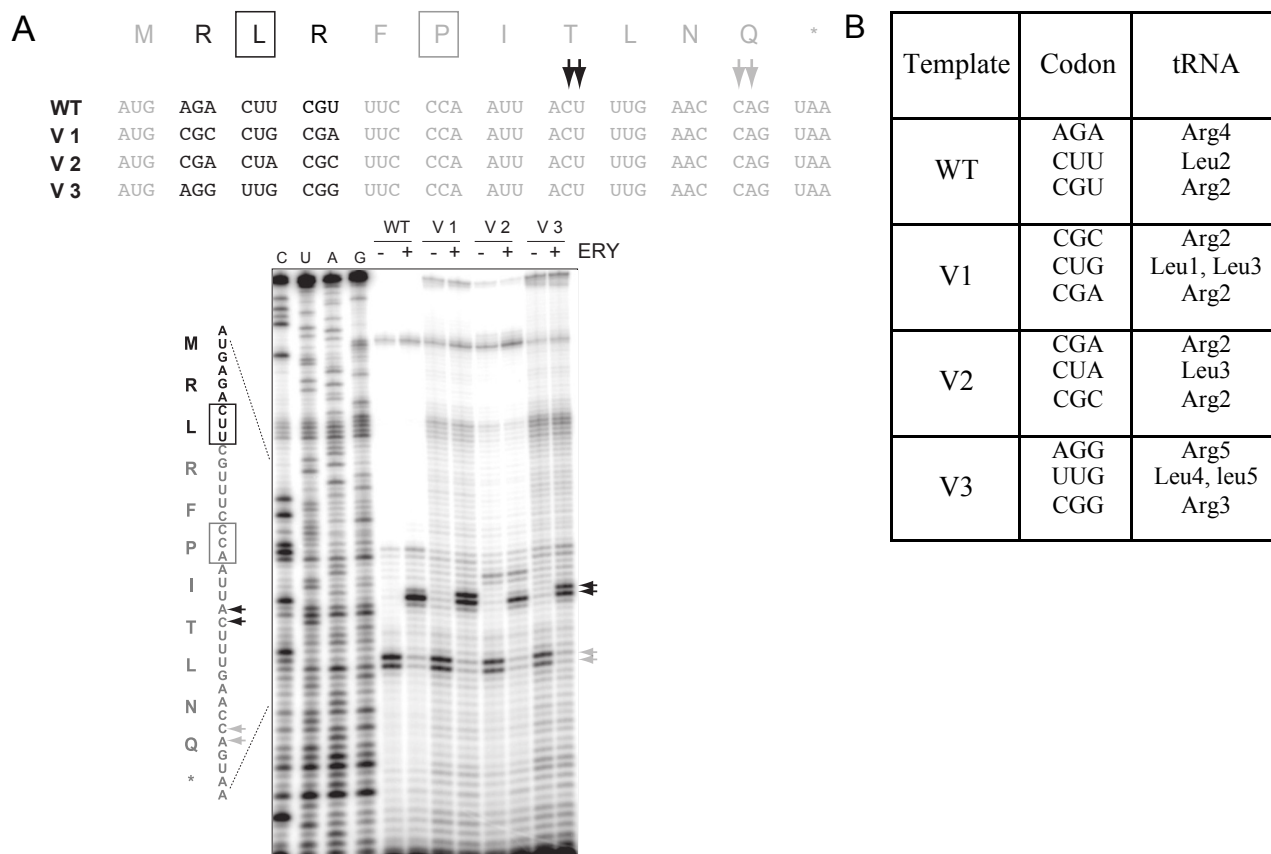


**Figure 3.1. ERY dependent translation arrest in the MRLR ORF is not dependent on the mRNA structure or the nature of its tRNA decoders.** (A) Amino acid and nucleotide sequences of the in vitro translation templates of the wt MRLR ORF and its variants (V1, V2, and V3) containing synonymous codons, and toeprinting analysis for ERY dependent translation arrest at the Leu-3 codon of the ORFs. The bands corresponding to ribosomes stalled with its P-site at the Leu-3 codon (black box) are marked with black arrows. The gray arrows indicate the toeprint band produced by the ribosomes that do not stall in response to ERY but are trapped at the downstream Pro-6 codon (gray box) due to the lack of Ile-tRNA in the reaction (because of the presence of the IleRS inhibitor mupirocin). Sequencing lanes are marked as C, U, A, G. Gel is representative of two independent experiments. (B) The different synonymous codons and corresponding tRNA(s) that decode them in each template are indicated.

peptide bond formation in the PTC of the drug-bound ribosome. First, we investigated the contributions of the second and third amino acids of the peptidyl moiety of the donor substrate, MRL-tRNA, to macrolide-dependent translation arrest. Codons 2 and 3 of the MRLR ORF, which encode the penultimate and the C-terminal residues of the nascent peptide, were mutated to specify all other 19 amino acids, and ERY-induced ribosome stalling in these templates was analyzed by toeprinting. Most of the alterations of the penultimate amino acid (Arg<sub>2</sub>) abolished stalling. Only the Arg<sub>2</sub>-to-Lys replacement maintained efficient translation arrest (Figure. 3.2A). In contrast, the nature of the C-terminal residue was of a much lesser importance: only changes of Leu<sub>3</sub> to Trp or Pro showed a somewhat increased bypass of the arrest site, whereas the majority of the mutants directed ribosome stalling as readily as the wt (Figure. 3.2B).

We then examined the role of the acceptor substrate. By mutating the fourth codon of the MRLR ORF we directed binding of the A site to aminoacyl-tRNAs linked to any of the 20 different amino acids. Similar to the effect observed for the penultimate position of the nascent peptide, only the Arg<sub>4</sub>-to-Lys (and to a much lesser extent the Arg<sub>4</sub>-to-Trp) substitution was conducive to ERY-induced stalling (Figure. 3.2C). Thus, ERY promotes formation of a stable stalled ribosome complex preferentially on those short templates where the second and fourth codons specify either Arg or Lys.

Because individual substitutions of Arg<sub>2</sub> or Arg<sub>4</sub> with Lys were compatible with ERY-induced stalling, we also tested whether simultaneous replacement of both Arg codons with Lys would still be conducive to the translation arrest. Indeed, we found that the majority of the ribosomes that reached the third codon of the MKLK template got arrested (Figure. 3.4, black arrowheads, lane 'L'). In addition, similar to the results

obtained with the MRLR template, mutations of the Leu<sub>3</sub> codon, sandwiched between the two Lys codons in the MKLK template, had little effect on the ERY-induced arrest (Figure. 3.4). An exception was the MKPK sequence. In this template, drug-bound ribosomes could not reach the 3<sup>rd</sup> codon because they stalled at the Lys<sub>2</sub> codon (Figure. 3.4, lane 'P'), likely due to the reported propensity of macrolides to inhibit peptide bond formation between a donor peptide ending with lysine and prolyl-tRNA (Kannan et al., 2014, Davis et al., 2014).

Altogether, our mutational studies showed that the antibiotic bound in the ribosomal exit tunnel efficiently and specifically prevents the transfer of the nascent peptides, which have Arg or Lys in their penultimate position, to an Arg or Lys acceptor.

### **3.3.3 The presence of Arg or Lys in the donor and acceptor substrates is critical for arrest of translation by diverse macrolide antibiotics.**

Regulatory stalling peptides of some *erm* genes exhibit strong antibiotic selectivity so that only C3 cladinose-containing macrolides (e.g. ERY), but not cladinose-lacking ketolides can direct ribosome stalling (Vazquez-Laslop et al., 2008, Vazquez-Laslop et al., 2011). In contrast, both cladinose-containing macrolides as well as ketolides arrest translation of the truncated ErmDL (Sothiselvam et al., 2014). We asked whether the identity of the second and fourth codons of the MRLR template, which are critical for ERY-induced arrest, are equally important for ribosome stalling directed by other macrolide antibiotics. Therefore, we tested two other drugs: the fluoro-ketolide solithromycin (SOL) and the cladinose-containing 15-member ring, azithromycin (AZI) (Figure. 3.5A).

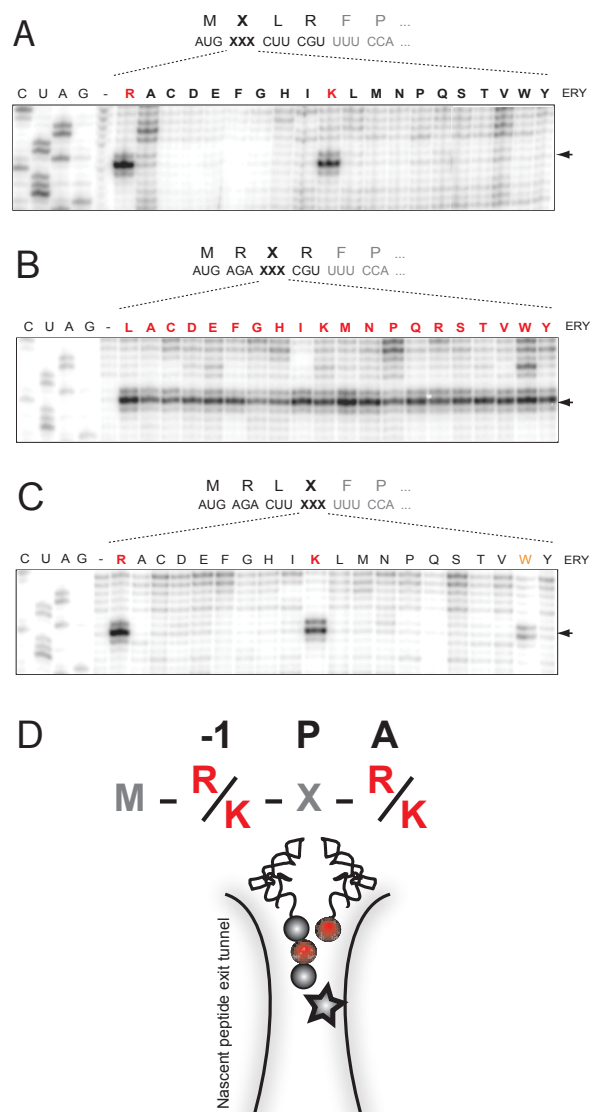


**Figure 3.2. Amino acid residues critical for ERY dependent translation arrest in MRLR ORF. Amino acid residues critical for ERY-dependent translation arrest in the MRLR sequence. (A-C) Mutational analysis of the residues 2 (A), 3 (B) and 4 (C) in the MRLR sequence. Arg<sub>2</sub>, Leu<sub>3</sub>, and Arg<sub>4</sub> codons of the wt MRLR template were individually mutated to code for all other 19 natural amino acids. The mutagenized codon is marked with X in the sequences over the corresponding gel. ERY-mediated translation arrest was evaluated by toeprinting analysis. The toeprint band produced by the stalled ribosomes, whose P-site is occupied by codon-3 of the templates, is indicated with an arrow. The control sample where ERY was absent is marked with '-'. Sequencing lanes prepared using wt template are indicated. Amino acids conducive to ERY-dependent stalling are colored red. Shown gels are representative of two independent experiments. Full gels are shown in Figure. 3.3. (D) Schematic representation of the stalled ribosome with MRL-tRNA in the P-site and Arg-tRNA in the A-site. Antibiotic is represented as a star. Antibiotic-mediated stalling is only supported when the penultimate amino acid of the nascent peptide and the incoming amino acid esterifying the A site tRNA are Arg or Lys residues (indicated with red circles).**

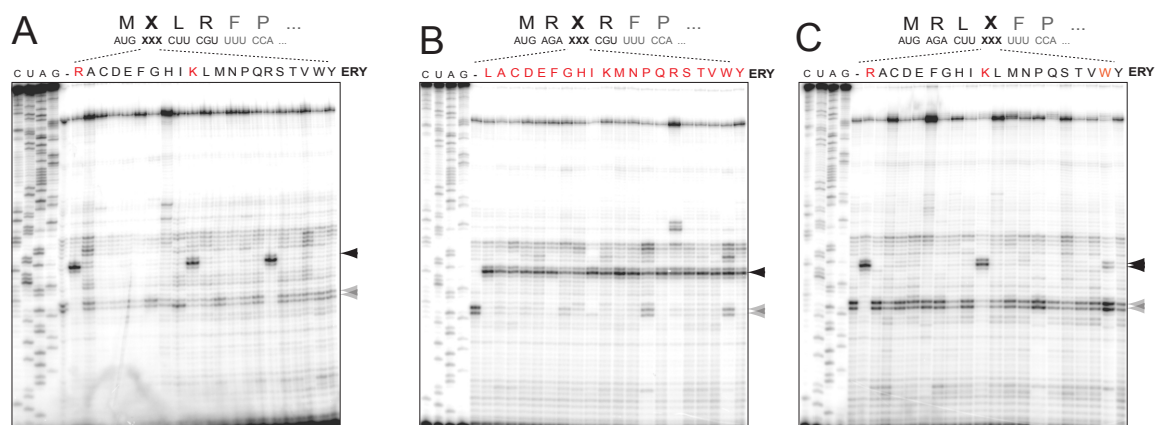


**Figure 3.3. ERY dependent translation arrest in mutants of the MRLR sequence.** Representative full-size toeprinting analysis gels (from two independent experiments) used to generate the gel panels shown in Figure. 3.2. Black arrows indicate ERY dependent translation arrest at codon 3 of the templates. The toeprint band marked with gray arrows correspond to the ribosomes that do not stall at codon 3 but are captured at the downstream Pro-6 codon due to lack of charged Ile-tRNA in the translation reactions because they contain the IleRS inhibitor mupirocin or indolmycin, TrpRS inhibitor (only in lanes marked 'I'). The lane of the control sample with no ERY is marked as '-'. Sequencing lanes are marked as C, U, A, G.

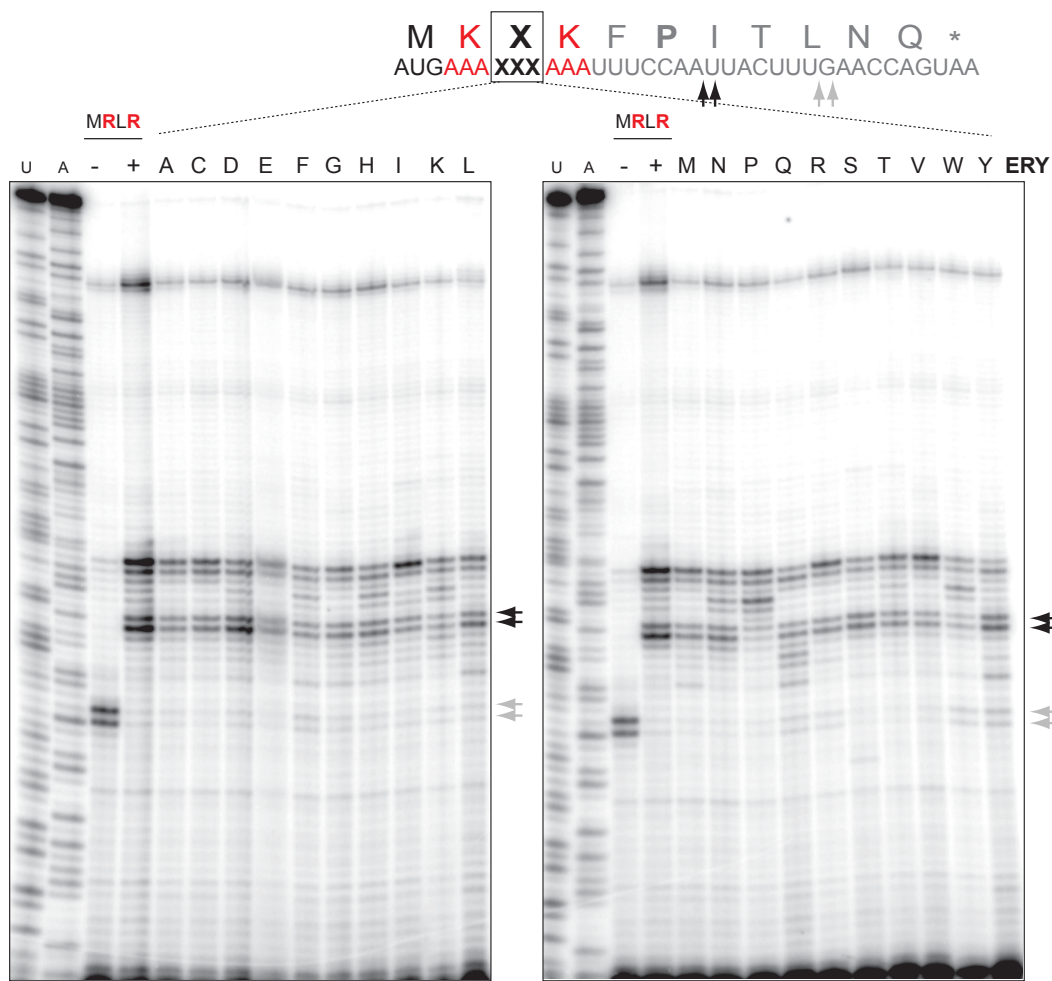


**Figure 3.4. ERY-mediated translation arrest is supported by the MKXX sequence regardless of the identity of the codon 3 of the ORF.** Toeprinting analysis for ERY mediated arrest at the MKLK ORF or its codon 3 variants. Leu-3 codon (denoted with xxx) of the template for *in vitro* translation was mutagenized to code for all other 19 amino acids. Black arrows indicate ERY dependent translation arrest at codon-3. Toeprint samples for ERY-mediated stalling at the original MRLR ORF (indicated as RLR) were included for comparison. The non-stalled ribosomes captured at the downstream Pro codon due to the presence of mupirocin, an IleRS inhibitor or indolmycin, a TrpRS inhibitor ( used in the lane marked 'I') produced the band denoted by gray arrows. Sequencing lanes are marked as U, A. Gels are representative of two independent experiments.

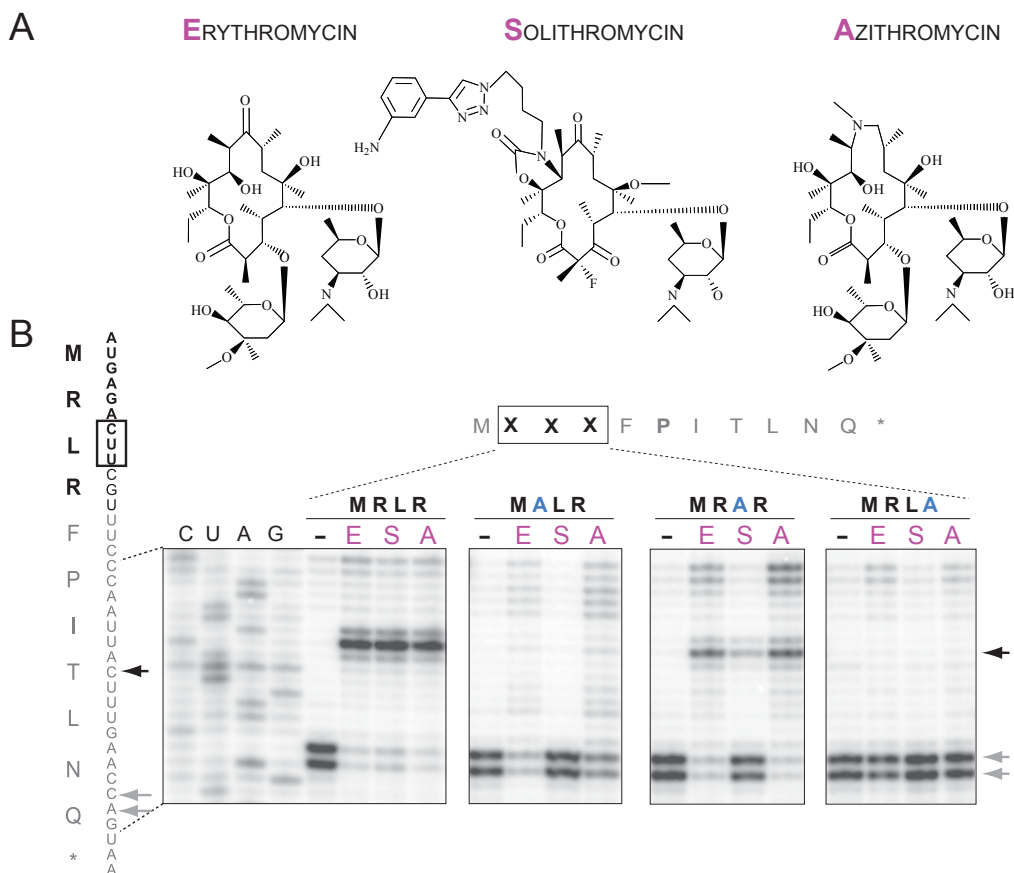


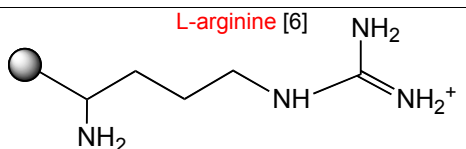
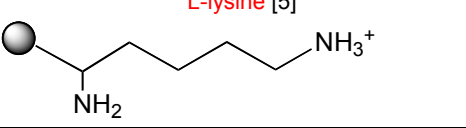
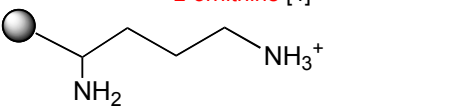
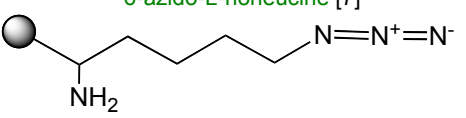
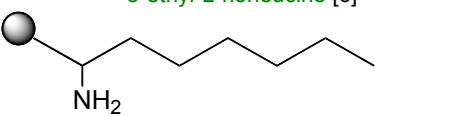
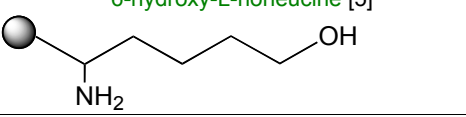
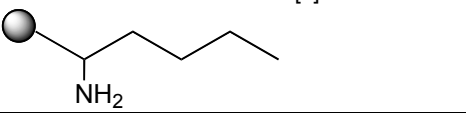
**Figure 3.5. Translation arrest triggered by diverse macrolides is similarly affected by alanine mutations of the MRLR sequence.** (A) Chemical structures of erythromycin (ERY), solithromycin (SOL), and azithromycin (AZI). (B) Toeprinting analysis for drug-mediated arrest in templates with alanine substitutions for Arg-2, Leu-3, or Arg-3 of the MRLR sequence. Black arrows indicate ERY, AZI or SOL dependent translation arrest at codon-3 of the templates. The toeprint band produced by ribosomes that do not stall in response to macrolides but are captured at the downstream Pro-6 codon is indicated by gray arrows. Sequencing lanes are marked as C, U, A, G. Gels are representative of two independent experiments.

Similar to the effects observed with ERY, the mutations of Arg<sub>2</sub> or Arg<sub>4</sub> to Ala completely abolished arrest induced by SOL or AZI. Furthermore, similar to the effect on ERY-mediated arrest, altering the third codon (Leu) to Ala had no effect on AZI-induced arrest, even though this mutation allowed for some read-through of the SOL-bound ribosome (Figure. 3.5B). We concluded that the nature of the penultimate residue of the short nascent peptide and the incoming amino acid are the most critical for arrest induced by a broad range of macrolide antibiotics.

#### **3.3.4 Arg- and Lys- acceptor substrate analogs react poorly with the MRL-tRNA donor in the presence and in the absence of antibiotic.**

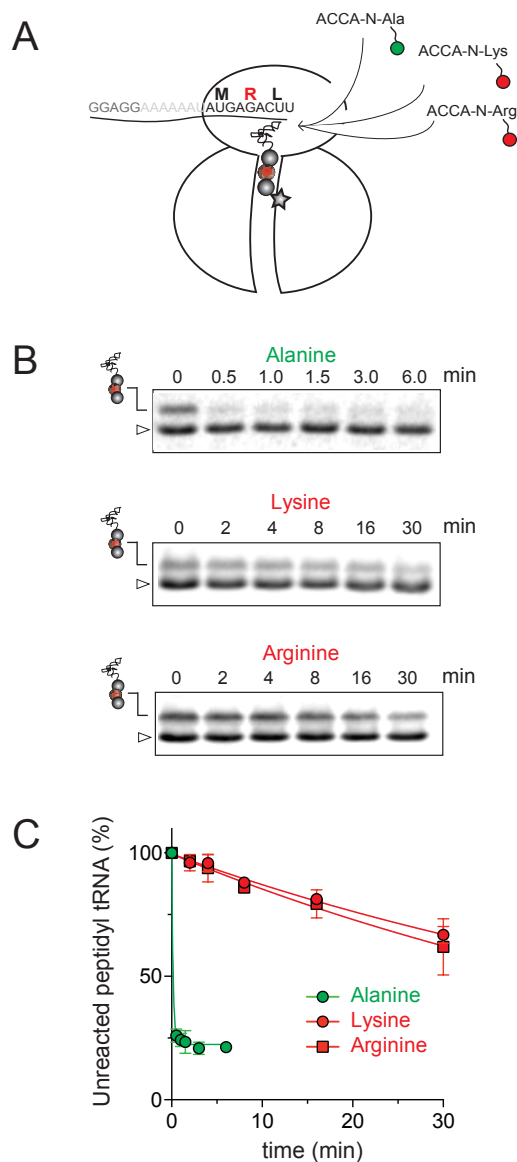
The results presented above strongly suggest that the ribosome with a macrolide antibiotic bound in the exit tunnel stalls when it needs to catalyze the transfer of tripeptides MRX or MKX to an Arg or Lys acceptor. In order to substantiate this conclusion, we followed the kinetics of peptide bond formation between the donor MRL-tRNA and different model acceptor substrates. For these experiments, we synthesized chemically stable substrates ACCA-N-X mimicking the aminoacyl-tRNA acceptor end (Table 3.2). Binding of these substrates to the ribosomal A site is independent of EF-Tu or mRNA codon and their acceptor ability depends exclusively on the nature of the amino acid residue. In the initial series of experiments, we used analogs that contained natural amino acid residues either conduce stalling (X = Arg or Lys) or abolish the arrest (X = Ala) (Table 3.2).

Table 3.2: Peptidyl transfer reaction with model A site substrates

Acceptor Substrate <sup>(a)</sup>	Donor Substrate			
	MRL		MAL	
	No drug $k_{app}$ (min <sup>-1</sup> )	ERY $k_{app}$ (min <sup>-1</sup> )	No drug $k_{app}$ (min <sup>-1</sup> )	ERY $k_{app}$ (min <sup>-1</sup> )
L-arginine [6] 	0.09 ± 0.15	0.01 ± 0.02	0.96 ± 0.23	0.87 ± 0.21
L-lysine [5] 	0.15 ± 0.03	0.01 ± 0.01	0.74 ± 0.14	1.17 ± 0.23
L-ornithine [4] 	0.08 ± 0.02	< 0.01 <sup>c)</sup>	1.03 ± 0.29	0.81 ± 0.22
6-azido-L-norleucine [7] 	> 1.8 <sup>b)</sup>	0.32 ± 0.08	> 1.8 *	> 1.8 *
5-ethyl-L-norleucine [6] 	> 1.8 *	0.31 ± 0.07	> 1.8 *	> 1.8 *
6-hydroxy-L-norleucine [5] 	> 1.8 *	0.34 ± 0.10	> 1.8 *	> 1.8 *
L-norleucine [4] 	> 1.8 *	> 1.8 *	> 1.8 *	> 1.8 *
L-alanine [1] 	> 1.8 *	> 1.8 *	> 1.8 *	> 1.8 *

(a) The gray balls represent ACCA moiety

The ribosome/mRNA/MRL-tRNA complex was prepared by translating a synthetic tri-codon MRL mRNA in the PURE cell-free translation system (Shimizu et al., 2001). Because the mRNA lacks the stop codon, the ribosome stalls at the third codon with the tripeptidyl-tRNA bound in the P site and a vacant A site regardless of the presence of ERY (Figure. 3.6A). The stalled ribosome complexes were then mixed with high concentrations (0.7 mM) of the acceptor substrates and the progression of the peptidyl transfer reaction was monitored by quantifying the amount of unreacted MRL-tRNA<sup>Leu</sup> resolved in Bis-Tris polyacrylamide gels (Figure. 3.6B and Figure. 3.8). Upon addition of the ACCA-N-Ala acceptor substrate, irrespective of the presence of ERY, the reaction was completed within 30 s (the shortest incubation time we could reliably measure with our experimental set-up) (apparent rate constant  $k_{app} > 1.8 \text{ min}^{-1}$ ) (Figure. 3.6B and C, Table 3.2, Figure. 3.8). This indicates that the drug-free and ERY-bound ribosomes efficiently catalyze transfer of MRL to the non-stalling Ala acceptor. In striking contrast, in the presence of ERY the majority of MRL-tRNA remained unreacted with the ACCA-N-Arg or ACCA-N-Lys acceptors even after 30 min of incubation (Figure. 3.6B,C). Interestingly, even though in the absence of the antibiotic the reaction with these analogs accelerated nearly 10-fold ( $k_{app} = 0.9\text{-}1.5 \text{ min}^{-1}$ ), it remained notably slower in comparison with the ACCA-N-Ala substrate (Table 3.2 and Figure. 3.8A and B). These results show that the transfer of the MRL donor to the Arg- or Lys- acceptors is intrinsically difficult for the ribosome but the presence of the antibiotic in the exit tunnel dramatically exacerbates the problem, essentially halting peptide bond formation.



**Figure 3.6. Arg and Lys are poor acceptors of the MRL-peptide in the stalled ribosome.** (A) Cartoon illustrating the experimental design: the ribosomes carrying ERY in the NPET and MRL-tRNA<sup>Leu</sup> in the P site and having an empty A-site are reacted with the model ACCA-N-X acceptor substrates. (B) Gel electrophoresis analysis of the remaining [<sup>35</sup>S]-MRL-tRNA<sup>Leu</sup> upon reaction with ACCA-N-Ala, ACCA-N-Lys or ACCA-N-Arg in the presence of ERY. The band marked with an open triangle corresponds to fMet-tRNA<sup>fMet</sup> present in the reaction mixture. (C) Quantification of the amount of unreacted MRL-tRNA<sup>Leu</sup> over the time course of the reaction estimated from the gels in B. The amount of MRL-tRNA<sup>Leu</sup> prior to addition of the A-site substrates (0 min) was set as 100%. Error bars show deviation from the mean in two independent experiments.

### **3.3.5 The positive charge of the A site substrates is the predominant factor that makes them poor acceptors of the MRL peptide.**

Arg and Lys are unique among 20 natural amino acids because they contain the longest side chains that are positively charged at physiological pH. We considered that either size, the charge, or the combination of these two features could make it difficult for the ribosome to utilize Arg-tRNA or Lys-tRNA as acceptors of the MRL peptide leading to translation arrest. To dissect the contribution of length and charge of the acceptor's side chain to antibiotic-mediated ribosome stalling, we prepared a new series of synthetic substrate analogs either lacking the positive charge, but maintaining the length of the side chain comparable to that of Lys and Arg, or carrying the positive charge but at a shortened side chain (Table 3.2). We then tested the acceptor activity of these substrates in the same experimental set-up that we used before with the Ala- Lys- or Arg- acceptor analogs. In the presence of ERY, the transfer of the MRL peptide to ACCA-N-6-azido-L-norleucine, ACCA-N-6-hydroxy-L-norleucine, or ACCA-N-5-ethyl-L-norleucine (otherwise known as 2-aminooctanoic acid), whose side chain ranges in length from 5 to 7 atoms but lacks the positive charge, occurs with the apparent rate constants  $k_{app}$  of ca.  $0.3 \text{ min}^{-1}$  (Figure. 3.7 and Table 3.2). Remarkably, shortening the uncharged side chain to 4 atoms (in ACCA-N-norleucine), significantly accelerated the reaction making it too fast to accurately determine the rate constant in our experiments ( $k_{app} > 1.8 \text{ min}^{-1}$ ) (Figure. 3.7 and Table 3.2). In the absence of the antibiotic, all the uncharged acceptor substrates reacted with kinetics too rapid to be accurately measured with our experimental set-up (Figure. 3.8 and Table 3.2). These results show that the length of the acceptor side chain

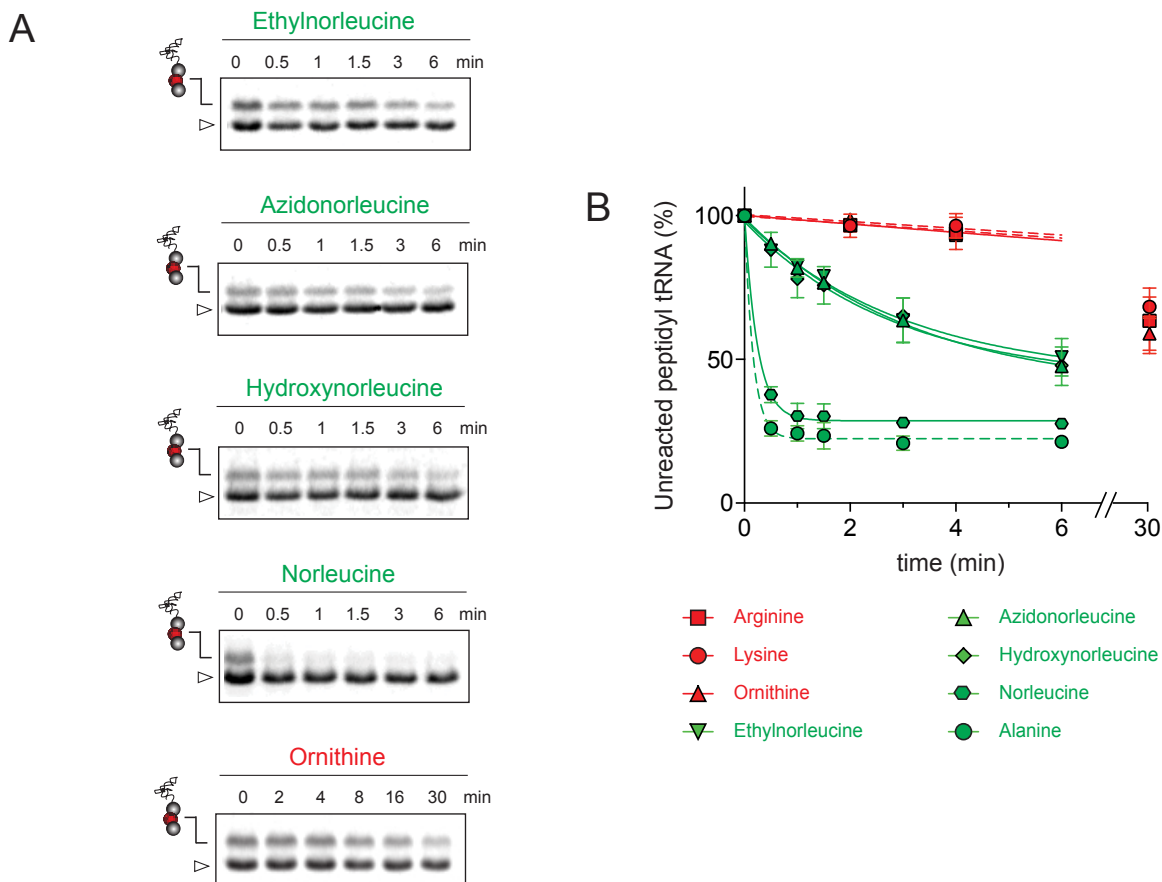


**Figure 3.7. Reactivity of substrate analogs reveals the charge of the amino acid side chain as the predominant factor of slow peptide bond formation. (A)** Gel electrophoresis analysis of the remaining  $[^{35}\text{S}]$ -MRL-tRNA<sup>Leu</sup> upon reaction with ACCA-N-X acceptor analogs in the presence of ERY. The band marked with an open triangle corresponds to fMet-tRNA<sup>fMet</sup> present in the reaction mixture. Substrates with the positively charged side chain of the amino acid moiety are shown in red and those with the neutral side chain are green. **(B)** Quantification of the gels shown in (A). Reaction plots with substrates carrying natural amino acids are shown as dashed lines. The amount of MRL-tRNA<sup>Leu</sup> prior to addition of the A-site substrates (0 min) was set as 100%. Error bars show deviation from the mean in two independent experiments.

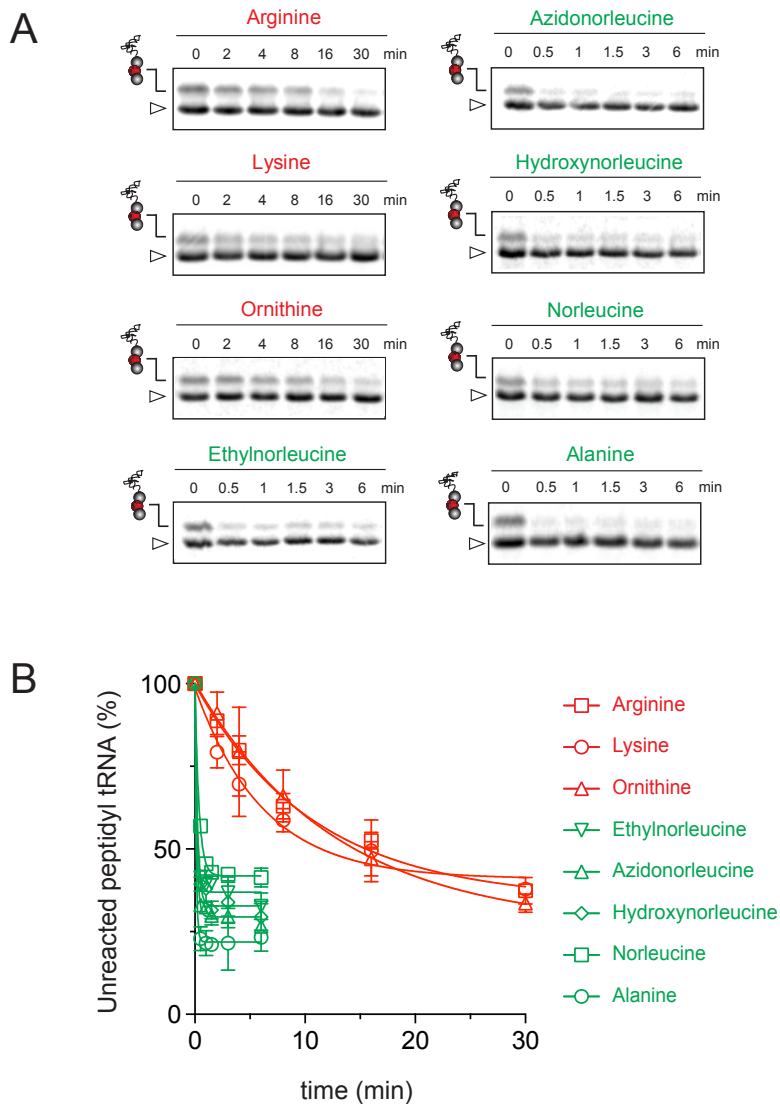


**Figure 3.8. Reaction of model A-site substrates with the MRL peptide in the absence of ERY.** (A) Gel electrophoresis analysis of the remaining  $[^{35}\text{S}]$ -MRL-tRNA<sup>Leu</sup> upon reaction with ACCA-N-X acceptor analogs in the absence of ERY. The band marked with an open triangle corresponds to fMet-tRNA<sup>fMet</sup> present in the reaction mixture. Substrates with the positively charged side chain of the amino acid moiety are shown in red and those with the neutral side chain are green. (B) Quantification of the gels shown in (A). Reaction plots with substrates carrying natural amino acids are shown as dashed lines. The amount of MRL-tRNA<sup>Leu</sup> prior to addition of the A-site substrates (0 min) was set as 100%. Error bars show deviation from the mean in two independent experiments.

contributes to the arrest mechanism because macrolides notably slow down the transfer of the MRL peptide to acceptors with extended side chains. Nevertheless, the transfer of the MRL peptide to the electro-neutral acceptors still proceeded at a considerable rate indicating that the extended length of the acceptor side chain is insufficient to support formation of a stable stalled complex.

Introduction of the positive charge to the side chain on the acceptor substrate had a by far more dramatic effect on the rate of reaction with the MRL donor. Replacement of the terminal methyl group of norleucine with a positively charged amino group in ACCA-N-ornithine resulted in a precipitous drop of the MRL transfer rate, essentially abolishing the reaction in the presence of ERY ( $k_{app} < 0.01 \text{ min}^{-1}$ ) (Table 3.2 and Figure. 3.6). Interestingly, even in the absence of ERY, the transfer of the MRL peptide to ACCA-N-ornithine was rather inefficient ( $k_{app} 0.08 \pm 0.02 \text{ min}^{-1}$ ) (Figure. 3.8 and Table 3.2). These results clearly indicate that the major obstacle for catalysis of the transfer of the MRL peptide to the acceptor in the PTC of the macrolide-bound ribosome is imposed by the charge of the A site amino acid.

The sluggish transfer of the MRL peptide to charged substrates ACCA-N-Lys, ACCA-N-Arg, and ACCA-N-ornithine critically depends on the presence of Arg (or Lys) in the penultimate position of the nascent chain. The control (non-stalling) donor peptide MAL, reacted fast with all the tested acceptor substrates irrespective of the antibiotic presence ( $k_{app} \geq 0.74 \text{ min}^{-1}$ ) (Figure. 3.9, Figure. 3.10 and Table 3.2) showing that the removal of a long positively charged side chain at the penultimate position of the donor substrate stimulates the reaction. This result is compatible with the view that the simultaneous presence of the charged long side chains in the penultimate position of the

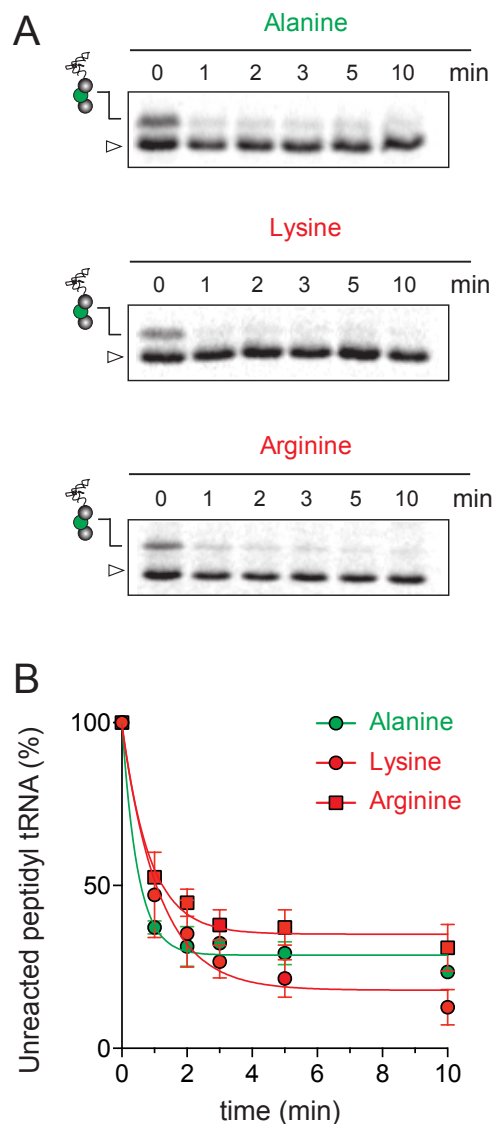


**Figure 3.9. Arg- and Lys- substrates are good acceptors of the non-stalling MAL-peptide in spite of the presence of ERY.** (A) Gel electrophoresis analysis of the remaining  $[^{35}\text{S}]\text{-MAL-tRNA}^{\text{Leu}}$  upon reaction with ACCA-N-Arg, ACCA-N-Lys or ACCA-N-Ala acceptor analogs in the presence of ERY. The band marked with an open triangle corresponds to fMet-tRNA<sup>fMet</sup> present in the reaction mixture. Substrates with the positively charged side chain of the amino acid moiety are indicated in red and the one with the neutral side chain is green. (B) Quantification of the gels shown in (A). Reaction plots with substrates carrying natural amino acids are shown as dashed lines. The amount of MAL-tRNA<sup>Leu</sup> prior to addition of the A-site substrates (0 min) was set as 100%. Error bars show deviation from the mean in two independent experiments.

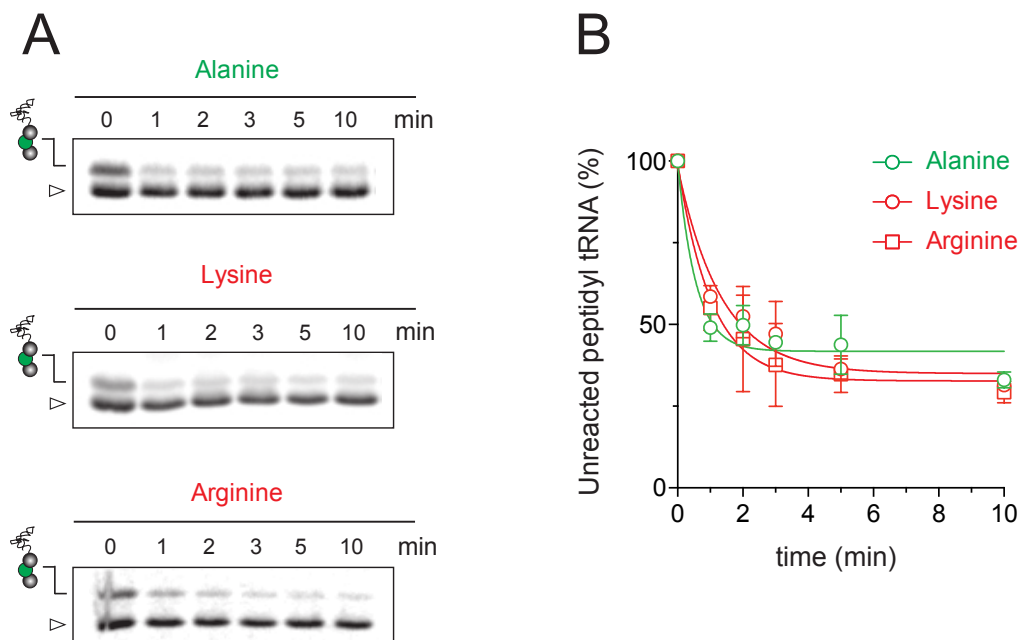


**Figure 3.10. Reaction of MAL peptide with model A-site substrates in the absence of ERY.** (A) Gel electrophoresis analysis of the  $[^{35}\text{S}]\text{-MAL-tRNA}^{\text{Leu}}$  upon reaction with neutral ACCA-N-Ala, -Lys or -Arg over the course of time at  $37^\circ\text{C}$  in the absence of ERY. The band marked with an open triangle corresponds to  $\text{fMet-tRNA}^{\text{fMet}}$  present in the reaction mixture. (B) Graph for the quantification of  $\text{MAL-tRNA}^{\text{Leu}}$  from the gels shown in A. The total accumulated  $\text{MAL-tRNA}^{\text{Leu}}$  at 0 min was set as 100%. Error bars show deviation from the mean based on two independent experiments.

donor substrate and in the aminoacyl acceptor presents the obstacle for catalysis of peptide bond formation by the macrolide-bound ribosome.

One possible model that follows from our findings is that a simple electrostatic repulsion between the penultimate residue of the peptidyl donor and the aminoacyl moiety of the acceptor may be sufficient to hamper the catalysis of the peptidyl transfer reaction in the macrolide-bound ribosome. If this were the case, then simultaneous replacement of the positively charged residues encoded in codons 2 and 4 of the MRLR ORF with negatively charged amino acids would be comparably detrimental for translation. We tested this hypothesis in a straightforward experiment by preparing two new templates for toeprinting analysis, in which the second and the fourth codons of the truncated *ermDL* ORF were mutated to specify peptides MDLD and MELE, which carry negatively charged amino acids in the critical positions. Interestingly, toeprinting showed that neither of these peptides could direct efficient arrest of the macrolide-bound ribosome (Figure. 3.11). Thus, it is not the simple repulsion of two equivalent charges, but the explicit presence of *positively* charged residues in the penultimate position of the P site peptidyl donor and in the A site aminoacyl acceptor that obstruct peptide bond formation in the ribosome with a macrolide antibiotic bound in the NPET.

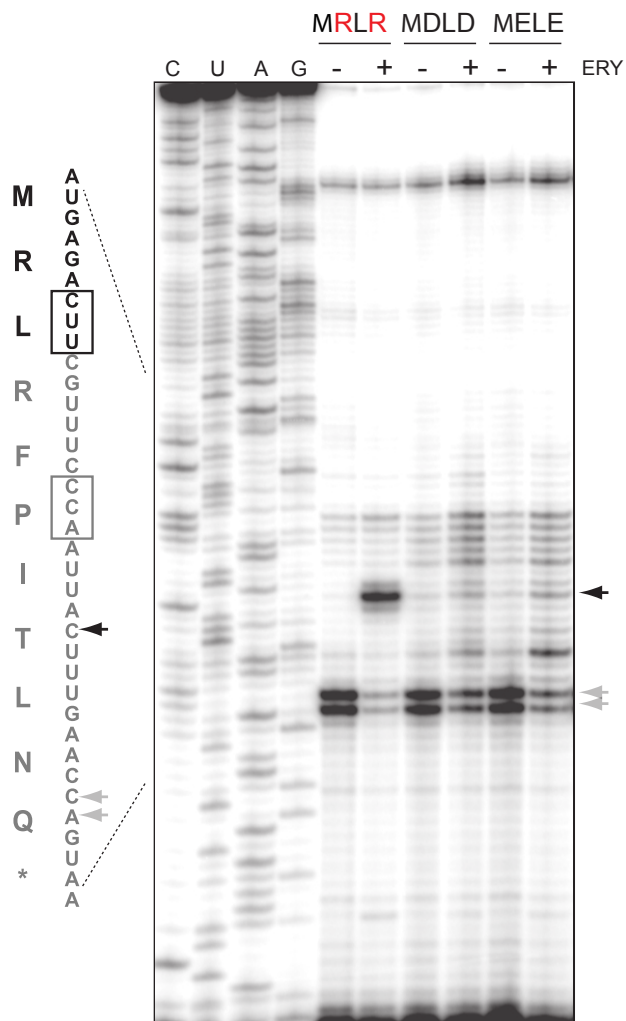


**Figure 3.11 Drug dependent translation arrest is not efficient when the PTC donor and acceptor substrates are negatively charged.** Toeprinting analysis ERY-mediated translation arrest for templates encoding MDLD and MELE sequences. Black arrows indicate ERY dependent translation arrest at the Leu-3 codon of the templates. Ery-induced arrest at the MRLR sequence was included for comparison. Ribosomes that do not stall due to ERY are captured at the downstream Pro-6 codon, producing the toeprint band marked with gray arrows. Sequencing lanes are indicated with C, U, A, G. Gels are representative of two independent experiments.

### 3.4 **Discussion**

It has been unknown why the ribosome is unable to polymerize certain protein sequences when macrolide antibiotics bind in the NPET. In order to address this question, we interrogated one of the most common problematic motifs for the macrolide-bound ribosome and found that specific physicochemical properties of the substrates of peptide bond formation are the major contributing factors to the drug-induced translation arrest.

During translation elongation, macrolides act as inhibitors of peptide bond formation between specific combinations of donor and acceptor substrates (Kannan et al., 2014). This mode of action is likely mediated by allosteric changes in the PTC properties induced by the drug (Sothiselvam et al., 2014), which may be additionally modulated by direct interactions between the nascent chain and the antibiotic in the NPET (Vazquez-Laslop et al., 2011, Arenz et al., 2014a, Arenz et al., 2014b). Our use of the shortest known peptide, MRL, capable of directing macrolide-dependent ribosome stalling (Sothiselvam et al., 2014), made it possible to simplify the system by decoupling the PTC events from the influence of a direct antibiotic-nascent peptide interaction. Furthermore, the small size of the stalling peptide made it possible to probe the contribution of each of its residues (with the exception of the N-terminal formyl-methionine) to translation arrest.

Strikingly, in the context of such a short donor substrate, the physicochemical characteristics of only one of its residues, the penultimate amino acid, are critical, whereas the properties of the C-terminal amino acid, which directly participates in peptide bond formation, is of a lesser importance. Our comprehensive mutational analysis showed that any combination of Lys and Arg residues in the penultimate peptide's position and in the acceptor substrate is sufficient for preventing fast peptide bond

formation in the macrolide-bound ribosome. Subsequent biochemical studies, which utilized two different peptidyl donors (MRL and MAL) and a series of synthetic acceptor substrate analogs, showed that the positive charge of the side chains of the critical amino acid residues, and to a lesser extent their size, are the key factors that render peptide bond formation inefficient in the drug-bound ribosome. All the positively charged acceptors of the MRL peptide (ACCA-N-Arg, -Lys, or -ornithine) reacted extremely slowly, but their replacement with electro-neutral analogs dramatically accelerated the reaction. Replacing the penultimate Arg in the MRL donor with an electro-neutral Ala, had a similar effect. Only in the absence of the charge, the contribution of the size of the side chain could be clearly revealed: the electro-neutral acceptors with the size of the side chain in the range of 5 to 7 atoms reacted rather slowly, but ACCA-N-norleucine, whose side chain contains only 4 atoms, reacted much faster (Table 3.2). Although the contribution of the side chain size could be generally concealed due to the dominance of the charge effect, it might nevertheless play a notable role in the mode of the drug action in the cell. Indeed, although in our in vitro experiments both ACCA-N-Lys and ACCA-N-Arg reacted too slowly to accurately distinguish the difference in their reactivity, ribosome profiling analysis showed a more pronounced enrichment of Arg containing sequences of the R/K-X-R/K motif in the sites of macrolide-induced translation stalling (Davis et al., 2014, Kannan et al., 2014). Because the guanidinium group of Arg and  $\epsilon$ -amino group of Lys are both completely protonated at physiological pH, it is possible that the longer side chain of Arg (6 atoms) compared to Lys (5 atoms) (Table 3.2) accounts for a more severe translation arrest at the Arg-containing motifs. In addition to providing mechanistic insights into the results of the recent ribosome profiling experiments (Davis et al., 2014,

Kannan et al., 2014), our studies of the translation arrest promoted by the R/K-X-R/K motif have clarified one of the oldest puzzling facts about the mode of macrolide action. In the early days of macrolide research, when only synthetic RNA homopolymers were available, it had been convincingly demonstrated that translation of poly(A) RNA, encoding poly-lysine, was efficiently inhibited by erythromycin and resulted in accumulation of very short, di- to penta-lysine, peptides (Mao et al, 1971, Otaka et al., 1975, Vazquez et al., 1966). At that time, it was difficult to explain the accumulation of such short peptides, whose progression through the NPET could be hardly obstructed by direct steric hindrance from the drug. It is easy to see, however, that poly-Lys sequence perfectly conforms to the R/K-X-R/K motif and thus it is not surprising that its synthesis would be interrupted at the very early rounds due to interference with the transfer of even very short nascent chains carrying Lys in the penultimate position to the incoming Lys-tRNA.

Our results show that the interplay of the penultimate nascent peptide residue and the incoming amino acid has a dramatic effect on macrolide-induced arrest at the R/K-X-R/K sites. Interestingly, the nature of the central amino acid of the motif, the C-terminal residue of the donor peptide that resides in the P-site of the catalytic site, appears to be by far less significant, at least in the case of ERY-induced arrest with the minimal peptide (Figure. 3.2B). Nevertheless, the role of the C-terminal residue in modulating, to some extent, the efficiency of peptide bond formation in the macrolide-bound ribosome, could be inferred from the somewhat varying relative intensity of the arrest bands in the toeprint gels (Figure. 3.2B and Figure. 3.3). Furthermore, the nature of the tunnel-bound antibiotic affects the importance of the C-terminal residue of the nascent chain for

translation arrest. While Leu<sub>3</sub>-to-Ala replacement had only a negligible effect on the transfer of the MRL peptide to Arg-tRNA in the ERY-bound ribosome, the same mutation notably diminished translation arrest when, instead of ERY, the fluoroketolide SOL was bound in the NPET (Figure. 3.5). This result is reminiscent of our recent findings that the nature of the C-terminal residue of another stalling regulatory peptide, ErmBL, which conforms to a different stalling motif, XDK (Kannan et al., 2014), defines which antibiotic is recognized as a stalling cofactor (Gupta et al., 2016).

In the absence of structural data on the ribosome stalled at the R/K-X-R/K motif, our data, which show that peptide bond formation is significantly inhibited when the penultimate residue of the nascent chain and the incoming amino acid carry ~~extended~~ positively charged side chains, could be accounted for by several scenarios. One possibility is that electrostatic repulsion between the incoming amino acid and the penultimate peptide residue, possibly exacerbated by direct steric hindrance, prevents proper accommodation of the aminoacyl-tRNA acceptor in the PTC A site. This could result either in an aberrant placement of the stably-bound aminoacyl-tRNA or in a rapid dissociation of Arg-tRNA or Lys-tRNA from the A site. Unfortunately, our ability to synthesize only limited amounts of the acceptor substrate analogs prevented us from carrying more detailed kinetic studies, which could potentially distinguish between these scenarios. It is also possible that binding of the positively charged substrate to the A site shifts the placement of the peptidyl-tRNA in the P site, if the penultimate position of the nascent chain carries a positively charged residue. Finally, both the P and the A site substrates could be mutually misplaced in the PTC active site, which would be detrimental for the efficient peptide bond formation.

While the positive charges of the penultimate peptide residue and the acceptor amino acid play the key role in macrolide-induced arrest, simultaneous replacement of both of the critical residues with negatively charged amino acids was not conducive to inhibition of peptide bond formation (Figure. 3.11). This observation clearly shows that the polarity of the charge of the donor and acceptor is central to the mechanism of stalling. In agreement with this conclusion, while R/K-X-R/K is one of the most predominant macrolide stalling motifs in Gram-positive and Gram-negative bacteria, no particular enrichment of the D/E-X-D/E sequences at the sites of drug-induced translation arrest was noted (Davis et al., 2014, Kannan et al., 2014). The strict polarity requirement suggests that electrostatic interactions of the substrates with additional charged group(s) of the ribosome or its ligands could be involved in the mechanism of stalling. It is conceivable, that the positively charged side chains of the peptide donor or aminoacyl acceptor could interact with the electro-negative phosphate group of one of the neighboring 23S rRNA nucleotides. Alternatively, the protonated 3' dimethyl-amino group of the macrolide molecule, located at a distance of ca. 8 Å from the PTC active site, could influence the placement of the positively charged substrates.

Only specific combinations of peptidyl transfer donor and acceptors are problematic for the ribosome corrupted by macrolides. Do these drugs exacerbate the intrinsic poor reactivity of some substrates or they make normally 'good' substrates problematic? The rate of the catalytic step of peptide bond formation in the drug-free ribosome depends on the nature of the reacting substrates (Bourd et al., 1982, Monro et al., 1968, Wohlgemuth et al., 2008, Johansson et al., 2011). However, this difference is normally masked by the slow rate of aminoacyl-tRNA binding and accommodation,

which is the rate-limiting step of translation elongation (Wintermeyer et al., 2004). It is conceivable, however, that if the general catalytic capacity of the PTC is sufficiently decreased, then formation of peptide bonds between certain generally ‘slow’ substrates could become rate limiting. From this standpoint, it is interesting that even in the absence of antibiotic, the reaction of the MRL peptide with the acceptor analogs carrying positively charged amino acids was notably slower than the reaction with electro-neutral acceptors (Table 3.2). This observation hints that peptide bond formation between substrates conforming to the R/K-X-R/K motif could be intrinsically slow. We are fully aware, however, that such a conclusion could be made only cautiously because the use of the model substrates may significantly slow down the reaction, which becomes much faster when the full length tRNA delivers the acceptor to the PTC A site (Wohlgemuth et al., 2008). Indeed, if the rate of peptidyl transfer measured in our model experiments reflects the *in vivo* reactivity of the substrates, one would expect to see pronounced ribosome stalling at the R/K-X-R/K motif even in the absence of antibiotic, which was reported (Davis et al., 2014, Kannan et al., 2014, Mohammad et al., 2016). However, if our assertion is correct then maybe inhibition of translation by macrolide antibiotics has revealed a general but concealed phenomenon of the dependence of the catalytic rate of peptidyl transfer on the interplay of the penultimate residue of the nascent chain and the incoming amino acid.

In summary our study exemplifies that the fundamental discriminative behavior of the ribosome towards its catalytic substrates can be exaggerated when small molecules like macrolide antibiotics bind to the ribosome leading to sequence specific translation arrest.

### 3.5 Cited Literature

Almutairi, M.M., Park, S.R., Rose, S., Hansen, D.A., Vazquez-Laslop, N., Douthwaite, S., Sherman, D.H., and Mankin, A.S. (2015). Resistance to ketolide antibiotics by coordinated expression of rRNA methyltransferases in a bacterial producer of natural ketolides. *Proceedings of the National Academy of Sciences of the United States of America* 112, 12956-12961.

Arenz, S., Meydan, S., Starosta, A.L., Berninghausen, O., Beckmann, R., Vazquez-Laslop, N., and Wilson, D.N. (2014a). Drug sensing by the ribosome induces translational arrest via active site perturbation. *Molecular cell* 56, 446-452.

Arenz, S., Ramu, H., Gupta, P., Berninghausen, O., Beckmann, R., Vazquez-Laslop, N., Mankin, A.S., and Wilson, D.N. (2014b). Molecular basis for erythromycin-dependent ribosome stalling during translation of the ErmBL leader peptide. *Nature communications* 5, 3501.

Bourd, S., Victorova, L., and Kukhanova, M. (1982). On substrate specificity of the donor site of the *Escherichia coli* ribosomal peptidyl transferase center. Synthesis of dipeptides from 3'-terminal fragments of aminoacyl-tRNA. *FEBS letters* 142, 96-100.

Bulkley, D., Innis, C.A., Blaha, G., and Steitz, T.A. (2010). Revisiting the structures of several antibiotics bound to the bacterial ribosome. *Proceedings of the National Academy of Sciences of the United States of America* 107, 17158-17163.

Davis, A.R., Gohara, D.W., and Yap, M.N. (2014). Sequence selectivity of macrolide-induced translational attenuation. *Proceedings of the National Academy of Sciences of the United States of America* 111, 15379-15384.

Dunkle, J.A., Xiong, L., Mankin, A.S., and Cate, J.H. (2010). Structures of the *Escherichia coli* ribosome with antibiotics bound near the peptidyl transferase center explain spectra of drug action. *Proceedings of the National Academy of Sciences of the United States of America* 107, 17152-17157.

Gryczan, T.J., Grandi, G., Hahn, J., Grandi, R., and Dubnau, D. (1980). Conformational alteration of mRNA structure and the posttranscriptional regulation of erythromycin-induced drug resistance. *Nucleic acids research* 8, 6081-6097.

Gupta, P., Liu, B., Klepacki, D., Gupta, V., Schulten, K., Mankin, A.S., and Vazquez-Laslop, N. (2016). Nascent peptide assists the ribosome in recognizing chemically distinct small molecules. *Nature chemical biology*.

Horinouchi, S., and Weisblum, B. (1980). Posttranscriptional modification of mRNA conformation: mechanism that regulates erythromycin-induced resistance. *Proceedings of the National Academy of Sciences of the United States of America* 77, 7079-7083.

Hue, K.K., and Bechhofer, D.H. (1992). Regulation of the macrolide-lincosamide-streptogramin B resistance gene *ermD*. *Journal of bacteriology* 174, 5860-5868.

Johansson, M., Jeong, K.W., Trobro, S., Strazewski, P., Aqvist, J., Pavlov, M.Y., and Ehrenberg, M. (2011). pH-sensitivity of the ribosomal peptidyl transfer reaction dependent on the identity of the A-site aminoacyl-tRNA. *Proceedings of the National Academy of Sciences of the United States of America* 108, 79-84.

Kannan, K., Kanabar, P., Schryer, D., Florin, T., Oh, E., Bahroos, N., Tenson, T., Weissman, J.S., and Mankin, A.S. (2014). The general mode of translation inhibition by macrolide antibiotics. *Proceedings of the National Academy of Sciences of the United States of America* 111, 15958-15963.

Kannan, K., Vazquez-Laslop, N., and Mankin, A.S. (2012). Selective protein synthesis by ribosomes with a drug-obstructed exit tunnel. *Cell* 151, 508-520.

Kwak, J.H., Choi, E.C., and Weisblum, B. (1991). Transcriptional attenuation control of *ermK*, a macrolide-lincosamide-streptogramin B resistance determinant from *Bacillus licheniformis*. *Journal of bacteriology* 173, 4725-4735.

Kwon, A.R., Min, Y.H., Yoon, E.J., Kim, J.A., Shim, M.J., and Choi, E.C. (2006). *ErmK* leader peptide : amino acid sequence critical for induction by erythromycin. *Archives of pharmacal research* 29, 1154-1157.

Mao, J.C., and Robishaw, E.E. (1971). Effects of macrolides on peptide-bond formation and translocation. *Biochemistry* 10, 2054-2061.

Mohammad, F., Woolstenhulme, C.J., Green, R., and Buskirk, A.R. (2016). Clarifying the Translational Pausing Landscape in Bacteria by Ribosome Profiling. *Cell reports* 14, 686-694.

Monro, R.E., Cerna, J., and Marcker, K.A. (1968). Ribosome-catalyzed peptidyl transfer: substrate specificity at the P-site. *Proceedings of the National Academy of Sciences of the United States of America* 61, 1042-1049.

Ramu, H., Mankin, A., and Vazquez-Laslop, N. (2009). Programmed drug-dependent ribosome stalling. *Molecular microbiology* 71, 811-824.

Ramu, H., Vazquez-Laslop, N., Klepacki, D., Dai, Q., Piccirilli, J., Micura, R., and Mankin, A.S. (2011). Nascent peptide in the ribosome exit tunnel affects functional properties of the A-site of the peptidyl transferase center. *Molecular cell* 41, 321-330.

Schlunzen, F., Zarivach, R., Harms, J., Bashan, A., Tocilj, A., Albrecht, R., Yonath, A., and Franceschi, F. (2001). Structural basis for the interaction of antibiotics with the peptidyl transferase centre in eubacteria. *Nature* 413, 814-821.

Shimizu, Y., Inoue, A., Tomari, Y., Suzuki, T., Yokogawa, T., Nishikawa, K., and Ueda, T. (2001). Cell-free translation reconstituted with purified components. *Nature biotechnology* 19, 751-755.

Sothivelvam, S., Liu, B., Han, W., Ramu, H., Klepacki, D., Atkinson, G.C., Brauer, A., Remm, M., Tenson, T., Schulten, K., et al. (2014). Macrolide antibiotics allosterically predispose the ribosome for translation arrest. *Proceedings of the National Academy of Sciences of the United States of America* 111, 9804-9809.

Starosta, A.L., Karpenko, V.V., Shishkina, A.V., Mikolajka, A., Sumbatyan, N.V., Schlutzen, F., Korshunova, G.A., Bogdanov, A.A., and Wilson, D.N. (2010). Interplay between the ribosomal tunnel, nascent chain, and macrolides influences drug inhibition. *Chemistry & biology* 17, 504-514.

Subramanian SL, Ramu H, Mankin AS. Inducible resistance to macrolide antibiotics. In: Dougherty TJ, Pucci, M. J. , editor. *Antibiotic Drug Discovery and Development*. New York, NY: Springer Publishing Company; 2011.

Vazquez, D. (1966). Antibiotics affecting chloramphenicol uptake by bacteria. Their effect on amino acid incorporation in a cell-free system. *Biochimica et biophysica acta* 114, 289-295.

Vazquez-Laslop, N., Klepacki, D., Mulhearn, D.C., Ramu, H., Krasnykh, O., Franzblau, S., and Mankin, A.S. (2011). Role of antibiotic ligand in nascent peptide-dependent ribosome stalling. *Proceedings of the National Academy of Sciences of the United States of America* 108, 10496-10501.

Vazquez-Laslop, N., Thum, C., and Mankin, A.S. (2008). Molecular mechanism of drug-dependent ribosome stalling. *Molecular cell* 30, 190-202.

Weisblum, B. (1995). Insights into erythromycin action from studies of its activity as inducer of resistance. *Antimicrobial agents and chemotherapy* 39, 797-805.

Wintermeyer, W., Peske, F., Beringer, M., Gromadski, K.B., Savelsbergh, A., and Rodnina, M.V. (2004). Mechanisms of elongation on the ribosome: dynamics of a macromolecular machine. *Biochemical Society transactions* 32, 733-737.

Wohlgemuth, I., Brenner, S., Beringer, M., and Rodnina, M.V. (2008). Modulation of the rate of peptidyl transfer on the ribosome by the nature of substrates. *The Journal of biological chemistry* 283, 32229-32235.

## **4. Context specific action of macrolide antibiotics in facilitating translation arrest**

### **4.1 Introduction and rationale**

Macrolide antibiotics, like erythromycin (ERY) and its newer derivatives, affect bacterial growth by inhibiting protein synthesis. They achieve the inhibitory effect by binding to the nascent peptide exit tunnel (NPET) of the ribosome, at a short distance from the peptidyl transferase center (PTC) (Dunkle et al., 2010, Schlunzen et al., 2001, Bulkley et al., 2010). The presence of a bulky macrolide molecule in a narrow segment of the NPET restricts the placement of the nascent chain and may obstruct its progression through the tunnel. Macrolides were thought to act exclusively like an NPET plug, preventing the passage of the nascent peptides and causing peptidyl-tRNA drop-off (Menninger, 1995, Tenson et al., 2003). However, recent studies have suggested that this may not be the predominant mode of action of these drugs (Kannan et al., 2014, Kannan et al., 2012). Emerging evidence indicates that the action of macrolides upon protein synthesis critically depends on the properties of the peptide being synthesized (Starosta et al., 2010, Kannan et al., 2012). While some protein sequences are conducive to early peptidyl-tRNA drop-off, other nascent peptide sequences can promote formation of a stable stalled translation complex at specific sites on the mRNA (reviewed in Vázquez-Laslop et al., 2014). Such drug-dependent ribosome stalling can occur at early or late stages of protein synthesis depending on the nature of the peptide (Kannan et al., 2012). In some occasions, proteins can evade the presence of the macrolide antibiotic, in which case, synthesis of such polypeptides continues to completion (Kannan et al., 2012). The prevalence of each of these scenarios critically depends on the nature of the peptide being

synthesized and the structure of the macrolide antibiotic bound in the NPET. However, the underlying molecular bases of these outcomes have remained elusive.

The recent ribosome profiling experiments in Gram-positive and Gram-negative bacteria provided the first genome-wide insights into sequence-specificity of macrolide action (Kannan et al., 2014, Davis et al., 2014). Several specific amino acid motifs have been identified, at which the antibiotic-bound ribosome stalls. One of the most prominent of such ‘problematic’ motifs is the sequence R/K-X-R/K (Kannan et al., 2014, Davis et al., 2014). The ribosome stalls within this motif, when it has to catalyze the transfer of a nascent peptide that contains an Arg or Lys residue in the penultimate position, to an aminoacyl-tRNA acylated with Arg or Lys.

Several bacteria exploit drug-dependent translation arrest to regulate the expression of their resistance genes (reviewed in Weisblum, 1995, Ramu et al., 2009, Subramanian et al., 2011). Programmed ribosome stalling, which in the presence of the antibiotic occurs at specific, evolutionary-selected sites of the upstream regulatory ORF (uORF), activates the expression of the downstream resistance genes. A large variety of these regulatory uORFs encode peptides that contain the sequences conforming to the R/K-X-R/K motif (Sothiselvam et al., 2014, Almutairi et al., 2015). In vitro analysis has shown that drug-mediated programmed translation arrest at the uORFs occurs exactly within this motif, when its second codon enters the ribosomal P site (Sothiselvam et al., 2014). One of the best-characterized regulatory peptides of this class is ErmDL, encoded in the regulatory uORF controlling expression of the resistance rRNA methyltransferase ErmD (Hue and Bechhofer, 1992, Kwak et al., 1991, Kwon et al., 2006). In the presence of macrolides, translation of the *ermDL* ORF is halted at the middle codon encoding the

R-L-R sequence, after the first 7 amino acids of the leader peptide (MTSHMRL) are polymerized and the Lys<sub>8</sub> codon enters the ribosomal A site (Vazquez-Laslop et al., 2010, Sothiselvam et al., 2014). Our previous experiments have shown that macrolides induce translation arrest even if the ErmDL peptide is N-terminally truncated. The shortest ORF at which the ribosome can be actively stalled by macrolides contains the sequence MRLR (Sothiselvam et al., 2014). Stalling within this ORF occurs when the nascent chain has only three amino acid residues (MRL). Experimenting with this short peptide, we have shown that the identities of the first and last residues of the R/K-X-R/K stalling motif are the most critical for macrolide-induced arrest. Mutating any of these amino acids to a residue different from Arg or Lys, completely abolished the arrest. Our studies have shown that the positive charge of the critical residues of the motif and the size of their side chains are the major factors that make the donor and acceptor substrates highly problematic for the drug-bound ribosome (Sothiselvam et al., in submission).

The use of the simplified MRLR experimental system made it possible to elucidate the critical details of the molecular mechanism of macrolide-induced translation stalling. However, the effect of macrolides on translation could be modulated by additional factors, which could not be recapitulated with the minimal sequence. For example, when examining the ribosome profiling data obtained with cells treated with high concentrations of macrolides, we noted a large variation in the prominence of translation arrest within the 'R/K-X-R/K' motifs (Kannan et al., 2014). While the differences in the sequence of the motif itself could account for some of the observed effects, they could not explain the broad range of the disparities. Indeed, we found several instances where the drug bound ribosomes continue translation of a gene past its

'R/K-X-R/K' sequence, when exactly the same motif could cause a strong arrest in a different gene (Figure. 4.1). These observations suggested that the context in which the 'R/K-X-R/K' sequence occurs might significantly modulate the efficiency of macrolide-induced translation arrest.

In this work, we used the ErmDL leader peptide, which carries the RLR sequence conforming to the R/K-X-R/K consensus, as a model for elucidating the influence of its context on macrolide-promoted ribosome stalling. Our results show that the sequence of the nascent peptide immediately upstream of the 'RLR' sequence may significantly influence the severity of translation arrest imposed by the macrolide drug. We propose a model in which the sequence preceding the arrest motif can function as an independent module with the ability to stimulate or counteract drug-induced ribosome stalling.

## **4.2 Materials and Methods**

### **Toeprinting assay.**

Linear DNA templates (0.5–1 pmol) encoding the ORF of interest preceded by the T7 promoter sequence were generated by PCR using primers indicated in Table 4.1. The resulting templates were used to direct coupled transcription–translation in the PURExpress cell-free system (New England Biolabs). The reactions were carried out in a total volume of 5  $\mu$ L and, where indicated, were supplemented with antibiotics (50  $\mu$ M final concentration). Following 10 min incubation at 37 °C, a 5-min primer extension initiated by addition of reverse primer NV1 (Table 4.1) and 3 U of reverse transcriptase (Roche Applied Science). The cDNA products along with sequencing reactions were separated in a 6% sequencing gel and visualized with a Typhoon imager (GE).

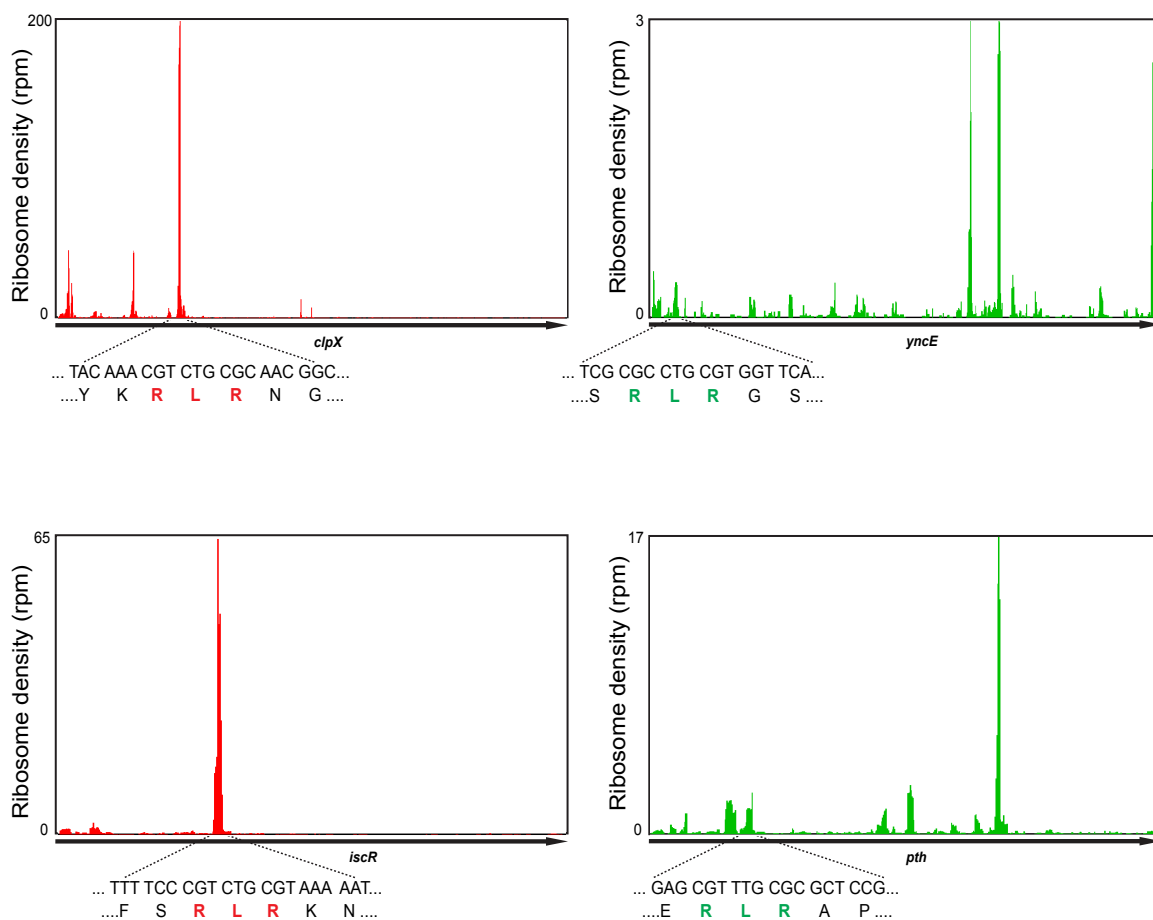


**Figure 4.1. Translation is not implicitly arrested at ‘RLR’ always in the presence of ERY.** Ribosome density in the *clpX*, *iscR*, *pth* and *yncE* genes derived from the ribosome profiling data of *E. coli* treated with ERY, previously reported (Kannan et al., 2014). The position and neighboring sequences of the internal RLR motif in each of these genes is indicated. The cartoons illustrate that drug-bound ribosomes stall at the RLR sequence of *clpX* and *iscR* but not at the similar internal motif of *yncE* and *pth*.

**Table 4.1: Primers used in this study**

<b>Primer name</b>	<b>Primer sequence</b>
T7	TAATACGACTCACTATAGGG
NV1	GGTTATAATGAATTTTGCTTATTAAC
ErmDL-Fwd	TAATACGACTCACTATAGGGCTTAAGTATAAGGAGGAAAAAATATGACA CACTCAATGAGACTTCGTTTCCCAATTACTTTGTAAGTG
Common-Rev	GGTTATAATGAATTTTGCTTATTAACGATAGAATTCTATCACTTACAAAG TAATTGGG
M1-Fwd	TAATACGACTCACTATAGGGCTTAAGTATAAGGAGGAAAAAATATGCACA CTCAATGTAGACTTCGTTTCCCAATTACTTTGTAAGTG
M2-Fwd	TAATACGACTCACTATAGGGCTTAAGTATAAGGAGGAAAAAATATGAACA CTCAATGTAGACTTCGTTTCCCAATTACTTTGTAAGTG
M3-Fwd	TAATACGACTCACTATAGGGCTTAAGTATAAGGAGGAAAAAATATGGACA CACTCAATAGACTTCGTTTCCCAATTACTTTGTAAGTG
M4-Fwd	TAATACGACTCACTATAGGGCTTAAGTATAAGGAGGAAAAAATATGAACA CACTCAATAGACTTCGTTTCCCAATTACTTTGTAAGTG
M5-Fwd	TAATACGACTCACTATAGGGCTTAAGTATAAGGAGGAAAAAATATGGACA CACTCATGAGACTTCGTTTCCCAATTACTTTGTAAGTG
M6-Fwd	TAATACGACTCACTATAGGGCTTAAGTATAAGGAGGAAAAAATATGGACA CATCAATGAGACTTCGTTTCCCAATTACTTTGTAAGTG
M7-Fwd	TAATACGACTCACTATAGGGCTTAAGTATAAGGAGGAAAAAATATGGACC ACTCAATGAGACTTCGTTTCCCAATTACTTTGTAAGTG
M8-Fwd	TAATACGACTCACTATAGGGCTTAAGTATAAGGAGGAAAAAATATGACA CACCTCAATAGACTTCGTTTCCCAATTACTTTGTAAGTG
Lpp-THSM-Fwd	TAATACGACTCACTATAGGGCTTAAGTATAAGGAGGAAAAAATATGAAAG CTACTAAACTGGTACTGGGCGCGGTAATCCTGGGTTCTATGACACACTCA
Lpp-THSM-Rev	GGTTATAATGAATTTTGCTTATTAACCTCTATCACTATCACGATAGAATTCT TACCAACGAAGTCTCATTGAGTGTGTCATAGAACC
Lpp-DTLN-Fwd	TAATACGACTCACTATAGGGCTTAAGTATAAGGAGGAAAAAATATGAAAG CTACTAAACTGGTACTGGGCGCGGTAATCCTGGGTTCTATGGACACACTC
Lpp-DTLN-Rev	GGTTATAATGAATTTTGCTTATTAACCTCTATCACTATCACGATAGAATTCT TACCAACGAAGTCTATTGAGTGTGTCATAGAACC
ErmDL-ALR-Fwd	TAATACGACTCACTATAGGGCTTAAGTATAAGGAGGAAAAAATATGACA CACTCAAUGGCACTTCGTATTTTCCCAACTTTGAACCAG
ErmDL-RLA-Fwd	TAATACGACTCACTATAGGGCTTAAGTATAAGGAGGAAAAAATATGACA CACTCAAUGAGACTTGCAATTTTCCCAACTTTGAACCAG
ErmDL-ALA-Fwd	TAATACGACTCACTATAGGGCTTAAGTATAAGGAGGAAAAAATATGACA CACTCAAUGGCACTTGCAATTTTCCCAACTTTGAACCAG
ErmDL-AAA-Fwd	TAATACGACTCACTATAGGGCTTAAGTATAAGGAGGAAAAAATATGACA CACTCAAUGGCACTTGCAATTTTCCCAACTTTGAACCAG
RLR-Ala-reverse	GGTTATAATGAATTTTGCTTATTAACGATAGAATTCTATCACTACTGGTTC AAAGTTGGGAA
MRLR-Fwd	TAATACGACTCACTATAGGGCTTAAGTATAAGGAGGAAAAAATATGAGAC TTCGTTTCCCAATTACTTTGAACCAGTAAGTGATAG
MRLA-Fwd	TAATACGACTCACTATAGGGCTTAAGTATAAGGAGGAAAAAATATGAGAC TTGCATTCCCAATTACTTTGAACCAGTAAGTGATAG
MRLR-Rev	GGTTATAATGAATTTTGCTTATTAACGATAGAATTCTATCACTACTGGTT CAA
ErmDL-T2A-Fwd	TAATACGACTCACTATAGGGCTTAAGTATAAGGAGGAAAAAATATGGCACA

	CTCAATGAGACTTCGTTTCCCAATTACTTTGTAAGTG
ErmDL-H3A-Fwd	TAATACGACTCACTATAGGGCTTAAGTATAAGGAGGAAAAAATATGACAGC ATCAATGAGACTTCGTTTCCCAATTACTTTGTAAGTG
ErmDL-S4A-Fwd	TAATACGACTCACTATAGGGCTTAAGTATAAGGAGGAAAAAATATGACACA CGCAATGAGACTTCGTTTCCCAATTACTTTGTAAGTG
ErmDL-M5A-Fwd	TAATACGACTCACTATAGGGCTTAAGTATAAGGAGGAAAAAATATGACACA CTCAGCAAGACTTCGTTTCCCAATTACTTTGTAAGTG
M3-BL-Fwd	TAATACGACTCACTATAGGGCTTAAGTATAAGGAGGAAAAAATATGGACAC ACTCAATAGACTTCGTTTGGTATTCCAAATGCGT
M3-BL-Rev	GGTTATAATGAATTTTGCTTATTAACGATAGAATTCTATCACTTACAAAGTA ATTTTATCTACATTACGCATTGGAATACCAAACG
Lpp-THSM-ALR-Rev	GGTTATAATGAATTTTGCTTATTAACCTTCTATCACTATCACGATAGAATTCTT ACCAACGAAGTGCCATTGAGTGTGTCATAGAACC
Lpp-THSM-RLA-Rev	GGTTATAATGAATTTTGCTTATTAACCTTCTATCACTATCACGATAGAATTCTT ACCATGCAAGTCTCATTGAGTGTGTCATAGAACC
Lpp-THSM-ALA-Rev	GGTTATAATGAATTTTGCTTATTAACCTTCTATCACTATCACGATAGAATTCTT ACCATGCAAGTGCCATTGAGTGTGTCATAGAACC
Lpp-THSM-AAA-Rev	GGTTATAATGAATTTTGCTTATTAACCTTCTATCACTATCACGATAGAATTCTT ACCATGCTGCTGCCATTGAGTGTGTCATAGAACC

### 4.3 Results

#### 4.3.1 Nascent peptide sequence preceding the RLR stalling motif affects

##### macrolide-dependent translation arrest.

Ribosome profiling analysis of *E. coli* treated with macrolide antibiotics revealed the R/K-X-R/K sequence as one of the most predominant motifs at which ribosome-bound antibiotic stalls (Kannan et al., 2014). However, the extent of ribosome stalling varied significantly between different R/K-X-R/K sites and in several genes no significant accumulation of ribosomal density was observed at this motif (Figure 4.1). Although the sequence variation within the motif could moderately affect the efficiency of macrolide-dependent stalling (Kannan et al., 2014, Sothiselvam et al, in submission), this could not explain the range of effects observed between multiple genomic R/K-X-R/K sites. Therefore, we considered the possibility that the context in which the stalling motif appears, could modulate the severity of the translation arrest.

We reasoned that the nascent chain segment immediately preceding the arrest motif, which is placed in the NPET side-by-side with the antibiotic molecule, would most likely strongly impact the efficiency of drug-induced stalling. In order to evaluate the influence of the nascent peptide sequence preceding the R/K-X-R/K arrest motif upon drug-induced ribosome stalling, we used as a model the RLR containing leader peptide ErmDL that controls the expression of the macrolide resistance gene *ermD* (Kwak et al., 1991, Hue and Bechhofer, 1992, Kwon et al., 2006). The regulatory *ermDL* ORF encodes the peptide of the sequence MTHSMRLR (Figure. 4.2A). In the presence of ERY, translation of *ermDL* is arrested at the Leu<sub>7</sub> codon, when the ribosome fails to catalyze peptide bond formation between the 7 amino acid long nascent peptide MTHSMRL and the incoming Arg-tRNA. ERY-promoted translation arrest, is revealed by *in vitro* toeprinting analysis (Figure. 4.2B, lanes 'WT'). In order to test whether the ErmDL segment preceding the RLR motif influences the efficiency of drug-induced ribosome stalling, we prepared a series of mutant templates in which the ErmDL N-terminal sequence was completely altered by introducing compensatory frameshifting mutations in the *ermDL* gene, affecting amino acid residues 2 to 5. The mutant templates coded for peptides in which the wt ErmDL N-terminal sequence MTHSM was changed to MHTQC (M1), MNTQC (M2), MDTLN (M3) or MNTLN (M4) (Figure. 4.2A). Strikingly, the complete replacement of the ErmDL sequence preceding the RLR stalling motif essentially abolished the arrest at the 7<sup>th</sup> codon (Figure. 4.2B). Although some of the mutants exhibited partial ERY-dependent arrest at the earlier codons, the fraction of the ribosomes reaching the RLR sequence was sufficiently high to clearly show that the



**Figure 4.2. Changing the amino acid sequence of the N-terminal segment of ErmDL abrogates translation arrest.** (A) The nucleotide and amino acid sequences of templates for cell-free translation of wt-ErmDL and its N-terminal segment variants (M1-4). The single nucleotides added or deleted to generate the desired compensatory frameshifting mutations (which allowed preservation of the RLR motifs in the templates) are indicated with dark or light blue arrows, respectively. (B) Toeprinting analysis of ERY-dependent ribosome stalling in the templates encoding wt-ErmDL or its N-terminal variants. The ribosomes that continue translation past the Leu<sub>7</sub> codon of the RLR sequence are captured at the downstream Pro<sub>10</sub> codon as a result of the presence of mupirocin (an IleRS inhibitor) in the reactions. Black and gray, arrowheads and boxes indicate the toeprint signals generated by arrested ribosomes at Leu<sub>7</sub> and Pro<sub>10</sub> codon respectively. Sequencing lanes are labeled as C, U, A, G. (C) Bar graph of the efficiency of ERY-mediated stalling at the Leu<sub>7</sub> codon, estimated by  $I_{Leu} / (I_{Leu} + I_{Pro})$  where  $I_{Leu}$  and  $I_{Pro}$  correspond to the intensity of toeprinting bands of ribosomes stalled at Leu<sub>7</sub> or Pro<sub>10</sub> codons, respectively. Error bars show deviation from the mean in two independent experiments.

altered protein sequence preceding the motif could dramatically reduce the efficiency of the arrest (to < 9 %) at RLR (Figure. 4.2C).

We then tested the contribution of individual amino acids in the wt ErmDL N-terminal segment for translation arrest at the RLR motif. We individually changed residues 2-5 of ErmDL to Ala and tested the efficiency of stalling (Figure. 4.3A). Toeprinting analysis showed that while mutations of Thr<sub>2</sub>, His<sub>3</sub>, Ser<sub>4</sub> and Met<sub>5</sub> to Ala slightly reduced ERY-dependent stalling at the *ermDL* 7<sup>th</sup> codon (Figure. 4.3B,C), none of the individual amino acid substitutions had an effect as significant as that observed when the entire sequence of the segment was changed (Figure. 4.2).

We then asked whether partial restoration of the wt ErmDL N-terminal sequence in the ‘non-stalling’ mutant MDTLNRLR (M3 in Figure. 4.2) could reinstate ERY-dependent arrest at the RLR motif (Figure. 4.4). Reverting to wt residue number 5, immediately preceding the RLR motif (construct M5, MDTLMRLR, where the wt

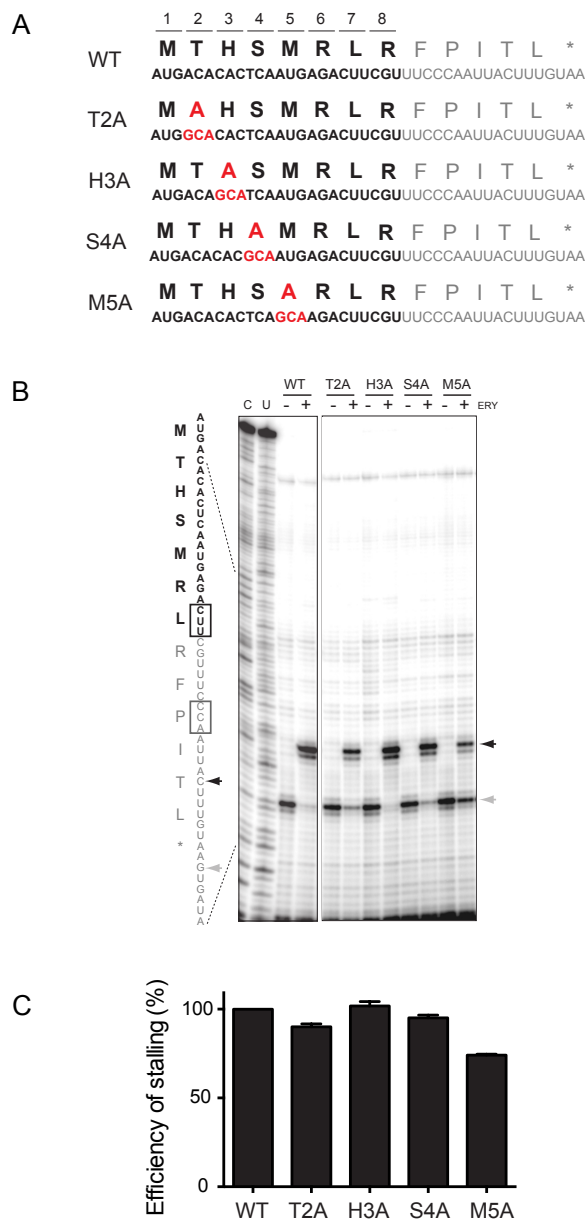


**Figure 4.3. Ala substitutions of the N-terminal amino acids of ErmDL do not significantly affect ERY-dependent translation arrest at the RLR motif. (A)** Nucleotide and amino acid sequences of cell-free translation templates for wt-ErmDL or the Ala-scanning mutagenesis of its N-terminal segment. **(B)** Toeprinting analysis of ERY-dependent translation arrest in the templates. Samples contained mupirocin (see legend of Figure. 4.2). Black and gray arrowheads indicate the toeprint signals of ribosomes whose P-site is at Leu<sub>7</sub> (boxed in black) or Pro<sub>10</sub> (boxed in gray), respectively. Sequencing lanes are marked as C, U. **(C)** Bar graph of the efficiency of ERY-mediated stalling at the Leu<sub>7</sub> codon, estimated by  $I_{Leu} / (I_{Leu} + I_{Pro})$  where  $I_{Leu}$  and  $I_{Pro}$  correspond to the intensity of toeprint bands due to stalling at Leu<sub>7</sub> and Pro<sub>10</sub> codon respectively. Error bars show deviation from the mean in two independent experiments.

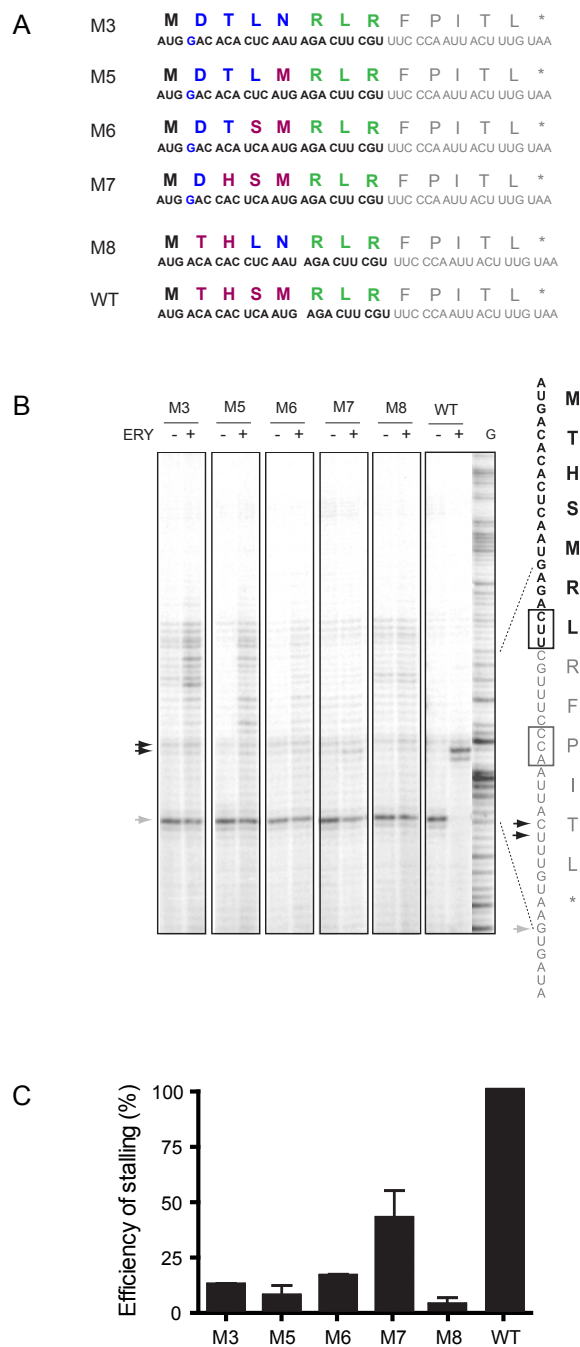


**Figure 4.4. Integrity of the N-terminal segment of ErmDL is required for efficient antibiotic dependent translation arrest (A)** The nucleotide and amino acid sequences of templates of wt-ErmDL and its N-terminal variants M3 (see Figure. 4.2) and M5-7 (which are hybrids generated by combining the wt and M3 templates). **(B)** Toeprinting analysis of ERY-dependent ribosome stalling in the different templates. Black or gray arrowheads indicate the toeprints of stalled ribosomes with their P-sites at the Leu<sub>7</sub> (boxed in black) or Pro<sub>10</sub> (boxed in gray) codons, respectively. Sequencing lane is marked as G. **(C)** Bar graph of the efficiency of ERY-mediated stalling at the Leu<sub>7</sub> codon (estimated as described in Figure. 4.2). Error bars show deviation from the mean in two independent experiments.

residue is underlined), had no effect and stalling still remained negligible. When residues 4 and 5 of the mutant were reverted to wt (construct M6, MDTSMRRLR), stalling efficiency remained as low as ca. 20 % relative to the wt ErmDL. When reverting residues 3-5 (construct M7, MDHSMRLR), where only one amino acid differed from that in wt ErmDL (Thr<sub>2</sub> to Asp), stalling was restored to the level of ca. 37%. These results of the ‘sliding’ mutagenesis seemed to suggest an exceptionally prominent role of one of the most distant residues from the stalling RLR motif. However, when in the final construct (M8, MTHLNRLR) we kept the wt MTH sequence but replaced residues 4 and 5 to their M3 mutant identities (LN), translation arrest was again alleviated.

Altogether, the results of the mutational analysis showed that the sequence preceding the RLR stalling motif could significantly modulate drug-dependent stalling. However, the contribution of individual amino acids in the N-terminal ErmDL sequence was not clearly assigned. It appears, instead, that the composite structure of the nascent chain segment upstream of the arrest motif controls whether ERY promotes ribosome stalling within the RLR motif, or it allows for translation to continue past this sequence in spite of the antibiotic presence.

#### **4.3.2 ERY remains bound to the ribosome, which translates through the RLR sequence.**

We considered the possibility that the N-terminal sequences of the ‘counter-stalling’ segment of the ErmDL mutants could displace the ERY molecule from its binding site in the NPET, as it has been previously shown for some short peptides (Tenson et al., 1996, Tenson et al., 1997, Tripathi et al, 1998, Vimberg et al., 2004).

Displacement of the antibiotic from its binding site would prevent arrest at the RLR sequence. In order to test this scenario, we analyzed whether ERY remained bound to the ribosomes that have synthesized the M3 mutant peptide MDTLNRLR. We prepared the hybrid template (M3-BL), where the sequence of the M3 *ermDL* mutant encoding the MDTLNRLR peptide was extended with the codons specifying the stalling segment LVFQMRNVDK of another stalling peptide, ErmBL (Figure. 4.5). In ErmBL, ERY-dependent translation arrest occurs at the aspartate codon within the VDK sequence (Min et al., 2008, Vazquez-Laslop et al., 2010, Arenz et al., 2014, Gupta et al., 2016). The use of thiostrepton, a drug that in the cell-free system arrests the ribosome at the initiation codon, showed that translation of the hybrid template initiates exclusively at the *ermDL* start codon (Figure. 4.5, lane ‘Ths’). When the M3-BL hybrid was translated in the presence of ERY, a single prominent toeprint band corresponding to the ribosomes stalled at the Asp<sub>17</sub> codon of the *ermBL* segment of the template was observed (Figure. 4.5). Because ERY is likely unable to rebind to the ribosome when a nascent chain is already in the NPET, this result demonstrated that ribosomes that translated through the RLR sequence of the ErmDL M3 mutant still retained the antibiotic. Thus, the mutant ErmDL N-terminal sequence allows translation of the RLR motif in spite of the antibiotic presence.

### **4.3.3 The counter-stalling sequence of the *ermDL* M3 mutant can operate inside the gene.**

In the wt *ermDL*, translation arrest takes place when the nascent chain is only 7 residues long and spans only a short NPET segment. Therefore, our finding that the



peptide sequence preceding the RLR site modulates the efficiency of the arrest could represent only a special case related only to the stalling sequences near the start of the gene. In order to test the generality of the observed phenomenon we asked whether the counter-stalling sequence MDTLN preceding the RLR motif in the M3 mutant would prevent ERY-induced arrest when placed farther away from the nascent chain N-terminus.

Ribosome profiling data showed that translation of the *E. coli* gene *lpp* continues at a high level in the cells treated with high concentrations of ERY (Kannan et al., 2014) (Figure. 4.6A). Thus, the 5'-terminal portion of the wt *lpp* gene has no intrinsic ERY stalling sites. When we fused the wt *ermDL* sequence after the first 15 codons of the *lpp* gene (Lpp<sub>15</sub>-MTHSMRLR template in Figure. 4.6A), translation was efficiently arrested at the Leu<sub>22</sub> codon, corresponding to the Leu codon of the RLR motif in the template, after a 22 amino acid long nascent chain was synthesized by the drug-bound ribosome (Figure. 4.6B, left gel). [The thiostrepton test (Figure. 4.6B, lane 'Ths') confirmed that the translation of the hybrid template is initiated at the *lpp* start codon, not at the methionine codons of the *ermDL*-encoded MTHSMRLR sequence]. Essentially no ERY-bound ribosomes were able to bypass the RLR motif (black arrow in Figure. 4.6B) of Lpp<sub>15</sub>-MTHSMRLR, as revealed by the absence of the toeprint band at the downstream 'catch' codon (grey arrow in Figure. 4.6B). In contrast, when the MTHSM segment of ErmDL was replaced with the counter-stalling MDTLN sequence within the *lpp* gene (Lpp<sub>15</sub>-MDTLNRLR template in Figure. 4.6A), stalling at the RLR motif dropped nearly three-fold and a large fraction of ERY-bound ribosomes could reach the catch codon (Figure. 4.6B-C). These results demonstrated that the amino acid context preceding the arrest sequence can modulate antibiotic-mediated stalling not only of the ribosomes

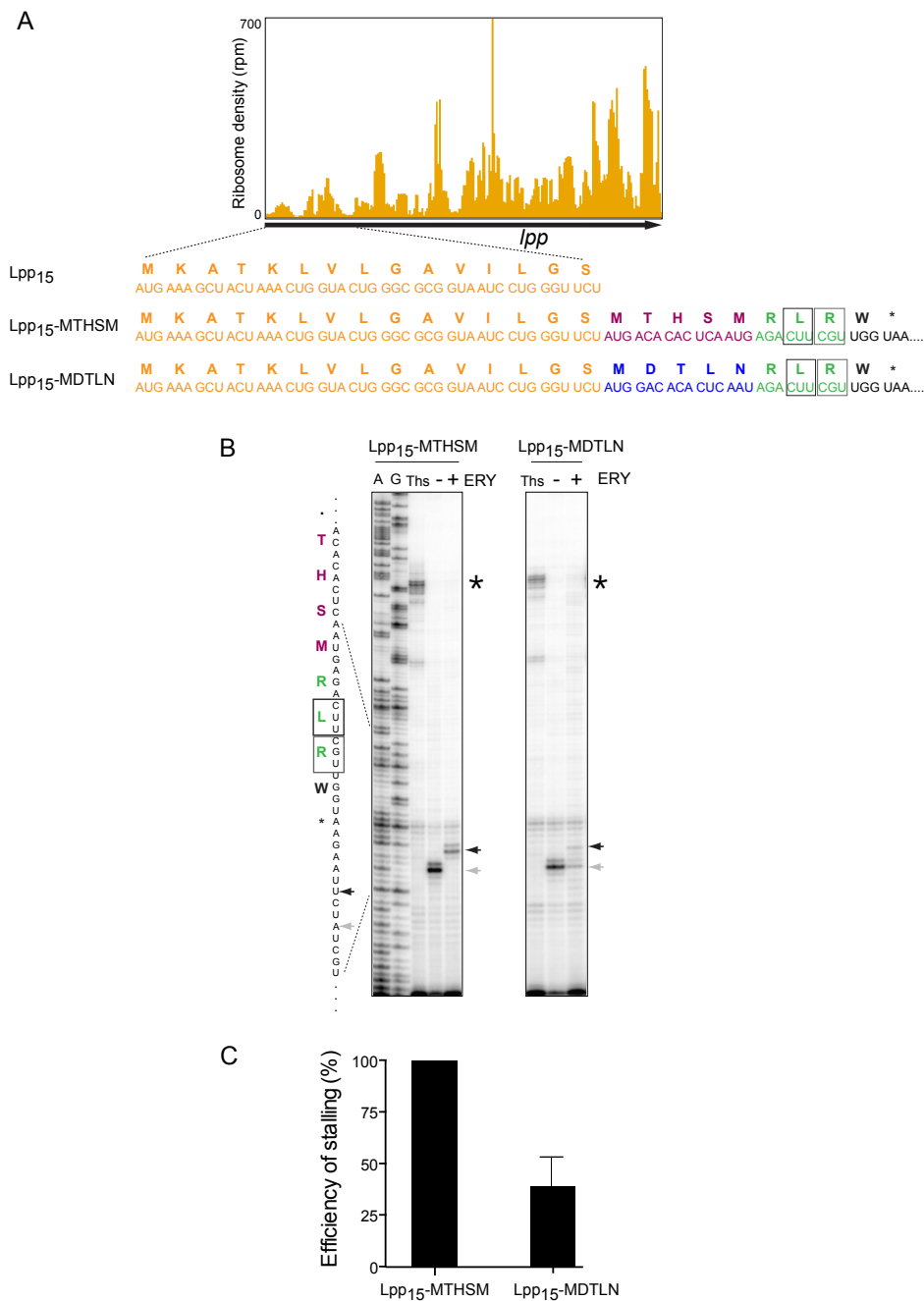


**Figure 4.6. Antibiotic-mediated late translation arrest at internal ‘RLR’ sequences is also context specific. (A)** Ribosome density at the *E. coli lpp* gene in the presence of ERY from the previously reported ribosome profiling data (Kannan et al, 2014). Below the panel is shown the nucleotide and amino acid sequences of the first 15 codons of *lpp* (Lpp<sub>15</sub>) used to generate cell free translation templates for Lpp<sub>15</sub>-MTHSM-RLR and Lpp<sub>15</sub>-MDTLN-RLR. **(B)** Toeprinting analysis of ERY-dependent ribosome stalling in the indicated templates. Ribosomes that continue translation past the Leu<sub>22</sub> codon are

trapped at the downstream Arg<sub>23</sub> codon due to the presence of TrpRS inhibitor indolmycin in the reactions. Black and gray arrowheads indicate the toeprint signals generated by arrested ribosomes whose P-site is located at the Leu<sub>22</sub> (black box in the sequence besides the gel) or Arg<sub>23</sub> (gray box) codon, respectively. The unique strong toeprint bands (marked with an asterisk) in the lanes of the samples that contained thiostrepton (Ths) (an inhibitor of initiation) show that translation only initiates at the first AUG codon of the templates. Sequencing lanes are marked as A, G. **(C)** The bar graph shows the efficiency of ERY-mediated arrest at the Leu<sub>22</sub> codon estimated by  $I_{Leu} / (I_{Leu} + I_{Arg})$  where  $I_{Leu}$  and  $I_{Arg}$  correspond to the intensity of toeprint bands due to arrest at Leu<sub>22</sub> or Arg<sub>23</sub> codon, respectively. Error bars show deviation from the mean in two independent experiments.

carrying short nascent peptides, but it can also counteract ERY-induced translation arrest at the R/K-X-R/K motifs located far away from the start of the gene.

#### **4.3.4 The N-terminal sequence of the ErmDL peptide acts as an independent stalling module that promotes translation arrest even at non-optimal stalling motifs.**

Given that the mutant N-terminal sequences of ErmDL prevent translation arrest at the 7<sup>th</sup> codon, whereas the wt sequence is highly conducive to it, we wondered whether the original ErmDL N-terminal segment could act as an independent stalling module, which would be able to promote ERY-dependent arrest even when the RLR arrest motif is corrupted by point mutations. To test this hypothesis, we analyzed antibiotic-triggered arrest using ErmDL templates where the individual amino acids of its RLR sequence were replaced with Ala residues, generating templates ALR, RLA, ALA, or AAA (Figure . 4.7A). In striking contrast with the results obtained with the truncated MRLR template, where the ALR and RLA mutations completely abolished ERY-induced translation arrest (Sothiselvam et al., in submission) (Figure. 4.8), the individual Ala mutations of the Arg residues of RLR had only a marginal effect upon stalling in the context of the full size ErmDL. Even the simultaneous replacement of both critical Arg

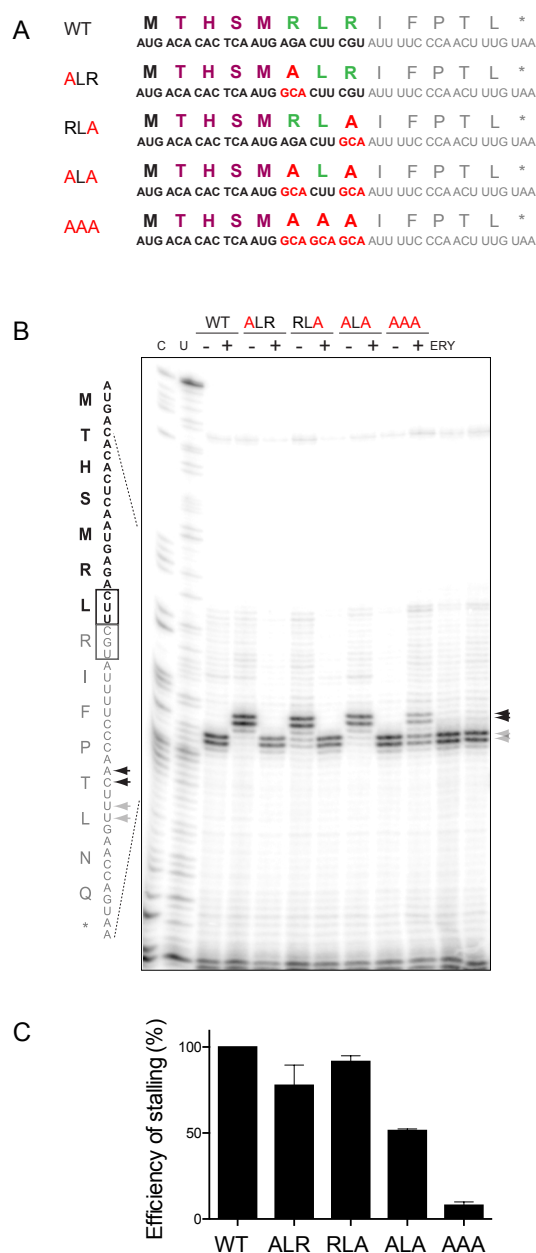


**Figure 4.7. The N-terminal segment of ErmDL can support translation arrest even when its arrest motif is altered. (A)** Nucleotide and amino acid sequences for the wt-ErmDL peptide or its arrest motif variants ALR, RLA, ALA and AAA. **(B)** Toeprinting analysis of ERY-dependent translation arrest. Samples contained mupirocin (see legend of Figure. 4.2). Black and gray arrowheads indicate the toeprint signals of ribosomes whose P site is at codon 7 (Leu or Ala) (boxed in black) or codon 8 (Arg or Ala) (boxed in gray), respectively. Sequencing lanes are marked as C, U. **(C)** Bar graph of the efficiency of ERY-mediated stalling at the codon-7 was estimated by  $I_{\text{codon-7}} / (I_{\text{codon-7}} + I_{\text{codon-8}})$  where  $I_{\text{codon-7}}$  and  $I_{\text{codon-8}}$  correspond to the intensity of toe printing bands due to stalling at codon-7 or codon-8 respectively. Error bars show deviation from the mean in two independent experiments.

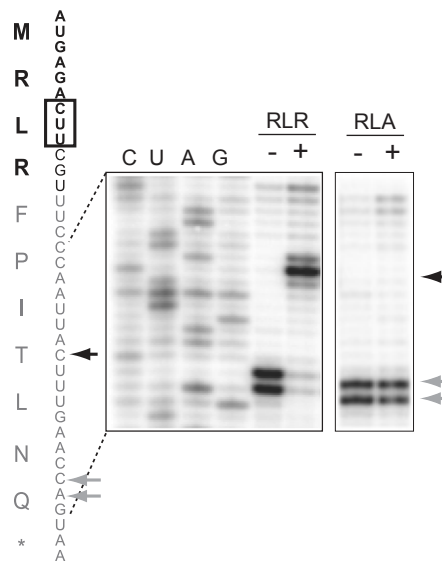


**Figure 4.8. Altering the arrest sequence abolishes ribosome stalling when there is no preceding n-terminal sequence.** Toeprinting analysis of ERY-dependent translation arrest on templates that code for MRLR and MRLA. Samples contained mupirocin (see legend of Figure. 4.2). Black and gray arrowheads indicate the toeprint signals of ribosomes whose P site is at codon 3 (Leu) (boxed in black) or codon 6 (Pro) respectively. Sequencing lanes are marked as C, U, A, G.



residues with Ala still allowed for ca. 50% efficient arrest. Only the simultaneous replacement of the entire RLR sequence with alanine residues finally prevented ERY-induced ribosome stalling at the 7<sup>th</sup> codon of the MTHSMAAA template (Figure. 4.7B, C). These results imply that, although the most efficient translation arrest occurs when the wt RLR sequence (fully conforming to the R/K-X-R/K motif) is present, the ErmDL N-terminal segment MTHSM widens the range of amino acid sequences at which the ERY-bound ribosome is prompt to stall. Thus, the N-terminal segment of ErmDL seems to function as an independent module with a specific function in the mechanism of programmed translation arrest. Interestingly, however, the stalling stimulatory effect of the MTHSM domain becomes evident only when this sequence is placed at the N-terminus of the nascent chain. When the MTHSM sequence was inserted after the first 15 codons of the *lpp* gene, changing any of the critical Arg residues of the RLR motif to Ala nearly eliminated stalling (Figure. 4.9).

#### 4.4 **Discussion**

Binding of a macrolide antibiotic to the ribosome makes specific sequence motifs problematic for the peptidyl transfer reaction. The ribosome, which in spite of the antibiotic being bound in the NPET is able to polymerize a broad array of amino acid sequences, halts when it has to catalyze peptide bond formation between certain combinations of donor and acceptor substrates. Previous genome-wide *in vivo* approaches and *in vitro* biochemical experiments have shown that the properties of amino acid residues at the C-terminus of the nascent peptide and the nature of the incoming aminoacyl acceptor are the key factors that determine the drug-induced translation arrest (Sothiselvam et al., 2014, Ramu et al., 2011, Gupta et al., 2016, Kannan et al., 2014, Davis et al., 2014, Vázquez-Laslop et al., 2014). However, the influence of the context, within which the problematic sequence occurs, remained unexplored. In this paper we have examined how the short segment of the nascent peptide chain preceding the problematic sequence, affects ribosome stalling within the RLR motif, a prime representative of one of the most prominent macrolide arrest consensus sequences, R/K-X-R/K. We have shown that replacement of the wt amino acid sequence MTHSM, which immediately precedes the RLR stalling site of the ErmDL leader peptide, with several unrelated sequences can nearly abolish ERY-induced ribosome stalling. The ‘counteracting’ sequences could also significantly reduce stalling at the RLR motif, when placed farther inside a gene. We also showed that the ErmDL wt N-terminal sequence could play an arrest-stimulatory role, expanding the range of sequences conducive to drug-induced stalling beyond the R/K-X-R/K consensus.

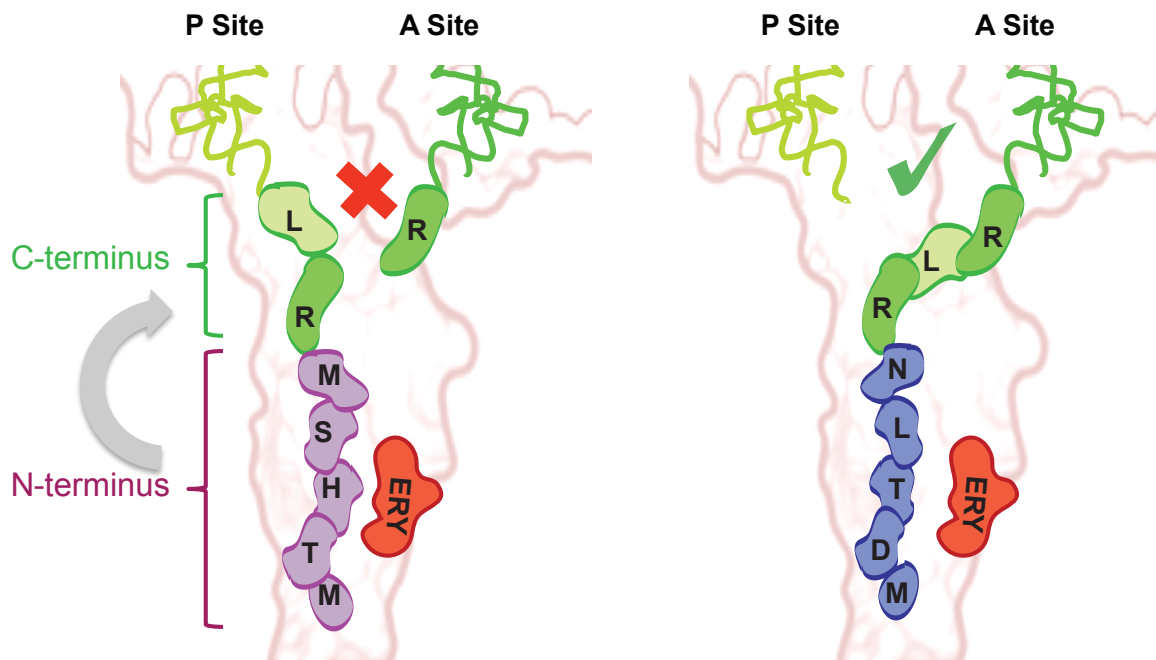


**Figure 4.10.** Cartoon representation of the effect of N-terminal sequence of the peptide on the C-terminal arrest motif in the exit tunnel of the antibiotic bound ribosome. N-terminal sequence MTHSM facilitates translation arrest at RLR while MDTLN abrogates arrest.

Our results strongly argue that the general structure of the N-terminal segment of ErmDL is functionally critical. However, we were not able to draw a clear conclusion about the contribution of individual amino acids within this segment for stimulating or counteracting the arrest. Replacement of any of the four amino acid residues (2-5) of the wild type sequence MTHSM with alanine had only marginal effects on arrest within the following RLR motif (Figure. 4.3). However, substitution of the wt Thr<sub>2</sub> residue to Asp was enough to reduce efficiency of stalling by ca. 70% (Figure. 4.4, mutant M7). Yet, when the first three amino acids of ErmDL, including Thr<sub>2</sub>, were left intact, but residues Ser<sub>4</sub> and Met<sub>5</sub> were changed to Leu and Asn, respectively, translation arrest was essentially alleviated (Figure. 4.4, mutant M8). Altogether these results are compatible with the possibility that it is not so much the nature of individual amino acids, but rather the overall structural or physicochemical properties of the entire nascent chain segment preceding the stalling motif that are important.

The observation that a variety of N-terminal sequences can prevent ribosome from stalling at the 7<sup>th</sup> codon of the *ermDL* gene within the RLR motif, suggests that not only the arrest sequence, but also the N-terminal portion of the leader peptide have been evolutionary optimized to direct efficient ribosome stalling. In agreement with this hypothesis, the presence of the wt N-terminal segment preceding RLR makes macrolide-induced arrest extremely robust. Remarkably, when N-terminal segment is completely absent, as it is the case in the short stalling sequence MRLR, the identities of the penultimate amino acid of the nascent chain (MRL) and the aminoacyl acceptor (Arg-tRNA) are critical. Substitution of the crucial residues with amino acids other than Arg or Lys, abolishes ribosome stalling (Sothiselvam et al, in submission) (Figure. 4.8).

However, in contrast, when the RLR motif is preceded by the wt ErmDL sequence MTHSM, the mutations of the critical positions of the stalling RLR motif to alanine are significantly tolerated (Figure. 4.8). Even when both of the critical Arg residues of the RLR motif are simultaneously mutated to Ala, the arrest at the 7<sup>th</sup> codon of *ermDL* still occurs with ca. 50% efficiency compared to wt (Figure. 4.8). Thus, the wt ErmDL N-terminal module makes macrolide-dependent ribosome stalling and thus, inducible expression of the downstream *ermD* resistance gene, much more tolerant to spontaneous mutations of the critical motif. The unexpected finding that the ribosome stalls at the ‘correct’ *ermDL* codon even when two of the three positions of the stalling RLR motif are mutated, also indicates that the N-terminal module preceding the arrest sequence possess an independent capacity to direct ribosome stalling. However, interestingly, this capacity is manifested only when the MTHSM sequence is present at the N-terminus of the nascent peptide. Its insertion at a gene location farther from the start abolished its ability to support stalling at the mutated RLR motifs (Figure. 4.9). The major difference between the presence of the module as the N-terminus or as an internal domain is the length of the nascent chain. At the early rounds of translation, a peptidyl-tRNA with a short peptide is prone to rapid dissociation from the ribosome (Heurgue-Hamard et al., 2000). Premature peptidyl-tRNA drop-off is additionally stimulated by the presence of the macrolide molecule in the NPET (Tenson et al., 2003). Thus, even if the ribosome pauses because it is incapable of polymerizing the RLR sequence, the stalled complex could be unstable due to rapid peptidyl-tRNA drop-off. Therefore, the ‘special’ task of the wt ErmDL sequence could be to stabilize the association of peptidyl-tRNA with the ribosome and increasing the life span of the stalled ribosome complex for the time-frame

required to isomerize the mRNA structure and activate the downstream resistance gene. Stabilization of the peptidyl-tRNA could be hypothetically achieved by tight contacts between the ErmDL N-terminal segment, jammed in the narrow opening of the NPET obstructed by the antibiotic, with the drug and/or with the ribosome (Figure. 4.10). Such jamming may not only stabilize the association of the peptidyl-tRNA with the ribosome, but also impede progression of the nascent chain through the tunnel, which could result in translation arrest at the 7<sup>th</sup> codon of *ermDL* even when the RLR stalling motif is mutated. These nascent peptide-antibiotic interactions could be significantly different when the corresponding ErmDL sequence is distant from the N-terminus. The longer nascent peptide, which has already threaded through the antibiotic-obstructed NPET, may assume a conformation that would prevent tight interactions between the ErmDL MTHSM sequence and the drug, and hence lose its stimulatory arrest effect on mutant RLR sequences.

Following a similar logic, the counteracting activity of the mutant MDTLN (M3) sequence upon stalling, could also be mediated by its interaction with the tunnel-bound antibiotic. Due to either its overall structure or its specific interactions with the drug and/or the ribosome, the MDTLN module could restrict the placement of the nascent chain to conformations that would facilitate its transfer to Arg-tRNA acceptor (Figure. 4.10). It is conceivable that a similar effect could be achieved even when a longer nascent chain precedes the site of arrest, which would explain the counteractive effect of the MDTLN sequence upon drug-induced arrest at an RLR motif placed inside the gene (Figure. 4.6).

Our findings that the ErmDL sequence preceding the critical arrest motif affects the efficiency of drug-induced ribosome stalling, formally resemble the results obtained with several other regulatory or artificial stalling peptides. In these cases, the structure of the nascent chain distant from the C-terminus plays a major role in the mechanism of arrest (Chiba et al., 2012, Nakatogawa et al., 2002, Woolstenhulme et al., 2013). Although all these systems share several similarities, it is important to recognize that macrolide-induced translation arrest is principally different. Unlike examples of the intrinsic, cofactor-independent, ribosome stalling, modulation of antibiotic-induced translation arrest is likely mediated by interactions of the nascent chain, encoded in the uORF, with the antibiotic. There is a superficial resemblance between macrolide-induced stalling at the regulatory ORFs of the resistance genes and tryptophan-mediated arrest of termination of the *tnaC* gene (Gong et al., 2002, Martinez et al., 2014). Indeed, biochemical and structural data suggest that the tryptophan cofactor binds at a location that overlaps with the macrolide-binding site in the NPET (Martinez et al., 2014, Bischoff et al., 2014). However, the ERY molecule is nearly 4 times bigger than Trp and thus obstructs the tunnel much more significantly. Furthermore, the arrest of the *tnaC* termination occurs when the nascent peptide is 24-residues long, and spans nearly the entire NPET, whereas translation of *ermDL* is halted at codon 7, when the nascent chain is still negotiating its PTC-proximal segment. Therefore, it may be that the peptide segments preceding the site(s) of macrolide-dependent arrest and those preceding the sites of arrest of other stalling peptides can inhibit the peptidyl transfer reaction by operating on significantly different principles.

In conclusion, our results revealed an important influence of the protein context sequence on the mode of antibiotic action. Not only the presence of the well-defined arrest motifs, but also the context in which they appear in the protein structure may modulate the extent of inhibition of translation by macrolide drugs. The same phenomenon seems to play an important role in the mechanism of inducible resistance, where the evolutionary selected context facilitates the operation of the ‘conventional’ stalling motif in the mechanism of gene regulation. Further unraveling of context specificity of macrolide action will illuminate the rational development of better drugs and new ways to combat resistance.

## 4.5 Cited Literature

Almutairi, M.M., Park, S.R., Rose, S., Hansen, D.A., Vazquez-Laslop, N., Douthwaite, S., Sherman, D.H., and Mankin, A.S. (2015). Resistance to ketolide antibiotics by coordinated expression of rRNA methyltransferases in a bacterial producer of natural ketolides. *Proceedings of the National Academy of Sciences of the United States of America* 112, 12956-12961.

Arenz, S., Meydan, S., Starosta, A.L., Berninghausen, O., Beckmann, R., Vazquez-Laslop, N., and Wilson, D.N. (2014a). Drug sensing by the ribosome induces translational arrest via active site perturbation. *Molecular cell* 56, 446-452.

Arenz, S., Ramu, H., Gupta, P., Berninghausen, O., Beckmann, R., Vazquez-Laslop, N., Mankin, A.S., and Wilson, D.N. (2014b). Molecular basis for erythromycin-dependent ribosome stalling during translation of the ErmBL leader peptide. *Nature communications* 5, 3501.

Bischoff, L., Berninghausen, O., and Beckmann, R. (2014). Molecular basis for the ribosome functioning as an L-tryptophan sensor. *Cell reports* 9, 469-475.

Bulkley, D., Innis, C.A., Blaha, G., and Steitz, T.A. (2010). Revisiting the structures of several antibiotics bound to the bacterial ribosome. *Proceedings of the National Academy of Sciences of the United States of America* 107, 17158-17163.

Chiba, S., and Ito, K. (2012). Multisite ribosomal stalling: a unique mode of regulatory nascent chain action revealed for MifM. *Molecular cell* 47, 863-872.

Davis, A.R., Gohara, D.W., and Yap, M.N. (2014). Sequence selectivity of macrolide-induced translational attenuation. *Proceedings of the National Academy of Sciences of the United States of America* 111, 15379-15384.

Dunkle, J.A., Xiong, L., Mankin, A.S., and Cate, J.H. (2010). Structures of the *Escherichia coli* ribosome with antibiotics bound near the peptidyl transferase center explain spectra of drug action. *Proceedings of the National Academy of Sciences of the United States of America* 107, 17152-17157.

Gong, F., and Yanofsky, C. (2002). Instruction of translating ribosome by nascent peptide. *Science* 297, 1864-1867.

Gupta, P., Liu, B., Klepacki, D., Gupta, V., Schulten, K., Mankin, A.S., and Vazquez-Laslop, N. (2016). Nascent peptide assists the ribosome in recognizing chemically distinct small molecules. *Nature chemical biology*.

Heurgue-Hamard, V., Dincbas, V., Buckingham, R.H., and Ehrenberg, M. (2000). Origins of minigene-dependent growth inhibition in bacterial cells. *The EMBO journal* 19, 2701-2709.

Hue, K.K., and Bechhofer, D.H. (1992). Regulation of the macrolide-lincosamide-streptogramin B resistance gene *ermD*. *Journal of bacteriology* 174, 5860-5868.

Kannan, K., Kanabar, P., Schryer, D., Florin, T., Oh, E., Bahroos, N., Tenson, T., Weissman, J.S., and Mankin, A.S. (2014). The general mode of translation inhibition by macrolide antibiotics. *Proceedings of the National Academy of Sciences of the United States of America* 111, 15958-15963.

Kannan, K., Vazquez-Laslop, N., and Mankin, A.S. (2012). Selective protein synthesis by ribosomes with a drug-obstructed exit tunnel. *Cell* 151, 508-520.

Kwak, J.H., Choi, E.C., and Weisblum, B. (1991). Transcriptional attenuation control of *ermK*, a macrolide-lincosamide-streptogramin B resistance determinant from *Bacillus licheniformis*. *Journal of bacteriology* 173, 4725-4735.

Kwon, A.R., Min, Y.H., Yoon, E.J., Kim, J.A., Shim, M.J., and Choi, E.C. (2006). *ErmK* leader peptide : amino acid sequence critical for induction by erythromycin. *Archives of pharmacal research* 29, 1154-1157.

Martinez, A.K., Gordon, E., Sengupta, A., Shirole, N., Klepacki, D., Martinez-Garriga, B., Brown, L.M., Benedik, M.J., Yanofsky, C., Mankin, A.S., et al. (2014). Interactions of the *TnaC* nascent peptide with rRNA in the exit tunnel enable the ribosome to respond to free tryptophan. *Nucleic acids research* 42, 1245-1256.

Menninger, J.R. (1995). Mechanism of inhibition of protein synthesis by macrolide and lincosamide antibiotics. *Journal of basic and clinical physiology and pharmacology* 6, 229-250.

Min, Y.H., Kwon, A.R., Yoon, E.J., Shim, M.J., and Choi, E.C. (2008). Translational attenuation and mRNA stabilization as mechanisms of *erm(B)* induction by erythromycin. *Antimicrobial agents and chemotherapy* 52, 1782-1789.

Nakatogawa, H., and Ito, K. (2002). The ribosomal exit tunnel functions as a discriminating gate. *Cell* 108, 629-636.

Nilsson, O.B., Hedman, R., Marino, J., Wickles, S., Bischoff, L., Johansson, M., Muller-Lucks, A., Trovato, F., Puglisi, J.D., O'Brien, E.P., et al. (2015). Cotranslational Protein Folding inside the Ribosome Exit Tunnel. *Cell reports* 12, 1533-1540.

Ramu, H., Mankin, A., and Vazquez-Laslop, N. (2009). Programmed drug-dependent ribosome stalling. *Molecular microbiology* 71, 811-824.

Ramu, H., Vazquez-Laslop, N., Klepacki, D., Dai, Q., Piccirilli, J., Micura, R., and Mankin, A.S. (2011). Nascent peptide in the ribosome exit tunnel affects functional properties of the A-site of the peptidyl transferase center. *Molecular cell* 41, 321-330.

Schlunzen, F., Zarivach, R., Harms, J., Bashan, A., Tocilj, A., Albrecht, R., Yonath, A., and Franceschi, F. (2001). Structural basis for the interaction of antibiotics with the peptidyl transferase centre in eubacteria. *Nature* 413, 814-821.

Sothiselvam, S., Liu, B., Han, W., Ramu, H., Klepacki, D., Atkinson, G.C., Brauer, A., Remm, M., Tenson, T., Schulten, K., et al. (2014). Macrolide antibiotics allosterically predispose the ribosome for translation arrest. *Proceedings of the National Academy of Sciences of the United States of America* 111, 9804-9809.

Subramanian SL, Ramu H, Mankin AS. Inducible resistance to macrolide antibiotics. In: Dougherty TJ, Pucci, M. J. , editor. *Antibiotic Drug Discovery and Development*. New York, NY: Springer Publishing Company; 2011.

Starosta, A.L., Karpenko, V.V., Shishkina, A.V., Mikolajka, A., Sumbatyan, N.V., Schlunzen, F., Korshunova, G.A., Bogdanov, A.A., and Wilson, D.N. (2010). Interplay between the ribosomal tunnel, nascent chain, and macrolides influences drug inhibition. *Chemistry & biology* 17, 504-514.

Tenson, T., DeBlasio, A., and Mankin, A. (1996). A functional peptide encoded in the *Escherichia coli* 23S rRNA. *Proceedings of the National Academy of Sciences of the United States of America* 93, 5641-5646.

Tenson, T., Lovmar, M., and Ehrenberg, M. (2003). The mechanism of action of macrolides, lincosamides and streptogramin B reveals the nascent peptide exit path in the ribosome. *Journal of molecular biology* 330, 1005-1014.

Tenson, T., Xiong, L., Kloss, P., and Mankin, A.S. (1997). Erythromycin resistance peptides selected from random peptide libraries. *The Journal of biological chemistry* 272, 17425-17430.

Tripathi, S., Kloss, P.S., and Mankin, A.S. (1998). Ketolide resistance conferred by short peptides. *The Journal of biological chemistry* 273, 20073-20077.

Vazquez-Laslop, N., Ramu, H., Klepacki, D., Kannan, K., and Mankin, A.S. (2010). The key function of a conserved and modified rRNA residue in the ribosomal response to the nascent peptide. *The EMBO journal* 29, 3108-3117.

Vázquez-Laslop, N., Mankin, A.S. (2014) Triggering peptide-dependent translation arrest by small molecules: ribosome stalling modulated by antibiotics. In: *Regulatory Nascent Polypeptides* (Ito, K., ed). Springer (Tokyo) 0, 165-186.

Vimberg, V., Xiong, L., Bailey, M., Tenson, T., and Mankin, A. (2004). Peptide-mediated macrolide resistance reveals possible specific interactions in the nascent peptide exit tunnel. *Molecular microbiology* 54, 376-385.

Weisblum, B. (1995). Erythromycin resistance by ribosome modification. *Antimicrobial agents and chemotherapy* 39, 577-585.

Woolstenhulme, C.J., Guydosh, N.R., Green, R., and Buskirk, A.R. (2015). High-precision analysis of translational pausing by ribosome profiling in bacteria lacking EFP. *Cell reports* 11, 13-21.

Woolstenhulme, C.J., Parajuli, S., Healey, D.W., Valverde, D.P., Petersen, E.N., Starosta, A.L., Guydosh, N.R., Johnson, W.E., Wilson, D.N., and Buskirk, A.R. (2013). Nascent peptides that block protein synthesis in bacteria. *Proceedings of the National Academy of Sciences of the United States of America* 110, E878-887.

## **APPENDICES**

### **Appendix A**

The following section includes work that I did during my graduate work in the Mankin Lab as part of my rotation project. The publication has been attached as it is and the permission to include the publication has been attached.

#### **Author Contributions**

Pulkit Gupta, Nora Vazquez-Laslop and Alexander Mankin designed the experiments. Pulkit Gupta and Shanmugapriya Sothiselvam performed the experiments. Pulkit Gupta, Nora Vazquez-Laslop and Alexander Mankin wrote the paper.

### **Permission requests from authors**

The authors of articles published by Nature Publishing Group, or the authors' designated agents, do not usually need to seek permission for re-use of their material as long as the journal is credited with initial publication. For further information about the terms of re-use for authors please see below.

### **Author Requests**

If you are the author of this content (or his/her designated agent) please read the following. Since 2003, ownership of copyright in original research articles remains with the Authors\*, and provided that, when reproducing the Contribution or extracts from it, the Authors acknowledge first and reference publication in the Journal, the Authors retain the following non-exclusive rights:

- a. To reproduce the Contribution in whole or in part in any printed volume (book or thesis) of which they are the author(s).
- b. They and any academic institution where they work at the time may reproduce the Contribution for the purpose of course teaching.
- c. To reuse Figures or tables created by them and contained in the Contribution in other works created by them.
- d. To post a copy of the Contribution as accepted for publication after peer review (in Word or Tex format) on the Author's own web site, or the Author's institutional repository, or the Author's funding body's archive, six months after publication of the printed or online edition of the Journal, provided that they also link to the Journal article on NPG's web site (eg through the DOI).

NPG encourages the self-archiving of the accepted version of your manuscript in your funding agency's or institution's repository, six months after publication. This policy complements the recently announced policies of the US National Institutes of Health, Wellcome Trust and other research funding bodies around the world. NPG recognizes the efforts of funding bodies to increase access to the research they fund, and we strongly encourage authors to participate in such efforts.

## Shanmugapriya Sothiselvam

900 S. Ashland Avenue Rm 3060 • Chicago, IL 60607 • Phone: 773-677-2753 • ssodhi2@uic.edu

Date: February 10, 2016

Pulkit Gupta, PhD  
Post Doctoral Research Associate.  
Merck, Inc.

Dear Pulkit,

I am writing to request permission to use the material from your publication (Deregulation of translation due to post-transcriptional modification of rRNA explains why erm genes are inducible *Nat Commun* 4, 1984 DOI: 10.1038/ncomms2984. ) in my thesis. This material will appear as originally published in the Appendix of my thesis. Unless you request otherwise, I will use the conventional style of the Graduate College of the University of Illinois at Chicago as acknowledgment.

A copy of this letter is included for your records. Thank you for your kind consideration of this request.

Sincerely,

Shanmugapriya Sothiselvam  
900 S. Ashland Avenue Rm 3060,  
Chicago IL 60607

The above request is approved.

Approved by: PULKIT GUPTA  Date: 02/10/16

**Deregulation of translation due to posttranscriptional modification of rRNA  
explains why *erm* genes are inducible**

**Introduction and rationale**

Resistance to antibiotics is a serious medical problem. It cripples the efficacy of drugs, especially those that have been in medical use for a considerable length of time. One of the oldest classes of antibacterials are the macrolides, which inhibit bacterial growth by binding to the nascent peptide exit tunnel (NPET) of the ribosome and interfering with protein synthesis (reviewed in (Gaynor and Mankin, 2003; Poehlsgaard and Douthwaite, 2005). The prototype macrolide, erythromycin (ERY), and its more modern derivatives are among the most successful antibacterials. Macrolides have been used for more than half a century for treatment of serious infections caused by a range of Gram-positive pathogens. The extensive and prolonged use of these drugs led to the spread of resistance. One of the main resistance mechanisms is based on dimethylation of a unique adenine residue in 23S rRNA, A2058 (*E. coli* numbering), located in the macrolide binding site in the NPET (Weisblum, 1995) (Figure. 1). This posttranscriptional modification prevents binding of the macrolides to the ribosome and renders cells resistant to very high concentrations of these drugs. The same modification confers resistance to two other classes of antibiotics, lincosamides and streptogramins B, whose binding sites in the ribosome overlap with that of macrolides (Sutcliffe and Leclercq, 2002). The methylation of A2058 is catalyzed by Erm methyltransferase. The *erm* genes that encode this enzyme are found in the genomes of various macrolide

producers, from which they have disseminated to other bacterial species, including many clinical pathogens (Cundliffe, 1989).

Early investigations of one of the first known genes of this class, *ermC*, led to the discovery of its inducibility: in the absence of the drug, the resistance gene was not expressed but resistance rapidly developed when cells were exposed to macrolides like ERY (Griffith et al., 1965; Weisblum and Demohn, 1969). The majority of more than 40 types of *erm* genes that are currently known show signatures of inducibility (Ramu et al., 2009; Roberts, 2004, 2008; Subramanian et al., 2011); most of the constitutive *erm*s appear to be merely the mutant versions of the originally inducible genes (Rosato et al., 1999; Schmitz et al., 2002; Werckenthin and Schwarz, 2000). While many examples of inducible resistance genes are now known, the drug-dependent activation of the *ermC* gene remains one of the most well-studied and paradigm-setting systems (Weisblum, 1995).

The molecular mechanism of *ermC* induction has been extensively characterized. It involves drug- and nascent peptide-controlled programmed translation arrest at the regulatory open reading frame that leads to mRNA isomerization and activation of *ermC* expression (Horinouchi and Weisblum, 1980; Shivakumar et al., 1980b; Vazquez-Laslop et al., 2008). It is likely that inducible expression plays a key role in the rapid dissemination of *erm*-mediated resistance (Andersson and Hughes, 2010). However, it remains unknown why bacteria favor *erm* genes to be inducible. Therefore, the driving force for evolving a complex regulatory scheme for the drug-dependent activation of expression of the Erm methyltransferase has remained obscure. It has been speculated that expression of the *erm* genes could be associated with an unspecified fitness cost

(Depardieu et al., 2007; Foucault et al., 2010). However, the assertion that *erm* expression reduces cell fitness and the reasons for the alleged fitness cost have never been experimentally demonstrated. Furthermore, it is not clear why production of Erm protein and the resulting addition of just two methyl groups with combined molecular weight of 30 Da to a site located 10 Å away from the nearest functional center of the 2.5 million Da ribosome would be disadvantageous for bacteria (Figure. 1).

Here, using the prototype macrolide resistance gene *ermC* as a model, we demonstrate that expression of Erm methyltransferase notably decreases the fitness of bacteria. We show that dimethylation of an RNA nucleotide located in the NPET affects the composition of the cellular proteome by altering the level of expression of specific polypeptides. Our experiments revealed that changes in the proteome likely result from anomalous interactions of the nascent peptide with the Erm-modified exit tunnel of the ribosome. These findings provide a molecular explanation of why the *erm* genes evolved to be inducible.

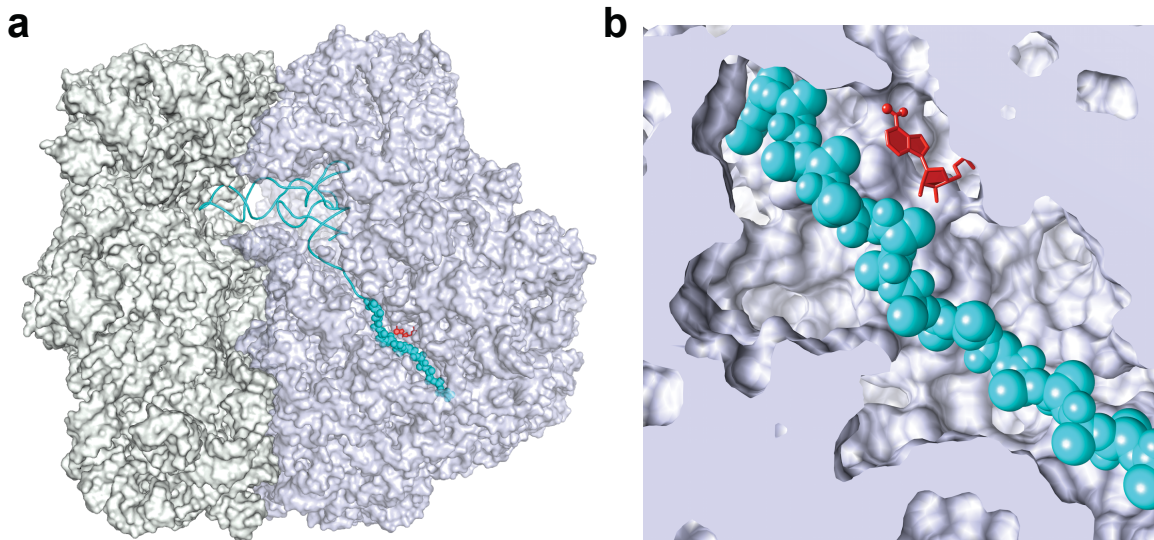


**Figure 1. Location of A2058, the target of Erm methyltransferase, in the ribosome.** (a) The structure of the bacterial ribosome with a model nascent peptide (cyan) in the exit tunnel (PDB accession numbers 2WWQ and 2WWL (Seidelt et al., 2009)) with the A2058 residue highlighted in red. The large ribosomal subunit is shown in pale blue and the small subunit is pale green. Some rRNA and protein residues have been removed to expose the peptidyl-tRNA and the NPET. (b) The close-up view of the nascent peptide and m<sub>26</sub>A2058 in the tunnel. Two methyl groups at the exocyclic amine of A2058 (shown as balls) were added computationally.

## **Materials and methods**

### **Strains and plasmids.**

*S. aureus* clinical strain USA300-P23, a derivative of NARSA strain USA300-0114 (McDougal et al., 2003; Tenover et al., 2006) rendered macrolide sensitive by curing it of plasmids 2 (30kb) and 3 (4.3kb), was generously provided by Dr. T. Bae (Indiana University School of Medicine). Plasmid 2 contains *msrA* gene that encodes for the drug transporter responsible for macrolide resistance. The laboratory strain RN4220 (Novick, 1991) was used as an alternative plasmid host.

The plasmid pErmCC, constitutively expressing the *ermC* gene under the control of the Pspac promoter (Yansura and Henner, 1984) was prepared by PCR-amplification of the *ermC* gene from the pE194 plasmid (Shivakumar et al., 1980a) using oligonucleotide primers spac-ermC-F1 and ermC-R, subsequent addition of the Pspac promoter by sequential PCRs using primer pairs spac-ermC-F2 + ermC-R, spac-ermC-F3 + ermC-R, spac-ermC-F4 + ermC-R, (Table 1), cutting the PCR product with restriction enzymes EcoRI and HindIII, and cloning it into pLI50 shuttle cloning vector (Lee et al., 1991) opened with the same enzymes. The pErmCC\* plasmid that encodes the catalytically inactive Tyr<sub>104</sub>-to-Ala mutant of ErmC (Maravic et al., 2003) was engineered by site-directed mutagenesis of the pErmCC plasmid in which the Tyr<sub>104</sub> *ermC* codon TAT was changed to the alanine codon GCT using primer ermC (Y104A) (Table 1). The plasmids expressing C-terminally His<sub>6</sub>-tagged wild type (pErmCC-His<sub>6</sub>) and mutant ErmC (pErmCC\*-His<sub>6</sub>) variants were prepared following the same strategy as described above for pErmCC and pErmCC\*, except that the C-terminal His<sub>6</sub>-tag was introduced during PCR amplification of the *ermC* gene using the reverse PCR primer ermC-His-R.



**Analysis of the extent of A2058 dimethylation.**

Total RNA was isolated from *S. aureus* cells as previously described (LaMarre et al., 2011). The extent of 23S rRNA A2058 dimethylation was assessed by primer extension using L2058 primer (Table 1) as described previously (Bailey et al., 2008; Vester and Douthwaite, 1994) with minor modifications. Specifically, 0.5 pmol of [5'-<sup>32</sup>P] labeled primer L2058 was annealed to 1 µg of total RNA and extended with AMV reverse transcriptase (Roche) in the presence of 0.25 mM dTTP and 1 mM of dGTP, dATP, and ddCTP. The cDNA products were resolved in a denaturing 12% polyacrylamide gel and visualized by phosphorimaging.

**Growth competition.**

*S. aureus* USA300 or RN4220 strains transformed with pErmCC, pErmCC\* or pLI50 plasmids were grown overnight in brain heart infusion (BHI) medium (BD Diagnostics) supplemented with 25 µg/ml of chloramphenicol. The overnight cultures were diluted to  $A_{600} = 0.05$  in fresh medium containing chloramphenicol and grown at 37°C with shaking until they reached  $A_{600}$  just above 0.5. The densities of the culture were then adjusted to identical values ( $A_{600} = 0.5$ ). Equal culture volumes were mixed in a pair-wise fashion (pErmCC/pLI50 and pErmCC/pErmCC\*) and grown overnight with shaking at 37°C. At each cycle, the cultures were diluted 1000 fold into fresh BHI/chloramphenicol medium and grown for 24 hrs. Cultures were grown for a total of four passages corresponding to ca. 40 cell generations.

The ratio of cells transformed with different plasmids was determined at each cycle by isolating total RNA from the co-culture and assaying the extent of dimethylation

of A2058 in 23S rRNA by primer extension. The fitness cost was calculated as previously described (Sander et al., 2002).

### **Microbiological testing.**

MIC for ERY was determined by microbroth dilution following the standard protocol (Standards, 2006).

### **Preparation of *S. aureus* ribosomes and cell-free translation.**

Ribosomes were purified from exponentially growing cultures of *S. aureus* RN4220 cells (either untransformed, or transformed with pErmCC). Cells were harvested by centrifugation from a 1L exponential culture grown in BHI medium and flash-frozen. Cell pellets were later resuspended in 25 ml of buffer containing 10 mM Hepes-KOH, pH 7.6, 50 mM KCl, 10 mM Mg(OAc)<sub>2</sub>, 7 mM β-mercaptoethanol, 0.1 mg/ml lysostaphin (Sigma- Aldrich) and disrupted by two passes through French press at 20,000 psi. Cell debris was removed by centrifugation at 20,000g for 30 min. Ribosomes were then purified from the cell lysates as previously described for *E. coli* (Ohashi et al., 2007). Status of A2058 modification was verified by primer extension analysis of the rRNA isolated by phenol extraction from the ribosome preparation.

*In vitro* translation and toeprinting were carried out essentially as previously described (Vazquez-Laslop et al., 2008) with some modifications. Specifically, *in vitro* transcription/translation was performed in a 5 µl reaction using the *E. coli* Δribosome PURExpress kit (New England Biolabs), which lacks ribosomes, supplemented with 10 pmoles of purified *S. aureus* ribosomes. Except for reducing the reaction volume down to

5  $\mu$ l and using heterologous ribosomes, the reactions were assembled following the manufacturer's protocol. DNA templates were prepared by PCR amplification of *S. aureus* genes with their ribosome binding sites, using genomic DNA prepared from the RN4220 strain as template (primers are listed in Table 1). The T7 promoter required for *in vitro* transcription was introduced on the forward PCR primer. The control *dhfr* template was provided with the PURExpress kit.

For introducing compensatory frameshift mutations, the *poxB* gene was first 3'-truncated and Asp<sub>137</sub> codon was mutated to a stop codon (TAA) using primers T7-poxB and poxB(short)-R (Table 1). The compensatory frameshift mutations that changed the sequence of the nascent peptide encoded in codons 102-117 in the *poxB* gene were introduced by two step PCR using primers T7-poxB and poxB.F-R in the first PCR reaction followed by PCR with primers T7-poxB and poxB(short)-R.

### **Sucrose gradient analysis of ribosomal subunits.**

The ribosomal subunits from *S. aureus* RN4220 cells transformed with pLI50 and pErmCC were analyzed as previously described (Siibak et al., 2011). Presence of ribosomal precursors was analyzed by primer extension carried out using total RNA isolated from pLI50- or pErmCC- transformed RN4220 cells. The primers SaS20 and SaL20 annealing close to the 5' ends of 16S and 23S rRNA, respectively, were used in the analysis.

**Proteomics.**

*S. aureus* RN4220 transformed with pErmCC, pErmCC\* or pLI50 plasmids were grown overnight in BHI medium supplemented with 25 µg/ml chloramphenicol. The overnight cultures were diluted to an optical density of  $A_{600} = 0.05$  in fresh chloramphenicol containing medium and grown at 37°C with shaking to an optical density of 0.5. Cells were pelleted, washed twice with PBS buffer and flash-frozen. Protein extraction, labeling and two-dimensional gel electrophoresis was performed by Applied Biomics, Hayward, CA using a linear pH gradient 4 to 7 in the first dimension (Ho et al., 2012; Li et al., 2012).

Gels were scanned using Typhoon TRIO (GE Healthcare). The images were analyzed by Image Quant and DeCyder software (GE Healthcare). Spots with consistent ratios below 0.67 or above 1.5 for the pLI50/pErmCC and pErmCC\*/pErmCC pairs but within the 0.83-1.2 range for the pLI50/pErmCC\* pair, were cut from the gel using a spot picker robot. Proteins were extracted and their tryptic digests analyzed by mass spectrometry at the proteomics facility of the University of Illinois at Chicago.

**Analysis of ErmC expression.**

*S. aureus* cells (RN4220) transformed with pErmCC-His<sub>6</sub> or pErmCC\*-His<sub>6</sub> plasmids were grown in 5 ml BHI medium supplemented with 25 µg/ml chloramphenicol. When cultures reached an optical density of  $A_{600} = 0.5$ , cells were pelleted and resuspended in 200 µl of the buffer: 10 mM Tris- HCl, pH7.5, 30 mM MgCl<sub>2</sub>, 30 mM NH<sub>4</sub>Cl, containing 0.5 mg/ml of lysostaphin (Sigma- Aldrich). Lysis was completed by incubating the cell suspensions at 37°C for 1h. Samples with 25 µg of

protein (ca. 20  $\mu$ l of the lysate) were loaded onto 4%-20% Mini- PROTEAN TGX gel (Bio-Rad) and resolved by electrophoresis. Proteins were then transferred to a PVDF membrane and probed using anti-His<sub>6</sub> HRP-coupled antibodies (Thermo Scientific). As a loading control, equal amounts of lysates were run on a separate gel and stained with Coomassie blue G-250.

## **Results**

### **Dimethylation of A2058 by the ErmC methyltransferase decreases fitness of *Staphylococcus aureus*.**

In order to test whether the expression of ErmC methyltransferase impacts the fitness of bacteria, we introduced the plasmid pErmCC that constitutively expresses the wild type enzyme into the ERY-sensitive variant of the clinical *S. aureus* strain USA300 (Figure. 2).

Primer extension analysis (Figure. 3a) showed that 60% of the ribosomes in the pErmCC-transformed *S. aureus* are dimethylated at A2058 in 23S rRNA. These cells exhibited high resistance to ERY (minimal inhibitory concentration [MIC] >1024  $\mu$ g/ml) (Table 2) whereas cells transformed with the empty vector (pLI50) retained unmodified A2058 (Figure. 3a) and remained sensitive to the drug (MIC 0.2  $\mu$ g/ml) (Table 2).

In order to test whether *ermC* expression affects cell fitness, we analyzed how efficiently the pErmCC-transformed *S. aureus* cells could compete with cells carrying the empty vector. The *S. aureus*/pErmCC cells were mixed in a liquid culture with equal number of *S. aureus*/pLI50 cells and cultures were grown for ca. 40 generations being passaged to a fresh medium after each 10-generation cycle. Changes in the ratio of the

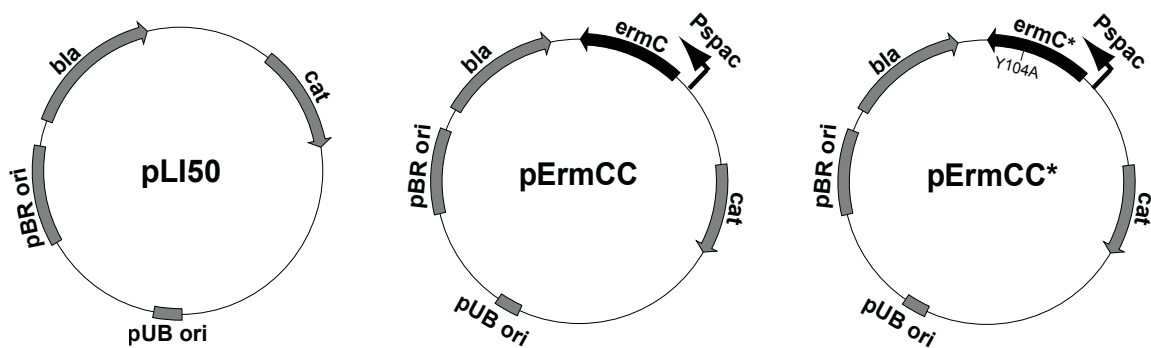


**Figure 2. Plasmids used in this study.** The shuttle plasmid pLI50 was used as a backbone to generate pErmCC and pErmCC\* plasmids, which constitutively express the *ermC* gene (pErmCC) or its catalytically inactive Tyr104 to Ala mutant (pErmCC\*), respectively, under the control of the *P<sub>spac</sub>* promoter.

**Table 2.** ERY MIC ( $\mu\text{g/ml}$ ) for *S. aureus* USA300 and RN4220 strains transformed with different plasmids.

Plasmid	Strain	
	USA300	RN4220
pLI50 (empty vector)	0.2	0.2
pErmCC	>1024	>1024
pErmCC*(Y104A)	0.2	0.2

pErmCC- and pLI50-bearing cells was monitored by determining the levels of dimethylation of A2058 in the total rRNA isolated from the mixed culture. We observed that cells expressing ErmC were fairly rapidly outcompeted by cells carrying an empty vector (Figure. 3b). The estimated fitness cost associated with the presence of the constitutively-expressed *ermC* gene in the *S. aureus* USA300 cells was  $6.5\% \pm 0.6$  per generation demonstrating that expression of ErmC has an adverse effect on cell growth in the absence of antibiotic selective pressure.

Is it the production of the ErmC protein *per se*, or is it the catalytic activity of ErmC that accounts for the fitness cost? In order to address this question, we introduced the Tyr<sub>104</sub>-to-Ala mutation in the ErmC enzyme, which has been previously reported to inactivate its catalytic activity (Maravic et al., 2003). This mutation was engineered in the *ermC* gene of the pErmCC plasmid and the resulting mutant plasmid pErmCC\* was introduced into *S. aureus*. Western blot analysis verified that the wild type (ErmC) and the mutant (ErmC\*) proteins were expressed at comparable levels (Figure. 4).

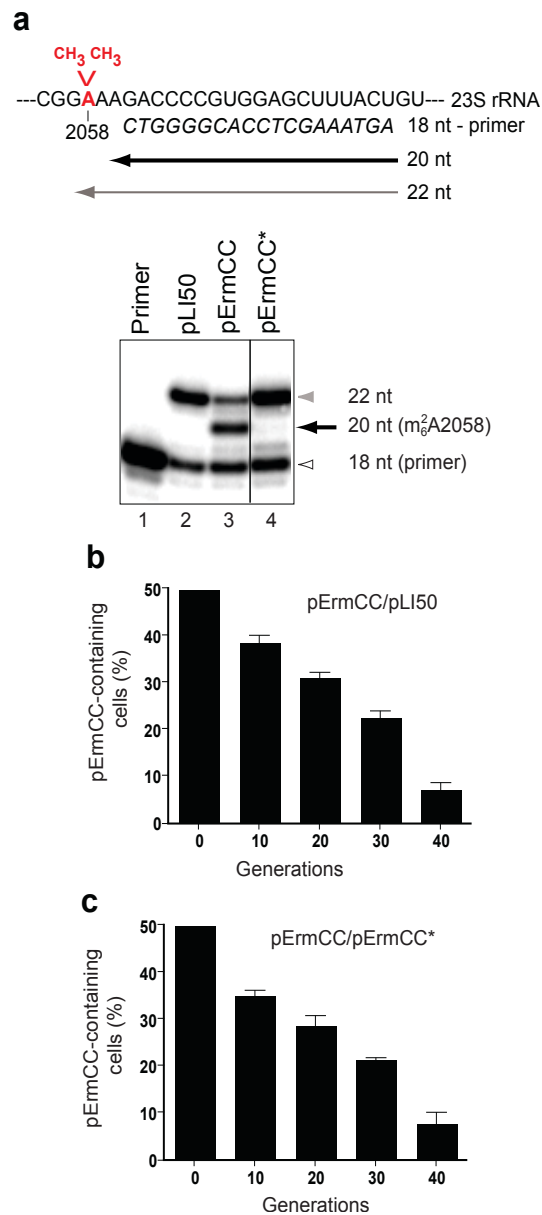


**Figure 3. Expression of catalytically active ErmC methyltransferase decreases the fitness of *S. aureus*.** (a) Principle of detection of A2058 dimethylation by primer extension. In the presence of dATP, dGTP, dTTP and ddCTP, reverse transcriptase extends the 18-nucleotide (nt) long primer by four nucleotides when A2058 is not modified but only by 2 nucleotides when the residue is dimethylated because extension is impeded by the modification. The gel shows the methylation status of A2058 in rRNA from *S. aureus* USA300 cells containing pLI50, pErmCC or pErmCC\* plasmids (lanes 2-4 respectively). Lane 1 contains the labeled primer. (b and c) Growth competition between *S. aureus* USA300 cells transformed with plasmids pErmCC and pLI50 (b), or pErmCC/ and pErmCC\* (c). The percentage of cells expressing active ErmC was estimated by measuring the level of A2058 methylation every 10 generations for a total of ca. 40 generations. Values are the mean of three independent experiments; error bars indicate the standard deviation of the mean.

As expected, A2058 remained unmodified in the pErmCC\*-transformed cells (Figure. 3a) which also remained sensitive to ERY (Table 2), thereby verifying that the Tyr<sub>104</sub>-Ala mutation eliminated the methyltransferase activity of the ErmC\* protein. Strikingly, in the co-growth experiment, the *S. aureus*/pErmCC cells were outcompeted by the *S. aureus*/pErmCC\* cells nearly as efficiently as by the cells transformed with an empty vector (Figure. 3c) with the relative fitness loss of cells expressing the active enzyme of  $6.3\% \pm 0.9$ . The deleterious effect of the expression of active ErmC was even more evident in the generally less-fit *S. aureus* laboratory strain RN4220 (Nair et al., 2011; Novick, 1991) where the relative fitness cost of expressing an active enzyme versus the mutationally-inactivated Erm was  $7.3\% \pm 0.8$ .

Altogether these results clearly demonstrated that the activity of the rRNA methyltransferase enzyme, rather than the mere production of the exogenous protein, is primarily responsible for the decrease in cell fitness and provided a clear biological 'reason' for the inducible nature of the *erm* genes.

### **Changes in the chemical makeup of the NPET lead to differential translation of specific cellular proteins.**

Having recognized that it is the action of the ErmC enzyme upon the ribosome that reduces fitness of *S. aureus*, we wanted to unravel the molecular basis of this effect. ErmC methylates 23S rRNA at the early steps of ribosome biogenesis (Kovalic et al., 1994; Vester et al., 1998). Conceivably, the interaction of the foreign enzyme with ribosomal precursors might interfere with this process by stalling or derailing the assembly, leading to accumulation of intermediates or off-pathway products (Maguire,

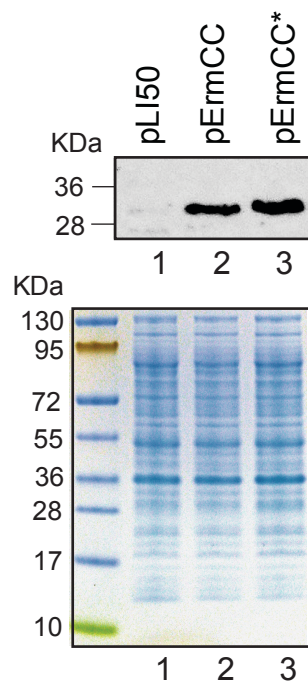


**Figure 4. Mutant ErmC\*(Y104A) protein is actively expressed in *S. aureus*.** Western blot with anti-His<sub>6</sub> antibodies used to assess the level of expression of His<sub>6</sub>-tagged ErmC and ErmC\* proteins in *S. aureus* RN4220 cells transformed with pLI50, pErmCC-His<sub>6</sub> and pErmCC\*-His<sub>6</sub> plasmids (lanes 1, 2 and 3 respectively). The Coomassie-stained gel, used as a loading control, contains the same amounts of total protein loaded in the gel used for Western blot analysis.

2009). However, sucrose gradient centrifugation showed no significant differences between in the ribosomal profiles of the pErmCC- or pLI50- transformed cells (Figure. 5a). Furthermore, no increase in accumulation of incompletely processed rRNA in Erm-expressing cells was detected by primer extension (Figure. 6). Thus, expression of Erm seems to have little effect, if any, on assembly of the ribosome.

An alternative possibility is that Erm-catalyzed dimethylation of A2058 affects properties of the mature ribosome. Because A2058 is located in the NPET, where functional interactions between the ribosome and the nascent peptide take place (Ito et al., 2010; Vázquez-Laslop, 2011), we hypothesized that changes in the chemical makeup of the tunnel surface may influence the production of certain cellular polypeptides. To explore this possibility, we used two-dimensional difference gel electrophoresis (2D-DIGE) to look for possible differences in the proteomes of *S. aureus* cells expressing active ErmC (from pErmCC), with those of cells expressing either the inactive ErmC mutant (from pErmCC\*) or no ErmC protein at all (pLI50 control). While the majority of the proteins did not show any significant deviation in their abundance (Figure. 5b and Figure. 7), we detected several distinct protein spots whose steady-state levels in the ErmC- positive cells consistently varied 1.5 to 2.5 fold relative to both controls. Fifteen protein spots (spots 3-17) showed higher intensity in the ErmC expressing cells, whereas two proteins (spots 1 and 2) were expressed at lower levels (Figure. 5b and c, Figure. 7).

The results of the 2D-DIGE analysis showed that expression of ErmC methylase, causing modification of an rRNA residue in the NPET, does not have a global effect on translation efficiency, but may lead to imbalanced translation of specific proteins resulting in a skewed composition of the cellular proteome.

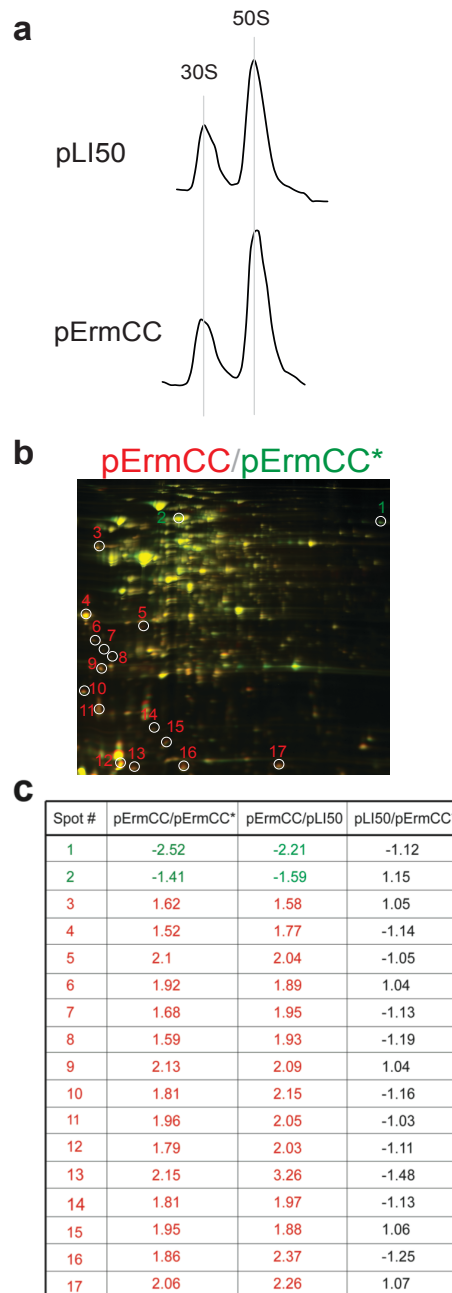


**Figure 5. Dimethylation of A2058 affects translation of specific polypeptides.** (a) ErmC expression does not affect ribosome assembly. Sucrose gradient profiles of ribosomal subunits from *S. aureus* RN4220 cells transformed with pLI50 or pErmCC plasmids. (b & c) Effect of dimethylation of A2058 on abundance of cellular proteins. 2D-DIGE comparison of proteomes of *S. aureus* RN4220 cells expressing active ErmC methyltransferase (pErmCC) vs. cells expressing catalytically inactive Erm protein (pErmCC\*) (see also Figure. 7). Spots with ratios exceeding 1.5 for the pErmCC/pErmCC\* and pErmCC/pLI50 pairs but being within 1.0-1.2 fold ratio for the pLI50/pErmCC\* pair are circled and numbered from 1-17. The spots of proteins that were expressed at lower levels in pErmCC-containing cells are circled in green and those expressed at a higher level are circled in red. The values of the ratios are shown in the table (c) color coded as in (b).

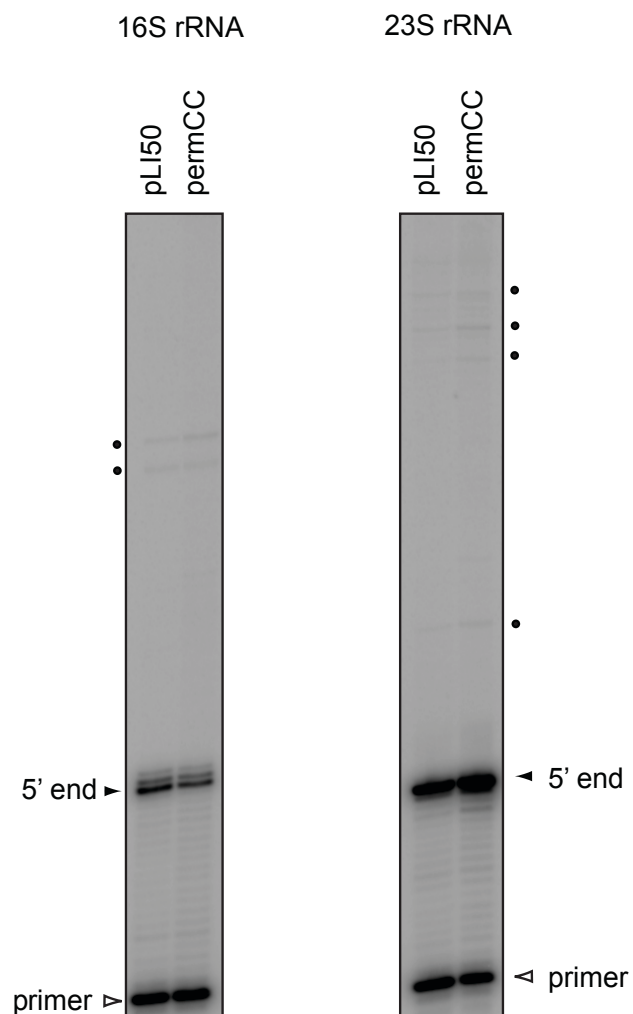


**Figure 6. ErmC expression does not cause accumulation of rRNA precursors.** Primer extension analysis of the 5' ends of 16S and 23S RNA using total RNA isolated from the exponential *S. aureus* RN4220 cells carrying pLI50 and pErmCC plasmids. The 5' ends of the mature 16S rRNA and 23S rRNA are indicated by the arrowheads; putative processing intermediates are indicated by black dots.

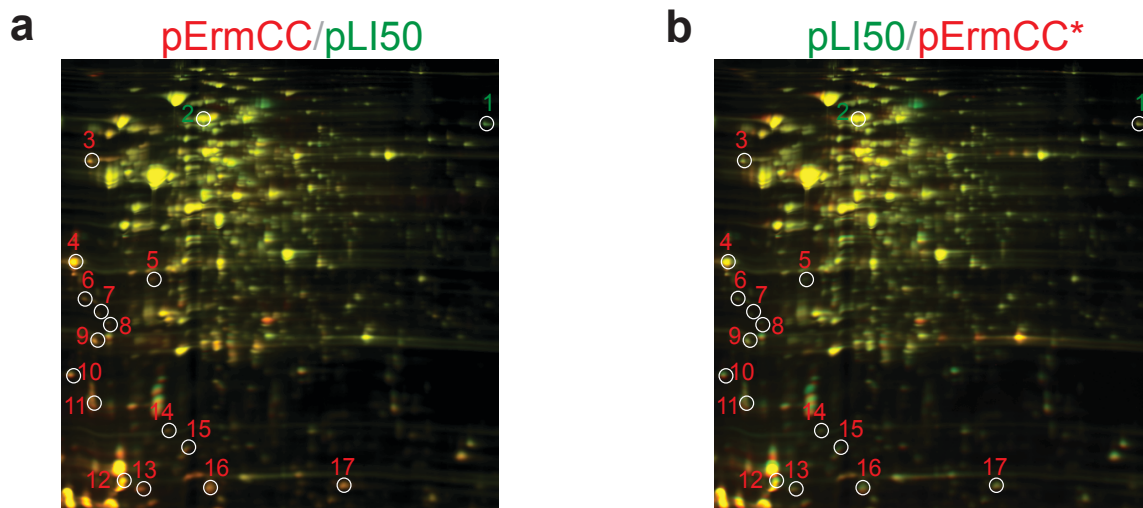


**Figure 7. 2D-DIGE comparison of proteomes of *S. aureus* RN4220 cells carrying (a) pErmCC vs. pLI50 plasmid, and (b) pLI50 vs. pErmCC\*. Spots with ratios exceeding 1.5 for the pErmCC/pLI50 and pErmCC/ pErmCC\* pairs but within the 1.0-1.2 ratio for the pLI50/pErmCC\* pair are circled and numbered from 1-17. The spots of proteins that were expressed at lower levels in pErmCC containing cells are numbered in green and those expressed at a higher level are numbered in red.**

**Modification of A2058 alters the translation efficiency of a protein in a nascent peptide - dependent manner.**

We suspected that translation of at least some of the proteins could be directly affected by the changes in the chemical structure of an rRNA residue in the NPET. Because up-regulation of protein expression is more likely to be a result of a stress-response (even though stress can also reduce protein expression) (Poole, 2012), we focused our attention on the protein (spot 1) that was most strongly down-regulated in the pErmCC-transformed cells. Mass spectrometry analysis uniquely assigned the protein in spot 1 as pyruvate oxidase (PoxB). We then examined whether the wild type and ErmC-modified ribosomes showed any difference in translation of the *poxB* gene. Because the nascent peptide - NPET interactions are known to affect progression of the ribosome along mRNA (Cruz-Vera et al., 2005; Mayford and Weisblum, 1989; Nakatogawa and Ito, 2002; Tanner et al., 2009; Vazquez-Laslop et al., 2008) we hypothesized that less efficient expression of pyruvate oxidase could stem from aberrant (more- or less-prolonged) ribosome “dwelling” at specific codon(s) within the gene. We examined potentially anomalous codon occupancy by analyzing the difference in distribution of unmodified and Erm-dimethylated ribosomes along the *poxB* mRNA during its *in vitro* translation.

Cell-free protein synthesis was carried out in a hybrid system composed of *S. aureus* ribosomes complemented with aminoacyl-tRNAs and purified translation factors from *E. coli*. (We verified beforehand that, similar to the previously reported *B. subtilis*/*E.coli* hybrid system (Chiba et al., 2011), the *S. aureus* ribosomes efficiently translate proteins *in vitro* with the assistance of *E. coli* factors [Figure. 8a]). Ribosomes

were prepared either from untransformed *S. aureus* RN4220 cells ('wild type') or from cells expressing catalytically active ErmC methyltransferase; 60% of ribosomes in the latter preparation were dimethylated at A2058. Direct measurements of the rate of *in vitro* production of PoxB were not sensitive enough to reliably detect the difference of *poxB* translation by unmodified and dimethylated ribosomes (Figure. 8b). This is not surprising because the differential steady state level of the protein observed *in vivo* could be additionally affected by translation-dependent folding and degradation, which could not be reproduced in the cell-free system. Therefore, in order to identify the *poxB* mRNA codons where the dwelling time of the Erm-modified ribosomes would be possibly different in comparison with the wild type ribosomes, we used primer extension inhibition analysis (toeprinting) (Hartz et al., 1988). This technique has been used to analyze programmed translation arrest where prolonged occupancy by ribosomes of a specific mRNA codon inhibits progression of the reverse transcriptase producing a fairly strong cDNA band on the gel (Muto et al., 2006; Vazquez-Laslop et al., 2008). Although we did not anticipate stable ribosome pausing in the *poxB* gene and thus did not expect appearance of strong toeprinting bands, we reasoned that primer extension could still reveal subtle differences in steady-state distribution of unmodified and dimethylated ribosomes along the mRNA during *in vitro* translation. The analysis showed that the A2058-dimethylated ribosomes reproducibly generated a stronger toeprint signal at codon Asn<sub>118</sub> compared to the wild type ribosomes (Figure. 8c).

The use of a primer annealing closer to codon 118 confirmed that the intensity of the toeprint band (representing the modified ribosomes paused at Asn<sub>118</sub> codon) was over

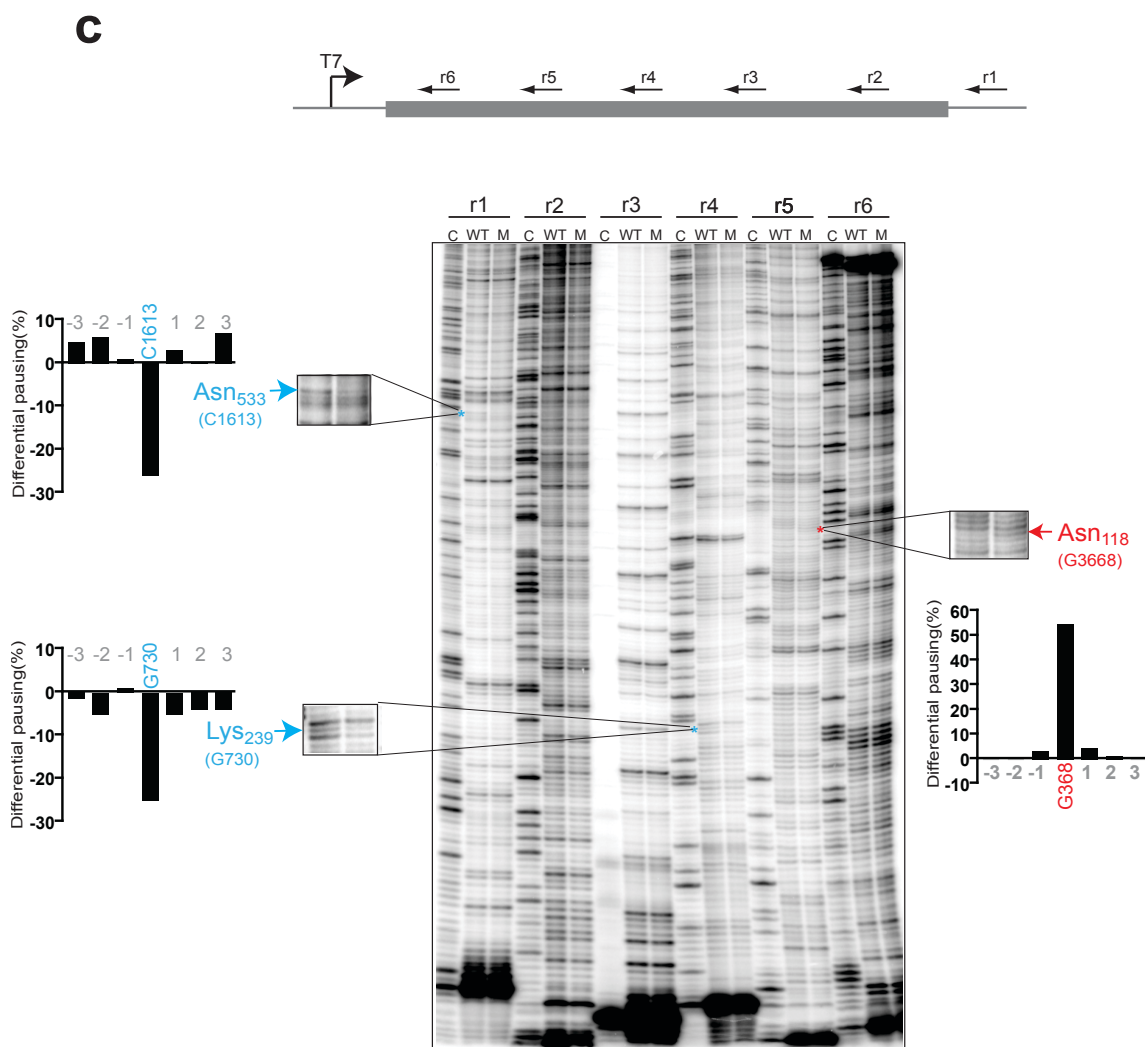
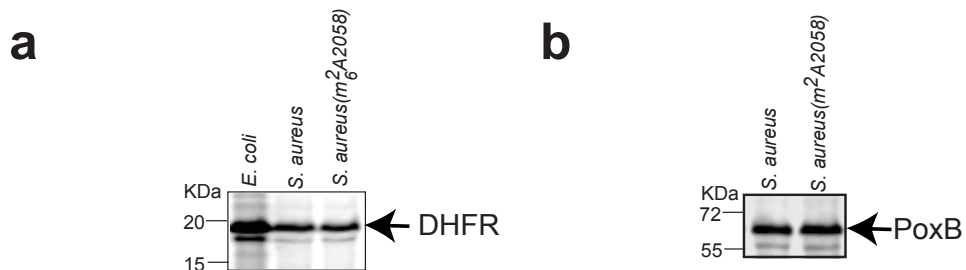


**Figure 8. Ribosomes with or without m<sup>26</sup>A2058 modification differentially pause at specific sites on the *poxB* mRNA.** (a, b) *S. aureus* ribosomes (unmethylated or dimethylated at A2058) efficiently translate the *dhfr* reporter gene (a) or *poxB* gene (b) in the *E. coli* !PURExpress cell-free translation system (NewEngland Biolabs) devoid of the endogenous ribosomes. Translation was carried out at 37 C for 30 min in the presence of [<sup>35</sup>S]-methionine. Translation products were resolved by SDS electrophoresis and visualized by phosphorimaging. The full size DHFR or PoxB proteins are indicated by arrowheads. (c) Differential lingering of methylated (M) or unmethylated (WT) *S. aureus* ribosomes at specific codons of the pyruvate oxidase (*poxB*) mRNA. Steady-state distribution of the translating ribosomes along mRNA mapped by toeprinting analysis with six different primers (r1-r6) as indicated. Sequencing reactions were carried out using ddG as the terminator and are marked on top of the gel as C. Asterisks (\*) indicate toeprint bands with substantial difference in intensity in the unmethylated and methylated ribosome samples. The toeprint bands with a higher intensity in the unmethylated ribosome sample, and the corresponding mRNA codons (Asn<sub>533</sub> and Lys<sub>239</sub>) are shown in blue. The band with a higher intensity in the methylated ribosome sample, and the corresponding mRNA codon Asn<sub>118</sub>, is shown in red. The corresponding sections of the gel are shown enlarged. Bar graphs show the result of quantification of the relative differential intensity of the toeprint signals (numbered nucleotide in color) of methylated over unmethylated ribosomes with the bands representing 3 preceding and 3 following nucleotides shown for the comparison.

50% greater relative to the band produced by the unmethylated ribosomes (Figure. 9a, lanes 1 and 2). This result showed that the modification of A2058 by the Erm methyltransferase leads to prolonged ribosome lingering after polymerizing 118 amino acids of the pyruvate oxidase nascent peptide. We additionally noted that at two other codons, Lys<sub>239</sub> and Asn<sub>533</sub>, methylated ribosomes produced a somewhat weaker toeprint than the wild type ribosomes (Figure. 8b). Altogether, the toeprinting data indicated that the methylation status of residue A2058 affects the rate of traversing specific codons at distinct locations of certain mRNAs.

In order to verify the generality of this conclusion, we searched for other proteins whose translation could be affected by dimethylation of A2058. Two other differentially

expressed and uniquely identified *S. aureus* proteins (spots 9 and 11, Figure. 5b and Table 3) did not show a clear difference in the toeprinting pattern (see Discussion), which prompted us to look for other examples. Analysis of polypeptides encoded in the *S. aureus* genome showed that protein TenA contains the sequence Trp-Pro-Pro<sub>108</sub>, which has been known to slow down translation (Tanner et al., 2009). We noticed that when this protein was translated in the cell-free system, *S. aureus* ribosomes isolated from ErmC-expressing cells idled for a longer time at the Pro<sub>107</sub> codon compared to unmodified ribosomes (Figure. 10a). Additionally, we tested translation of a *Bacillus subtilis* protein MifM, where several translation pause sites within the sequence Asp-Ala-Gly-Ser<sub>92</sub> have been previously identified (Chiba and Ito, 2012). Again, the A2058-dimethylated *S. aureus* ribosome showed a somewhat prolonged pausing at the Ser<sub>92</sub> codon in comparison with the wild type ribosome (Figure. 10b). Thus, it appears that dimethylation of A2058 in 23S rRNA may affect in a subtle way translation of various cellular polypeptides.

The A2058 residue is located in a section of the NPET that is known to be involved in recognition of the nascent peptide (Lawrence et al., 2008; Nakatogawa and Ito, 2002; Seidelt et al., 2009; Vazquez-Laslop et al., 2011) (Figure. 1). Therefore, it is conceivable that its modification may alter interaction of the ribosome with a defined nascent peptide sequence within the tunnel. To test this idea we introduced two compensatory frameshift mutations in the *poxB* mRNA, which changed the sequence of amino acid residues Gly<sub>102</sub>-Thr<sub>117</sub>; these 16 residues form the segment of the nascent peptide which would be located within close proximity to A2058 when the ribosome

**Table 3. Identification by mass-spectrometry of the proteins differentially expressed in cells with and without active Erm methyltransferase.**

<b>Spot #</b>	<b>Protein (95% confidence, ≥2 unique peptides)</b>
1	pyruvate oxidase
5	translation elongation factor-P and putative epimerase/dehydratase
9	Hexulose-6-phosphate synthase
10	hexulose-6-phosphate synthase and glucose/glucoside porter component IIA
11	Transcription elongation factor GreA
13	ribosomal protein S5, ribosomal protein L14, regulatory protein SpoVG
14	ribosomal protein S5, ribosomal protein L10, ribosomal protein L15, hypothetical protein MW 0363
17	ribosomal protein S17, cell cycle protein GpsB, hypothetical protein MW1812

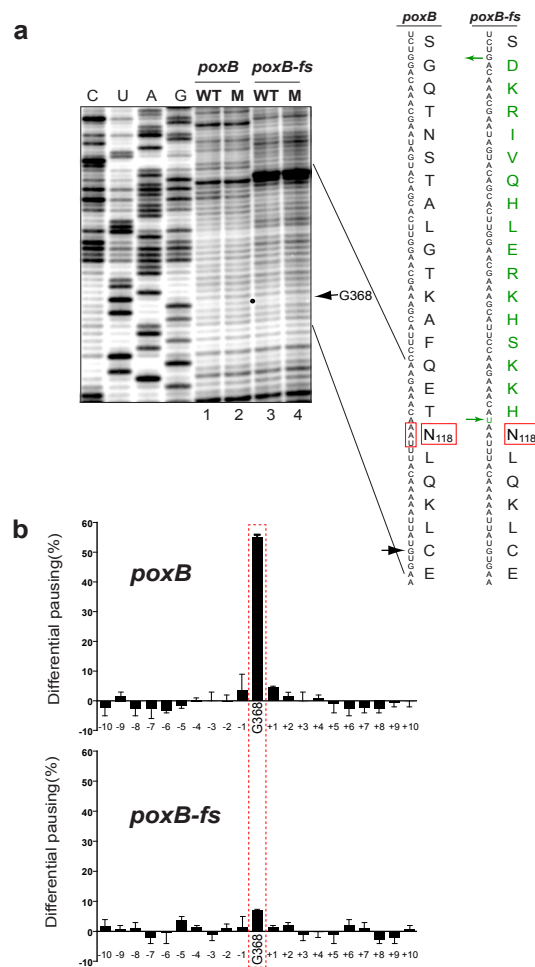


**Figure 9. Differential translation of *poxB* by ribosomes with unmethylated or dimethylated A2058 depends on the nascent peptide.** (a) Toeprinting analysis of distribution of translating unmethylated (WT) or methylated (M) ribosomes along the segment of the *poxB* mRNA containing the codon Asn<sub>118</sub>. The sequences of the mRNA templates encoding the wild-type PoxB (lanes 1 and 2) or the frameshift mutant PoxB-fs (lanes 3 and 4), with the altered sequence of amino acid residues 102-117 (amino acid residues shown in green), are shown on the right with the green arrows indicating the single nucleotide deletion and insertion used to generate the frameshift mutant. The intensity of the toeprint band at the *poxB* nucleotide G368 (an arrow and a dot on the gel), reflects the occupancy of the codon Asn<sub>118</sub> (boxed in red in the sequences). (b) Quantification of the differential pausing (differential intensity of the toeprint band) at G368 of *poxB* or *poxB-fs* of methylated over unmethylated ribosomes. For comparison, differential intensities of bands of the 10 nucleotides preceding and following position G368 were also calculated after the background intensity was subtracted. The integrated density of 5 consecutive bands with the seemingly similar intensities was used to normalize the data in order to account for potential difference in loading. Mean values were originated from 3 independent experiments; error bars represent the standard deviation of the mean. ImageJ software (<http://rsbweb.nih.gov/ij/>) was used for quantification.

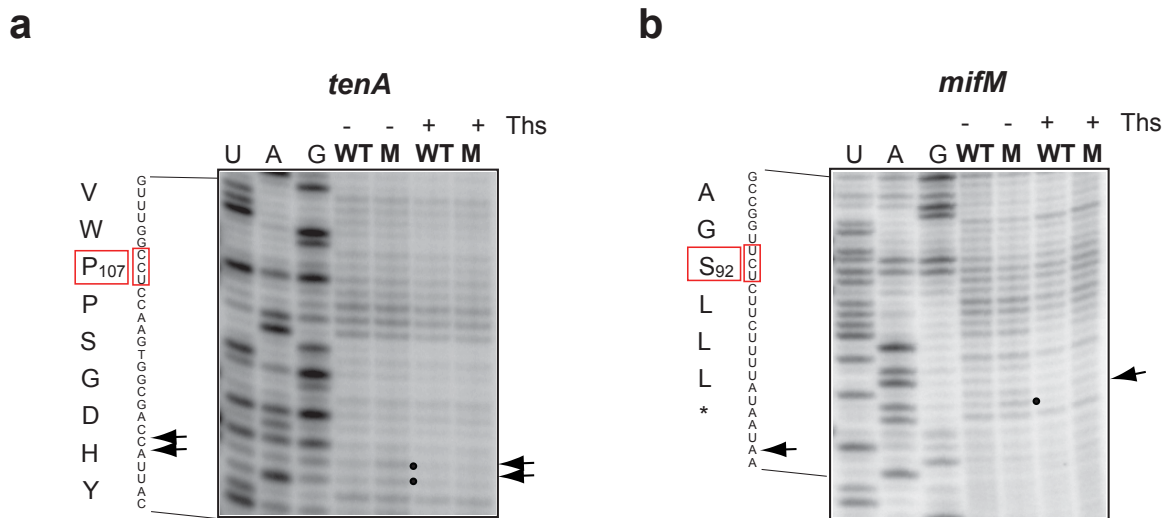


**Figure 10. Differential translation of *tenA* and *mifM* genes by the ribosomes with or without m<sub>26</sub>A2058 modification.** Differential idling of Erm-modified (M) or unmodified (WT) *S. aureus* ribosomes at a specific site in (a) *S. aureus tenA* mRNA or (b) *B. subtilis mifM* mRNA revealed by toeprinting analysis. Thioestrepton (Ths), which in our conditions inhibits translation initiation, was added to the indicated reactions to demonstrate that appearance of toeprint signals on *tenA* and *mifM* ORFs depends on their active translation. The bands revealing differential ribosome idling are marked by dots and arrows. The codon located in the P site of the stalled ribosome is boxed. Sequencing lanes are marked. The *tenA* DNA template under the control of T7 promoter was prepared by PCR using *tenA*-F, *tenA*-R1 primers and *S. aureus* genomic DNA as the template. The *mifM* DNA template was prepared by two sequential PCR reactions using first primers *mifM*-F1, *mifM*-R and *B. subtilis* genomic DNA as the template followed by the second PCR reaction using primers *mifM*-F2 and *mifM*-R. Primer extension on *tenA* and *mifM* ORF's was carried out using primers *tenA*-R2 and r1, respectively.

occupies the Asn<sub>118</sub> codon. Importantly, the mutations completely alter the amino acid sequence but have minimal effect on the structure of the mRNA. Remarkably, when the mutant *poxB* mRNA was expressed in the hybrid cell-free translation system, wild type and Erm-methylated ribosomes showed essentially no difference in pausing at the Asn<sub>118</sub> codon (Figure. 9a, lanes 3 & 4 and Figure. 9b). This result argues that the increased pausing of the Erm-modified ribosome at codon 118 of *poxB* is a consequence of aberrant interactions of the altered NPET with a specific nascent peptide structure.

### **Discussion**

Even though *erm*s were among the first known inducible antibiotic resistance genes, the evolutionary and molecular basis for their inducibility has remained unknown. Here we showed that expression of functionally active Erm methyltransferase reduces fitness of the bacterial cell because dimethylation of a unique rRNA residue in the ribosomal tunnel skews expression of a subset of proteins, likely due to aberrant interactions of specific nascent peptides with the modified ribosomal exit tunnel.

The fitness cost of expression of the *erm* gene in a clinical *S. aureus* strain observed in our experiments likely underestimates the cost expected to be found in nature. Expression of the ErmC methyltransferase from the engineered pErmCC plasmid resulted in a relatively modest degree of ribosome modification: only ca. 60% of ribosomes in the pErmCC-transformed *S. aureus* USA300 cells were modified (Figure. 3a). The higher level of *ermC* expression in other genetic environments (Weisblum et al., 1979) or the higher activity of other Erm variants (Douthwaite et al., 2005) can produce a nearly completely modified ribosomal population which would further increase the

fitness cost. We also noted that properties of the host cell can exacerbate the competitive disadvantage of the chemically-altered ribosome. Expression of catalytically active ErmC was more burdensome for the less fit laboratory strain RN4220 (Nair et al., 2011), than for the clinical strain USA300. In addition, the rich laboratory media used in our experiments may further dampen the fitness difference between the wild type and Erm-expressing cells (Sergiev et al., 2006). Finally, the different structural context of A2058 in ribosomes of different species may potentially influence the fitness cost associated with its modification (Pfister et al., 2005). Therefore, in the native bacterial strains living in their natural habitats, the unnecessary expression of Erm methyltransferase may be highly detrimental.

The considerable fitness cost of having A2058-dimethylated ribosomes would impose a strong evolutionary pressure upon bacteria to suppress expression of the *erm* genes in the absence of the antibiotic. Elegant mechanisms have been selected in the course of evolution of the *erm* genes that hinder their expression when no antibiotic is present. Remarkably, operation of these mechanisms is controlled by the modification status of A2058. In the absence of antibiotic, the unimpeded translation of the regulatory leader ORF prevents expression of the resistance gene. In the presence of the inducing antibiotic, the unmodified ribosome binds the drug and stalls at the leader ORF in a drug- and nascent peptide – dependent manner leading to activation of *erm* expression. The Erm-catalyzed dimethylation of A2058 not only abolishes antibiotic binding, but may also affect nascent peptide recognition thereby preventing translation arrest at the regulatory ORF and providing for an efficient feed-back loop that adjusts the extent of ribosome modification in response to the level of antibiotic in the environment

(Weisblum, 1995). This mechanism enables the cell to generate the minimal amount of A2058-modified ribosomes that is sufficient to maintain the adequate level of translation in the presence of the antibiotic.

One of the probable explanations for the growth deficiency of Erm-expressing cells is that translation of some proteins by A2058-modified ribosomes is different compared to the 'native' ribosome. Two extra methyl groups at the exocyclic amine of A2058 notably change its chemical properties by increasing the hydrophobicity of the base edge and preventing the amino group from participating in hydrogen bonding interactions. The alteration in the chemical structure of the A2058 residue may significantly affect the functional properties of the NPET. A2058 is located in the NPET segment that is intimately involved in modulating translation in response to specific nascent peptides (Ito et al., 2010; Vázquez-Laslop, 2011; Wilson and Beckmann, 2011). Mutations of A2058 prevent peptide-dependent ribosome stalling during translation of the regulatory SecM peptide (Nakatogawa and Ito, 2002), whereas dimethylation of the residue was reported to negatively affect chloramphenicol-dependent translation arrest at the open reading frame that controls expression of the chloramphenicol resistance gene *cmlA* (Lawrence et al., 2008). Extrapolating these findings, it seems reasonable to expect that A2058 may also be involved in operation of more subtle regulatory circuits, where nascent peptide - ribosome interactions modulate translation elongation in a more delicate mode. The Erm-catalyzed modification of A2058 could lead to deregulation of such circuits, selectively affecting expression of specific proteins. This idea is supported by our finding that dimethylation of A2058, even in a fraction of cellular ribosomes, is sufficient to notably skew production of a number of cellular polypeptides (Figure. 5b

and c). While changes in expression of some of these proteins could be an indirect consequence of a stress response, we presented evidence that progression of the ribosome along mRNA of at least one polypeptide, pyruvate oxidase (PoxB), is directly affected by dimethylation of A2058. PoxB expression was diminished more than two fold in cells in which only 60% of the ribosomes were modified. This change correlated with the apparent difference in the occupancy of the codons 118, 239 and 533 during *in vitro* translation of the *poxB* mRNA by A2058-modified ribosomes compared to the unmodified ribosomes. The prolonged dwelling of the Erm-methylated ribosomes at codon 118 was eliminated when the PoxB nascent peptide sequence in the NPET was mutated. This data clearly reveals that the chemical makeup of A2058 influences the ribosomal response to specific nascent peptides. It should be noted that not only slowing down, but also a needless acceleration of the evolutionary-optimized translation rate might negatively affect protein expression (Zhang et al., 2009). The observed *in vitro* reduced occupancy of the *poxB* codons Lys<sub>239</sub> and Asn<sub>533</sub> by the modified ribosome indicates a faster traverse rate may interfere *in vivo* with proper protein folding and thus, stability (Ciryam et al., 2013). It is conceivable that a similar negative effect of A2058 methylation upon accumulation of a regulatory protein, (e.g. a transcription repressor) may lead to up-regulation of expression of some cellular polypeptides, including those present in spots 3-17 in Figure. 5b. This consideration might explain why we did not observe any definite difference in the toeprinting pattern when the genes of the proteins identified in spots 9 and 11 were tested in the cell-free translation assay (data not shown). Of note, the lack of detectable ribosome assembly defects in the Erm-expressing cells

(Figure. 5a) argues that expression of ribosomal proteins is not significantly influenced by A2058 dimethylation.

Previously, we have shown that an indigenous posttranscriptional modification of another NPET residue, A2053, is required for the proper operation of the mechanism of programmed translation arrest (Vazquez-Laslop, 2010), revealing the importance of fine structural details of the NPET for the functional recognition of the nascent peptide. Our present finding expands this observation by showing that an unwarranted modification of an rRNA residue in the NPET by an acquired rRNA methyltransferase can disrupt proper nascent peptide recognition, which leads to deregulation of expression of specific proteins. It remains to be elucidated whether A2058 functions in immediate recognition of the peptide or in relaying the signal to the peptidyl transferase center (Fulle and Gohlke, 2009; Seidelt et al., 2009; Vazquez-Laslop et al., 2011).

## **Cited Literature**

Andersson, D.I., and Hughes, D. (2010). Antibiotic resistance and its cost: is it possible to reverse resistance? *Nat Rev Microbiol* 8, 260-271.

Bailey, M., Chettiath, T., and Mankin, A.S. (2008). Induction of *ermC* expression by 'non-inducing' antibiotics. *Antimicrob Agents Chemother* 52, 866-874.

Chiba, S., and Ito, K. (2012). Multisite ribosomal stalling: a unique mode of regulatory nascent chain action revealed for MifM. *Molecular cell* 47, 863-872.

Chiba, S., Kanamori, T., Ueda, T., Akiyama, Y., Pogliano, K., and Ito, K. (2011). Recruitment of a species-specific translational arrest module to monitor different cellular processes. *Proceedings of the National Academy of Sciences of the United States of America* 108, 6073-6078.

Ciryam, P., Morimoto, R.I., Vendruscolo, M., Dobson, C.M., and O'Brien, E.P. (2013). In vivo translation rates can substantially delay the cotranslational folding of the *Escherichia coli* cytosolic proteome. *Proceedings of the National Academy of Sciences of the United States of America* 110, E132-140.

Cruz-Vera, L.R., Rajagopal, S., Squires, C., and Yanofsky, C. (2005). Features of ribosome-peptidyl-tRNA interactions essential for tryptophan induction of *tna* operon expression. *Molecular cell* 19, 333-343.

Cundliffe, E. (1989). How antibiotic-producing organisms avoid suicide. *AnnuRevMicrobiol* 43, 207-233.

Depardieu, F., Podglajen, I., Leclercq, R., Collatz, E., and Courvalin, P. (2007). Modes and modulations of antibiotic resistance gene expression. *Clin Microbiol Rev* 20, 79-114.

Douthwaite, S., Jalava, J., and Jakobsen, L. (2005). Ketolide resistance in *Streptococcus pyogenes* correlates with the degree of rRNA dimethylation by Erm. *Molecular microbiology* 58, 613-622.

Foucault, M.L., Depardieu, F., Courvalin, P., and Grillot-Courvalin, C. (2010). Inducible expression eliminates the fitness cost of vancomycin resistance in enterococci. *Proceedings of the National Academy of Sciences of the United States of America* 107, 16964-16969.

Fulle, S., and Gohlke, H. (2009). Statics of the ribosomal exit tunnel: implications for cotranslational peptide folding, elongation regulation, and antibiotics binding. *J Mol Biol* 387, 502-517.

Gaynor, M., and Mankin, A.S. (2003). Macrolide antibiotics: binding site, mechanism of action, resistance. *Curr Top Med Chem* 3, 949-961.

- Griffith, L.J., Ostrander, W.E., Mullins, C.G., and Beswick, D.E. (1965). Drug Antagonism between Lincomycin and Erythromycin. *Science (New York, NY)* *147*, 746-747.
- Hartz, D., McPheeters, D.S., Traut, R., and Gold, L. (1988). Extension inhibition analysis of translation initiation complexes. *Methods in enzymology* *164*, 419-425.
- Ho, N.K., Ossa, J.C., Silphaduang, U., Johnson, R., Johnson-Henry, K.C., and Sherman, P.M. (2012). Enterohemorrhagic *Escherichia coli* O157:H7 Shiga toxins inhibit gamma interferon-mediated cellular activation. *Infection and immunity* *80*, 2307-2315.
- Horinouchi, S., and Weisblum, B. (1980). Posttranscriptional modification of mRNA conformation: mechanism that regulates erythromycin-induced resistance. *Proc Natl Acad Sci USA* *77*, 7079-7083.
- Ito, K., Chiba, S., and Pogliano, K. (2010). Divergent stalling sequences sense and control cellular physiology. *Biochemical and biophysical research communications* *393*, 1-5.
- Kovalic, D., Giannattasio, R.B., Jin, H.-J., and Weisblum, B. (1994). 23S rRNA domain V, a fragment that can be specifically methylated in vitro by the ErmSF (TlrA) methyltransferase. *Journal of Bacteriology* *176*, 6992-6998.
- LaMarre, J.M., Locke, J.B., Shaw, K.J., and Mankin, A.S. (2011). Low fitness cost of the multidrug resistance gene cfr. *Antimicrob Agents Chemother* *55*, 3714-3719.
- Lawrence, M., Lindahl, L., and Zengel, J.M. (2008). Effects on translation pausing of alterations in protein and RNA components of the ribosome exit tunnel. *J Bacteriol* *190*, 5862-5869.
- Lee, C.Y., Buranen, S.L., and Ye, Z.H. (1991). Construction of single-copy integration vectors for *Staphylococcus aureus*. *Gene* *103*, 101-105.
- Li, G., Cai, W., Hussein, A., Wannemuehler, Y.M., Logue, C.M., and Nolan, L.K. (2012). Proteome response of an extraintestinal pathogenic *Escherichia coli* strain with zoonotic potential to human and chicken sera. *Journal of proteomics* *75*, 4853-4862.
- Maguire, B.A. (2009). Inhibition of bacterial ribosome assembly: a suitable drug target? *Microbiol Mol Biol Rev* *73*, 22-35.
- Maravic, G., Feder, M., Pongor, S., Flogel, M., and Bujnicki, J.M. (2003). Mutational analysis defines the roles of conserved amino acid residues in the predicted catalytic pocket of the rRNA:m6A methyltransferase ErmC'. *J Mol Biol* *332*, 99-109.
- Mayford, M., and Weisblum, B. (1989). ermC leader peptide. Amino acid sequence critical for induction by translational attenuation. *J Mol Biol* *206*, 69-79.

- McDougal, L.K., Steward, C.D., Killgore, G.E., Chaitram, J.M., McAllister, S.K., and Tenover, F.C. (2003). Pulsed-field gel electrophoresis typing of oxacillin-resistant *Staphylococcus aureus* isolates from the United States: establishing a national database. *Journal of clinical microbiology* *41*, 5113-5120.
- Muto, H., Nakatogawa, H., and Ito, K. (2006). Genetically encoded but nonpolypeptide prolyl-tRNA functions in the A site for SecM-mediated ribosomal stall. *Molecular cell* *22*, 545-552.
- Nair, D., Memmi, G., Hernandez, D., Bard, J., Beaume, M., Gill, S., Francois, P., and Cheung, A.L. (2011). Whole genome sequencing of *Staphylococcus aureus* strain RN4220, a key laboratory strain used in virulence research, identifies mutations that affect not only virulence factors but also the fitness of the strain. *J Bacteriol* *193*, 2332-2335.
- Nakatogawa, H., and Ito, K. (2002). The ribosomal exit tunnel functions as a discriminating gate. *Cell* *108*, 629-636.
- Novick, R.P. (1991). Genetic systems in staphylococci. *Methods in enzymology* *204*, 587-636.
- Ohashi, H., Shimizu, Y., Ying, B.W., and Ueda, T. (2007). Efficient protein selection based on ribosome display system with purified components. *Biochemical and biophysical research communications* *352*, 270-276.
- Pfister, P., Corti, N., Hobbie, S., Bruell, C., Zarivach, R., Yonath, A., and Bottger, E.C. (2005). 23S rRNA base pair 2057-2611 determines ketolide susceptibility and fitness cost of the macrolide resistance mutation 2058A-->G. *Proceedings of the National Academy of Sciences of the United States of America* *102*, 5180-5185.
- Poehlsgaard, J., and Douthwaite, S. (2005). The bacterial ribosome as a target for antibiotics. *Nat Rev Microbiol* *3*, 870-881.
- Poole, K. (2012). Bacterial stress responses as determinants of antimicrobial resistance. *The Journal of antimicrobial chemotherapy* *67*, 2069-2089.
- Ramu, H., Mankin, A., and Vazquez-Laslop, N. (2009). Programmed drug-dependent ribosome stalling. *Molecular microbiology* *71*, 811-824.
- Roberts, M.C. (2004). Distribution of macrolide, lincosamide, streptogramin, ketolide and oxazolidinone (MLSKO) resistance genes in Gram-negative bacteria. *Current drug targets* *4*, 207-215.
- Roberts, M.C. (2008). Update on macrolide-lincosamide-streptogramin, ketolide, and oxazolidinone resistance genes. *FEMS microbiology letters* *282*, 147-159.

Rosato, A., Vicarini, H., and Leclercq, R. (1999). Inducible or constitutive expression of resistance in clinical isolates of streptococci and enterococci cross-resistant to erythromycin and lincomycin. *Journal of Antimicrobial Chemotherapy* 43, 559-562.

Sander, P., Springer, B., Prammananan, T., Sturmfels, A., Kappler, M., Pletschette, M., and Bottger, E.C. (2002). Fitness cost of chromosomal drug resistance-conferring mutations. *Antimicrob Agents Chemother* 46, 1204-1211.

Schmitz, F.J., Petridou, J., Jagusch, H., Astfalk, N., Scheuring, S., and Schwarz, S. (2002). Molecular characterization of ketolide-resistant erm(A)-carrying *Staphylococcus aureus* isolates selected in vitro by telithromycin, ABT-773, quinupristin and clindamycin. *The Journal of antimicrobial chemotherapy* 49, 611-617.

Seidelt, B., Innis, C.A., Wilson, D.N., Gartmann, M., Armache, J.P., Villa, E., Trabuco, L.G., Becker, T., Mielke, T., Schulten, K., *et al.* (2009). Structural insight into nascent polypeptide chain-mediated translational stalling. *Science (New York, NY)* 326, 1412-1415.

Sergiev, P.V., Lesnyak, D.V., Bogdanov, A.A., and Dontsova, O.A. (2006). Identification of *Escherichia coli* m2G methyltransferases: II. The *ygjO* gene encodes a methyltransferase specific for G1835 of the 23 S rRNA. *J Mol Biol* 364, 26-31.

Shivakumar, A.G., Gryczan, T.J., Kozlov, Y.I., and Dubnau, D. (1980a). Organization of the pE194 genome. *Mol Gen Genet* 179, 241-252.

Shivakumar, A.G., Hahn, J., Grandi, G., Kozlov, Y., and Dubnau, D. (1980b). Posttranscriptional regulation of an erythromycin resistance protein specified by plasmic pE194. *Proceedings of the National Academy of Sciences of the United States of America* 77, 3903-3907.

Siibak, T., Peil, L., Donhofer, A., Tats, A., Remm, M., Wilson, D.N., Tenson, T., and Remme, J. (2011). Antibiotic-induced ribosomal assembly defects result from changes in the synthesis of ribosomal proteins. *Molecular microbiology* 80, 54-67.

Standards, N.C.f.C.L. (2006). Methods for dilution antimicrobial susceptibility tests for bacteria that grow aerobically; approved standard M7-A7. , Vol 26, 7th edition edn (Wayne, PA, Clinical and Laboratory Standards Institute, Wayne, PA).

Subramanian, S.L., Ramu, H., and Mankin, A.S. (2011). Inducible resistance to macrolide antibiotics. In *Antibiotic Drug Discovery and Development*, T.J. Dougherty, Pucci, M. J. , ed. (New Yoork, NY, Springer Publishing Company).

Sutcliffe, J., and Leclercq, R. (2002). Mechanisms of resistance to macrolides, lincosamides, and ketolides. In *Macrolide Antibiotics*, W. Schönfeld, and H.A. Kirst, eds. (Basel-Boston-Berlin, Birkhäuser Verlag).

## Appendix B

The following are the rights and permissions as mentioned on the PNAS website for the publication “Sothiselvam, S., Liu, B., Han, W., Ramu, H., Klepacki, D., Atkinson, G.C., Brauer, A., Remm, M., Tenson, T., Schulten, K., Vázquez-Laslop, N., Mankin, A.S. (2014) **Macrolide antibiotics allosterically predispose the ribosome for translation arrest.** *Proc Natl Acad Sci USA* 111, 9804-9809” that comprises Chapter 2 of this thesis.

### **Permission to reuse published material (as mentioned in PNAS website)**

PNAS authors need not obtain permission for the following cases:

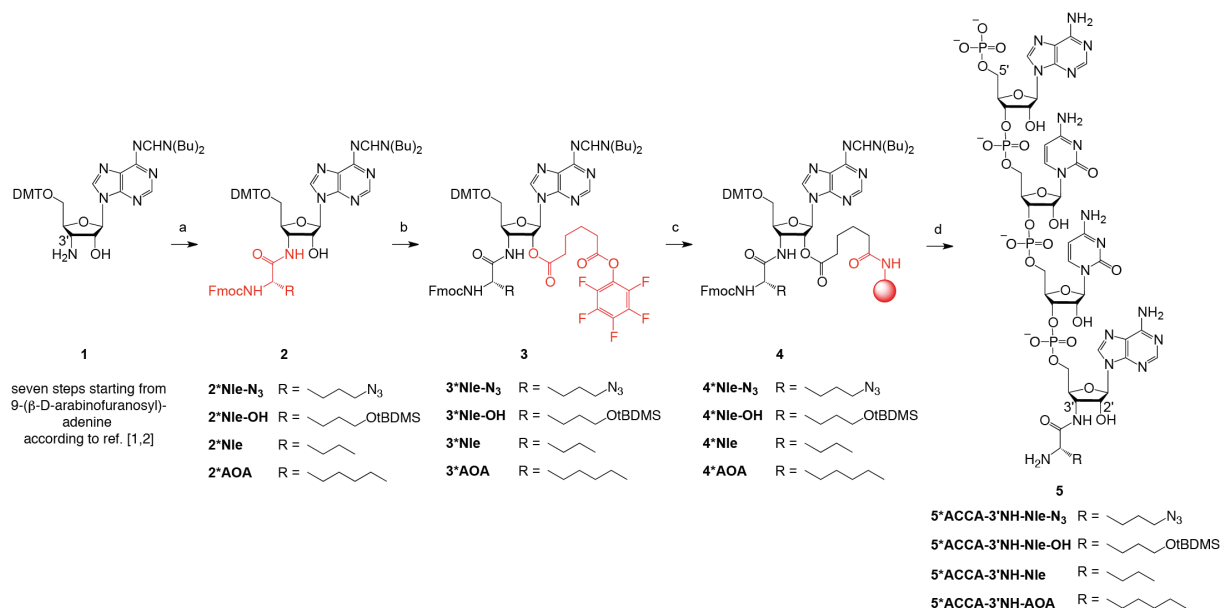
- (1) to use their original figures or tables in their future works;
- (2) to make copies of their papers for their own personal use, including classroom use, or for the personal use of colleagues, provided those copies are not for sale and are not distributed in a systematic way;
- (3) to include their papers as part of their dissertations; or
- (4) to use all or part of their articles in printed compilations of their own works. Citation of the original source must be included and copies must include the applicable copyright notice of the original report.

## Appendix C

The following section details the synthesis of ACCA substrates used in Chapter 2 of this thesis. This section was contributed by Lukas Rigger, Sandra Neuner and Ronald Micura, Institute of Organic Chemistry and Center for Molecular Biosciences (CMBI) Leopold-Franzens University, Innrain 80-82, 6020 Innsbruck (Austria)

### Chemical synthesis of ACCA-amino acid conjugates

The ACCA-amino acid conjugates (containing 6-azido-L-norleucine, 6-hydroxy-6-norleucine, norleucine or (2*S*)-2-aminooctanoic acid) were synthesized as outlined in Scheme S1 and described below. The ACCA-amino acid conjugates (containing L-lysine, L-ornithine, L-arginine or L-alanine) were synthesized following the lines as described in reference [1].



**Scheme S1.** Synthesis of solid supports and RNA-amino acid conjugates. Reaction conditions: **a)** 1.3 equiv Fmoc-amino acid-OBt, 1.5 equiv DIPEA, in *N,N*-dimethylformamide, r.t., 5 h, r.t., 12 h; **b)** 5 equiv of adipic acid bis(pentafluorophenyl)ester, 1 equiv DMAP in *N,N*-dimethylformamide/pyridine (1/1, v/v), r.t., 1 h; **c)** ~3 equiv (w/w) amino-functionalized polystyrene support (*GE Healthcare*, Custom Primer Support<sup>TM</sup> 200 Amino), ~2 equiv (w/w) pyridine, *N,N*-dimethylformamide, r.t., 1 day; **d)** automated RNA solid-phase synthesis, deprotection, and purification. Fmoc = *N*-(9-fluorenyl)methoxycarbonyl, Bt = Benzotriazol-1-yl, DIPEA = *N,N*-diisopropylethylamine, DMAP = 4-(*N,N*-dimethylamino)pyridine.

### Chemical synthesis of solid supports 4

*General remarks.* Reagents were purchased in the highest available quality from commercial suppliers (Sigma-Aldrich, Acros, IRIS Biotech GmbH) and used without further purification. Organic solvents for reactions were dried overnight over freshly activated molecular sieves (4Å). The reactions were carried out under argon atmosphere. <sup>1</sup>H and <sup>13</sup>C spectra were recorded on a Bruker DRX 300 MHz spectrometer. Chemical shifts (δ) are reported relative to tetramethylsilane (TMS) referenced to the residual proton signal of the deuterated solvent

DMSO- $d_6$  (2.50 ppm for  $^1\text{H}$  NMR spectra and 39.52 ppm for  $^{13}\text{C}$  spectra). The following abbreviations were used to denote multiplicities: s = singlet, d = doublet, t = triplet, m = multiplet, b = broad. Signal assignments were based on  $^1\text{H}$ - $^1\text{H}$ -COSY and  $^1\text{H}$ - $^{13}\text{C}$ -HSQC experiments. MS experiments were performed on a Finnigan LCQ Advantage MAX ion trap instrumentation (Thermo Fisher Scientific) with an electrospray ion source. Samples were analyzed in the positive- or negative-ion mode. Reaction control was performed via analytical thin-layer chromatography (TLC, Macherey-Nagel) with fluorescent indicator. Spots were further visualized using cerium molybdate or anisaldehyde staining reagents. Column chromatography was carried out on silica gel 60 (70-230 mesh). Custom Primer Support<sup>TM</sup> 200 Amino was purchased from GE Healthcare. Derivatized amino acids Fmoc-L-Nle(6- $\text{N}_3$ )-OH (also coined Fmoc-L-Lys( $\text{N}_3$ )-OH), Fmoc-L-Nle(6-OtBDMS)-OH, Fmoc-L-Nle-OH and Fmoc-L-2Aoc-OH (also coined Fmoc-L-2Aoc-OH) were purchased from *Iris Biotech GmbH*. Solid supports **4** containing other amino acids (L-Lys, L-Orn, L-Arg, L-Ala) were prepared as described in reference [1].

$\text{N}^6$ -[*(Di-n-butylamino)methylene*]-3'-[*N*-(9-fluorenyl)methoxycarbonyl-6-azido-L-norleuciny]*l*]amino-3'-deoxy-5'-*O*-(4,4'-dimethoxytrityl)-D-adenosine (**2\*Nle-N<sub>3</sub>**). Fmoc protected L-6-azidonorleucine (100 mg, 0.26 mmol) was dissolved in DMF (10 mL) followed by addition of *O*-(benzotriazol-1-yl)-*N,N,N',N'*-tetramethyluronium hexafluorophosphate (HBTU, 96 mg, 0.26 mmol), 1-hydroxybenzotriazole hydrate (HOBt, 39 mg, 0.26 mmol) and *N,N*-diisopropylethylamine (DIPEA, 52  $\mu\text{L}$ , 0.30 mmol). After 3 minutes of activation, 3'-amino- $\text{N}^6$ -[*(di-n-butylamino)methylene*]-3'-deoxy-5'-*O*-(4,4'-dimethoxytrityl)-D-adenosine **1**<sup>[2]</sup> (140 mg, 0.20 mmol, in 1 mL DMF) was added and the mixture was stirred overnight at room temperature. Then, the solvent was evaporated, the residue dissolved in  $\text{CH}_2\text{Cl}_2$  and washed consecutively with half-saturated aqueous  $\text{NaHCO}_3$  solution, 5% citric acid solution, and saturated aqueous  $\text{NaCl}$  solution. The organic layer was dried ( $\text{Na}_2\text{SO}_4$ ), evaporated and the crude product was purified via  $\text{SiO}_2$  chromatography yielding 162 mg of compound **2\*Nle-N<sub>3</sub>** as white foam (75 %).

$^1\text{H}$  NMR (300 MHz,  $\text{CDCl}_3$ )  $\delta$  9.04 (s, 1H, HC=N(6)), 8.47 (s, 1H, H-C(2)), 8.17 (s, 1H, H-C(8)), 7.71 (m, 2H, HC(ar)), 7.53 (m, 2H, HC(ar)), 7.38-7.16 (m, 13H, HC(ar) and  $\text{CDCl}_3$ ), 6.91 (s, 1H, NH(3')), 6.77 (d, 4H,  $J = 9.0$ , CH(ar)), 6.02 (s, 1H, H-C(1')), 5.50 (d, 1H,  $J = 7.5$ , H-N(Nle)), 4.69 (s, 2H, H-C(2') and H-C(3')), 4.32 (m, 3H, H-C(4') and O- $\text{CH}_2$ (Fmoc)), 4.17 (m, 2H, H-C(9, Fmoc) and CH( $\alpha$ , Nle)), 3.72 (s, 6H, 2xOCH<sub>3</sub>(DMT)), 3.67 (m, 2H, N(CH<sub>2</sub>CH<sub>2</sub>CH<sub>2</sub>CH<sub>3</sub>)), 3.45-3.30 (m, 4H, H<sub>2</sub>C(5') and N(CH<sub>2</sub>CH<sub>2</sub>CH<sub>2</sub>CH<sub>3</sub>)), 3.16 (t, 2H,  $J = 6.7$ , H<sub>2</sub>C-N<sub>3</sub>), 1.69-1.26 (m, 14H, N(CH<sub>2</sub>CH<sub>2</sub>CH<sub>2</sub>CH<sub>3</sub>)<sub>2</sub> and 3xCH<sub>2</sub>), 1.00-0.91 (m, 6H, N(CH<sub>2</sub>CH<sub>2</sub>CH<sub>2</sub>CH<sub>3</sub>)<sub>2</sub>).  $^{13}\text{C}$  NMR (75 MHz,  $\text{CDCl}_3$ ):  $\delta$  172.3, 162.7, 160.5, 159.0 (HC=N(6)), 156.4, 152.4 (C(2)), 150.5, 144.5, 143.8, 143.7, 141.4, 139.6, 135.7, 130.2 (C(ar)), 128.3 (C(ar)), 128.0 (C(ar)), 127.2 (C(ar)), 125.1 (C(ar)), 120.1 (C(ar)), 113.3 (C(ar)), 91.4 (C(1')), 86.6, 83.2 (C(4')), 74.7 (C(2')), 67.3 (O- $\text{CH}_2$ (Fmoc)), 63.0 (C(5')), 55.3 (2xOCH<sub>3</sub>(DMT)), 55.0 (C( $\alpha$ , Nle)), 52.0 (C(3') and N(CH<sub>2</sub>CH<sub>2</sub>CH<sub>2</sub>CH<sub>3</sub>)<sub>2</sub>), 51.1 (CH<sub>3</sub>-N<sub>3</sub>), 47.2 (CH(Fmoc)), 45.4 (N(CH<sub>2</sub>CH<sub>2</sub>CH<sub>2</sub>CH<sub>3</sub>)<sub>2</sub>), 38.7, 36.6, 32.4 (CH<sub>2</sub>), 31.1 (CH<sub>2</sub>), 29.4 (CH<sub>2</sub>), 28.5 (CH<sub>2</sub>), 22.7 (CH<sub>2</sub>), 20.3 (CH<sub>2</sub>), 19.9 (CH<sub>2</sub>), 14.0 (CH<sub>3</sub>), 13.8 (CH<sub>3</sub>). ESI-MS ( $m/z$ ):  $[\text{M}+\text{H}]^+$  calcd for  $\text{C}_{61}\text{H}_{70}\text{N}_{11}\text{O}_8$ , 1084.54; found 1084.57.

$\text{N}^6$ -[*(Di-n-butylamino)methylene*]-3'-[*N*-(9-fluorenyl)methoxycarbonyl-6-azido-L-norleuciny]*l*]amino-3'-deoxy-5'-*O*-(4,4'-dimethoxytrityl)-2'-*O*-[1,6-dioxo-6-(pentafluorophenyl)hexyl]-D-adenosine (**3\*Nle-N<sub>3</sub>**). To a solution of compound **2\*Nle-N<sub>3</sub>** (162 mg, 0.15 mmol) in DMF (1.5 mL) and pyridine (1.0 mL) was added DMAP (20 mg, 0.16 mmol) and bis(pentafluorophenyl) adipate (143 mg, 0.30 mmol). The mixture was stirred for one hour followed by evaporation of the solvents. The crude product was purified via  $\text{SiO}_2$

chromatography (CH<sub>2</sub>Cl<sub>2</sub>/acetone, 7/3) yielding 112 mg of compound **3\*Nle-N<sub>3</sub>** as white foam (55%).

<sup>1</sup>H NMR (300 MHz, CDCl<sub>3</sub>) δ 8.96 (s, 1H, HC=N(6)), 8.49 (s, 1H, H-C(2)), 8.09 (s, 1H, H-C(8)), 7.75 (m, 2H, H-C(ar)), 7.55 (m, 2H, H-C(ar)), 7.40-7.19 (m, 13H, H-C(ar) and CDCl<sub>3</sub>), 6.77 (d, 4H, J = 8.6, H-C(ar)), 6.77 (d, 1H, J = 7.1, H-N(3')), 6.15 (d, 1H, J = 2.9, H-C(1')), 5.82 (m, 1H, H-C(2')), 5.33-5.22 (m, 2H, H-N(Nle) and H-C(3')), 4.49-4.35 (m, 2H, O-CH<sub>2</sub>(Fmoc)), 4.20 (m, 2H, H-C(4') and H-C(9, Fmoc)), 4.03 (m, C-H(α, Nle)), 3.76 (s, 6H, OCH<sub>3</sub>(DMT)), 3.64 (t, 2H, J = 6.1, N(CH<sub>2</sub>CH<sub>2</sub>CH<sub>2</sub>CH<sub>3</sub>)<sub>2</sub>), 3.45-3.35 (m, 4H, H-C(5') and N(CH<sub>2</sub>CH<sub>2</sub>CH<sub>2</sub>CH<sub>3</sub>)<sub>2</sub>), 3.21-3.16 (m, 2H, N<sub>3</sub>-CH<sub>2</sub>), 2.58 and 2.40 (s, 2H, OOCCH<sub>2</sub>CH<sub>2</sub>CH<sub>2</sub>CH<sub>2</sub>COO), 1.74-1.46 (m, 12H, N(CH<sub>2</sub>CH<sub>2</sub>CH<sub>2</sub>CH<sub>3</sub>)<sub>2</sub> and OOCCH<sub>2</sub>CH<sub>2</sub>CH<sub>2</sub>CH<sub>2</sub>COO and 3 x CH<sub>2</sub>(Nle)), 1.39-1.26 (m, 4H, N(CH<sub>2</sub>CH<sub>2</sub>CH<sub>2</sub>CH<sub>3</sub>)<sub>2</sub>), 0.97-0.88 (m, 6H, N(CH<sub>2</sub>CH<sub>2</sub>CH<sub>2</sub>CH<sub>3</sub>)<sub>2</sub>). <sup>13</sup>C NMR (75 MHz, CDCl<sub>3</sub>): δ 171.6, 169.5, 162.9, 159.9, 158.7 (HC=N(6)), 156.5, 152.8 (C(2)), 151.0, 144.4, 143.7, 141.4 (C(8)), 140.1, 135.6, 135.5, 130.2 (C(ar)), 129.3 (C(ar)), 128.3, 128.0, 127.2, 127.0 (C(ar)), 125.9 (C(ar)), 125.0, 124.9 (C(ar)), 120.2 (C(ar)), 113.3 (C(ar)), 87.7 (C(1')), 86.8, 82.4 (C(4')), 75.3 (C(2')), 67.2 (O-CH<sub>2</sub>(Fmoc)), 63.1 (C(5')), 55.3 (2xOCH<sub>3</sub>), 54.8 (C(α, Nle)), 52.1, 51.1 (N<sub>3</sub>-CH<sub>2</sub>), 50.6 (C(3')), 47.2 (HC(Fmoc)), 45.4 (N(CH<sub>2</sub>CH<sub>2</sub>CH<sub>2</sub>CH<sub>3</sub>)<sub>2</sub>), 38.7, 36.7, 33.3 (OOCCH<sub>2</sub>CH<sub>2</sub>CH<sub>2</sub>CH<sub>2</sub>COO), 32.9 (OOCCH<sub>2</sub>CH<sub>2</sub>CH<sub>2</sub>CH<sub>2</sub>COO), 31.6 (CH<sub>2</sub>), 31.4 (CH<sub>2</sub>), 31.0 (CH<sub>2</sub>), 29.3 (CH<sub>2</sub>), 28.5 (CH<sub>2</sub>), 24.0 (CH<sub>2</sub>), 23.9 (CH<sub>2</sub>), 20.2 (CH<sub>2</sub>), 19.9 (CH<sub>2</sub>), 13.9 (2x CH<sub>3</sub>). ESI-MS (m/z): [M+H]<sup>+</sup> calcd for C<sub>73</sub>H<sub>76</sub>N<sub>11</sub>O<sub>11</sub>, 1378.57; found 1378.56.

*DMTO-rA*<sup>3'-NH</sup>-(*N*-Fmoc-6-N<sub>3</sub>-Nle) solid support (**4\*Nle-N<sub>3</sub>**). Compound **3\*Nle-N<sub>3</sub>** (112 mg, 0.083 mmol) was dissolved in dry DMF (2.0 mL) and pyridine (15 μL) was added. To this solution, amino-functionalized support (*GE Healthcare, Custom Primer Support*<sup>TM</sup> 200 Amino, 300 mg) was added, and the suspension was agitated for 20 hours at room temperature. Subsequently, the beads were collected on a Büchner funnel and washed with DMF, methanol, and CH<sub>2</sub>Cl<sub>2</sub>. For capping of unreacted amino groups, the beads were treated with a mixture of solution A (0.2 M phenoxy acetic anhydride in THF, 10 mL) and solution B (0.2 M *N*-methyl imidazole, 0.2 M *sym*-collidine in THF, 10 mL) and agitated for 10 min at room temperature. The suspension was filtrated again, the beads were washed with THF, methanol and CH<sub>2</sub>Cl<sub>2</sub>, and dried under vacuum. Loading of the support **4\*Nle-N<sub>3</sub>** was 40 μmol/g.

*N*<sup>6</sup>-[(*Di-n*-butylamino)methylene]-3'-[*N*-(9-fluorenyl)methoxycarbonyl-6-*O*-tert.butyl dimethylsilyloxy-L-norleucinyl]amino-3'-deoxy-5'-*O*-(4,4'-dimethoxytrityl)-D-adenosine (**2\*Nle-OH**). *N*-Fluorenylmethoxycarbonyl-*O*-tert.butyl dimethylsilyl-6-hydroxy-L-norleucine (144 mg, 0.30 mmol) was dissolved in DMF (3 mL) followed by addition of *O*-(benzotriazol-1-yl)-*N,N,N',N'*-tetramethyluronium hexafluorophosphate (HBTU, 113 mg, 0.30 mmol), 1-hydroxybenzotriazole hydrate (HOBt, 46 mg, 0.30 mmol) and *N,N*-diisopropylethylamine (DIPEA, 60 μL, 0.34 mmol). After 3 minutes of activation, 3'-amino-*N*<sup>6</sup>-[(*di-n*-butylamino)methylene]-3'-deoxy-5'-*O*-(4,4'-dimethoxytrityl)-D-adenosine **1**<sup>[2]</sup> (162 mg, 0.23 mmol, in 1 mL DMF) was added and the mixture was stirred overnight at room temperature. Then, the solvent was evaporated, the residue dissolved in CH<sub>2</sub>Cl<sub>2</sub> and washed consecutively with half-saturated aqueous NaHCO<sub>3</sub> solution, 5% citric acid solution, and saturated aqueous NaCl solution. The organic layer was dried (Na<sub>2</sub>SO<sub>4</sub>), evaporated and the crude product was purified via SiO<sub>2</sub> chromatography yielding 240 mg of compound **2\*Nle-OH** as white foam (90 %).

<sup>1</sup>H NMR (300 MHz, CDCl<sub>3</sub>) δ 9.10 (s, 1H, HC=N(6)), 8.45 (s, 1H, H-C(2)), 8.16 (s, 1H, H-C(8)), 7.72 (m, 2H, H-C(ar)), 7.56 (m, 2H, H-C(ar)), 7.34-7.18 (m, 13H, H-C(ar) and CDCl<sub>3</sub>), 6.89 (b, 1H, HN(3')), 6.77 (d, 4H, J = 8.2, HC(ar)), 6.00 (s, 1H, H-C(1')), 5.50 (d, 1H, J = 6.3,

H-N(Nle)), 4.76 (m, 1H, H-C(2')), 4.68 (s, 1H, H-C(3')), 4.35 (m, 3H, H-C(4') and O-CH<sub>2</sub>(Fmoc)), 4.18 (t, 2H, J = 6.9, H-C( $\alpha$ , Fmoc) and H-C(9, DMT)), 3.74 (s, 8H, 2x OCH<sub>3</sub>(DMT) and OCH<sub>2</sub>(Nle)), 3.64-3.61 (m, 2H, N(CH<sub>2</sub>CH<sub>2</sub>CH<sub>2</sub>CH<sub>3</sub>)<sub>2</sub>), 3.55 (m, 2H, H-C(5')), 3.38 (m, 2H, N(CH<sub>2</sub>CH<sub>2</sub>CH<sub>2</sub>CH<sub>3</sub>)<sub>2</sub>), 1.63 (m, 4H, N(CH<sub>2</sub>CH<sub>2</sub>CH<sub>2</sub>CH<sub>3</sub>)<sub>2</sub>), 1.59-1.41 (m, 6H, 3xH<sub>2</sub>C(Nle)), 1.37 (m, 4H, N(CH<sub>2</sub>CH<sub>2</sub>CH<sub>2</sub>CH<sub>3</sub>)<sub>2</sub>), 0.98-0.89 (m, 6H, N(CH<sub>2</sub>CH<sub>2</sub>CH<sub>2</sub>CH<sub>3</sub>)<sub>2</sub>), 0.86 (s, 9H, 3xCH<sub>3</sub>(TBDMS)), 0.02 (s, 6H, 2xSi-CH<sub>3</sub>(TBDMS)). <sup>13</sup>C NMR (75 MHz, CDCl<sub>3</sub>)  $\delta$  172.6, 159.2, 158.6 (HC=N(6)), 156.5, 152.0 (C(2)), 150.6, 144.5, 143.9, 141.4, 139.9 (C(8)), 135.8, 130.2 (C(ar)), 128.3 (C(ar)), 127.9 (C(ar)), 127.2 (C(ar)), 125.2 (C(ar)), 120.1 (C(ar)), 113.3 (C(ar)), 91.3 (C(1')), 86.7, 83.7 (C(4')), 74.7 (C(2')), 67.3 (OCH<sub>2</sub>(Fmoc)), 62.9 (C(5')), 55.3 (C( $\alpha$ , Nle) and 2x OCH<sub>3</sub>), 52.2 (C(3') and N(CH<sub>2</sub>CH<sub>2</sub>CH<sub>2</sub>CH<sub>3</sub>)<sub>2</sub>), 47.2 (CH(Fmoc)), 45.5 (OCH<sub>2</sub>(Nle)), 38.7, 32.4 and 31.1 and 29.3 (N(CH<sub>2</sub>CH<sub>2</sub>CH<sub>2</sub>CH<sub>3</sub>)<sub>2</sub> and CH<sub>2</sub>(Nle)), 26.1 (3x CH<sub>3</sub>(TBDMS)), 22.1 and 20.4 and 19.9 (N(CH<sub>2</sub>CH<sub>2</sub>CH<sub>2</sub>CH<sub>3</sub>)<sub>2</sub> and CH<sub>2</sub>(Nle)), 18.4, 14.1 (N(CH<sub>2</sub>CH<sub>2</sub>CH<sub>2</sub>CH<sub>3</sub>)<sub>2</sub>), 13.8 (N(CH<sub>2</sub>CH<sub>2</sub>CH<sub>2</sub>CH<sub>3</sub>)<sub>2</sub>), -5.2 (2x Si-CH<sub>3</sub>). ESI-MS (m/z): [M+H]<sup>+</sup> calcd for C<sub>67</sub>H<sub>85</sub>N<sub>8</sub>O<sub>9</sub>Si, 1173.62; found 1173.55.

N<sup>6</sup>-[*(Di-n-butylamino)methylene*]-3'-[N-(9-fluorenyl)methoxycarbonyl-6-O-tert-butylidimethylsilyloxy-L-norleucinyl]amino-3'-deoxy-5'-O-(4,4'-dimethoxytrityl)-2'-O-[1,6-dioxo-6-(pentafluorophenoxy)hexyl]-D-adenosine (**3\*Nle-OH 6**). To a solution of compound **2\*Nle-OH** (230 mg, 0.20 mmol) in DMF (2.5 mL) and pyridine (2.0 mL) was added DMAP (26 mg, 0.22 mmol) and bis(pentafluorophenyl) adipate (188 mg, 0.39 mmol). The mixture was stirred for one hour followed by evaporation of the solvents. The crude product was purified via SiO<sub>2</sub> chromatography (CH<sub>2</sub>Cl<sub>2</sub>/acetone, 7/3) yielding 167 mg of compound **3\*Nle-OH** as white foam (58%).

<sup>1</sup>H NMR (300 MHz, CDCl<sub>3</sub>)  $\delta$  8.96 (s, 1H, HC=N(6)), 8.49 (s, 1H, H-C(2)), 8.08 (s, 1H, H-C(8)), 7.74 (d, 2H, J = 7.4, H-C(ar)), 7.54 (d, 2H, J = 7.2, H-C(ar)), 7.41-7.19 (m, 13H, H-C(ar) and CDCl<sub>3</sub>), 6.76 (d, 4H, J = 8.6, H-C(ar)), 6.50 (b, 1H, H-N(3')), 6.16 (d, 1H, J = 3.0, H-C(1')), 5.83 (m, 1H, H-C(2')), 5.20 (m, 2H, H-C(3') and H-N(Nle)), 4.47-4.26 (m, 3H, O-CH<sub>2</sub>(Fmoc) and H-C(9, Fmoc)), 4.18 (m, 1H, H-C(4')), 3.99 (m, 1H, H-C( $\alpha$ , Nle)), 3.75 (s, 6H, 2xOCH<sub>3</sub>(DMT)), 3.64 (m, 2H, N(CH<sub>2</sub>CH<sub>2</sub>CH<sub>2</sub>CH<sub>3</sub>)<sub>2</sub>), 3.56 (t, 2H, J = 6.3 (OCH<sub>2</sub>(Nle)), 3.45 (m, 2H, H-C(5')), 3.38 (t, 2H, J = 7.2, N(CH<sub>2</sub>CH<sub>2</sub>CH<sub>2</sub>CH<sub>3</sub>)<sub>2</sub>), 2.57 (s, 2H, (OOCCH<sub>2</sub>CH<sub>2</sub>CH<sub>2</sub>CH<sub>2</sub>COO)), 2.41 (s, 2H, (OOCCH<sub>2</sub>CH<sub>2</sub>CH<sub>2</sub>CH<sub>2</sub>COO)), 1.78-1.28 (m, 18H, 3xCH<sub>2</sub>(Nle) and (OOCCH<sub>2</sub>CH<sub>2</sub>CH<sub>2</sub>CH<sub>2</sub>COO) and N(CH<sub>2</sub>CH<sub>2</sub>CH<sub>2</sub>CH<sub>3</sub>)<sub>2</sub>), 0.93 (m, 6H, N(CH<sub>2</sub>CH<sub>2</sub>CH<sub>2</sub>CH<sub>3</sub>)<sub>2</sub>), 0.88 (s, 9H, 3xCH<sub>3</sub>(TBDMS)), 0.04 (s, 6H, 2xSi-CH<sub>3</sub>). <sup>13</sup>C NMR (75 MHz, CDCl<sub>3</sub>)  $\delta$  171.9, 171.6, 169.4, 160.0, 158.7 (HC=N(6)), 152.9 (C(2)), 151.1, 144.4, 143.7, 141.4 140.0 (C(8)), 139.6, 135.7, 130.2 (C(ar)), 129.3 (C(ar)), 128.4 (C(ar)), 128.0 (C(ar)), 127.2 (C(ar)), 127.0 (C(ar)), 125.9 (C(ar)), 125.0 (C(ar)), 120.2 (C(ar)), 113.3 (C(ar)), 87.5 (C(1')), 86.9, 82.6 (C(4')), 75.2 (C(2')), 67.3 (OCH<sub>2</sub>(Fmoc)), 63.3 (C(5')), 62.8 (N(CH<sub>2</sub>CH<sub>2</sub>CH<sub>2</sub>CH<sub>3</sub>)<sub>2</sub>), 55.3 (C( $\alpha$ , Nle) and 2xOCH<sub>3</sub>(DMT)), 52.0 (N(CH<sub>2</sub>CH<sub>2</sub>CH<sub>2</sub>CH<sub>3</sub>)<sub>2</sub>), 50.6 (C(3')), 47.2 (CH(Fmoc)), 45.4 (OCH<sub>2</sub>(Nle)), 38.7, 33.3 and 32.9 (OOCCH<sub>2</sub>CH<sub>2</sub>CH<sub>2</sub>CH<sub>2</sub>COO), 32.4-29.4 (OOCCH<sub>2</sub>CH<sub>2</sub>CH<sub>2</sub>CH<sub>2</sub>COO and/or CH<sub>2</sub>(Nle) and/or N(CH<sub>2</sub>CH<sub>2</sub>CH<sub>2</sub>CH<sub>3</sub>)<sub>2</sub>), 26.1 (2x CH<sub>3</sub>(TBDMS)), 24.0-18.5 (OOCCH<sub>2</sub>CH<sub>2</sub>CH<sub>2</sub>CH<sub>2</sub>COO and/or CH<sub>2</sub>(Nle) and/or N(CH<sub>2</sub>CH<sub>2</sub>CH<sub>2</sub>CH<sub>3</sub>)<sub>2</sub>), 13.9 and 13.8 (2x CH<sub>3</sub>), 1.1, -5.2 (2x Si-CH<sub>3</sub>). ESI-MS (m/z): [M+H]<sup>+</sup> calcd for C<sub>79</sub>H<sub>92</sub>F<sub>5</sub>N<sub>8</sub>O<sub>12</sub>Si, 1467.65; found 1467.63.

DMTO-*rA*<sup>3'-NH</sup>-(N-Fmoc-6-OtBDMS-Nle) solid support (**4\*Nle-OH**). Compound **3\*Nle-OH** (167 mg, 0.11 mmol) was dissolved in dry DMF (3.0 mL) and pyridine (21  $\mu$ L) was added. To this solution, amino-functionalized support (*GE Healthcare, Custom Primer Support<sup>TM</sup> 200 Amino*, 400 mg) was added, and the suspension was agitated for 20 hours at room temperature. Subsequently, the beads were collected on a Büchner funnel and washed with

DMF, methanol, and CH<sub>2</sub>Cl<sub>2</sub>. For capping of unreacted amino groups, the beads were treated with a mixture of solution A (0.2 M phenoxy acetic anhydride in THF, 10 mL) and solution B (0.2 M *N*-methyl imidazole, 0.2 M *sym*-collidine in THF, 10 mL) and agitated for 10 min at room temperature. The suspension was filtrated again, the beads were washed with THF, methanol and CH<sub>2</sub>Cl<sub>2</sub>, and dried under vacuum. Loading of the support **4\*Nle-OH** was 75 μmol/g.

*N*<sup>6</sup>-[(*Di-n-butylamino*)methylene]-3'-[*N*-(9-fluorenyl)methoxycarbonyl-*L*-norleucinyl]amino-3'-deoxy-5'-*O*-(4,4'-dimethoxytrityl)-*D*-adenosine (**2\*Nle**). Fmoc protected *L*-6-azidonorleucine (79 mg, 0.22 mmol) was dissolved in DMF (3 mL) followed by addition of *O*-(benzotriazol-1-yl)-*N,N,N',N'*-tetramethyluronium hexafluorophosphate (HBTU, 81 mg, 0.22 mmol), 1-hydroxybenzotriazole hydrate (HOBt, 27 mg, 0.17 mmol) and *N,N*-diisopropylethylamine (DIPEA, 45 μL, 0.26 mmol). After three minutes of activation, 3'-amino-*N*<sup>6</sup>-[(*di-n-butylamino*)methylene]-3'-deoxy-5'-*O*-(4,4'-dimethoxytrityl)-*D*-adenosine **1**<sup>[21]</sup> (122 mg, 0.17 mmol, in 1 mL DMF) was added and the mixture was stirred overnight at room temperature. Then, the solvent was evaporated, the residue dissolved in CH<sub>2</sub>Cl<sub>2</sub> and washed consecutively with half-saturated aqueous NaHCO<sub>3</sub> solution, 5% citric acid solution, and saturated aqueous NaCl solution. The organic layer was dried (Na<sub>2</sub>SO<sub>4</sub>), evaporated and the crude product was purified via SiO<sub>2</sub> chromatography yielding 116 mg of compound **2\*Nle** as white foam (65%).

<sup>1</sup>H NMR (300 MHz, CDCl<sub>3</sub>) δ 9.04 (s, 1H, HC=N(6)), 8.48 (s, 1H, H-C(2)), 8.14 (s, 1H, H-C(8)), 7.72 (m, 1H, H-C(ar)), 7.54 (m, 2H, H-C(ar)), 7.36-7.16 (m, 13H, H-C(ar) and CDCl<sub>3</sub>), 6.83 (s, 1H, H-N(3')), 6.76 (d, 4H, *J* = 8.5, H-C(ar)), 5.99 (s, 1H, H-C(1')), 5.39 (d, 1H, *J* = 7.3, H-N(Nle)), 4.77 (m, 1H, H-C(2')), 4.66 (m, 1H, H-C(3')), 4.34 (m, 3H, O-CH<sub>2</sub>(Fmoc) and H-C(4')), 4.18 (m, 2H, H-C(α, Nle) and H-C(9, Fmoc)), 3.75 (s, 6H, 2xOCH<sub>3</sub>(DMT)), 3.69 (m, 2H, N(CH<sub>2</sub>CH<sub>2</sub>CH<sub>2</sub>CH<sub>3</sub>)<sub>2</sub>), 3.39 (m, 4H, H-C(5') and N(CH<sub>2</sub>CH<sub>2</sub>CH<sub>2</sub>CH<sub>3</sub>)<sub>2</sub>), 1.66 (m, 6H, H<sub>2</sub>C(β, Nle) and N(CH<sub>2</sub>CH<sub>2</sub>CH<sub>2</sub>CH<sub>3</sub>)<sub>2</sub>), 1.38 (m, 4H, N(CH<sub>2</sub>CH<sub>2</sub>CH<sub>2</sub>CH<sub>3</sub>)<sub>2</sub>), 1.26 (m, 4H, 2xH<sub>2</sub>C(Nle)), 0.94 (m, 6H, N(CH<sub>2</sub>CH<sub>2</sub>CH<sub>2</sub>CH<sub>3</sub>)<sub>2</sub>), 0.84 (t, 3H, *J* = 6.6, H<sub>3</sub>C(Nle)). <sup>13</sup>C NMR (75 MHz, CDCl<sub>3</sub>) δ 172.6 (HC=N(6)), 160.5, 158.9, 158.6, 156.4, 152.5 (C(2)), 150.7, 144.5, 143.9, 143.8, 141.4, 139.6 (C(8)), 135.8, 135.7, 130.2 (C(ar)), 128.3 (C(ar)), 128.0 (C(ar)), 127.9 (C(ar)), 127.2 (C(ar)), 126.9 (C(ar)), 125.2 (C(ar)), 120.1 (C(ar)), 113.3 (C(ar)), 91.4 (C(1')), 86.6, 83.6 (C(4')), 74.7 (C(2')), 67.3 (O-CH<sub>2</sub>(Fmoc)), 63.4 (C(5')), 55.3 (C(α, Nle) and 2xOCH<sub>3</sub>(DMT)), 52.4 (C(3')), 52.1 (N(CH<sub>2</sub>CH<sub>2</sub>CH<sub>2</sub>CH<sub>3</sub>)<sub>2</sub>), 47.2 (CH(Fmoc)), 46.3, 45.4 (N(CH<sub>2</sub>CH<sub>2</sub>CH<sub>2</sub>CH<sub>3</sub>)<sub>2</sub>), 32.5 (N(CH<sub>2</sub>CH<sub>2</sub>CH<sub>2</sub>CH<sub>3</sub>)<sub>2</sub> and CH<sub>2</sub>(Nle)), 31.1 (N(CH<sub>2</sub>CH<sub>2</sub>CH<sub>2</sub>CH<sub>3</sub>)<sub>2</sub>), 29.4, 27.7 (CH<sub>2</sub>(Nle)), 22.4 (CH<sub>2</sub>(Nle)), 20.3 (N(CH<sub>2</sub>CH<sub>2</sub>CH<sub>2</sub>CH<sub>3</sub>)<sub>2</sub>), 19.9 (N(CH<sub>2</sub>CH<sub>2</sub>CH<sub>2</sub>CH<sub>3</sub>)<sub>2</sub>), 14.0, 14.0 (N(CH<sub>2</sub>CH<sub>2</sub>CH<sub>2</sub>CH<sub>3</sub>)<sub>2</sub>), 13.8 (CH<sub>3</sub>(Nle)), 11.0. ESI-MS (*m/z*): [M+H]<sup>+</sup> calcd for C<sub>61</sub>H<sub>71</sub>N<sub>8</sub>O<sub>8</sub>, 1043.54; found 1043.55.

*N*<sup>6</sup>-[(*Di-n-butylamino*)methylene]-3'-[*N*-(9-fluorenyl)methoxycarbonyl-*L*-norleucinyl]amino-3'-deoxy-5'-*O*-(4,4'-dimethoxytrityl)-2'-*O*-[1,6-dioxo-6-(pentafluorophenoxy)hexyl]-*D*-adenosine (**3\*Nle**). To a solution of compound **2\*Nle** (62 mg, 0.06 mmol) in DMF (1.5 mL) and pyridine (1.0 mL) was added DMAP (7 mg, 0.06 mmol) and bis(pentafluorophenyl) adipate (89 mg, 0.19 mmol). The mixture was stirred for one hour followed by evaporation of the solvents. The crude product was purified via SiO<sub>2</sub> chromatography (CH<sub>2</sub>Cl<sub>2</sub>/acetone, 7/3) yielding 36 mg of compound **2\*Nle** as white foam (46%).

<sup>1</sup>H NMR (300 MHz, CDCl<sub>3</sub>) δ 8.97 (s, 1H, HC=N(6)), 8.48 (s, 1H, H-C(2)), 8.01 (s, 1H, H-C(8)), 7.73 (m, 2H, HC(ar)), 7.75 (m, 2H, HC(ar)), 7.40-7.18 (m, 13H, HC(ar) and CDCl<sub>3</sub>), 6.75 (d, 4H, *J* = 7.8, HC(ar)), 6.54 (m, 1H, HN(3')), 6.14 (d, 1H, *J* = 2.6, HC(1')), 5.83 (m, 1H, HC(2')), 5.27 (m, 1H, HN(Nle)), 5.20 (m, 1H, HC(3')), 4.43 (m, 2H, OCH<sub>2</sub>(Fmoc)), 4.18 (m, 2H, HC(4') and HC(9, Fmoc)), 4.01 (m, 1H, HC(α, Fmoc)), 3.75 (s, 6H, 2xOCH<sub>3</sub>(DMT)),

3.67 (m, 2H, N(CH<sub>2</sub>CH<sub>2</sub>CH<sub>2</sub>CH<sub>3</sub>)<sub>2</sub>), 3.45-3.35 (m, 4H, HC(5')) and N(CH<sub>2</sub>CH<sub>2</sub>CH<sub>2</sub>CH<sub>3</sub>)<sub>2</sub>), 2.57 (m, 2H, OOCCH<sub>2</sub>CH<sub>2</sub>CH<sub>2</sub>CH<sub>2</sub>COO), 2.39 (m, 2H, OOCCH<sub>2</sub>CH<sub>2</sub>CH<sub>2</sub>CH<sub>2</sub>COO), 1.65 (m, 8H, CH<sub>2</sub>(AOA) and OOCCH<sub>2</sub>CH<sub>2</sub>CH<sub>2</sub>CH<sub>2</sub>COO and N(CH<sub>2</sub>CH<sub>2</sub>CH<sub>2</sub>CH<sub>3</sub>)<sub>2</sub>), 1.36 (m, 2H, N(CH<sub>2</sub>CH<sub>2</sub>CH<sub>2</sub>CH<sub>3</sub>)<sub>2</sub>), 1.23 (m, 4H, 2xCH<sub>2</sub>(Nle)), 0.93 (q, 6H, N(CH<sub>2</sub>CH<sub>2</sub>CH<sub>2</sub>CH<sub>3</sub>)<sub>2</sub>), 0.84 (t, 3H, CH<sub>3</sub>(Nle)). <sup>13</sup>C NMR (75 MHz, CDCl<sub>3</sub>) δ 172.1, 171.6, 169.6, 169.5, 162.7, 160.3, 158.6 (HC=N(6)), 158.5, 156.5, 153.1 (C(2)), 151.3, 144.5, 143.8, 141.4, 140.0 (C(8)), 135.7, 130.2 (C(ar)), 128.4 (C(ar)), 127.9 (C(ar)), 127.2 (C(ar)), 125.1 (C(ar)), 120.1 (C(ar)), 113.3 (C(ar)), 87.5 (C(1')), 86.8, 82.5 (C(4')), 75.2 (C(2')), 67.2 (OCH<sub>2</sub>), 63.4 (C(5')), 55.3 (C(α, Nle) and 2xOCH<sub>3</sub>(DMT)), 52.0 (N(CH<sub>2</sub>CH<sub>2</sub>CH<sub>2</sub>CH<sub>3</sub>)<sub>2</sub>), 50.7 (C(3')), 47.2 (CH(Fmoc)), 46.3, 45.3 (N(CH<sub>2</sub>CH<sub>2</sub>CH<sub>2</sub>CH<sub>3</sub>)<sub>2</sub>), 36.6, 34.7 (OOCCH<sub>2</sub>CH<sub>2</sub>CH<sub>2</sub>CH<sub>2</sub>COO), 33.3 (OOCCH<sub>2</sub>CH<sub>2</sub>CH<sub>2</sub>CH<sub>2</sub>COO), 32.9, 31.6, 31.1 (CH<sub>2</sub>(Nle)), 29.4 (2x OOCCH<sub>2</sub>CH<sub>2</sub>CH<sub>2</sub>CH<sub>2</sub>COO), 27.8 (CH<sub>2</sub>(Nle)), 25.7, 24.0 and 23.9 (N(CH<sub>2</sub>CH<sub>2</sub>CH<sub>2</sub>CH<sub>3</sub>)<sub>2</sub>), 22.4 (CH<sub>2</sub>(Nle)), 20.3 (N(CH<sub>2</sub>CH<sub>2</sub>CH<sub>2</sub>CH<sub>3</sub>)<sub>2</sub>), 19.9, 14.0 (N(CH<sub>2</sub>CH<sub>2</sub>CH<sub>2</sub>CH<sub>3</sub>)<sub>2</sub>), 13.8 (CH<sub>3</sub>(Nle)), 8.8. ESI-MS (m/z): [M+H]<sup>+</sup> calcd for C<sub>75</sub>H<sub>82</sub>F<sub>5</sub>N<sub>8</sub>O<sub>11</sub>, 1337.57; found 1337.46.

*DMTO-rA<sup>3'-NH</sup>-(N-Fmoc-Nle) solid support (4\*Nle)*. Compound **3\*Nle** (36 mg, 0.03 mmol) was dissolved in dry DMF (1.5 mL) and pyridine (5 μL) was added. To this solution, amino-functionalized support (*GE Healthcare, Custom Primer Support<sup>TM</sup> 200 Amino*, 200 mg) was added, and the suspension was agitated for 20 hours at room temperature. Subsequently, the beads were collected on a Büchner funnel and washed with DMF, methanol, and CH<sub>2</sub>Cl<sub>2</sub>. For capping of unreacted amino groups, the beads were treated with a mixture of solution A (0.2 M phenoxy acetic anhydride in THF, 10 mL) and solution B (0.2 M *N*-methyl imidazole, 0.2 M *sym*-collidine in THF, 10 mL) and agitated for 10 min at room temperature. The suspension was filtrated again, the beads were washed with THF, methanol and CH<sub>2</sub>Cl<sub>2</sub>, and dried under vacuum. Loading of the support **4\*Nle** was 40 μmol/g.

*N<sup>6</sup>-[(Di-*n*-butylamino)methylene]-3'-[(2*S*)-*N*-(9-fluorenyl)methoxycarbonyl-2-amino-octanamido]-3'-deoxy-5'-O-(4,4'-dimethoxytrityl)-D-adenosine (2\*AOA)*. (2*S*)-*N*-(9-fluorenyl)methoxycarbonyl-2-amino-octanic acid (83 mg, 0.20 mmol) was dissolved in DMF (3 mL) followed by addition of *O*-(benzotriazol-1-yl)-*N,N,N',N'*-tetramethyluronium hexafluorophosphate (HBTU, 66 mg, 0.17 mmol), 1-hydroxybenzotriazole hydrate (HOBt, 27 mg, 0.17 mmol) and *N,N*-diisopropylethylamine (DIPEA, 35 μL, 0.20 mmol). After 3 minutes of activation, 3'-amino-*N<sup>6</sup>*-[(di-*n*-butylamino)methylene]-3'-deoxy-5'-O-(4,4'-dimethoxytrityl)-D-adenosine **1**<sup>[2]</sup> (95 mg, 0.13 mmol, in 1 mL DMF) was added and the mixture was stirred overnight at room temperature. Then, the solvent was evaporated, the residue dissolved in CH<sub>2</sub>Cl<sub>2</sub> and washed consecutively with half-saturated aqueous NaHCO<sub>3</sub> solution, 5% citric acid solution, and saturated aqueous NaCl solution. The organic layer was dried (Na<sub>2</sub>SO<sub>4</sub>), evaporated and the crude product was purified via SiO<sub>2</sub> chromatography yielding 62 mg of compound **2\*AOA** as white foam (43%).

<sup>1</sup>H NMR (300 MHz, CDCl<sub>3</sub>) δ 9.05 (s, 1H, HC=N(6)), 8.49 (s, 1H, H-C(2)), 8.17 (s, 1H, H-C(8)), 7.71 (m, 2H, H-C(ar)), 7.54 (m, 2H, H-C(ar)), 7.39-7.14 (m, 13H, H-C(ar)), 6.87 (m, 1H, H-N(3')), 6.75 (d, 4H, J = 8.4, H-C(ar)), 6.01 (s, 1H, H-C(1')), 5.48 (d, 1H, J = 7.4, H-N(AOA)), 4.79 (m, 1H, H-C(2')), 4.69 (m, 1H, H-C(3')), 4.36 (m, 3H, OCH<sub>2</sub>(Fmoc) and H-C(4')), 4.18 (m, 2H, H-C(α, AOA) and H-C(9, Fmoc)), 3.74 (s, 6H, OCH<sub>3</sub>(DMT)), 3.72-3.60 (m, 2H, N(CH<sub>2</sub>CH<sub>2</sub>CH<sub>2</sub>CH<sub>3</sub>)<sub>2</sub>), 3.48-3.36 (m, 4H, N(CH<sub>2</sub>CH<sub>2</sub>CH<sub>2</sub>CH<sub>3</sub>)<sub>2</sub> and H-C(5')), 1.62 (m, 6H, N(CH<sub>2</sub>CH<sub>2</sub>CH<sub>2</sub>CH<sub>3</sub>)<sub>2</sub> and CH<sub>2</sub>(AOA)), 1.38-1.29 (m, 6H, N(CH<sub>2</sub>CH<sub>2</sub>CH<sub>2</sub>CH<sub>3</sub>)<sub>2</sub> and CH<sub>2</sub>(AOA)), 1.24 (br, 6H; 3xCH<sub>2</sub>(AOA)), 0.97-0.83 (m, 9H, 3xCH<sub>3</sub>). <sup>13</sup>C NMR (75 MHz, CDCl<sub>3</sub>) δ 173.1, 160.7, 158.8 (HC=N(6)), 156.5, 152.5 (C(2)), 150.8, 144.7, 144.1, 141.5, 139.8 (C(8)), 136.0, 130.2, 128.3, 128.0, 127.2, 125.2, 120.1, 113.3, 91.4(C(1')), 86.8, 83.7 (C(4')), 74.9 (C(2')), 67.4 (O-CH<sub>2</sub>(Fmoc)), 63.5 (C(5')), 55.4 (C(α, AOA) and

2xOCH<sub>3</sub>(DMT)), 52.5 (C(3')), 52.1 (N(CH<sub>2</sub>CH<sub>2</sub>CH<sub>2</sub>CH<sub>3</sub>)<sub>2</sub>), 47.3, 46.5 (CH(Fmoc)), 45.5 (N(CH<sub>2</sub>CH<sub>2</sub>CH<sub>2</sub>CH<sub>3</sub>)<sub>2</sub>), 38.9, 32.9, 31.8 and 31.2 (N(CH<sub>2</sub>CH<sub>2</sub>CH<sub>2</sub>CH<sub>3</sub>)<sub>2</sub> and CH<sub>2</sub>(AOA)), 29.4 and 29.1 (N(CH<sub>2</sub>CH<sub>2</sub>CH<sub>2</sub>CH<sub>3</sub>)<sub>2</sub> and CH<sub>2</sub>(AOA)), 25.7 (CH<sub>2</sub>(AOA)), 22.7 (CH<sub>2</sub>(AOA)), 20.4 and 20.0 (N(CH<sub>2</sub>CH<sub>2</sub>CH<sub>2</sub>CH<sub>3</sub>)<sub>2</sub>), 14.3-13.9 (N(CH<sub>2</sub>CH<sub>2</sub>CH<sub>2</sub>CH<sub>3</sub>)<sub>2</sub> and CH<sub>3</sub>(AOA)), 8.9. ESI-MS (m/z): [M+H]<sup>+</sup> calcd for C<sub>63</sub>H<sub>75</sub>N<sub>8</sub>O<sub>8</sub>, 1071.57; found 1071.44.

N<sup>6</sup>-[(Di-*n*-butylamino)methylene]-3'-[(2*S*)-N-(9-fluorenyl)methoxycarbonyl-2-amino-octanamido]-3'-deoxy-5'-O-(4,4'-dimethoxytrityl)-2'-O-[1,6-dioxo-6-(pentafluorophenyl)hexyl]-D-adenosine (**3\*AOA**). To a solution of compound **2\*AOA** (62 mg, 0.06 mmol) in DMF (1.5 mL) and pyridine (1.0 mL) was added DMAP (7 mg, 0.06 mmol) and bis(pentafluorophenyl) adipate (89 mg, 0.19 mmol). The mixture was stirred for one hour followed by evaporation of the solvents. The crude product was purified via SiO<sub>2</sub> chromatography (CH<sub>2</sub>Cl<sub>2</sub>/acetone, 7/3) yielding 36 mg of compound **3\*AOA** as white foam (46%).

<sup>1</sup>H NMR (300 MHz, CDCl<sub>3</sub>) δ 8.99 (s, 1H, HC=N(6)), 8.49 (s, 1H, H-C(2)), 8.08 (s, 1H, H-C(8)), 7.75 (m, 2H, H-C(ar)), 7.56 (m, 2H, H-C(ar)), 7.41-7.16 (m, 13H, H-C(ar)), 6.78 (d, 4H, J = 8.7, H-C(ar)), 6.52 (br, 1H, H-N(3')), 6.16 (d, 1H, J = 3.1, H-C(1)), 5.83 (m, 1H, H-C(2')), 5.24 (m, 2H, H-C(3') and H-N(AOA)), 4.47-4.29 (m, 2H, O-CH<sub>2</sub>(Fmoc)), 4.18 (m, 2H, H-C(4') and H-C(9, Fmoc)), 4.01 (m, 1H, H-C(α, AOA)), 3.75 (s, 6H, 2xO-CH<sub>3</sub>(DMT)), 3.64 (m, 2H, N(CH<sub>2</sub>CH<sub>2</sub>CH<sub>2</sub>CH<sub>3</sub>)<sub>2</sub>), 3.45-3.36 (m, 4H, H<sub>2</sub>C(5') and N(CH<sub>2</sub>CH<sub>2</sub>CH<sub>2</sub>CH<sub>3</sub>)<sub>2</sub>), 2.57 (s, 2H, OOCCH<sub>2</sub>CH<sub>2</sub>CH<sub>2</sub>CH<sub>2</sub>COO), 2.41 (s, 2H, OOCCH<sub>2</sub>CH<sub>2</sub>CH<sub>2</sub>CH<sub>2</sub>COO), 1.65-1.57 (m, 8H, CH<sub>2</sub>(AOA) and OOCCH<sub>2</sub>CH<sub>2</sub>CH<sub>2</sub>CH<sub>2</sub>COO and N(CH<sub>2</sub>CH<sub>2</sub>CH<sub>2</sub>CH<sub>3</sub>)<sub>2</sub>), 1.39-1.29 (m, 4H, N(CH<sub>2</sub>CH<sub>2</sub>CH<sub>2</sub>CH<sub>3</sub>)<sub>2</sub>), 1.28-1.19 (m, 8H, CH<sub>2</sub>(AOA)), 0.97-0.84 (m, 9H, 3xCH<sub>3</sub>). <sup>13</sup>C NMR (75 MHz, CDCl<sub>3</sub>) δ 172.0, 171.6, 169.5, 159.9, 158.7 (HC=N(6)), 156.5, 152.7 (C(2)), 151.1, 144.4, 143.7, 141.4 (C(8)), 140.1, 139.6, 135.6, 130.2 (C(ar)), 129.3, 128.4(C(ar)), 128.0, 127.2, 127.0, 125.9, 125.0 (C(ar)), 120.1 (C(ar)), 113.3 (C(ar)), 87.6 (C(1')), 86.8, 82.5 (C(4')), 75.2 (C(2')), 67.2 (OCH<sub>2</sub>(Fmoc)), 63.2 (C(5')), 55.3 (C(α, Nle) and 2xOCH<sub>3</sub>(DMT)), 52.1 (N(CH<sub>2</sub>CH<sub>2</sub>CH<sub>2</sub>CH<sub>3</sub>)<sub>2</sub>), 50.6 (C(3')), 47.2 (HC(Fmoc)), 45.4 (N(CH<sub>2</sub>CH<sub>2</sub>CH<sub>2</sub>CH<sub>3</sub>)<sub>2</sub>), 33.3 (OOCCH<sub>2</sub>CH<sub>2</sub>CH<sub>2</sub>CH<sub>2</sub>COO), 32.9 (OOCCH<sub>2</sub>CH<sub>2</sub>CH<sub>2</sub>CH<sub>2</sub>COO), 31.7 (CH<sub>2</sub>(AOA)), 31.1 (OOCCH<sub>2</sub>CH<sub>2</sub>CH<sub>2</sub>CH<sub>2</sub>COO), 29.3, 29.0 (2xCH<sub>2</sub>(AOA)), 25.7 (CH<sub>2</sub>(AOA)), 24.0, 23.8 (N(CH<sub>2</sub>CH<sub>2</sub>CH<sub>2</sub>CH<sub>3</sub>)<sub>2</sub>), 22.7 (CH<sub>2</sub>(AOA)), 20.2, 19.9 (N(CH<sub>2</sub>CH<sub>2</sub>CH<sub>2</sub>CH<sub>3</sub>)<sub>2</sub>), 14.1-13.7 (3xCH<sub>3</sub>). ESI-MS (m/z): [M+H]<sup>+</sup> calcd for C<sub>75</sub>H<sub>82</sub>F<sub>5</sub>N<sub>8</sub>O<sub>11</sub>, 1365.60; found 1366.48.

DMTO-*rA*<sup>3'-NH</sup>-(*N*-Fmoc-AOA) solid support (**4\*AOA**). Compound **3\*AOA** (36 mg, 0.03 mmol) was dissolved in dry DMF (1.5 mL) and pyridine (5 μL) was added. To this solution, amino-functionalized support (*GE Healthcare, Custom Primer Support*<sup>TM</sup> 200 Amino, 200 mg) was added, and the suspension was agitated for 20 hours at room temperature. Subsequently, the beads were collected on a Büchner funnel and washed with DMF, methanol, and CH<sub>2</sub>Cl<sub>2</sub>. For capping of unreacted amino groups, the beads were treated with a mixture of solution A (0.2 M phenoxy acetic anhydride in THF, 10 mL) and solution B (0.2 M *N*-methyl imidazole, 0.2 M *sym*-collidine in THF, 10 mL) and agitated for 10 min at room temperature. The suspension was filtrated again, the beads were washed with THF, methanol and CH<sub>2</sub>Cl<sub>2</sub>, and dried under vacuum. Loading of the support **4\*AOA** was 45 μmol/g.

### **RNA solid-phase synthesis, deprotection and purification**

*Automated synthesis on solid supports 4.* The 5'-p-ACC moiety was assembled on an *ABI 392 Nucleic Acid Synthesizer* following standard synthesis protocols using 2'-*O*-[(Triisopropylsilyl)oxy]methyl (TOM) protected nucleoside phosphoramidites<sup>[3,4]</sup> and the above described solid supports **4**. Detritylation (120 s): dichloroacetic acid/1,2-dichloroethane (4/96); coupling (120 s): phosphoramidites (0.1 M in acetonitrile, 130 mL) were activated with benzylthiotetrazole (0.3 M in acetonitrile, 180  $\mu$ L); capping (2 x 10 s, Cap A/Cap B = 1/1): Cap A: phenoxyacetic anhydride (0.2 M in THF), Cap B: *N*-methyl imidazole (0.2 M), sym-collidine (0.2 M) in THF; oxidation (20 s): I<sub>2</sub> (0.2 M) in THF/pyridine/H<sub>2</sub>O (35/10/5). Nucleoside phosphoramidites, benzylthiotetrazole, and capping solutions were dried over activated molecular sieves (4 Å) overnight.

*Deprotection of the 5'-p-ACCA<sup>3NH</sup>-amino acid conjugates. Step A) Fmoc deprotection.* In the *ABI* synthesis column, the solid support was treated with a solution of 20 % piperidine in acetonitrile (10 mL, 10 min), washed with acetonitrile and dried. *Step B) Acyl deprotection and cleavage from the solid support.* For the conjugates synthesized on solid support **4**, the beads were transferred into an Eppendorf tube and equal volumes of methylamine in ethanol (8 M, 0.5 mL) and methylamine in H<sub>2</sub>O (40 %, 0.5 mL) were added. After 6 h shaking at room temperature the supernatant was filtered and evaporated to dryness. *Step C) 2'-O-TOM and 6-OtBDMS-Nle deprotection.* The obtained residue was treated with TBAF·3 H<sub>2</sub>O in THF (1 M, 1 mL) overnight at room temperature. The reaction was quenched by the addition of triethylammonium acetate (TEAA) (1 M, pH 7.4, 1 mL). After reducing the volume of the solution, it was applied on a size-exclusion chromatography column (*GE Healthcare*, HiPrep 26/10 Desalting, 2.6 x 10 cm, Sephadex G25). By eluting with H<sub>2</sub>O, the conjugate-containing fractions were collected, evaporated to dryness, and the residue was dissolved in H<sub>2</sub>O (1 mL). Analysis of the crude products was performed by anion-exchange chromatography on a *Dionex DNAPac PA-100* column (4 x 250 mm) at 60 °C. Flow rate: 1 mL min<sup>-1</sup>; eluent A: 25 mM Tris·HCl (pH 8.0), 6 M urea; eluent B: 25 mM Tris·HCl (pH 8.0), 0.5 M NaClO<sub>4</sub>, 6 M urea; gradient: 0–60 % B in A within 45 min or 0–40 % B in A within 30 min, UV detection at  $\lambda = 260$  nm.

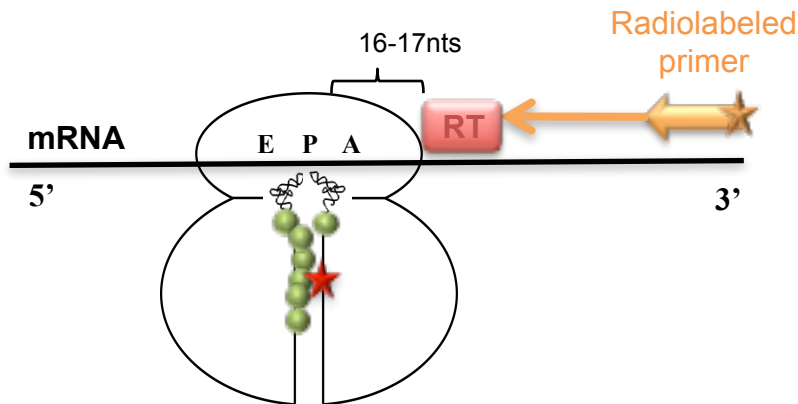
*Purification of the 5'-p-ACCA<sup>3NH</sup>-amino acid conjugates.* The crude conjugate was purified on a semipreparative *Dionex DNAPac PA-100* column (9 x 250 mm) at 60 °C with flow rate of 2 mL min<sup>-1</sup> (for eluents see above). Fractions containing the conjugate were loaded on a C18 SepPak Plus cartridge (*Waters/Millipore*), washed with 0.1–0.15 M (Et<sub>3</sub>NH)<sup>+</sup>HCO<sub>3</sub><sup>-</sup>, H<sub>2</sub>O, and eluted with H<sub>2</sub>O/CH<sub>3</sub>CN (1:1). Conjugate-containing fractions were evaporated to dryness and dissolved in H<sub>2</sub>O (1 mL). The quality of the purified conjugate was analyzed by analytical anion-exchange chromatography (for conditions see above). The molecular weight of the synthesized conjugate was confirmed by LC-ESI mass spectrometry. Yields were determined by UV photometrical analysis of conjugate solutions. The final compound was dissolved in water to achieve ~50 mM concentration for stock solutions and later used for soaking.

**Cited Literature**

- [1] Moroder, H., Steger, J., Graber, D., Fauster, K., Trappl, K., Marquez, V., Polacek, N., Wilson, D. N., Micura, R. (2009). Non-Hydrolyzable RNA-Peptide Conjugates: A Powerful Advance in the Synthesis of Mimics for 3'-Peptidyl tRNA Termini. *Angew. Chem. Int. Ed.*, 48, 4056–4060.
- [2] Geiermann, A.-S., Micura, R. (2015). Native chemical ligation of hydrolysis-resistant 3'-NH-cysteine-modified RNA. *Curr. Protoc. Nucleic Acid Chem.* 62:4.64.1-4.64.36.
- [3] Pitsch, S., Weiss, P. A., Jenny, L., Stutz, A., Wu, X. (2001). Reliable Chemical Synthesis of Oligoribonucleotides (RNA) with 2'-O-[(Triisopropylsilyl)oxy]methyl (2'-O-tom)-Protected Phosphoramidites. *Helvetica Chimica Acta*, 84(12), 3773–3795.
- [4] Micura, R. (2002). Small interfering RNAs and their chemical synthesis. *Angew. Chem. Int. Ed.*, 41, 2265–2269.

## Appendix D

### Principle of toe printing assay



Cell-free translation and toeprinting analyses were carried out as described in section 2.2. Linear DNA templates (0.5–1 pmol) encoding the ORF of interest preceded by the T7 promoter were generated by PCR. The templates were used to direct transcription–translation in the ribosome PURExpress cell-free system (New England Biolabs). The reactions were supplemented with antibiotics in a total volume of 5  $\mu$ L. The reactions were incubated for 10 min at 37 °C followed by a 5-min primer extension initiated by addition of reverse transcriptase. cDNA products were separated in a 6% sequencing gel and visualized with a Typhoon imager (GE). cDNA products from arrest site result in unique band 16-17 nucleotides from the P site of the arrested ribosome. From the sequencing lanes on the gel of the corresponding templates, the codon corresponding to the P site of the arrested ribosome can be mapped.

## VITA

### EDUCATION

University of Illinois at Chicago (UIC), USA

**Ph.D., Pharmaceutical Biotechnology**

Minor: Certified Associate in Project Management (CAPM)

Anna University, India

**B. Tech, Industrial Biotechnology**

2006 – 2010

### INDUSTRIAL RESEARCH EXPERIENCE

**Genentech Inc.**

*Infectious Diseases, South San Francisco, CA*

June 2015-Sep 2015

Constructed a genetically engineered library of E.coli strains for discovery of novel antibiotics.

**Thermo Fisher Scientific Inc.**

*Particles Team, Eugene, OR*

May 2014-Aug 2014

Developed next generation of fluorescent probes for immunology applications.

### PUBLICATIONS

**Sothiselvam, S.**, Liu, B., Han, W., Ramu, H., Klepacki, D., Atkinson, G.C., Brauer, A., Remm, M., Tenson, T., Schulten, K., Vázquez-Laslop, N., Mankin, A.S. (2014) Macrolide antibiotics allosterically predispose the ribosome for translation arrest. *PNAS USA* 111, 9804-9809.

Gupta, P., **Sothiselvam, S.**, Vázquez-Laslop, N., Mankin, A.S. (2013) Deregulation of translation due to post-transcriptional modification of rRNA explains why erm genes are inducible *Nature Communications* 4, 1984 DOI: 10.1038/ncomms2984.

- This article was recommended in *Faculty of 1000*.

### ORAL PRESENTATIONS

Antibiotic corrupts the ribosome into discriminating its catalytic substrates based on charge and size. **Cold spring harbor laboratories conferences (Translation control)**. New York, 2014.

Macrolide antibiotics allosterically alter the catalytic center of the ribosome. **The MIKI Meeting 2014: The 52<sup>nd</sup> Annual Medicinal Chemistry Meeting**. Chicago, 2014.

### POSTER PRESENTATIONS

**Shanmugapriya Sothiselvam**, Nora Vasquez-Laslop and Alexander Mankin. *Context specific action of macrolide antibiotics in causing translation arrest*. **College of Pharmacy Research Day**, UIC, Chicago, 2015.

**Shanmugapriya Sothiselvam**, Haripriya Ramu, Nora Vasquez-Laslop and Alexander Mankin. *Structurally different macrolides induce antibiotic resistance*. **ICAAC**, Denver, 2013.

**Shanmugapriya Sothiselvam**, Lukas Rigger, Ronald Micura, Nora Vazquez-Laslop and Alexander Mankin. *Antibiotic alters substrate specificity of the ribosome*. **Ribosomes Conference**, Napa, 2013.

Lukas Rigger, **Shanmugapriya Sothiselvam**, Nora Vasquez-Laslop, Alexander Mankin and Ronald Micura. *Chemical Synthesis of 3'-Aminoacyl-tRNA Mimics to Investigate Antibiotic Induced Ribosome Stalling*. **Annual meeting of the RNA society**, Davos, Switzerland, 2013.

Lauren Callahan, **Shanmugapriya Sothiselvam**, Nora Vasquez-Laslop and Alexander Mankin. **College of Science Joint Annual Meeting**. University of Notre dame, 2013.

**Shanmugapriya Sothiselvam**, Haripriya Ramu, Nora Vasquez-Laslop and Alexander Mankin. *The shortest nascent peptide that directs ribosome stalling*. **ASBMB Conference**, San Diego, 2012.

**Shanmugapriya Sothiselvam**, Haripriya Ramu, Nora Vasquez-Laslop and Alexander Mankin. *The shortest nascent peptide that directs ribosome stalling*. **College of Pharmacy Research Day**, UIC, 2012.

Pulkit Gupta, **Shanmugapriya Sothiselvam**, Nora Vasquez-Laslop and Alexander Mankin. *Why are erm genes inducible?* **ICAAC**, Chicago, 2011.

Pulkit Gupta, **Shanmugapriya Sothiselvam**, Nora Vasquez-Laslop, Alexander Mankin. *Why is the expression of erythromycin resistance inducible?* **College of Pharmacy research day**, UIC, 2011.

**Shanmugapriya Sothiselvam**, Marrielle Gruenig and Michael Cox; *Purification and Characterization of Bacteriophage-P1 Ref protein*. **33<sup>rd</sup> Steenbock Symposium**, Madison, 2009.

## ACADEMIC RESEARCH EXPERIENCE

### **Graduate Research Assistant**

**Center for Pharmaceutical Biotechnology, UIC**

April 2011 - Present

Elucidated the mechanism of antibiotic dependent arrest of protein synthesis to understand

- Action of antibiotics at a molecular level that will lead to the discovery of novel antibiotics.
- Mechanism of Antibiotic resistance.
- Inhibition of protein synthesis by small molecules.

### **Summer Research Fellow**

**Center for Biotechnology, Anna University, India**

December 2009 - June 2010

- Cloned and purified recombinant filarial proteins as potential diagnostic markers for lymphatic filariasis.
- Characterized the use of recombinant filarial protein Bm-33 as a marker in different stages of the filarial disease prognosis.

### **Summer research intern**

**University of Wisconsin-Madison, USA**

May 2009 - July 2009

Purified the Bacteriophage P1 Recombination enhancement factor, implicated in DNA recombination in bacteria, and characterized its DNA-binding properties.

### **HONORS AND AWARDS**

- Chancellor's Graduate Research Award, UIC, 2013 & 2014
- Provost and Deiss Graduate Student Award, UIC, 2013
- Myron Goldsmith Graduate Student Award, UIC, 2013
- Student Travel Presenters Award, UIC, 2013
- Graduate Student Council Travel Award, UIC, 2013
- American Society for Biochemistry and Molecular Biology (ASBMB) Travel Award, 2012
- Khorana Scholar, Indo-US Research Fellowship, Awarded by Dept of biotechnology, India, 2009
- National Talent Search Fellowship, Awarded by Govt. of India, 2005

### **LEADERSHIP ROLES** (Most recent)

- Marketing Head of the Graduate Student Consulting Club (GSCC), UIC
- Team Lead and Commercialization and Strategy Consultant at Enterprise Works, Chicago
- Invited Science Fair Judge at Gunsaulus Academy Elementary, Chicago, 2011, 2012 & 2013